UCLouvain

École polytechnique de Louvain

Design and modelling of a passive bearingless motor with buried permanent magnets

Authors: **Simon Herrman, Adrien Robert**
Supervisors: **Bruno Dehez, Joachim Van Verdeghem**
Reader: **Marc Bekemans**
Academic year 2021–2022
Master [120] in Electro-mechanical Engineering

ACKNOWLEDGEMENTS

We would like to first express our sincere gratitude to our supervisor, Prof. Bruno Dehez, for this incredible experience. More precisely, we would like to thank him for his availability, his constant optimism, his rigorousness and for his small but always well-dosed jokes. His implication and his passion for electrical machines motivated us more than ever. Few students have the chance to receive such support and it was a pleasure to have his guidance.

We are also thankful to our second supervisor, the Dr. Joachim Van Verdeghem, for his accompaniment and his availability, but also for his good mood and his sens of humour despite his headaches on Monday afternoon, and his answers to emails at ever more surprising hours on weekends (do you ever sleep ?). It was truly a pleasure to benefit from your great knowledge and advises during this year.

We would also like to thank the Dr. Benoît Herman for his great advice and the numerous discussions about the design of the rotor. It is always a pleasure to talk with him.

Thanks also to the Prof. Marc Bekemans for accepting to read our Master's thesis. We hope you will enjoy the reading it as much as we enjoy making it.

Finally, we would like to thank our respecting families who supported us during those five years of study. They always encouraged ourselves to give our very best, to never give up and were always ready to carefully listen to us when needed. We would not be there without them.

ABSTRACT

Bearingless machines are developed for applications which require high rotation speed, power density, long lifetime and high purity environment. The most compact machines of this category are the combined winding machines which gather both suspension and driving functions in only one set of winding. During the last few years, an Electrodynamic Thrust Self-Bearing Machine (ETSBM) has been developed by Dr. Joachim Van Verdeghem and Prof. Bruno Dehez. This motor is an Axial Flux Permanent Magnet (AFPM) machine which drives a flat disc rotor that passively levitates at high speed due to a specific connection of the windings. However the rotor topology of this machine uses a basic structure of Surface Mounted PMs (SMPMs) without any ferromagnetic part present on the rotor. More generally, the current researches in the field of axial bearingless machine have not yet explored the use of rotors with Buried PMs (BPMs). This kind of rotor should improve the suspension performance at low speed by increasing the inductance coefficients. Moreover, these parts will add axial and angular variations of the same coefficients which will create reluctant force components. With this in mind, this Master's thesis aims to study the influence of a BPM rotor on the ETSBM performances.

First, a review of the literature dealing with the AFPM machines using a rotor with buried permanent magnets (BPMs) is done. Thanks to it, a topology is chosen and a first design proposal is given. After that, an electromechanical model suited to the selected topology is developed. It describes the axial and spin behaviours of the machine. This model also highlights the modulation capability of the suspension through the motor currents and the reluctant effects generated by the structure of the rotor. Then static FEM simulations determine the parameters of the model and validate the assumptions made in this one. Next a bi-objective optimisation process consisting of the minimisation of the losses and the maximisation of the axial stiffness is realised in order to size the AFPM BPM machine. Finally a case study based on the best candidate previously computed is done. It aims to compare SMPM and BPM rotor topologies through both a quasi-static and a dynamic analysis. These analyses show that the BPM rotor can significantly upgrade the suspension performance. However, the analyses point out that the motor currents do not have enough influence on the suspension to modulate it. Besides of that, a comparison with a modified BPM rotor design shows that better performances could still be achieved. This paves the way for future researches concerning bearingless motors with a BPM rotor.

CONTENTS

LIST OF SYMBOLS

α	Angular position of the rotor (Notation of [1])	[rad]
θ_{em}	Electrical angular position	[rad]
θ_{m}	Angular position of the rotor	[rad]
$\boldsymbol{\Phi_{\mathbf{L}}}$	Lower winding magnetic flux linkage	[Wb]
$\boldsymbol{\Phi_{\mathbf{M}}}$	Motor magnetic flux	[Wb]
$\boldsymbol{\Phi_{\mathbf{S}}}$	Suspension magnetic flux	[Wb]
$\boldsymbol{\Phi_{\mathbf{U}}}$	Upper winding magnetic flux linkage	[Wb]
ω	Rotation speed	[rad/s]
A	Magnetic potential vector	[T/m]
$\mathrm{C_z}$	Axial damping coefficient	[kg/s]
$\mathrm{C}_{\theta_{\mathrm{m}}}$	Angular damping coefficient	[kg·m^2/s]
dL	Axial variation of cyclic inductance	[H]
$\mathrm{dL_0}$	Axial derivative of $\mathrm{L_0}$	[H/m]
$\mathrm{dL_2}$	Axial derivative of $\mathrm{L_2}$	[H/m]
$\mathrm{dL_d}$	Axial derivative of the direct inductance	[H/m]
$\mathrm{dL_q}$	Axial derivative of the quadrature inductance	[H/m]
$\mathrm{dM_0}$	Axial derivative of $\mathrm{M_0}$	[H/m]
$\mathrm{F_z}$	Axial force	[N]
$\mathrm{F_{z,d}}$	Detent axial force	[N]

$F_{z,e}$	External axial force	[N]
$F_{z,Ed}$	Electrodynamic axial force	[N]
$F_{z,rel}$	Reluctant axial force	[N]
I_L	Current circulating in the lower winding	[A]
$I_{M,d}$	Direct motor current	[A]
$I_{M,q}$	Quadrature motor current	[A]
$I_{S,d}$	Direct suspension current	[A]
$I_{S,q}$	Quadrature suspension current	[A]
I_U	Current circulating in the upper winding	[A]
J_p	Polar moment of inertia of the rotor	[m^2·kg]
J	Current density vector	[A/m^2]
K_{θ_m}	Amplitude of the magnetic flux linkage when the rotor is axially centered	[Wb]
K_z	Gradiant of magnetic flux linkage according to the axial position of the rotor	[Wb/m]
$k_{z,d}$	Detent stiffness	[N/m]
$\mathbf{L_0}$	Constant term of $\mathbf{L_{U/L}}(z, \theta_{em})$ according to θ_{em}	[H]
L_0	Self inductance of one phase of the upper or lower winding	[H]
L_2	Amplitude of the angular variation of L_0	[H]
L_{Av}	Average matrix defined in 2.13	[H]
L_d	Direct inductance	[H]
$\mathbf{L_L}(z, \theta_{em})$	Matrix of inductance of the lower winding	[H]
$L_{M,c}$	Motor cyclic inductance (notation from [1])	[H]
$L_{M,d}$	Direct motor inductance	[H]
$L_{M,q}$	Quadrature motor inductance	[H]
L_q	Quadrature inductance	[H]
$L_{S,c}$	Suspension cyclic inductance (notation from [1])	[H]
$L_{S,d}$	Direct suspension inductance	[H]
$L_{S,q}$	Quadrature suspension inductance	[H]

$\mathbf{L_U}(z, \theta_{em})$	Matrix of inductance of the upper winding	[H]
L_v	Variation matrix defined in 2.14	[H]
m	Mass of the rotor	[kg]
M_0	Mutual inductance between two phases of the upper winding (same for lower)	[H]
M_2	Amplitude of the angular variation of M_{UL}	[H]
M_d	Direct mutual inductance	[H]
M_{ii}	Mutual inductance between an upper and a lower winding of the same phase	[H]
M_{ij}	Mutual inductance between an upper and a lower winding of two different phases	[H]
M_q	Quadrature mutual inductance	[H]
M_{UL}	Matrix of mutual inductance between upper and lower windings	[H]
p	Number of pole pair	[-]
R	Resistance of a phase of the upper/lower winding	[Ω]
$T_{\alpha,D}$	Drag torque (Notation of [1])	[Nm]
$T_{\alpha,M}$	Driving torque (Notation of [1])	[Nm]
$T_{\theta_m,D}$	Drag torque	[Nm]
$T_{\theta_m,M}$	Driving torque	[Nm]
$T_{\theta_m,e}$	External torque	[Nm]
$T_{\theta_m,rel}$	Reluctant torque	[Nm]
U_d	Direct-axis voltage	[V]
U_q	Quadrature-axis voltage	[V]
z	Axial position of the rotor	[m]
$\ldots^{\infty}$	Asymptotic value	[-]
$\ldots^{S}$	Matrix in the Concordia domain	[-]
$\ldots^{P}$	Matrix in the Park domain	[-]

LIST OF ACRONYMS

INTRODUCTION

One of the most common failures in classical high-speed electrical motors is caused by the breaking of the contact type-bearings. Moreover, these ball bearings can create some vibrations and losses which are no more negligible when the speed becomes important. Lubrication is sometimes used to reduce these losses, but the lubricant prevents from using this system in vacuum or high purity application [1, 2]. All these reasons have motivated the development of the contact-less bearings which are divided in two main categories: the air-foils aerodynamic bearings and the magnetic bearings. The former [3] provides a purely passive suspension which is well adapted for small shaft and a specific speed range but, of course, cannot be used in vacuum environment.

The latter can be split into two subcategories: The Active Magnetic Bearings (AMBs) and the Passive Magnetic Bearings (PMBs). On the one hand, AMBs consist in electromagnets where the current which regulates the stiffness is actively regulated according to the application and the position of the rotor [4]. It must be noted that AMBs are expensive and complicated to integrate.

On the other hand, PMBs use only passive phenomena and are constituted of PMs. Many topologies are already developed [5], but as stated by Earnshaw's theorem, it is impossible to reach a fully magnetic levitation by using a static magnetic field to stabilise all the Degrees Of Freedom (DOF) of the rotor: at least one DOF must be controlled with an alternative, which means PMBs must be combined with another technology.

Passive magnetic bearings avoid the problem of friction and lubrication. But using them leads to another problem [6]. Indeed, the passive magnetic bearings occupy a non-negligible part of the shaft compare to classical bearings and thus they decrease the global power density of the system, which is problematic when the purpose is to reach high rotation speed with a reasonable torque. Moreover, the length of the shaft is limited to avoid the flexible modes. Then for a same shaft length, the reachable power range is lower than with classical bearings because the length available for the armature winding of the motor is smaller, as illustrated in Figure 1.

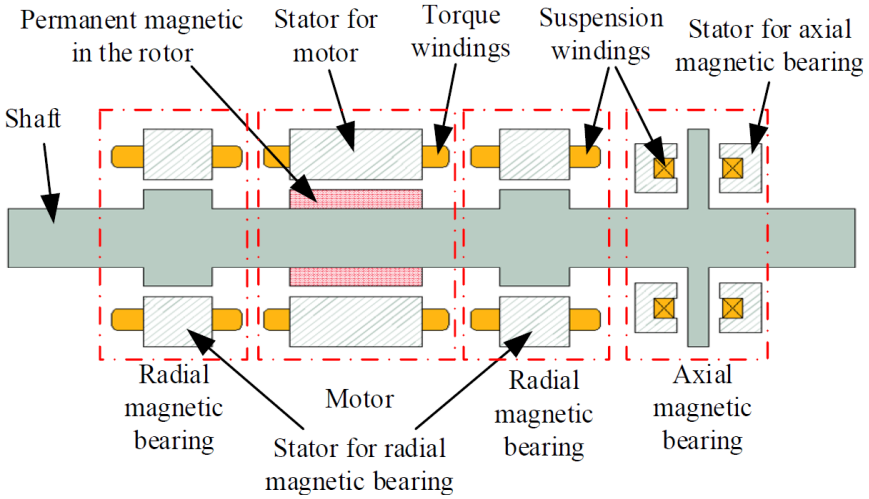

Figure 1: Schematic structure of the motor with AMBs (from [7]).

The bearingless machines, also called self-bearing machines, are used to compensate these defaults and increase the power density. This technology uses a single structure to provide both motor (or generator) and magnetic suspension functions [8]. These motors usually combine two sets of windings, the first one for the motor function and the second one for the magnetic suspension [9]. They are developed for different high-speed applications like centrifugal pump and compressor [10–12], fans and blowers [13–15], flywheels [16–18] and reaction wheels [19, 20]. Furthermore, this technology is used in situation where lubricant of a classical machine could be dangerous for the proper functioning of the system, like in high purity mixing devices for bioreactors [21–24] or in centrifugal blood pumps and in ventricular assist devices [25–28].

Currently, some researches propose new motors which combine both functions in one set of windings [1, 29–40], usually called Combined Winding BearingLess Machine (CWBLM). These systems improve the compactness and the power density of the machines while reducing the Joules losses. The basic structure of this type of machine is available in Figure 2 and highlights the gain of space available for the motor windings compare to Figure 1.

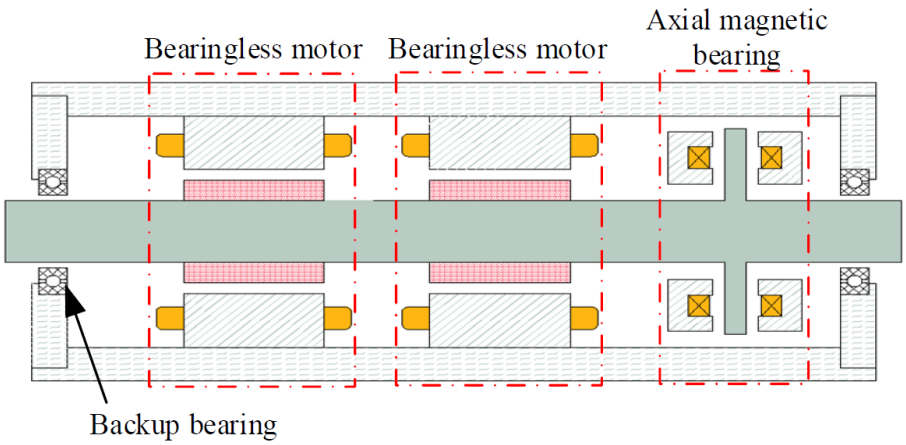

Figure 2: Schematic structure of the CWBLM (from [7]).

As for conventional motors, there are axial flux machines and radial flux machines, but this Master thesis will focus on the first category. The classical machines with Axial Flux Permanent Magnet (AFPM) are used for a wide variety of applications which require axial compactness, high efficiency and high torque density [41]. Axial Flux BearingLess Machine (AFBLM) keeps these qualities while reducing the losses due to mechanical friction and increasing the reachable rotation speed.

Topologies of axial-flux bearingless machine

This section presents the state of the art of the AFBLM. Its purpose is to complete the state of the art proposed by J.Van Verdeghem in [1], then some topologies presentations will be mainly inspired from his work and be marked by blue title.

(Ueno et al., 2000)

The prototype presented in [30] is shown in Figure 3(a). It is an axial-flux structure where the stator includes a three-phase armature winding disposed in a slotted ferromagnetic circuit. The rotor is composed of a ferromagnetic disc on which the PMs have an alternate polarisation. The PMs are either surface mounted or inserted. This machine provides only a motor torque and an attractive axial force f_m which depends on both direct and quadrature currents and tends to bring closer the rotor to the stator. Then this force must be compensate by a restoring force, called bias force f_b in the paper, to reach the nominal position. The axial position of the rotor is controlled by injecting more or less current into the coils. As the driving torque solely depends on the quadrature current, it is limited by the bias force.

The prototype presented in [31] is an improved version of the one presented in [30]. As it can be seen in Figure 3(b), the prototype was symmetrised to remove the need of a bias force and then remove the torque limitation. Nevertheless this symmetry requires to use two sets of three-phase windings. Concerning the radial and tilt DOF, they are magnetically supported by two classic PM centering bearings.

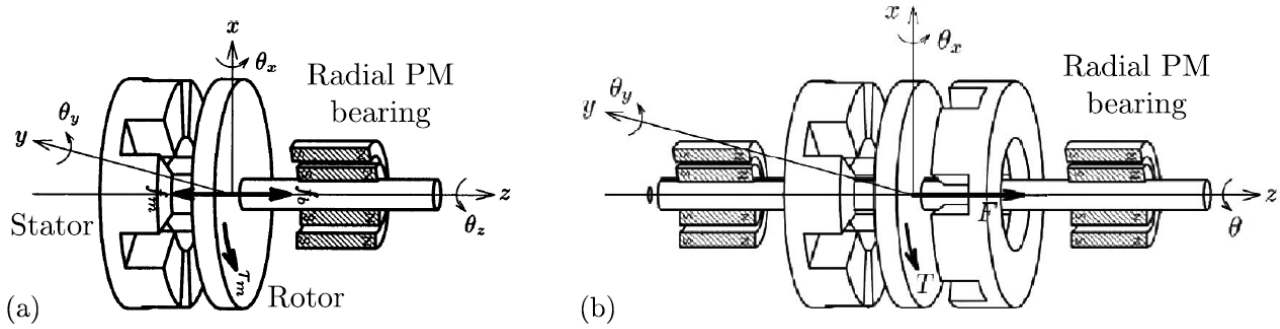

Figure 3: Axial-flux structure with a slotted stator and a flat disc rotor (from [30]) (a) Unidirectional variant. (b) Bidirectional variant (from [31]) (© 2000 IEEE).

(Asper et al.,2003)

The paper [32] presents an electrodynamic thrust bearing machine. The rotor, shown in Figure 4, is composed of a PM arrangement of highlighted by the number 1 and 2 in Figure 4(a). These magnets are alternately magnetised in the axial direction. Two sets of windings are visible in Figure 4(b): The suspension winding L_A and L_B, which are short-circuited through their opposition connection (3), and the additional motor windings L_X and L_Y, which are connected in series to the power supply (13). This configuration allows to control the driving torque with the current $I_{X,Y}$ while the axial levitation comes from the induced current flowing into the suspension winding. The other DOF can be passively stabilised with classical PM bearings. This topology can be improved to achieved the axial suspension and the rotor drive to become a passively levitated thrust self-bearing machine.

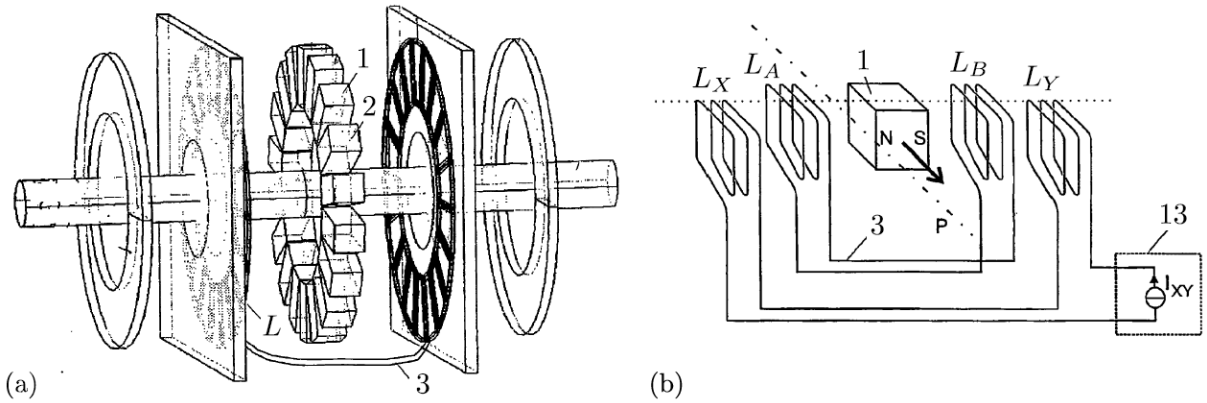

Figure 4: Thrust self-bearing machine (from [32]). (a) Exploded view. (b) Detailed view.

(Asama et al.2013)

The principle of [31] has inspired [33] to propose this topology which offers in addition the single-drive characteristic. Figure 5 shows the structure of the machine. Its rotor is composed of two sets of PMs axially magnetised and fixed on back iron which are themselves connected on each sides of the rotor shaft. The stator is made of two ferromagnetic circuits, each one in front of one set of PMs. The symmetry of this structure allows to have a centred position where the attractive magnetic forces acting on both rotor sides compensate each other. The left ferromagnetic circuit receives a three-phases armature winding. This winding allows to regulate the strengthening of the axial magnetic flux and the torque by injecting respectively direct and quadrature current. Indeed, as depicted in Figures 5(a) and 5(b), increasing the direct current that strengthens the magnetic flux. The two last Figures, 5(c) and 5(d), depict the passive stabilisation of the tilt and radial DOF due to the interaction between the PMs and the ferromagnetic circuits of the rotor.

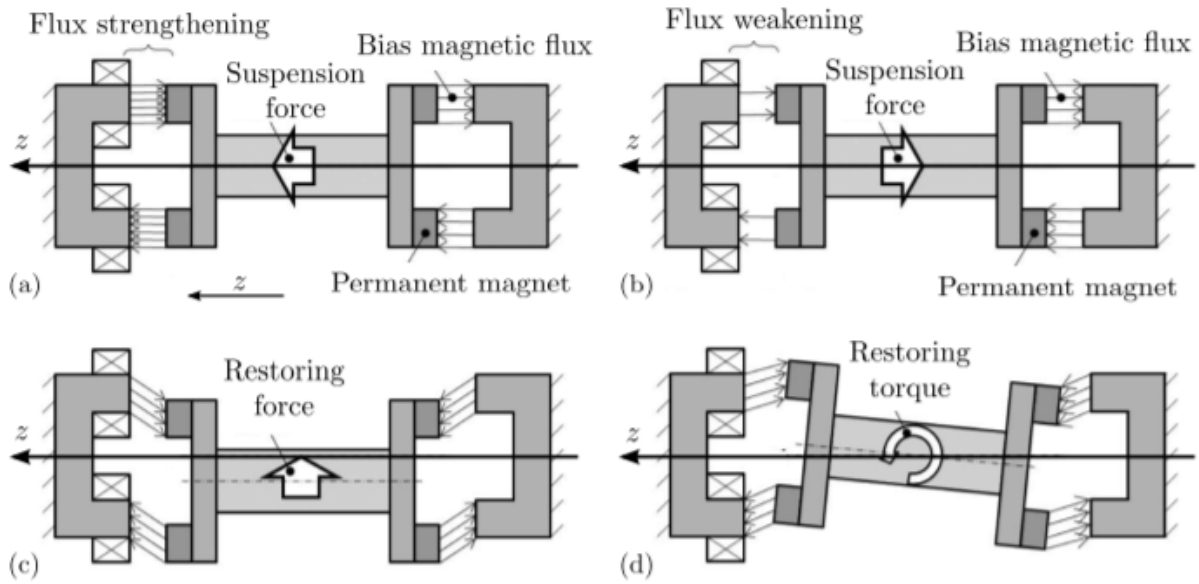

Figure 5: Exploded and detailed views of the self-bearing machine (from [33]). (a) Positive axial force. (b) Negative axial force. (c) Passive radial stabilisation. (d) Passive tilt stabilisation.

(Asama et al., 2014)

The machine described in [34] and [35] is a single-drive machine which has a classic single-sided axial flux configuration. Figure 6(a) allows to see how the PM are fixed on the back yoke to form the rotor. The stator is made of coreless coils. Figure 6(b) shows how the interaction between the radial and azimuthal components of the magnetic field with the armature currents provides the magnetic suspension force according to Laplace's law. Concerning the axial component of the magnetic field, it provides the driving torque. Suspension force and driving torque are completely independent as they are respectively produced by the direct and quadrature currents. The last DOF, (tilt and radial DOF) are stabilised by a PM bearing with a high length to diameter ratio.

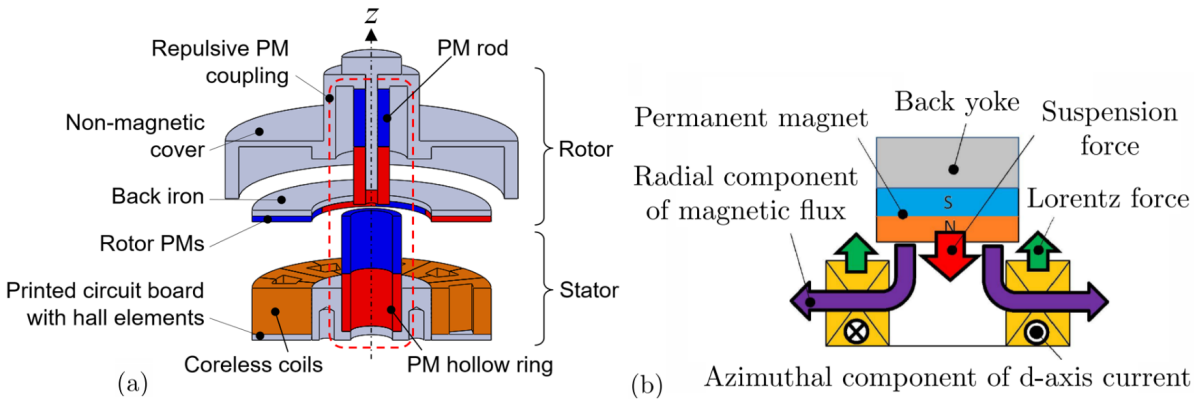

Figure 6: Single-drive single-sided axial flux machine (from[34]). (a) Exploded view of the machine. (b) Axial force generation.

(Ueno et al.,2021)

The prototype presented in [38], similar to the previous one, proposes an axial flux self-bearing machine described as a combination of an axial flux motor and a thrust magnetic bearing. The main difference with the previous machine resides in the supplementary stator core. The machine is a single stator structure. This stator is positioned above the rotor, and permanent magnetic bearings are used to stabilise the tilt and radial DOF. The rotor can reach a speed of about 1600 [rpm] but produces vibrations due to the conical mode.

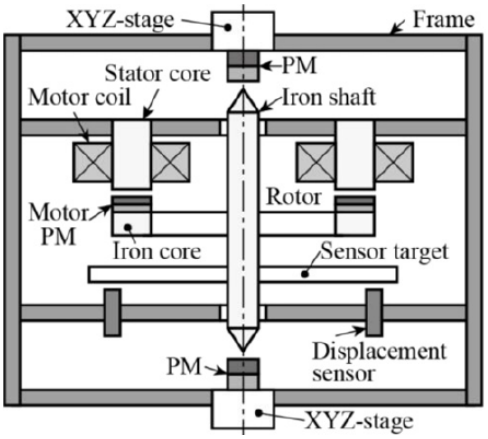

Figure 7: Structure of the axial self-bearing motor (from [38]).

(Van Verdeghem et al.,2020)

The article [37] describes a fully passively levitated Electrodynamic Thrust Self-Bearing Machine (ETSBM) which is the evolution of the bearingless machine proposed in [29]. This Master's thesis is based on the modification of this machine, therefore the following pages will be dedicated to its detailed description and its working principle.

The tilt and radial DOF of the rotor are passively controlled by two PM centring bearings while the rotor drive and the passive axial suspension are provided by the single winding of an ETSBM. Figures 8(a) and (b) show respectively that the ETSBM can be either based on a axial flux topology or on a radial flux topology. The prototype and the model developed in the paper have been made for the first case.

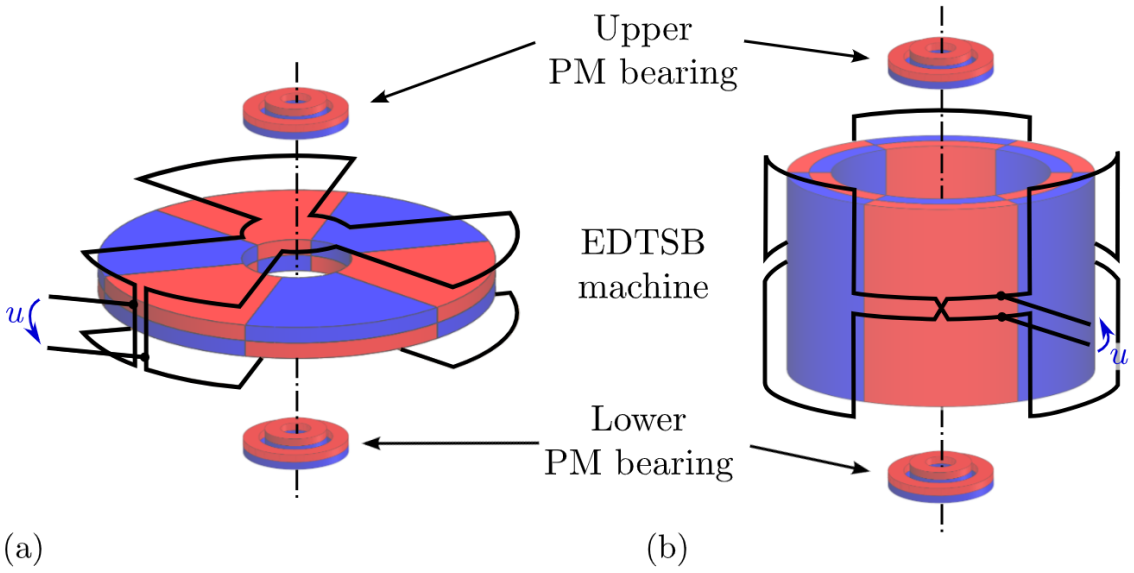

Figure 8: Fully passively levitated machine (only one phase). (a) Axial flux configuration. (b) Radial flux configuration (from [37]).

The developed prototype is a Double Stator Single Rotor (DSSR) axial flux permanent magnet machine. It is composed of two sets of three-phase armature windings connected in parallel, an upper and a lower one, wound on a non-magnetic yoke and positioned on each side of an axial flux rotor. A simplified view of the structure is proposed in Figure 8(a). The rotor is constituted of two arrangements of PM placed in attraction on both side of a ferromagnetic yoke.

This prototype uses the null-flux principle to stabilise the rotor in the axial direction. The upper and lower fluxes compensate each other when the rotor is in its centred position, therefore there is no axial force generated on the rotor in this position. It also means that the rotor axial DOF is stabilised through passive electrodynamic force. No sensor, power electronic or controller is needed to achieve the rotor levitation, which improves the compactness and the reliability. The control of the motor function is made through a commercial electronic.

The prototype structure and its main components are detailed in Figure 9 and are listed below:

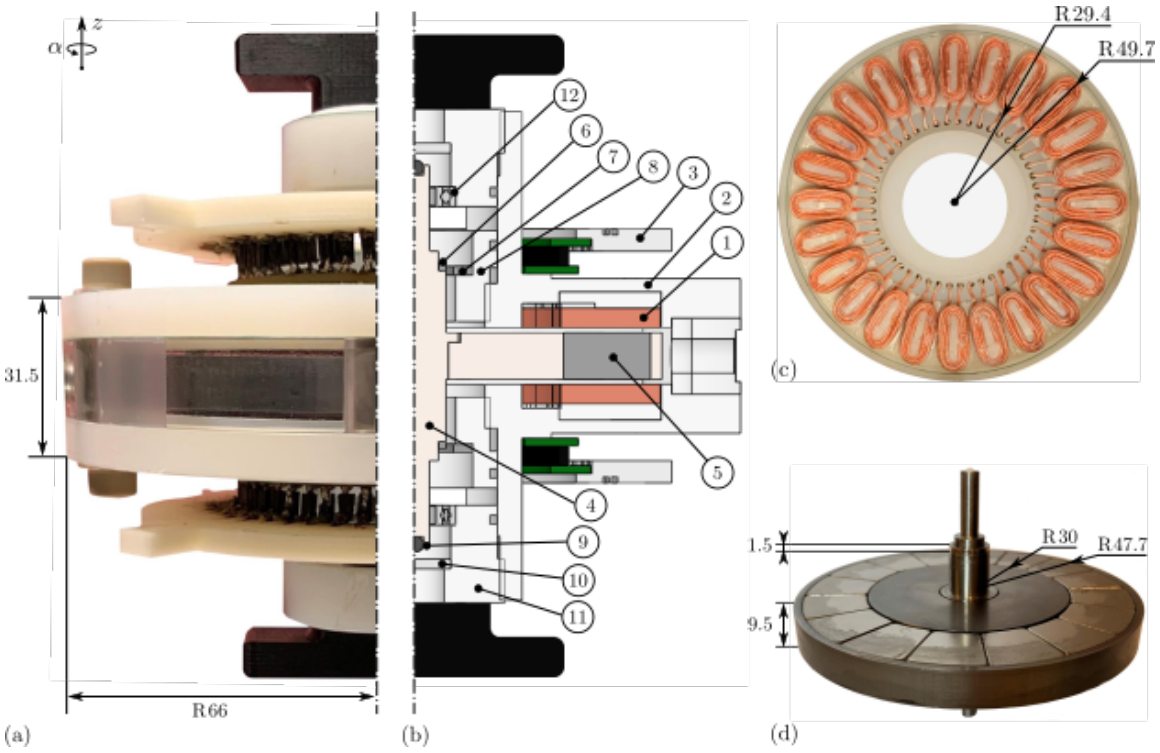

Figure 9: Fully passively levitated machine prototype (from [37]). (a) Picture of the machine. (b) Cross-sectional view with (1) the coils, (2) the non-magnetic non-conductive frame, (3) the printed circuit board, (4) the stainless steel shaft, (5) the PM arrangement, (6) the rotating PM rings and (7) their corresponding stationary rings, (8) and (11) the threaded parts screwed on (2), (9) the landing bearings constituted of a ceramic ball, (10) the stainless steel plate and (12) the radial safety bearings larger than the shaft used in case of instability or failure. (c) Picture of the armature winding. (d) Picture of the rotor.

Operation principle

The purpose of this section is to describe the operation principle of the ETSBM presented by Van Verdeghem et al. in [37], by emphasizing the interaction between the different currents and the magnetic field, and then the different forces and torques created by them. As presented previously, [37] describes the first fully passive levitated self-bearing machine with combined windings. The four radial and tilt DOF are passively stabilised while the suspension in the axial direction and the driving torque are provided with a single set of three-phase[1] winding distributed between the upper and lower winding.

As shown in Figure 10, the rotor comprises an arrangement of PMs with alternating polarisation to obtain "p" pairs of pole. The topology, based on the null-flux principle, has 3 identical and evenly distributed phases composing the stator, each one being formed by the parallel connection of an upper and a lower winding. Each upper/lower winding is made of "p" identical and evenly distributed coils connected in series.

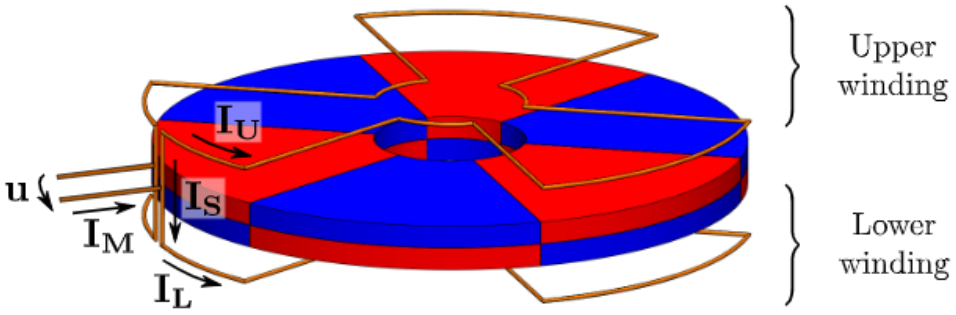

Figure 10: Schematic representation of ETSBM topology with three poles and limited to one phase winding (from [29]).

To fully understand the principle and the figure 11, the motor current I_M and the suspension current I_S must be defined:

$$\begin{cases} I_U = \frac{I_M}{2} + I_S \\ I_L = \frac{I_M}{2} - I_S \end{cases} \iff \begin{cases} I_M = I_L + I_U \\ I_S = \frac{I_U - I_L}{2} \end{cases} \quad (1)$$

I_M is injected by the power supply and provides the driving torque, while I_S will be passively induced by the relative axial movement between the coils and the PMs. The latter can also be interpreted as the unbalance of current between the upper and lower windings, this unbalance depending on the axial position of the rotor.

As presented in Figure 11(a), when the rotor is axially centred ($z = 0$), the amplitude of the PM flux linkages related to each upper and lower winding of each phase Φ_U and Φ_L are equal. The motor current is then evenly distributed between each upper and lower winding as the ElectroMotive Forces (EMFs) are equal for both. This current generates a driving

[1] In [37], the principle is generalised to "N" phase, but the number of phase have been fixed to work with classical tree-phase power supply.

torque $T_{\alpha,M}$ by interacting with the axial component of the magnetic field produced by the PMs along the coil radial section. Besides, the interaction with the azimuthal component of the magnetic field with these upper and lower currents creates two axial forces which compensate each other. Figure 12(a) illustrates these interactions for a centred position.

Figure 11(b) describes the effect of a rotor displacement along the z-axis: Φ_U and Φ_L are no more equal, that means that EMFs are not either. Consequently, the total current is no more evenly distributed between upper and lower windings. This is represented by an additional current, the suspension current I_S, which increases the current in the coils closest to the rotor, and conversely for the farthest.

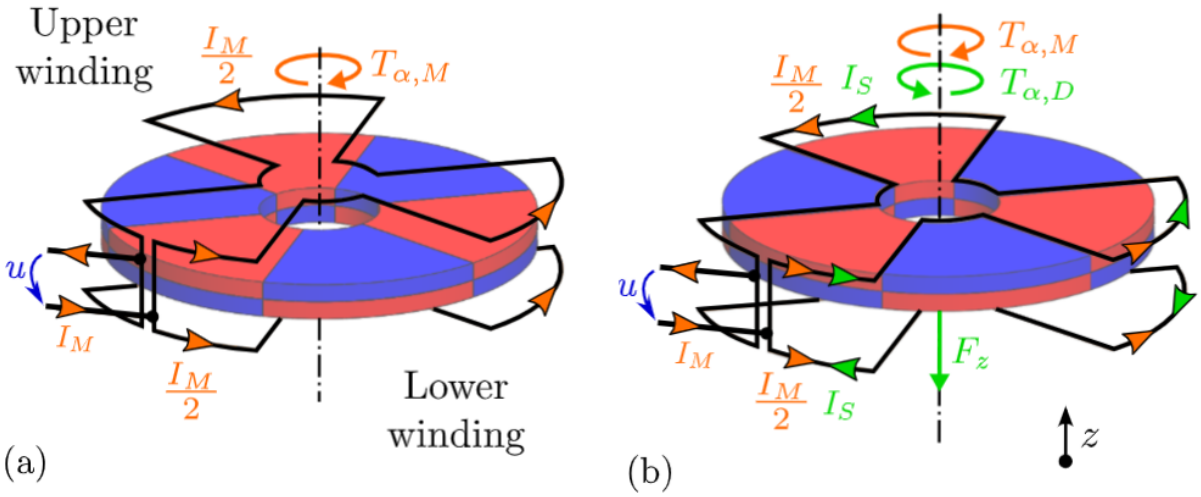

Figure 11: Electrodynamic thrust self-bearing machine operation (from [37]). (a) Centred position ($z = 0$). (b) Decentred position ($z \neq 0$).

Concerning the forces in this situation, since the PM magnetic flux density is divergence free and the relation between the axial component and the axial position is linear, the azimuthal component of the PM magnetic flux is independent of the axial position. Therefore the motor current I_M still solely provides the driving torque $T_{\alpha,M}$ even when the rotor is axially decentred. However as the path of circulation of the suspension current I_S is different, this current interacts with the azimuthal PM magnetic field to produce an axial force F_z that tends to restore the rotor in its centered position. But this current also interacts with the field axial component, resulting in an undesirable drag torque $T_{\alpha,d}$, that goes against the rotation of the machine. All these interactions are illustrated in Figure 12(b).

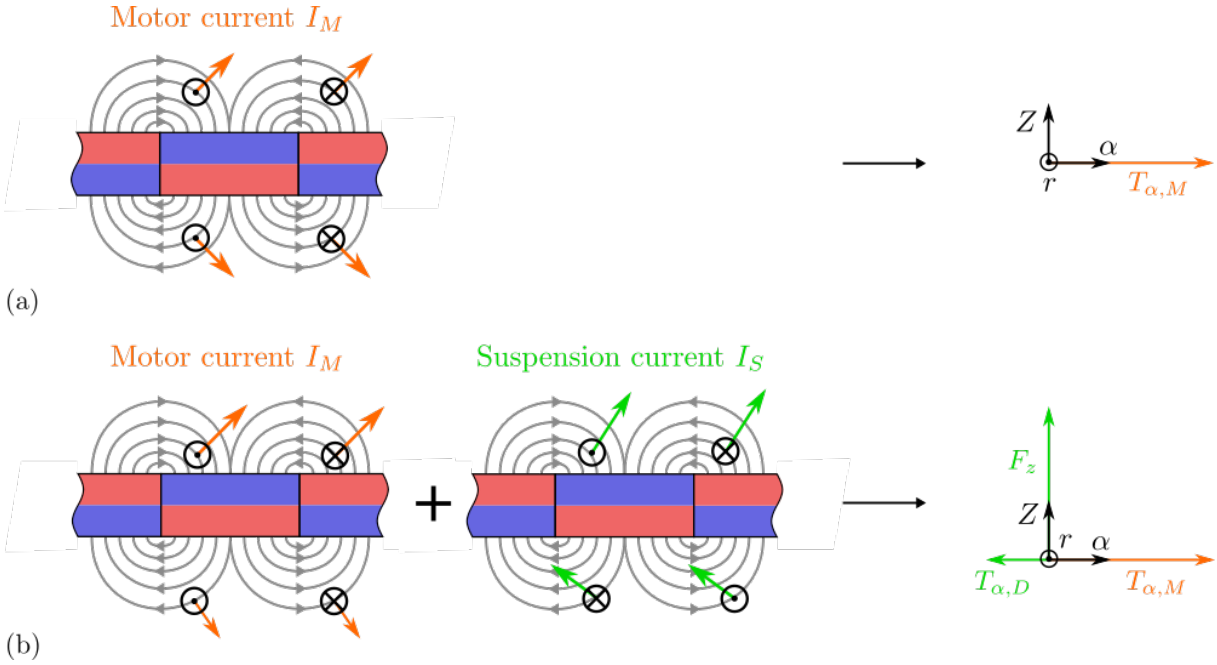

Figure 12: Motor and suspension forces generation : unrolled representation of the self-bearing machine (from [1]). (a) Centred position (z = 0). (b) Decentred position (z ≠ 0).

Small rotor displacements allow to consider a linear dependence of the flux linkages to the axial displacement. It means that one winding will experience an increase I_S of its total current while the other will experience a decrease of the same amount. I_U and I_L can therefore be constructed with the superposition principle with the summation of the motor and suspension currents.

Objectives of this Master's thesis

All the motors presented previously are using rotor with Surface Mounted Permanent Magnet (SMPM), which are relatively simple topologies in their designs and their influence on the magnetic circuit linking the rotor and armature windings. However a more complex magnetic circuit can be obtained by using rotor with Buried Permanent Magnet (BPM), since the ferromagnetic parts on this kind of rotor add axial and angular dependence of the inductance coefficients. Furthermore, the proximity of the ferromagnetic parts will increase the inductances coefficients [42]. All theses elements should have positive influence on the machine performances. Indeed greater inductances coefficient should improve the thrust function of the machine while their angular and axial variation should add a new reluctant component to the suspension force and to the driving torque. This Master's thesis aims to study the influence of a rotor with BPM on the performances of the machine proposed by J. Van Verdeghem et al in [37]. The initial objectives of this work included the design and the optimisation of its dimensions, the modelling but also the prototyping of the ETSBM with a BPM rotor. However due to the unexpected duration of the FEM-simulations which have considerably slowed down the optimisation process, it was decided not to carry out the prototype to ensure the proper development of other parts of the work. The fact remains that all the choices made during the design and the FEM simulations have been made in order to realise this prototype, which will be carry out by the research team in the future.

This work is subdivided in five chapters. The first one aims to present the different BPM rotors existing in the literature, compare them, and choose the most appropriate one for the ETSBM proposed in [37]. Then chapter 2 provides the adaptation of the analytical modelling describing the axial and angular dynamic of the ETSBM to a BPM rotor. This model will allow to highlight the influence of the axial and angular variation of inductance coefficients. The third chapter describes the Finite Elements Method (FEM) models which have been developed to compute the different coefficients identified in the analytical model of chapter 2. The assumptions which are related to the BPM and the rotor topology will also be validated in this section. The next chapter, the fourth one, is dedicated to different optimisations realised during this Master's thesis. The last chapter is focused on a case study based on the best topology found by the optimisation. The performances at start-up and high speed will be studied and compared to the performances published by J.Van Verdeghem et al. for the ETSBM with SMPM rotor.

CHAPTER 1

DESIGN

This chapter aims to present the design which adapts the ETSBM to a rotor with BPM. To do so, the state of the art of BPM rotor is proposed in Section 1.1, followed by a the selection of a topology which will be used for the optimisation and the case study in Section 1.2. In Section 1.3, the topology of winding which will be used for the FEM simulations of chapter 3 and the case study of chapter 5 is chosen. Finally the mechanical design of the rotor is proposed in Section 1.4, this one representing the design validated by the research team for the prototype which will be realised in the future.

1.1 State of the Art of buried permanent magnet rotor topology

Through this section, a review of the different topologies of axial flux rotor with BPM presented in the literature is done. The topologies can be classified in three main categories as explained in [43]: the single-sided AFPM machines, the double-sided AFPM machines and finally the multi-stage or multidisc AFPM machines, which are in fact combination of doubled-sided topologies. Their benefits and drawbacks are highlighted in order to select the topology which will be used in this Master's thesis.

(Peeters et al., 2003)
The configuration described in [44] and [45] aims to the mass production. This specific topology is called AXIFUS, which means AXIal Flux with U-shaped Stator coils. Cylindrical PMs are buried into a non-magnetic rotor as represented in Figure 1.1a and coated by two flux distribution plates. As it is shown in Figure 1.1b, a plate presents a laser-cut pattern in order to reduce the Eddy current losses.

The major advantage of this topology is its versatility and ease of manufacturing. Indeed, basic components are needed like NdFeB for the magnets, epoxy hard paper for the rotor,... Furthermore, by modifying the value of some key parameters such as the length of the airgap between the rotor and the stator, the number of stator, the number of rotor,... It is possible to designed a tailor-made machine.

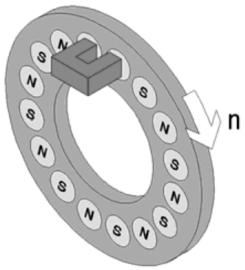

(a) 2D layout of the PMs with one U-shaped stator coil represented.

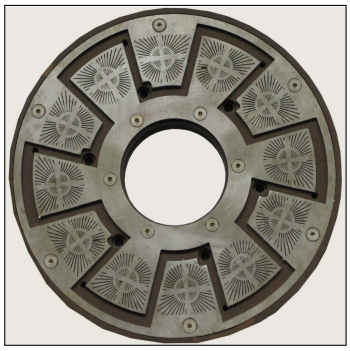

(b) Flux distribution plate.

Figure 1.1: Axial flux machine with U-shaped stator coils (from [44] and [45]).

(Neethu et al., 2017)
A high speed Axial Flux Buried Permanent Magnet (AFBPM) synchronous motor is described in [46]. It consists of a single-sided machine, which means one stator and one rotor. The PMs are buried in the rotor as shown in Figure 1.2. The specific features of this topology are the specific shape and position of the magnets. As it is pointed out in Figure 1.3, the span and shift angle of the magnets are modified to improve the sinusoidal form of the back-EMFs and to reduce the torque ripple.

A single-sided machine is cheap but has one major drawback, it is subjected to an unbalanced axial force between the stator and the rotor. This force is proportional to the airgap flux density, which means that to limit this force, the B-field in the airgap has to be limited and that reduces the torque of the machine. Burying the magnets allows to counter the force coming from centrifugal effect. It means that BPM can reach high rotation speed without additional protection such as retaining sleeve unlike axial-flux machine with SMPM[47].

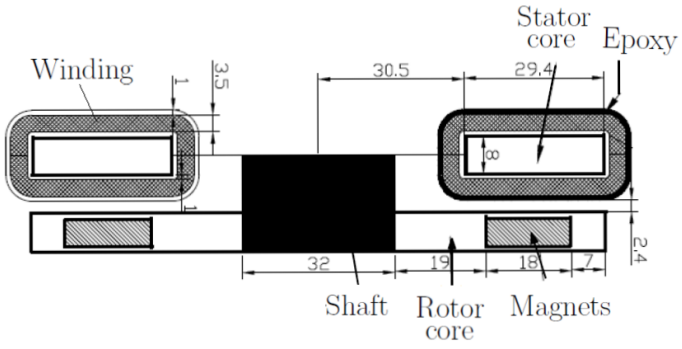

Figure 1.2: 2D cut of the machine (from [46]).

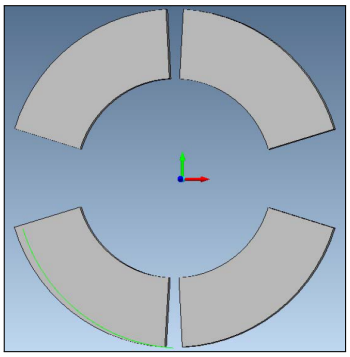

Figure 1.3: Position of the magnets for a two pole pairs machine, the angular span and shift of the magnet have been optimised to reduce the torque ripple (from [46]).

(Tegkun et al., 2017)
The topology detailed in [42], is a particular double-sided AFBPM machine. Indeed as it is presented in Figures 1.4 and 1.5, this machine has a special arrangement of magnets. Two consecutive PMs form a V-shape. As the rotor is thicker due to this combination of magnets, a second layer of magnets is inserted into the rotor, which leads to a Λ shape. Moreover, the PMs have flux barriers on their edges to reduce the flux leakage and to increase the anisotropy.

By having these PMs inclination, the machine has an higher salience and inductance compare to other AFBPM. These higher saliencies will lead to the production of a higher reluctance torque, increasing the total output torque of the machine. For the same power, this type of machine will need less PM. These angles will also lead to an increasing airgap flux density. Another benefit is the range of rotation speed where the performances are maintained that is wider than for both AFBPM and axial flux SMPM classical machines.

But this topology has two main drawbacks. The first one is its poor manufacturability. Both stator and rotor have to be made from several pieces that are then glued together. The second one is that due the thicker rotor, the mass of the machine increases, leading to a lower torque density than in axial flux SMPM.

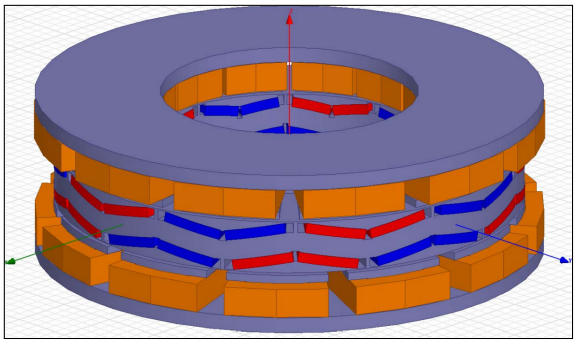

Figure 1.4: 3D representation of the AFBPM V-shaped machine (from [42]).

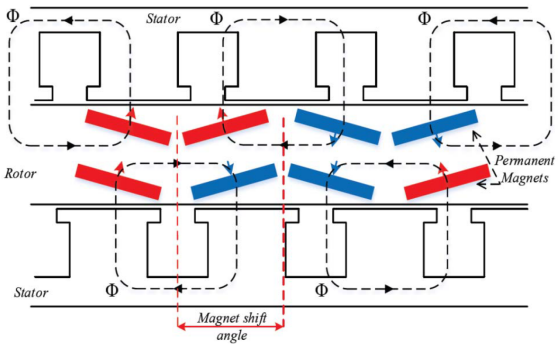

Figure 1.5: Representation of the flux path in the AFBPM V-shaped machine (from [42]).

Spoke type topologies

Double Stator Single Rotor (DSSR)

(Chai et al., 2018, 2019)

As illustrated in Figures 1.6a and 1.6b, two rotor structures are introduced and then compared in [48]. They are respectively called single-layer Spoke Type (ST) AFBPM and Two-Layer Spoke Type (TLST) AFBPM. In the second case, the shape of the PM is different as it can be observed in Figure 1.7. In the ST AFBPM, λ is the pole pitch and τ is the ratio between the arc length of PM and the pole pitch. In [49] a focus is made on the TLST AFBPM. The PM is seen as a combination of two rectangles, the narrow one has an axial length L1 and the second L2 as it is shown in Figure 1.6b. The Optimisation consists of tuning the design parameters of the PM in order to minimise the Total Harmonic Distortion (THD) and maximise the airgap flux density. The smaller this THD is, the more sinusoidal the airgap flux density will be. For example, by varying the proportion of the narrow part, it is possible to diminish the THD and to improve the magnetic flux density. 2D FEM highlights the fact that the TLST machine has the lowest THD. The price to pay is a more complex way to optimise the design of the PMs due to their specific shapes. However, compare to SMPM, the BPM need less PM for the same airgap flux density.

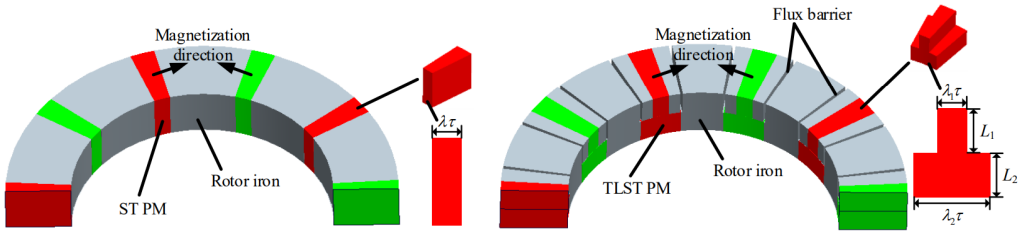

(a) ST AFBPM rotor.

(b) TLST AFBPM rotor with flux barriers.

Figure 1.6: Quarter of symmetry of ST and TLST topologies (from [48]).

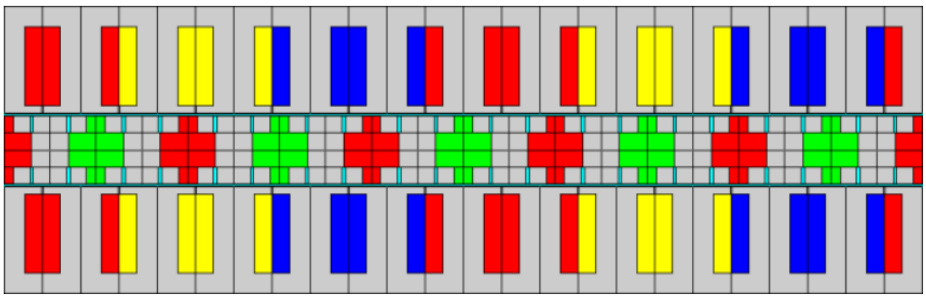

Figure 1.7: Unrolled view of the TLST AFBPM machine (from [48]).

Double Rotor Single Stator (DRSS)

(Aydin et al., 2016) Contrarily to [48] and [49], the machine described in [50] is based on one stator sandwiched by two rotors as it can be seen in Figure 1.8. It is shown that for the same amount of PM a SMPM axial flux machine has less airgap flux density than this topology. The important feature of this topology is that the rotor is made of sinusoidal segments. Using this type of segment leads to a variable airgap, as shown on Figure 1.9, which improves the sinusoidal form of the Back-EMFs. One advantage of this rotor is the simple way of manufacturing with material that has a good manufacturability and high magnetic permeability. By optimising the rotor segment to pole pitch ratios $\frac{\tau_{seg}}{\tau_{pole-arc}}$, the THD can be minimised. Then, another parameter to optimise is the airgap variation denoted d_{gap} shown in Figure 1.9. By increasing it, the THD is decreased but also the airgap flux which means a lower back-EMFs. The ratio defined just before can be also chosen to minimise the torque ripple but in this case, it is a compromise.

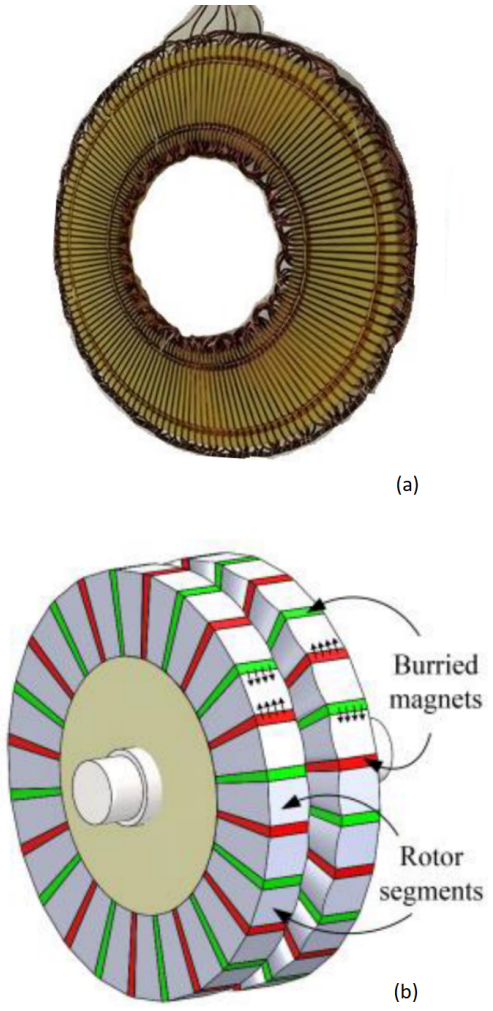

Figure 1.8: 3D view of a) one layer of a ST coreless AFBPM motor stator and b) IPM rotor with sinusoidal rotor segments (from [50]).

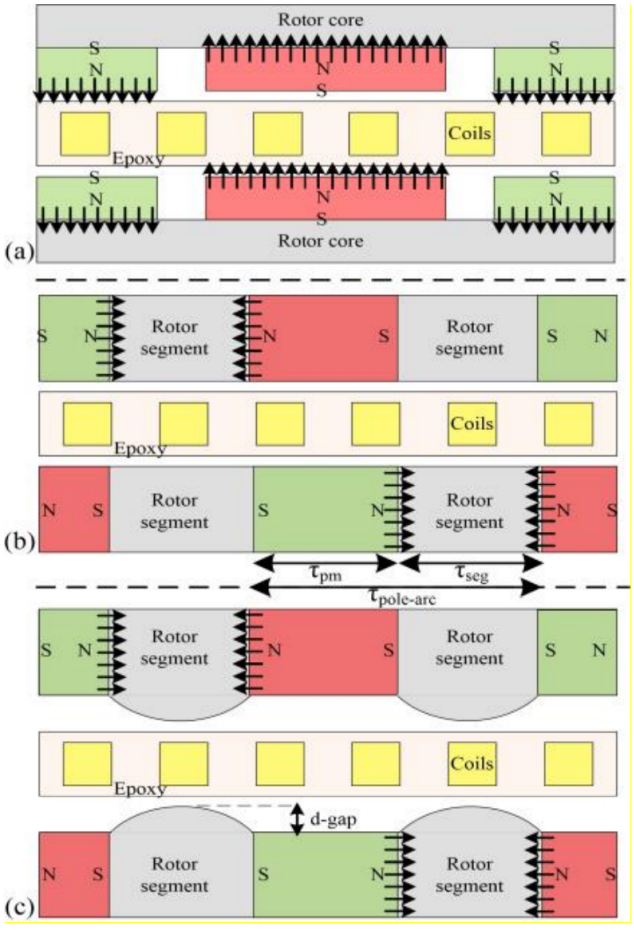

Figure 1.9: 2D views of a) coreless AFPM SMPM motor b) spoke-type coreless AFBPM with non-sinusoidal and c) with sinusoidal rotor segments (from [50]).

1.2 Choice of the rotor topology

The ETSBM is a DSSR topology, then among all the solution proposed above, only one need adaptation: the topology presented by Aydin et al. which can be switch from a DRSS to a DSSR topology by symmetrising one of its two rotors. However, this adaptation leads to a rotor very similar to the ST topology. In the following comparison, the Aydin et al. topology will therefore be noted as Spoke Type with Sinusoidal Segment (STSS). Concerning the topology proposed by Neethu et al. which is a single-sided topology, it could be considered as very similar to the AXIFUS topology since the difference resides in the optimisation of the shape and the position of the PM. The five rotor topologies that will be compared are the V-shaped, the rotor of AXIFUS machine, the TLST, the ST and the STSS.

Five criteria are used to compare the topologies. The first one is the manufacturability and takes into account the complexity of manufacturing and assembly. The second criterion is the improvement of the THD of the air-gap flux density, which can be made through the sinusoidal segments or the use of flux barriers. After that comes the rated speed where the rotor has already been used: the rotors already tested for high rotation speeds are more trusted candidates. The fourth criterion is the shape of the magnet. This criterion could be considered as very similar to the first one, but complex magnet shapes will also consequently increase the price of the PMs and their delivery time. It was then an important criterion during this Master's thesis while the manufacturing of a prototype was still considered. Finally, the optimisation of the reluctant torque is considered but unknown for the majority of the topologies, thus it will be the least important criterion. The Table 1.1 allows to compare the different rotors based on these criteria and on the informations provided in literature. The ST topology is arbitrarily taken as reference:

	ST	V-shaped	Axifus	STSS	TLST
Manufacturability	0	- -	+	-	0
THD of the air-gap flux density	0	+	/	+	+
Rated speed	0	- -	-	/	0
Magnet shape	0	0	0	0	-
Optimised reluctant torque	/	+	/	/	/

Table 1.1: Comparison of the five potential rotor topologies. The use of sign "+" is based on the positive meaning of the sign, i.e. a sign "++" used for manufacturability means that the rotor is much more easily to manufacture than ST-topology. Cell with a "/" means that no information is available for this criterion for this rotor. "0" means that the topology is considered as good as the ST machine.

The V-shaped machine is interesting with its high total torque. However, its manufacture is complex, which also means high cost. Furthermore, the specific pattern of the magnets

has to be investigated from a mechanical point of view to avoid problem arising from the mechanical stress due to the rotation speed. Indeed V-shaped machine has until now not been tested for rotation speed higher than 2000 [rpm].

Then, the AXIFUS machine is the simplest machine which obtains good THD by optimising the shape and the position of PMs as shown by Neethu et al. However, this type of machine is mostly used for medium to high power application, as hybrid electric vehicles [44] and wind turbines for example [45]. This topology is then not really suitable for the ETSBM.

Next the STSS topology is, by definition, very similar to the ST-topology, but offers a better THD of the flux density thanks to the more complex shape of ferromagnetic parts.

Finally there is the TLST machine. Its biggest advantage comes from the specific shapes of the magnets which provide a high flux density with a good THD compare to the ST-topology. The shape of the magnet is however also a disadvantage for the fourth criterion. The manufacturability is supposed as easy as for the ST topology. Indeed even if the ferromagnetic parts have more complex shapes in the TLST, the assembling will be facilitate by the interlocking of the parts compare to the ST topology. This topology has been chosen for this Master's thesis and will be used for the final design of the machine. However a modification of the topology has been made and must be contextualised: The choice of the topology was made during the first half of the academic year when the prototype was still in the objectives of this Master's thesis. The delivery time of the magnets being an important factor but uncertain, it has been decided, a few months later, to use more classical PMs with segment shapes to accelerate the delivery process. It means that in the machine studied in chapters 3, 4 and 5, no PM is disposed on the height L_1 represented in Figure 1.6b. The consequences of this choice will be discussed in chapter 5.

1.2.1 Adaptation of the connection for the TLST topology

The topology of the TLST rotor creates a circulation of the magnetic field which is different from the one produced by the SMPM rotor of Figure 12, which requires a modification of the winding connection to have a good operation of the machine.

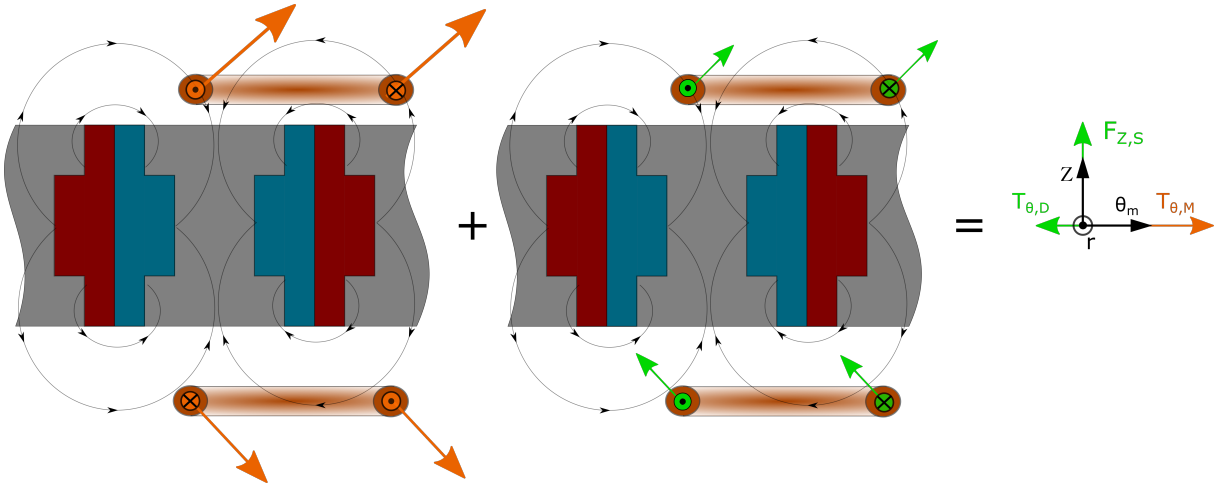

Figure 1.10: Unrolled view of the TLST rotor in a decentred position and direction of the applied forces.

As it can be seen in Figure 1.10, the lower current must flows in the opposite direction compare to the one represented in Figure 12(b) to provide the same direction force, which results in an anti-parallel connection of the upper and lower winding. Figure 1.11 sums up the connection and all the flowing currents, as well as the forces created in a decentred position. It must be noted that the motor currents are still coming through the homologous terminals, which is the convention used for the developments produced in Section 2.2.

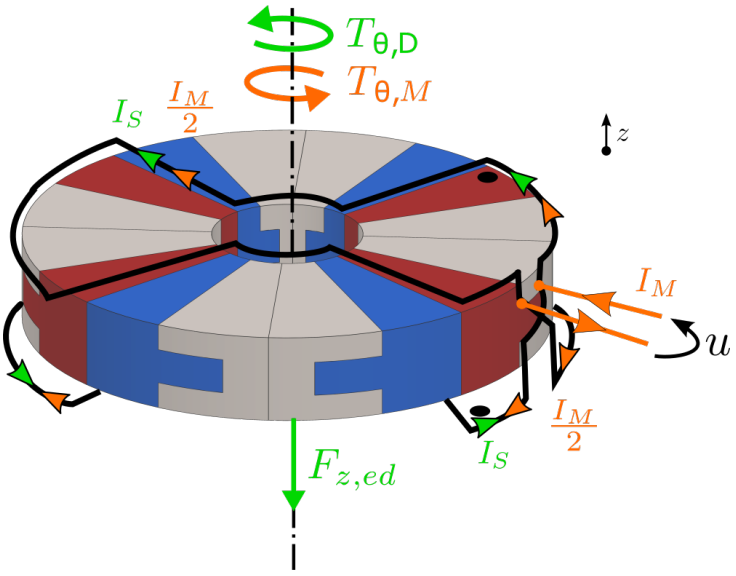

Figure 1.11: Representation of the currents directions for a simplified rotor with one phase winding and two poles.

1.3 Winding topologies

The windings and more precisely their layout are crucial to obtain high value of torque and to minimise the losses in the machine. The two most used configurations of windings are the non-overlapping concentrated windings and the distributed windings.

The first one consists of windings whose turns all wound together in series to form a multi-turn coil. They are characterised by small end windings, high capability for flux weakening and have a good manufacturability [1]. However, this kind of configuration leads to a higher harmonic content than for distributed windings and their small saliency ratio, defined as $\frac{L_d}{L_q}$, leads to a small reluctant torque[51].

On the opposite, distributed windings are evenly spread windings on multiple slots which allow to decrease the harmonic content while increasing the saliency ratio. However, it is more difficult to build, it takes more space and induces more copper losses than concentrated windings.

The second topology has been arbitrarily chosen for the rest of this work, and will be used for all the FEM simulations of chapter 3. Indeed, even if at first glance, the overlapped topology allows to take advantage of the reluctant effect more than concentrated windings, the small number of study already carried out on the ETSBM does not yet allow to affirm that it is objectively the best choice. The comparison between both topologies of winding should be the topic of a future work to improve the performances of the ETSBM.

1.4 Design proposal

This chapter aims to describe the design proposal depicted in Figure 1.12 which has been realised during this Master's thesis. It will not be manufactured for this work but will open the way for a future prototype to be realised by the research team. The proportions used are similar to the machine presented in [29], but there is no fixed dimension, it is a functional design, not a dimensional one.

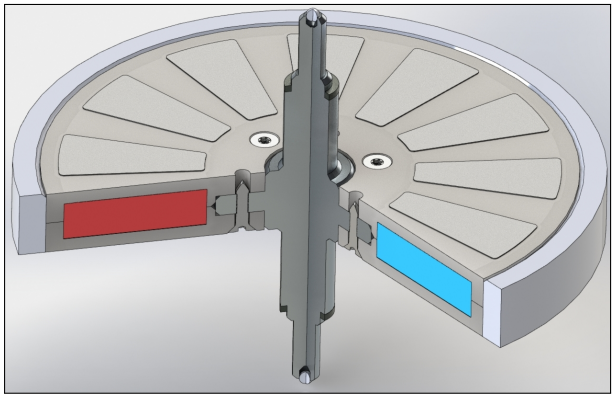

Figure 1.12: Vertical sectional view of a rotor with six pole pairs.

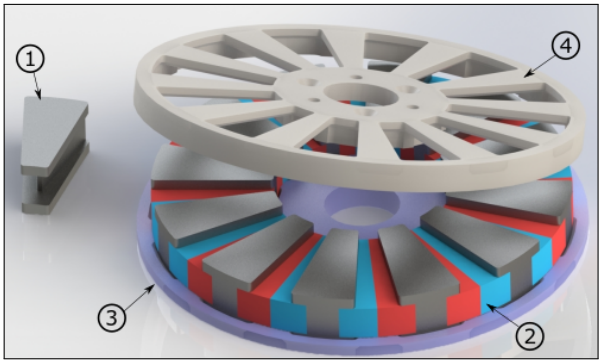

Figure 1.13: Assembling of the crown of PMs and iron parts with the 3d-printed tool, and clamping of the Onyx part.

As explained in Section 1.2, it has been chosen to design the TLST rotor with segment-shaped magnets because they are cheaper and easier to obtain. Therefore the topology of PMs does not correspond exactly to the one presented initially in Figure 1.11.

It is first composed of a crown alternating iron parts (1) and segment-shaped PMs (2). A 3D-printed tool (3) is used to position the parts and adjust radially the PMs as represented in Figure 1.13. This crown is intended to be encapsulated between two symmetrical 3D-printed parts (4) composed of Onyx [52] reinforced with Kevlar. These parts prevent a radial movement of the PMs, which explains the need of a 3D-printed tool to first place them into the ferromagnetic parts before the encapsulation. The crown is placed in the first 3D-printed part (4) where each part of iron is embedded in clamping. The crown is still in the tool (3) when it is fixed in (4) on its other face to ensure a good positioning of the PMs, as shown in Figure 1.13.

The second step of assembling is represented in Figure 1.14. Then a shaft (5) similar to the one presented in Figure 9, with its PM rings (6) and ceramic balls (7), is placed in the center of the rotor. This shaft has a central disc with 6 tapped holes which will be clamped between both parts (4) and fixed with 3 screws (8) in each direction. Finally, an aluminium sleeve (9) is held tightly around the rotor.

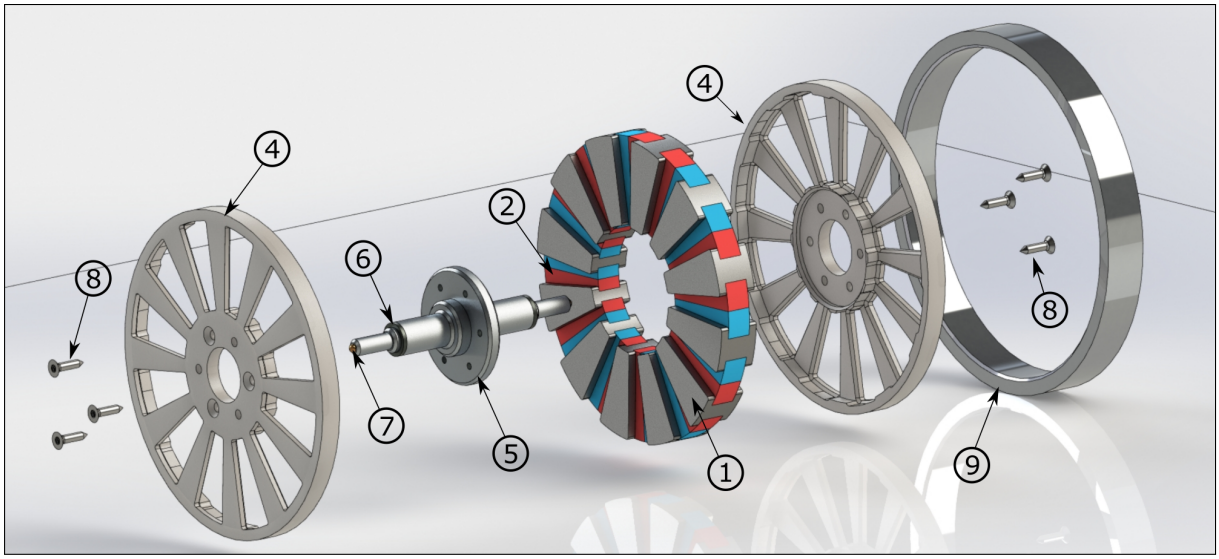

Figure 1.14: Exploded view of the design of a rotor with six pairs of poles.

CHAPTER 2

ANALYTICAL MODELLING

This chapter presents a dynamical model describing the axial and spin behaviour of a fully passive self-bearing machine with BPM. Based on a set of global parameters, it is then adapted to a broad range of topologies and allows to determine their performances. This model is a generalisation of the electromechanical model presented in [29], since it takes into account both the angular and axial variations of the winding inductance coefficients. Then, numerous comparisons with [29] highlight the supplementary elements brought by the BPM.

Section 2.1 lists assumptions made to derive the model. Then, the electromagnetic and mechanical equations are respectively developed in Section 2.2 and 2.3. The results are combine to obtain the general electromechanical model of the machine in Section 2.4. In this last section, a gradual comparison highlights the differences brought first by axial variation of inductance and secondly the inductance variation introduced by the magnetic saliency.

2.1 Assumptions

The dynamical model describing the axial and spin behaviour of this self-bearing machine is developed under the following assumptions :

1. The materials have linear magnetic properties, which supposes hysteresis and saturation are neglected.
2. The proximity and skin effects in the armature winding are neglected.
3. The eddy currents induced locally in the armature winding as well as in all other conductive materials are neglected.
4. The upper and lower windings are supposed perfectly balanced, signifying that their resistances are identical and that their flux linkages exhibit a symmetrical evolution with respect to the rotor axial displacements.
5. Only the fundamental component of the magnetic field arising from permanent magnet arrangement is considered.

6. The angular variation of the inductance coefficients is supposed purely sinusoidal, with a period half the electrical one.

7. The rotor axial displacements are supposed to be small, thus allowing linearisation of the axial variation of magnetic flux linkage and inductance coefficients.

The five first assumptions are already used in [29], so their validity and relevance will not be discussed, excepted the fifth one that will be validated for the TLST topology. The two last assumptions, particularly those dealing with the axial and the angular variation of the inductance coefficients, will also be validated for the TLST topology.

2.2 Electromagnetic model

The purpose of this section is first to express the electrical equations of the machine which take into account the axial and angular variations of inductance coefficients, and secondly to develop the three components of the electromagnetic forces : the electrodynamic, the detent and the reluctant forces. The first two were already present in the model developed in 10, so the results are similar but necessary for further developments in this master thesis. However, the reluctant component appears by definition thanks to the magnetic saliencies and is then a new component to consider for the electromechanical model developed in Section 2.4.

2.2.1 Inductance coefficients

2.2.1.a The self inductance

Assumption 6 allows to consider the self inductance matrix as the summation of a constant term and a sinusoidal function depending on the double of the electrical position:

$$\mathbf{L_{U/L}}(\mathrm{z}, \theta_{\mathrm{em}}) = \mathbf{L_0}(\mathrm{z}) + \mathrm{L}_2(\mathrm{z}) \cdot [\boldsymbol{2\theta_{em}}] \tag{2.1}$$

And assumption 7 allows to apply a first order Taylor approximation:

$$\mathbf{L_U}(\mathrm{z}, \theta_{\mathrm{em}}) = \mathbf{L_0} + \mathrm{z} \cdot \mathbf{dL_0} + (\mathrm{L}_2 + \mathrm{z} \cdot \mathrm{dL}_2) \cdot [\boldsymbol{2\theta_{em}}] \tag{2.2}$$

$$\mathbf{L_L}(\mathrm{z}, \theta_{\mathrm{em}}) = \mathbf{L_0} - \mathrm{z} \cdot \mathbf{dL_0} + (\mathrm{L}_2 - \mathrm{z} \cdot \mathrm{dL}_2) \cdot [\boldsymbol{2\theta_{em}}] \tag{2.3}$$

The three matrices used in this expression are defined as:

$$\mathbf{L_0} = \begin{pmatrix} \mathrm{L}_0 & \mathrm{M}_0 & \mathrm{M}_0 \\ \mathrm{M}_0 & \mathrm{L}_0 & \mathrm{M}_0 \\ \mathrm{M}_0 & \mathrm{M}_0 & \mathrm{L}_0 \end{pmatrix} \qquad \mathbf{dL_0} = \begin{pmatrix} \mathrm{dL}_0 & \mathrm{dM}_0 & \mathrm{dM}_0 \\ \mathrm{dM}_0 & \mathrm{dL}_0 & \mathrm{dM}_0 \\ \mathrm{dM}_0 & \mathrm{dM}_0 & \mathrm{dL}_0 \end{pmatrix}$$

and

$$[\boldsymbol{2\theta_{em}}] = \begin{pmatrix} \cos(2\theta_{\mathrm{em}}) & \cos(2\theta_{\mathrm{em}} - 2\pi/3) & \cos(2\theta_{\mathrm{em}} - 4\pi/3) \\ \cos(2\theta_{\mathrm{em}} - 2\pi/3) & \cos(2\theta_{\mathrm{em}} - 4\pi/3) & \cos(2\theta_{\mathrm{em}}) \\ \cos(2\theta_{\mathrm{em}} - 4\pi/3) & \cos(2\theta_{\mathrm{em}}) & \cos(2\theta_{\mathrm{em}} - 2\pi/3) \end{pmatrix} \tag{2.4}$$

The notations used in these expressions are defined as:

- $\mathbf{L_0} = \mathbf{L_0}(0)$
- $\mathbf{dL_0} = \left.\frac{\partial \mathbf{L_0}(z)}{\partial z}\right|_{z=0}$
- $L_2 = L_2(0)$
- $dL_2 = \left.\frac{\partial L_2(z)}{\partial z}\right|_{z=0}$
- $L_0 = L_0(0)$
- $dL_0 = \left.\frac{\partial L(z)}{\partial z}\right|_{z=0}$
- $M_0 = M_0(0)$
- $dM_0 = \left.\frac{\partial M_0(z)}{\partial z}\right|_{z=0}$

with $i, j = a, b$ or c and $i \neq j$

2.2.1.b The mutual inductance matrix between the upper and lower set of windings

Assumption 8 also allows us to express the mutual inductance as a summation of a constant term and a sinusoidal term where the matrix $[\mathbf{2\theta_{em}}]$ is defined in 2.4:

$$\mathbf{M_{UL}}(z, \theta_{em}) = \mathbf{M_{UL_0}}(z) + M_{UL_2}(z) \cdot [\mathbf{2\theta_{em}}]$$

By applying a first order Taylor approximation the following expression is obtained:

$$\mathbf{M_{UL}}(z, \theta_{em}) = \mathbf{M_{UL_0}} + z \cdot \left.\frac{\partial \mathbf{M_{UL_0}}(z)}{\partial z}\right|_{z=0} + \left[M_2 + z \cdot \left.\frac{\partial M_{UL_2}(z)}{\partial z}\right|_{z=0}\right] \cdot [\mathbf{2\theta_{em}}]$$

Where:

- $\mathbf{M_{UL_0}} = \begin{pmatrix} M_{ii} & M_{ij} & M_{ij} \\ M_{ij} & M_{ii} & M_{ij} \\ M_{ij} & M_{ij} & M_{ii} \end{pmatrix}$
- $\mathbf{M_{UL_0}} = \mathbf{M_{UL_0}}(0)$
- $M_2 = M_{UL_2}(0)$
- $M_{ii} = M_{U_iL_i}(0)$
- $M_{ij} = M_{U_iL_j}(0)$

with $i, j = a, b$ or c and $i \neq j$

The mutual inductance has by definition the same value from the perspective of upper and lower currents, which means that this mutual inductance must be an even function regarding to the axial position dependency. Indeed its value will evolve in a same way when the rotor is shifted by a positive or negative Δz along the z-axis. It means that the odd derivatives of $\mathbf{M_{UL_0}}$ and M_2 are equal to 0. Moreover, assumption 7 allows to consider the quadratic and other superior terms of the Taylor approximation as negligible. Then the z-dependency of the mutual inductance coefficient is removed and the expression of $\mathbf{M_{UL}}(z, \theta)$ becomes:

$$\mathbf{M_{UL}}(\theta_{\theta_{em}}) = \mathbf{M_{UL_0}} + M_2 \cdot [\mathbf{2\theta_{em}}] \tag{2.5}$$

This reasoning will be validated in Section 3.3 as assumptions 7 and 8.

2.2.2 PM magnetic flux

The magnetic flux intercepted by each coil only depends on the axial and angular position of the rotor θ_{m}. Moreover, assumptions 4, 5 and 6 allow to express the flux intercepted by upper or lower windings as:

$$\boldsymbol{\Phi}_{\mathbf{U}} = (\mathrm{K}_{\theta_{\mathrm{m}}} + \mathrm{zK}_{\mathrm{z}}) \begin{pmatrix} \cos(\theta_{\mathrm{em}}) \\ \cos(\theta_{\mathrm{em}} - \frac{2\pi}{3}) \\ \cos(\theta_{\mathrm{em}} - \frac{4\pi}{3}) \end{pmatrix} \qquad \boldsymbol{\Phi}_{\mathbf{L}} = (\mathrm{K}_{\theta_{\mathrm{m}}} - \mathrm{zK}_{\mathrm{z}}) \begin{pmatrix} \cos(\theta_{\mathrm{em}}) \\ \cos(\theta_{\mathrm{em}} - \frac{2\pi}{3}) \\ \cos(\theta_{\mathrm{em}} - \frac{4\pi}{3}) \end{pmatrix} \tag{2.6}$$

with $\mathrm{K}_{\theta_{\mathrm{m}}}$, the flux magnitude when the rotor is axially centered, K_{z}, the flux magnitude gradient with the axial position and $\theta_{\mathrm{em}} = \mathrm{p} \cdot \theta_{\mathrm{m}}$, the electric angular position where p is the number of pole pair.

2.2.3 Electrical equations

Starting from Faraday's Law, the electrical equations for the upper and lower windings connected to the power supply can be expressed as:

$$\begin{cases} \mathbf{U} = \mathrm{R} \cdot \mathbf{I_U} + \dfrac{\mathrm{d}(\mathbf{L_U} \cdot \mathbf{I_U})}{\mathrm{dt}} + \dfrac{\mathrm{d}(\mathbf{M_{UL}} \cdot \mathbf{I_L})}{\mathrm{dt}} + \dfrac{\mathrm{d}\boldsymbol{\Phi}_{\mathbf{U}}}{\mathrm{dt}} \\ \mathbf{U} = \mathrm{R} \cdot \mathbf{I_L} + \dfrac{\mathrm{d}(\mathbf{L_L} \cdot \mathbf{I_L})}{\mathrm{dt}} + \dfrac{\mathrm{d}(\mathbf{M_{UL}} \cdot \mathbf{I_U})}{\mathrm{dt}} + \dfrac{\mathrm{d}\boldsymbol{\Phi}_{\mathbf{L}}}{\mathrm{dt}} \end{cases} \tag{2.7}$$

With:

$$\mathbf{U} = \begin{pmatrix} \mathrm{U}_1 \\ \mathrm{U}_2 \\ \mathrm{U}_3 \end{pmatrix} \qquad \mathbf{I_U} = \begin{pmatrix} \mathrm{I}_{\mathrm{U},1} \\ \mathrm{I}_{\mathrm{U},2} \\ \mathrm{I}_{\mathrm{U},3} \end{pmatrix} \qquad \mathbf{I_L} = \begin{pmatrix} \mathrm{I}_{\mathrm{L},1} \\ \mathrm{I}_{\mathrm{L},2} \\ \mathrm{I}_{\mathrm{L},3} \end{pmatrix} \tag{2.8}$$

The upper and lower windings being connected in parallel to the source, the voltage vector $\mathbf{U}$ is the same for the upper and the lower windings as expressed in 2.7. However, the currents flowing through them are different and respectively noted $\mathbf{I_U}$ and $\mathbf{I_L}$. The electrical circuit corresponding to equations 2.7 is represented in Figure 2.1.

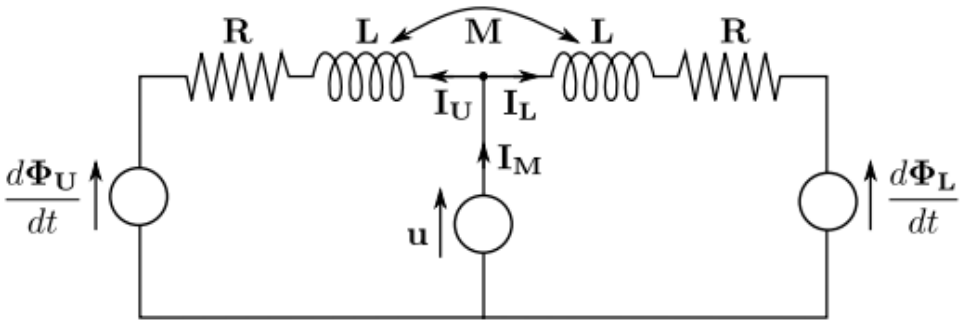

Figure 2.1: Equivalent electrical circuit of the EDTSB motor [29]

2.2.3.a Motor and suspension equations

As expressed in Equation 1, the motor and suspension currents are defined as $\mathbf{I_M}$ and $\mathbf{I_S}$:

$$\begin{cases} \mathbf{I_U} = \frac{\mathbf{I_M}}{2} + \mathbf{I_S} \\ \mathbf{I_L} = \frac{\mathbf{I_M}}{2} - \mathbf{I_S} \end{cases} \iff \begin{cases} \mathbf{I_M} = \mathbf{I_L} + \mathbf{I_U} \\ \mathbf{I_S} = \frac{\mathbf{I_U} - \mathbf{I_L}}{2} \end{cases} \tag{2.9}$$

Furthermore the motor and suspension fluxes $\boldsymbol{\Phi_M}$ and $\boldsymbol{\Phi_S}$ are expressed as:

$$\begin{aligned} \boldsymbol{\Phi_M} &= \frac{\boldsymbol{\Phi}_\mathrm{L} + \boldsymbol{\Phi}_\mathrm{U}}{2} \\ &= \mathrm{K}_{\theta_\mathrm{m}} \begin{pmatrix} \cos(\theta_\mathrm{em}) \\ \cos(\theta_\mathrm{em} - \frac{2\pi}{3}) \\ \cos(\theta_\mathrm{em} - \frac{4\pi}{3}) \end{pmatrix} \end{aligned} \tag{2.10}$$

$$\begin{aligned} \boldsymbol{\Phi_S} &= \boldsymbol{\Phi}_\mathrm{U} - \boldsymbol{\Phi}_\mathrm{L} \\ &= 2\mathrm{z}\mathrm{K}_\mathrm{z} \begin{pmatrix} \cos(\theta_\mathrm{em}) \\ \cos(\theta_\mathrm{em} - \frac{2\pi}{3}) \\ \cos(\theta_\mathrm{em} - \frac{4\pi}{3}) \end{pmatrix} \end{aligned} \tag{2.11}$$

Introducing these motor and suspension variables in the system of equations 2.7 provides the following system of equations[1]:

$$\begin{cases} \mathbf{U} = \frac{\mathrm{R}}{2} \cdot \mathbf{I_M} + \frac{\mathrm{d}}{\mathrm{dt}} \left(\left(\frac{\mathbf{L_{AV}} + \mathbf{M_{UL}}}{2} \right) \cdot \mathbf{I_M} + \mathbf{L_V} \cdot \mathbf{I_S} \right) + \frac{\mathrm{d}\boldsymbol{\Phi_M}}{\mathrm{dt}} \\ 0 = 2\mathrm{R} \cdot \mathbf{I_S} + \frac{\mathrm{d}}{\mathrm{dt}} \left(\mathbf{L_V} \cdot \mathbf{I_M} + 2 \left(\mathbf{L_{AV}} - \mathbf{M_{UL}} \right) \cdot \mathbf{I_S} \right) + \frac{\mathrm{d}\boldsymbol{\Phi_S}}{\mathrm{dt}} \end{cases} \tag{2.12}$$

Where the matrix of average inductance $\mathbf{L_{AV}}$ and the variation inductance matrix $\mathbf{L_V}$ are defined in 2.13 and 2.14:

$$\begin{aligned} \mathbf{L_{AV}} &= \frac{\mathbf{L_U} + \mathbf{L_L}}{2} \\ &= \mathbf{L_0} + \mathrm{L}_2 \cdot [\boldsymbol{2\theta_{em}}] \end{aligned} \tag{2.13}$$

$$\begin{aligned} \mathbf{L_V} &= \frac{\mathbf{L_U} - \mathbf{L_L}}{2} \\ &= \mathrm{z} \cdot (\mathbf{dL_0} + \mathrm{dL}_2 \cdot [\boldsymbol{2\theta_{em}}]) \end{aligned} \tag{2.14}$$

2.2.3.b Concordia transformation

The transformation of Concordia can be applied to all variables[2], i.e. the voltages, the currents and the fluxes, to switch from a three-phase system to a two-phase equivalent system since the homopolar component x_0 is equal to 0 if the system is balanced. This transformation is defined as:

$$\mathbf{x^S} = \begin{pmatrix} \mathrm{x}_0 \\ \mathrm{x}_\alpha \\ \mathrm{x}_\beta \end{pmatrix} = \mathbf{T}^{-1} \begin{pmatrix} \mathrm{x}_1 \\ \mathrm{x}_2 \\ \mathrm{x}_3 \end{pmatrix} = \mathbf{T}^{-1}\mathbf{x} \qquad \text{with} \qquad \mathbf{T} = \sqrt{\frac{2}{3}} \begin{pmatrix} \frac{1}{\sqrt{2}} & 1 & 0 \\ \frac{1}{\sqrt{2}} & \frac{-1}{2} & \frac{\sqrt{3}}{2} \\ \frac{1}{\sqrt{2}} & \frac{-1}{2} & \frac{-\sqrt{3}}{2} \end{pmatrix} \tag{2.15}$$

[1] Developments available in Appendix A

[2] Developments available in Appendix B

As the homopolar component for current and voltage does not participate to the electrodynamic behaviour of the machine, they will not be represented in the next developments. Then the inductance matrices become 2×2-matrices and current, voltage, flux vectors become 2×1-vectors. Applying the transformation provides :

$$\begin{cases} \mathbf{U^S} = \dfrac{\mathrm{R}}{2} \cdot \mathbf{I_M^S} + \dfrac{\mathrm{d}}{\mathrm{dt}} \left(\left(\dfrac{\mathbf{L_{AV}^S} + \mathbf{M_{UL}^S}}{2} \right) \cdot \mathbf{I_M^S} + \mathbf{L_V^S} \cdot \mathbf{I_S^S} \right) + \dfrac{\mathrm{d}\boldsymbol{\Phi}_\mathbf{M}^\mathbf{S}}{\mathrm{dt}} \\ 0 = 2\mathrm{R} \cdot \mathbf{I_S^S} + \dfrac{\mathrm{d}}{\mathrm{dt}} \left(\mathbf{L_V^S} \cdot \mathbf{I_M^S} + 2 \left(\mathbf{L_{AV}^S} - \mathbf{M_{UL}^S} \right) \cdot \mathbf{I_S}^{\mathrm{S}} \right) + \dfrac{\mathrm{d}\boldsymbol{\Phi}_\mathbf{S}^\mathbf{S}}{\mathrm{dt}} \end{cases} \tag{2.16}$$

Where the three following matrices can be defined as:

$$\mathbf{L_{AV}^S} = \mathbf{T^{-1}} \cdot \mathbf{L_{AV}} \cdot \mathbf{T} = \begin{pmatrix} \mathrm{L}_0 - \mathrm{M}_0 & 0 \\ 0 & \mathrm{L}_0 - \mathrm{M}_0 \end{pmatrix} + \frac{3}{2}\mathrm{L}_2 \begin{pmatrix} \cos(2\theta_{\mathrm{em}}) & \sin(2\theta_{\mathrm{em}}) \\ \sin(2\theta_{\mathrm{em}}) & -\cos(2\theta_{\mathrm{em}}) \end{pmatrix} \tag{2.17}$$

$$\mathbf{M_{UL}^S} = \mathbf{T^{-1}} \cdot \mathbf{M_{UL}} \cdot \mathbf{T} = \begin{pmatrix} \mathrm{M}_{\mathrm{ii}} - \mathrm{M}_{\mathrm{ij}} & 0 \\ 0 & \mathrm{M}_{\mathrm{ii}} - \mathrm{M}_{\mathrm{ij}} \end{pmatrix} + \frac{3}{2}\mathrm{M}_2 \begin{pmatrix} \cos(2\theta_{\mathrm{em}}) & \sin(2\theta_{\mathrm{em}}) \\ \sin(2\theta_{\mathrm{em}}) & -\cos(2\theta_{\mathrm{em}}) \end{pmatrix} \tag{2.18}$$

$$\mathbf{L_V^S} = \mathbf{T^{-1}} \cdot \mathbf{L_V} \cdot \mathbf{T} = \mathrm{z} \cdot \begin{pmatrix} \mathrm{dL}_0 - \mathrm{dM}_0 & 0 \\ 0 & \mathrm{dL}_0 - \mathrm{dM}_0 \end{pmatrix} + \frac{3}{2}\mathrm{z} \cdot \mathrm{dL}_2 \begin{pmatrix} \cos(2\theta_{\mathrm{em}}) & \sin(2\theta_{\mathrm{em}}) \\ \sin(2\theta_{\mathrm{em}}) & -\cos(2\theta_{\mathrm{em}}) \end{pmatrix} \tag{2.19}$$

And the derivatives of both fluxes can be expressed as:

$$\frac{\mathrm{d}\boldsymbol{\Phi}_\mathbf{M}^\mathbf{S}}{\mathrm{dt}} = \sqrt{\frac{3}{2}} \cdot \mathrm{K}_{\theta\mathrm{m}} \mathrm{p} \dot{\theta}_{\mathrm{m}} \cdot \begin{pmatrix} -\sin(\theta_{\mathrm{em}}) \\ \cos(\theta_{\mathrm{em}}) \end{pmatrix} \tag{2.20}$$

$$\frac{\mathrm{d}\boldsymbol{\Phi}_\mathbf{S}^\mathbf{S}}{\mathrm{dt}} = \sqrt{6}\mathrm{K}_{\mathrm{z}} \cdot \left[\dot{\mathrm{z}} \cdot \begin{pmatrix} \cos(\theta_{\mathrm{em}}) \\ \sin(\theta_{\mathrm{em}}) \end{pmatrix} + \mathrm{z} \cdot \mathrm{p} \dot{\theta}_{\mathrm{m}} \begin{pmatrix} -\sin(\theta_{\mathrm{em}}) \\ \cos(\theta_{\mathrm{em}}) \end{pmatrix} \right] \tag{2.21}$$

2.2.3.c Park transformation

Park transformation can be applied on the α and β components of Equations 2.16 to suppress the dependence with respect to the electric angular position θ_{em} and to obtain equations depending on direct and quadrature components of motor and suspension currents[3]. As a reminder, the transformation is defined as:

$$\mathbf{x^P} = \begin{pmatrix} \mathrm{x_d} \\ \mathrm{x_q} \end{pmatrix} = \mathbf{P}^{-1} \begin{pmatrix} \mathrm{x}_\alpha \\ \mathrm{x}_\beta \end{pmatrix} = \mathbf{P}^{-1} \mathbf{x^S} \tag{2.22}$$

$$\text{with } \mathbf{P} = \begin{pmatrix} \cos(\theta_{\mathrm{em}}) & -\sin(\theta_{\mathrm{em}}) \\ \sin(\theta_{\mathrm{em}}) & \cos(\theta_{\mathrm{em}}) \end{pmatrix}$$

[3]Developments available in Appendix C.1

Applying this transformation on the motor electrical equation of the system 2.16 provides the following result:

$$\begin{aligned}\mathbf{U^P} = \frac{\mathrm{R}}{2}\cdot\mathbf{I_M^P} + \mathrm{p}\dot{\theta}_\mathrm{m}\cdot\begin{pmatrix}0 & -\frac{\mathrm{L_{M,q}}}{2}\\ \frac{\mathrm{L_{M,d}}}{2} & 0\end{pmatrix}\cdot\mathbf{I_M^S} + \begin{pmatrix}\frac{\mathrm{L_{M,d}}}{2} & 0\\ 0 & \frac{\mathrm{L_{M,q}}}{2}\end{pmatrix}\cdot\frac{\mathrm{d}\mathbf{I_M^P}}{\mathrm{dt}} \\ + \begin{pmatrix}\dot{\mathrm{z}}\mathrm{dL_d} & -\mathrm{zp}\dot{\theta}_\mathrm{m}\mathrm{dL_q}\\ \mathrm{zp}\dot{\theta}_\mathrm{m}\mathrm{dL_d} & \dot{\mathrm{z}}\mathrm{dL_q}\end{pmatrix}\cdot\mathbf{I_S^P} + \begin{pmatrix}\mathrm{z}\cdot\mathrm{dL_d} & 0\\ 0 & \mathrm{z}\cdot\mathrm{dL_q}\end{pmatrix}\cdot\frac{\mathrm{d}\mathbf{I_S^P}}{\mathrm{dt}} + \sqrt{\frac{3}{2}}\mathrm{K}_{\theta_\mathrm{m}}\cdot\mathrm{p}\cdot\dot{\theta}_\mathrm{m}\cdot\begin{pmatrix}0\\1\end{pmatrix}\end{aligned} \tag{2.23}$$

The transformation is also applied on the suspension electrical equation of the system 2.16 and provides the following result:

$$\begin{aligned}0 = 2\mathrm{R}\cdot\mathbf{I_S^P} + 2\mathrm{p}\dot{\theta}_\mathrm{m}\cdot\begin{pmatrix}0 & -\mathrm{L_{S,q}}\\ \mathrm{L_{S,d}} & 0\end{pmatrix}\cdot\mathbf{I_S^P} + 2\cdot\begin{pmatrix}\mathrm{L_{S,d}} & 0\\ 0 & \mathrm{L_{S,q}}\end{pmatrix}\cdot\frac{\mathrm{d}\mathbf{I_S^P}}{\mathrm{dt}} \\ + \begin{pmatrix}\dot{\mathrm{z}}\mathrm{dL_d} & -\mathrm{zp}\dot{\theta}_\mathrm{m}\mathrm{dL_q}\\ \mathrm{zp}\dot{\theta}_\mathrm{m}\mathrm{dL_d} & \dot{\mathrm{z}}\mathrm{dL_q}\end{pmatrix}\cdot\mathbf{I_M^P} + \begin{pmatrix}\mathrm{z}\cdot\mathrm{dL_d} & 0\\ 0 & \mathrm{z}\cdot\mathrm{dL_q}\end{pmatrix}\cdot\frac{\mathrm{d}\mathbf{I_M^P}}{\mathrm{dt}} + \sqrt{6}\mathrm{K_z}\cdot\begin{pmatrix}\dot{\mathrm{z}}\\ \mathrm{p}\dot{\theta}_\mathrm{m}\mathrm{z}\end{pmatrix}\end{aligned} \tag{2.24}$$

The following coefficients are introduced in these expressions:

- The direct and quadrature inductance coefficients for a winding set (upper or lower):

$$\mathrm{L_d} = \mathrm{L_0} - \mathrm{M_0} + \frac{3}{2}\mathrm{L_2} \tag{2.25}$$

$$\mathrm{L_q} = \mathrm{L_0} - \mathrm{M_0} - \frac{3}{2}\mathrm{L_2} \tag{2.26}$$

- The direct and quadrature mutual inductance coefficients between upper and lower windings:

$$\mathrm{M_d} = \mathrm{M_{ii}} - \mathrm{M_{ij}} + \frac{3}{2}\mathrm{M_2} \tag{2.27}$$

$$\mathrm{M_q} = \mathrm{M_{ii}} - \mathrm{M_{ij}} - \frac{3}{2}\mathrm{M_2} \tag{2.28}$$

- The direct and quadrature motor inductance coefficients:

$$\mathrm{L_{M,d}} = \mathrm{L_d} + \mathrm{M_d} \tag{2.29}$$

$$\mathrm{L_{M,q}} = \mathrm{L_q} + \mathrm{M_q} \tag{2.30}$$

- The direct and quadrature suspension inductance coefficients:

$$\mathrm{L_{S,d}} = \mathrm{L_d} - \mathrm{M_d} \tag{2.31}$$

$$\mathrm{L_{S,q}} = \mathrm{L_q} - \mathrm{M_q} \tag{2.32}$$

- And finally the z-gradient of the direct and quadrature inductance coefficients for a winding set (upper or lower):

$$\mathrm{dL_d} = \mathrm{dL_0} - \mathrm{dM_0} + \frac{3}{2}\mathrm{dL_2} \tag{2.33}$$

$$\mathrm{dL_q} = \mathrm{dL_0} - \mathrm{dM_0} - \frac{3}{2}\mathrm{dL_2} \tag{2.34}$$

[8] Developments available in Appendix C.2

Gathering the system of equations 2.23 and 2.24 provides the following system of four equations describing the behaviours of the direct and quadrature components of the motor and suspension currents:

$$\begin{cases} \mathrm{U_d} = \dfrac{\mathrm{R}}{2}\cdot \mathrm{I_{M,d}} & + \dfrac{\mathrm{L_{M,d}}}{2}\dot{\mathrm{I}}_{\mathrm{M,d}} & - \mathrm{p}\dot{\theta}_{\mathrm{m}}\cdot \dfrac{\mathrm{L_{M,q}}}{2}\cdot \mathrm{I_{M,q}} & + \mathrm{dL_d}\cdot \dfrac{\mathrm{d}}{\mathrm{dt}}(\mathrm{z}\cdot \mathrm{I_{S,d}}) & - \mathrm{dL_q}\cdot \mathrm{z}\cdot \mathrm{p}\dot{\theta}_{\mathrm{m}}\cdot \mathrm{I_{S,q}} & \\ \mathrm{U_q} = \dfrac{\mathrm{R}}{2}\cdot \mathrm{I_{M,q}} & + \dfrac{\mathrm{L_{M,q}}}{2}\dot{\mathrm{I}}_{\mathrm{M,q}} & + \mathrm{p}\dot{\theta}_{\mathrm{m}}\cdot \dfrac{\mathrm{L_{M,d}}}{2}\cdot \mathrm{I_{M,d}} & + \mathrm{dL_q}\cdot \dfrac{\mathrm{d}}{\mathrm{dt}}(\mathrm{z}\cdot \mathrm{I_{S,q}}) & + \mathrm{dL_d}\cdot \mathrm{z}\cdot \mathrm{p}\dot{\theta}_{\mathrm{m}}\cdot \mathrm{I_{S,d}} & + \sqrt{\dfrac{3}{2}}\mathrm{K}_{\theta_{\mathrm{m}}}\mathrm{p}\dot{\theta}_{\mathrm{m}} \\ 0 = 2\mathrm{R}\cdot \mathrm{I_{S,d}} & + 2\mathrm{L_{S,d}}\dot{\mathrm{I}}_{\mathrm{S,d}} & - 2\mathrm{p}\dot{\theta}_{\mathrm{m}}\mathrm{L_{S,q}}\cdot \mathrm{I_{S,q}} & + \mathrm{dL_d}\cdot \dfrac{\mathrm{d}}{\mathrm{dt}}(\mathrm{z}\cdot \mathrm{I_{M,d}}) & - \mathrm{dL_q}\cdot \mathrm{z}\cdot \mathrm{p}\dot{\theta}_{\mathrm{m}}\cdot \mathrm{I_{M,q}} & + \sqrt{6}\mathrm{K_z}\cdot \dot{\mathrm{z}} \\ 0 = 2\mathrm{R}\cdot \mathrm{I_{S,q}} & + 2\mathrm{L_{S,q}}\dot{\mathrm{I}}_{\mathrm{S,q}} & + 2\mathrm{p}\dot{\theta}_{\mathrm{m}}\mathrm{L_{S,d}}\cdot \mathrm{I_{S,d}} & + \mathrm{dL_q}\cdot \dfrac{\mathrm{d}}{\mathrm{dt}}(\mathrm{z}\cdot \mathrm{I_{M,q}}) & + \mathrm{dL_d}\cdot \mathrm{z}\cdot \mathrm{p}\dot{\theta}_{\mathrm{m}}\cdot \mathrm{I_{M,d}} & + \sqrt{6}\mathrm{K_z}\mathrm{p}\dot{\theta}_{\mathrm{m}}\cdot \mathrm{z} \end{cases} \tag{2.35}$$

Theses equations show that the two systems are fully decoupled if the rotor is axially centred:

2.2.4 Electrodynamic forces and torques

The magnetic fluxes linkages defined in 2.6 being only dependent on the axial and spin position, the only electrodynamics forces and torques existing are the axial ones.
The former, noted $\mathrm{F_{z,Ed}}$, is defined as the superposition of the forces produced by the upper and lower windings:

$$\mathrm{F_{z,Ed}} = \left[\mathbf{I_U}\right]^{\mathrm{T}}\cdot \frac{\partial \Phi_{\mathbf{U}}}{\partial \mathrm{z}} + \left[\mathbf{I_L}\right]^{\mathrm{T}}\cdot \frac{\partial \boldsymbol{\Phi}_{\mathbf{L}}}{\partial \mathrm{z}}$$

The motor and suspension fluxes and currents can be highlighted[4] to provide:

$$\mathrm{F_{z,Ed}} = \left[\mathbf{I_M}\right]^{\mathrm{T}}\cdot \frac{\partial \boldsymbol{\Phi}_{\mathbf{M}}}{\partial \mathrm{z}} + \left[\mathbf{I_S}\right]^{\mathrm{T}}\cdot \frac{\partial \boldsymbol{\Phi}_{\mathbf{S}}}{\partial \mathrm{z}}$$

Knowing that the motor flux $\boldsymbol{\Phi}_{\mathbf{M}}$ does not depend on the axial position, the first term can be discarded. Applying the Concordia and Park transformations allow to reach the final expression of this force in the d-q frame:

$$\mathrm{F_{z,Ed}} = \sqrt{6}\mathrm{K_z}\cdot \mathrm{I_{S,d}} \tag{2.36}$$

The electrodynamic suspension is completely independent from the power supply and only depends on the direct suspension current.

Concerning the electrodynamic torque, it is defined as[5]:

$$\mathrm{T}_{\theta_{\mathrm{m}},\mathrm{Ed}} = \left[\mathbf{I_U}\right]^{\mathrm{T}}\cdot \frac{\partial \Phi_{\mathbf{U}}}{\partial \theta_{\mathrm{m}}} + \left[\mathbf{I_L}\right]^{\mathrm{T}}\cdot \frac{\partial \boldsymbol{\Phi}_{\mathbf{L}}}{\partial \theta_{\mathrm{m}}}$$

[4] Developments available in Appendix D.1
[5] Developments available in Appendix D.2

Which is equivalent to:

$$\mathrm{T}_{\theta_\mathrm{m},\mathrm{Ed}} = [\mathbf{I_M}]^\mathrm{T} \cdot \frac{\partial \boldsymbol{\Phi}_\mathbf{M}}{\theta_\mathrm{m}} + [\mathbf{I_S}]^\mathrm{T} \cdot \frac{\partial \boldsymbol{\Phi}_\mathbf{S}}{\theta_\mathrm{m}}$$

Finally, by again applying the Concordia and Park transformations, the following expression is obtained:

$$\mathrm{T}_{\theta_\mathrm{m},\mathrm{Ed}} = \underbrace{\mathrm{pK}_{\theta_\mathrm{m}} \sqrt{\frac{3}{2}} \cdot \mathrm{I}_{\mathrm{M,q}}}_{\mathrm{T}_{\theta_\mathrm{m},\mathrm{M}}} + \underbrace{\mathrm{pzK_z}\sqrt{6} \cdot \mathrm{I}_{\mathrm{S,q}}}_{\mathrm{T}_{\theta_\mathrm{m},\mathrm{D}}} \tag{2.37}$$

As it can be seen, the torque has two components, the first one being provided by the quadrature motor current coming from the power supply and the second by the quadrature suspension current. The former is the driving torque, noted $\mathrm{T}_{\theta_\mathrm{m},\mathrm{M}}$, and is completely independent from the axial behaviour of the machine. The second one is a parasitic torque, called the drag torque $\mathrm{T}_{\theta_\mathrm{m},\mathrm{D}}$, which appears when the rotor is not in it its centered axial position and will oppose the driving torque.

2.2.5 Reluctant force and torque

The ferromagnetic parts in the rotor will add an axial reluctant force and torque, each one respectively due to the axial and spin variation of the inductance coefficients.

The former can be defined as[6]:

$$\begin{aligned}
\mathrm{F}_{\mathrm{z,rel}} &= \frac{1}{2} \cdot \begin{pmatrix} \mathbf{I_U} \\ \mathbf{I_L} \end{pmatrix}^\mathrm{T} \cdot \frac{\partial}{\partial \mathrm{z}} \cdot \begin{pmatrix} \mathbf{L_U} & \mathbf{M_{UL}} \\ \mathbf{M_{UL}}^\mathrm{T} & \mathbf{L_L} \end{pmatrix} \cdot \begin{pmatrix} \mathbf{I_U} \\ \mathbf{I_L} \end{pmatrix} \\
&= \frac{1}{2} \cdot [\mathbf{I_U}]^\mathrm{T} \cdot \frac{\partial \mathbf{L_U}}{\partial \mathrm{z}} \cdot \mathbf{I_U} + \frac{1}{2} \cdot [\mathbf{I_L}]^\mathrm{T} \cdot \frac{\partial \mathbf{L_L}}{\partial \mathrm{z}} \cdot \mathbf{I_L} + [\mathbf{I_U}]^\mathrm{T} \cdot \frac{\partial \mathbf{M_{UL}}}{\partial \mathrm{z}} \cdot \mathbf{I_L}
\end{aligned}$$

It is then possible to make appear the motor and suspension currents. After that, by applying the Concordia and Park transformations, the expression finally becomes:

$$\mathrm{F}_{\mathrm{z,rel}} = \mathrm{I}_{\mathrm{M,d}} \cdot \mathrm{I}_{\mathrm{S,d}} \cdot \mathrm{dL_d} + \mathrm{I}_{\mathrm{M,q}} \cdot \mathrm{I}_{\mathrm{S,q}} \cdot \mathrm{dL_q} \tag{2.38}$$

Concerning the reluctant torque[7], it is defined as:

$$\begin{aligned}
\mathrm{T}_{\theta_\mathrm{m},\mathrm{rel}} &= \frac{1}{2} \cdot \begin{pmatrix} \mathbf{I_U} \\ \mathbf{I_L} \end{pmatrix}^\mathrm{T} \cdot \frac{\partial}{\partial \theta_\mathrm{m}} \cdot \begin{pmatrix} \mathbf{L_U} & \mathbf{M_{UL}} \\ \mathbf{M_{UL}}^\mathrm{T} & \mathbf{L_L} \end{pmatrix} \cdot \begin{pmatrix} \mathbf{I_U} \\ \mathbf{I_L} \end{pmatrix} \\
&= \frac{1}{2} \cdot [\mathbf{I_U}]^\mathrm{T} \cdot \frac{\partial \mathbf{L_U}}{\partial \theta_\mathrm{m}} \cdot \mathbf{I_U} + \frac{1}{2} \cdot [\mathbf{I_L}]^\mathrm{T} \cdot \frac{\partial \mathbf{L_L}}{\partial \theta_\mathrm{m}} \cdot \mathbf{I_L} + [\mathbf{I_U}]^\mathrm{T} \cdot \frac{\partial \mathbf{M_{UL}}}{\partial \theta_\mathrm{m}} \cdot \mathbf{I_L}
\end{aligned}$$

Using the same method as the one used for the axial reluctant force allows to obtain the final expression of the reluctant torque:

$$\begin{aligned}
\mathrm{T}_{\theta_\mathrm{m},\mathrm{rel}} = \quad & 3\mathrm{p} \cdot (\mathrm{L_2} + \mathrm{M_2}) \cdot \left[\frac{\mathrm{I}_{\mathrm{M,d}}\mathrm{I}_{\mathrm{M,q}}}{2}\right] \\
& + 3\mathrm{p} \cdot (\mathrm{L_2} - \mathrm{M_2}) \cdot [2\mathrm{I}_{\mathrm{S,d}}\mathrm{I}_{\mathrm{S,q}}] \\
& + 3\mathrm{p} \cdot \mathrm{z} \cdot \mathrm{dL_2} \cdot [\mathrm{I}_{\mathrm{M,d}}\mathrm{I}_{\mathrm{S,q}} + \mathrm{I}_{\mathrm{S,d}}\mathrm{I}_{\mathrm{M,q}}]
\end{aligned} \tag{2.39}$$

[6] Developments available in Appendix E.1

[7] Developments available in Appendix E.2

2.2.6 Detent force

The axial detent force $F_{z,d}$ is produced by the interaction between the PMs and the ferromagnetic parts in the armature. Using assumption 7 allows to express this force as:

$$F_{z,d} = -k_{z,d} \cdot z \tag{2.40}$$

where $k_{z,d}$ is the stiffness of the system.

2.3 Mechanical equations

Assuming a rigid and damped rotor allows to write its mechanical model as:

$$\begin{cases} m\ddot{z} + C_z\dot{z} = F_{z,Ed} + F_{z,d} + F_{z,rel} + F_{z,e} \\ J_p\ddot{\theta}_m + C_{\theta_m}\dot{\theta}_m = T_{\theta_m,D} + T_{\theta_m,M} + T_{\theta_m,rel} + T_{\theta_m,e} \end{cases} \tag{2.41}$$

where m and J_p are the rotor mass and polar moment of inertia, $F_{z,e}$ and $T_{\theta_m,e}$ are the axial external force and torque, C_z and C_{θ_m} are the axial and spin damping coefficients, both being either inherent to the machine, comprising e.g. the aerodynamic effects, or being introduced for stability purposes.

2.4 Electromechanical model

This section will first introduce the state-space model governing the axial and spin dynamic of a passive bearingless motor with BPM. Then the forces applied on the rotor are analysed for two cases: both with an axial dependence of the inductance coefficients, but only the second one with magnetic saliency. It will allow to gradually study the effect of each element on the performances of the machine. Both cases are then compared to the quasi-static equation of [29] to highlight the contribution of the ferromagnetic parts of the rotor.

2.4.1 State-space model

The purpose is to express the axial and spin dynamics of the rotor with a state-space representation. The six state variables which will be used are the direct and quadrature motors currents $I_{M,d}$ and $I_{M,q}$, the axial electrodynamic force $F_{z,Ed}$, the ratio between the drag torque and the axial position $\left(\frac{T_{\theta_m,D}}{z}\right)$, the axial position z and the mechanical angular speed $\dot{\theta}_m$,

The state-space representation will be based on Equations 2.35 and 2.41. The first step is to express all the terms of these equations in term of the six state variables. To do so, Equations 2.36, 2.37, 2.38, 2.39 and 2.40 are modified to be injected in the six equations of 2.35 and 2.41[8].

[8]Developments available in Appendix F

The model presented below is a generalisation of the non-linear model proposed in [29], the latter can be retrieve by removing the axial and angular dependencies of the inductance coefficients.

- $$\begin{aligned}\dot{\mathrm{I}}_{\mathrm{M,d}} =& \frac{1}{\mathrm{L_{M,d}L_{S,d}} - \mathrm{z}^2\mathrm{dL_d^2}} \Big[\quad 2\mathrm{U_d} \cdot \mathrm{L_{S,d}} \quad + \quad \left(\mathrm{dL_d^2} \cdot \mathrm{z} \cdot \dot{\mathrm{z}} - \mathrm{RL_{S,d}}\right) \cdot \mathrm{I_{M,d}} \\ & + \quad \mathrm{p}\dot{\theta}_\mathrm{m} \cdot \left(\mathrm{L_{M,q}L_{S,d}} - \mathrm{z}^2 \cdot \mathrm{dL_d dL_q}\right) \cdot \mathrm{I_{M,q}} \quad + \quad \sqrt{\frac{2}{3}} \frac{\mathrm{dL_d}}{\mathrm{K_z}} \cdot \left(\mathrm{z} \cdot \mathrm{R} - \dot{\mathrm{z}} \cdot \mathrm{L_{S,d}}\right) \cdot \mathrm{F_{z,Ed}} \\ & + \quad \sqrt{\frac{2}{3}} \frac{\mathrm{L_{S,d}dL_q} - \mathrm{L_{S,q}dL_d}}{\mathrm{K_z}} \cdot \mathrm{z} \cdot \dot{\theta}_\mathrm{m} \cdot \left(\frac{\mathrm{T}_{\theta_\mathrm{m},\mathrm{D}}}{\mathrm{z}}\right) \quad + \quad \sqrt{6}\mathrm{K_z dL_d} \cdot \mathrm{z} \cdot \dot{\mathrm{z}} \Big] \end{aligned} \tag{2.42}$$

- $$\begin{aligned}\dot{\mathrm{I}}_{\mathrm{M,q}} =& \frac{1}{\left(\mathrm{L_{M,q}L_{S,q}} - \mathrm{z}^2 \cdot \mathrm{dL_q^2}\right)} \cdot \Big[\quad 2\mathrm{U_q} \cdot \mathrm{L_{S,q}} \quad + \quad \left(\mathrm{dL_q^2} \cdot \mathrm{z} \cdot \dot{\mathrm{z}} - \mathrm{RL_{S,q}}\right) \cdot \mathrm{I_{M,q}} \\ & + \quad \mathrm{p}\dot{\theta}_\mathrm{m} \cdot \left[\mathrm{z}^2 \cdot \mathrm{dL_d dL_q} - \mathrm{L_{M,d}L_{S,q}}\right] \cdot \mathrm{I_{M,d}} \quad + \quad \sqrt{\frac{2}{3}} \frac{\mathrm{dL_q}}{\mathrm{pK_z}} \cdot \left(\mathrm{z} \cdot \mathrm{R} - \dot{\mathrm{z}} \cdot \mathrm{L_{S,q}}\right) \cdot \left(\frac{\mathrm{T}_{\theta_\mathrm{m},\mathrm{D}}}{\mathrm{z}}\right) \\ & - \quad \sqrt{\frac{2}{3}} \frac{\mathrm{L_{S,q}dL_d} - \mathrm{L_{S,d}dL_q}}{\mathrm{K_z}} \cdot \mathrm{z} \cdot \mathrm{p}\dot{\theta}_\mathrm{m} \cdot \mathrm{F_{z,Ed}} \quad + \quad \sqrt{6} \left(\mathrm{z}^2 \cdot \mathrm{K_z dL_q} - \mathrm{K}_{\theta_\mathrm{m}}\mathrm{L_{S,q}}\right) \cdot \mathrm{p}\dot{\theta}_\mathrm{m} \Big] \end{aligned} \tag{2.43}$$

- $$\begin{aligned}\dot{\mathrm{F}}_{\mathrm{z,Ed}} =& \quad \frac{1}{\mathrm{L_{M,d}L_{S,d}} - \mathrm{z}^2 \cdot \mathrm{dL_d^2}} \cdot \Big[\left(\mathrm{z} \cdot \dot{\mathrm{z}} \cdot \mathrm{dL_d^2} - \mathrm{RL_{M,d}}\right) \cdot \mathrm{F_{z,Ed}} \quad + \quad \left(\mathrm{L_{M,d}L_{S,q}} - \mathrm{z}^2 \cdot \mathrm{dL_d dL_q}\right) \cdot \dot{\theta}_\mathrm{m} \cdot \left(\frac{\mathrm{T}_{\theta_\mathrm{m},\mathrm{D}}}{\mathrm{z}}\right) \\ & + \quad \sqrt{\frac{3}{2}}\mathrm{K_z dL_d} \cdot \left(\mathrm{z} \cdot \mathrm{R} - \dot{\mathrm{z}} \cdot \mathrm{L_{M,d}}\right) \cdot \mathrm{I_{M,d}} \quad + \quad \sqrt{\frac{3}{2}}\mathrm{K_z} \left(\mathrm{L_{M,d}dL_q} - \mathrm{L_{M,q}dL_d}\right) \cdot \mathrm{z} \cdot \mathrm{p}\dot{\theta}_\mathrm{m} \cdot \mathrm{I_{M,q}} \\ & - \quad \sqrt{6}\mathrm{K_z dL_d} \cdot \mathrm{U_d} \cdot \mathrm{z} \quad - \quad 3\mathrm{K_z^2 L_{M,d}} \cdot \dot{\mathrm{z}} \Big] \end{aligned} \tag{2.44}$$

- $$\begin{aligned}\left(\frac{\dot{\mathrm{T}}_{\theta_\mathrm{m},\mathrm{D}}}{\mathrm{z}}\right) =& \quad \frac{1}{\mathrm{L_{M,q}L_{S,q}} - \mathrm{z}^2 \cdot \mathrm{dL_q^2}} \left[\left(\mathrm{z} \cdot \dot{\mathrm{z}} \cdot \mathrm{dL_q^2} - \mathrm{RL_{M,q}}\right) \left(\frac{\mathrm{T}_{\theta_\mathrm{m},\mathrm{D}}}{\mathrm{z}}\right) \quad - \quad \left(\mathrm{L_{M,q}L_{S,d}} - \mathrm{z}^2 \cdot \mathrm{dL_d dL_q}\right) \cdot \mathrm{p}^2\dot{\theta}_\mathrm{m} \cdot \mathrm{F_{z,Ed}} \right. \\ & + \quad \sqrt{\frac{3}{2}}\mathrm{pK_z dL_q} \cdot \left(\mathrm{z} \cdot \mathrm{R} - \dot{\mathrm{z}} \cdot \mathrm{L_{M,q}}\right) \cdot \mathrm{I_{M,q}} \quad + \quad \sqrt{\frac{3}{2}}\mathrm{K_z} \left(\mathrm{L_{M,d}dL_q} - \mathrm{L_{M,q}dL_d}\right) \cdot \mathrm{z} \cdot \mathrm{p}^2\dot{\theta}_\mathrm{m} \cdot \mathrm{I_{M,d}} \\ & \left. - \quad \sqrt{6}\mathrm{pK_z dL_q} \cdot \mathrm{U_q} \cdot \mathrm{z} \quad + \quad 3\mathrm{p}^2\mathrm{K_z} \cdot \left(\mathrm{K}_{\theta_\mathrm{m}}\mathrm{dL_q} - \mathrm{K_z L_{M,q}}\right) \cdot \dot{\theta}_\mathrm{m} \cdot \mathrm{z} \right] \end{aligned} \tag{2.45}$$

- $$\ddot{\mathrm{z}} = \frac{\mathrm{F_{z,Ed}}}{\mathrm{m}} - \frac{\mathrm{k_{z,d}}}{\mathrm{m}} \cdot \mathrm{z} + \frac{1}{\sqrt{6}\mathrm{mK_z}} \left[\mathrm{dL_d} \cdot \mathrm{I_{M,d}} \cdot \mathrm{F_{z,Ed}} + \frac{\mathrm{dL_q}}{\mathrm{p}} \cdot \mathrm{I_{M,q}} \cdot \left(\frac{\mathrm{T}_{\theta_\mathrm{m},\mathrm{D}}}{\mathrm{z}}\right)\right] - \frac{\mathrm{C_z}}{\mathrm{m}}\dot{\mathrm{z}} + \frac{\mathrm{F_{z,e}}}{\mathrm{m}} \tag{2.46}$$

- $$\begin{aligned}\ddot{\theta}_\mathrm{m} =& \left(\frac{\mathrm{T}_{\theta_\mathrm{m},\mathrm{D}}}{\mathrm{z}}\right) \cdot \frac{\mathrm{z}}{\mathrm{J_p}} + \frac{\mathrm{pK}_{\theta_\mathrm{m}}}{\mathrm{J_p}} \sqrt{\frac{3}{2}} \cdot \mathrm{I_{M,q}} - \frac{\mathrm{C}_{\theta_\mathrm{m}}}{\mathrm{J_p}}\dot{\theta}_\mathrm{m} + \frac{3\mathrm{p} \cdot (\mathrm{L_2} + \mathrm{M_2})}{\mathrm{J_p}} \cdot \left[\frac{\mathrm{I_{M,d}I_{M,q}}}{2}\right] \\ & + \frac{(\mathrm{L_2} - \mathrm{M_2})}{\mathrm{J_p K_z^2}} \cdot \left[\mathrm{F_{z,Ed}} \cdot \left(\frac{\mathrm{T}_{\theta_\mathrm{m},\mathrm{D}}}{\mathrm{z}}\right)\right] + \sqrt{\frac{3}{2}} \frac{\mathrm{z} \cdot \mathrm{dL_2}}{\mathrm{J_p K_z}} \cdot \left[\mathrm{I_{M,d}} \cdot \left(\frac{\mathrm{T}_{\theta_\mathrm{m},\mathrm{D}}}{\mathrm{z}}\right) + \mathrm{p} \cdot \mathrm{F_{z,Ed}} \cdot \mathrm{I_{M,q}}\right] + \frac{\mathrm{T}_{\theta_\mathrm{m},\mathrm{e}}}{\mathrm{J_p}} \end{aligned} \tag{2.47}$$

2.4.2 Quasi-Static analysis of a rotor without magnetic saliency

To observe the contributions of the axial variation of inductance and the saliency in the performances of the machine, a quasi-static analysis is realised in a gradual approach where both elements will be successively added. The section is then a intermediate analysis since it only takes into account the axial variation of inductance coefficients.

Considering the quasi-static conditions, which means $\dot{I}_{M,d} = \dot{I}_{M,q} = \left(\frac{\dot{T}_{\theta_m,D}}{z}\right) = \dot{F}_{z,Ed} = \dot{z} = \ddot{z} = \ddot{\theta}_m = 0$ and a constant spin speed $\dot{\theta}_m = \omega$, it is possible to modify Equations 2.44 and 2.45 to obtain the expression of the electrodynamic force and the drag torque with respect to the rotation speed [9]. In this section, direct and quadrature inductance coefficients are equal, thus notations used in [29], Equations 2.48 and 2.49, are apply to facilitate comparison with the SMPM rotor[10]in Section 2.4.2:

$$L_{M,d} = L_{M,q} \rightarrow L_{M_c} \tag{2.48}$$
$$L_{S,d} = L_{S,q} \rightarrow L_{S_c} \tag{2.49}$$
$$dL_d = dL_q \rightarrow dL \tag{2.50}$$

These new definitions allow to obtain the expression of the electrodynamic force:

$$F_{z,Ed} = \sqrt{\frac{3}{2}} \cdot K_z \cdot z \left[\frac{dL}{R} \cdot \left(1 - \frac{\omega^2}{\left[\frac{R^2}{p^2 L_{S_c}^2} + \omega^2 \right]} \right) \cdot p\omega \cdot I_{M,q} - \frac{\omega^2}{\left[\frac{R^2}{p^2 L_{S_c}^2} + \omega^2 \right]} \cdot \left[\sqrt{6} \cdot \frac{K_z}{L_{S_c}} + \frac{dL}{L_{S_c}} \cdot I_{M,d} \right] \right] \tag{2.51}$$

By considering a speed significantly higher than the electrical pole $\omega_e = \frac{R}{pL_{S_c}}$, one can obtain the asymptotic value of this force and then of the stiffness:

$$F_{z,Ed}^{\infty} = \lim_{\omega \to \infty} F_{z,Ed} = -\sqrt{\frac{3}{2}} \cdot \frac{K_z}{L_{S_c}} \cdot z \cdot \left[\sqrt{6} \cdot K_z + dL \cdot I_{M,d} \right] \tag{2.52}$$

The same reasoning can be applied for the drag torque which is expressed as:

$$T_{\theta_m,D} = -z^2 \cdot \sqrt{\frac{3}{2}} \cdot \frac{K_z \cdot R}{L_{S_c}^2} \cdot \frac{\omega}{\left[\frac{R^2}{p^2 L_{S_c}^2} + \omega^2 \right]} \cdot \left[\sqrt{6} \cdot K_z + dL \cdot I_{M,d} + \frac{L_{S_c} \cdot dL}{R} \cdot p\omega \cdot I_{M,q} \right] \tag{2.53}$$

It has three components, each of them being proportional either to the axial variation of the flux or to the axial variation of inductance. Only the first one was already present in [29].

[9] Developments available in Appendix G

[10] In [29], factors $\frac{1}{2}$ and 2 are respectively used in the definitions of L_{M_c} and L_{S_c}, which is not the case in definition 2.29,2.30,2.31 and 2.32. These coefficients are compensate in the equations and thus have no influence on the result. To avoid confusion during the following comparison, equations of [29] have been adapted with coefficients L_{M_c} and L_{S_c} which do not have the factor $\frac{1}{2}$ and 2 in their definitions.

The main difference with the model [29] lies in the asymptotic value of the drag torque since this one no longer tends towards 0 in non-centred position at high speed, as shown below:

$$T^{\infty}_{\theta_m,D} = -z^2 \cdot \sqrt{\frac{3}{2}} \cdot p \cdot K_z \cdot \frac{dL}{L_{S_c}} \cdot I_{M,q} \tag{2.54}$$

2.4.2.a Expression and origin of the suspension currents

The following analysis is made considering a higher speed than the electrical pole and then asymptotic values for all the expressions.

The suspensions currents have been introduced to express the unbalanced current distribution between upper and lower windings appearing when the rotor is axially shifted from its centred position. Equations 2.36, 2.37, 2.52 and 2.54 allow to express the suspension currents generated at high speed according to the direct and quadrature motor currents:

$$\begin{aligned} I^{\infty}_{S,d} &= \frac{F^{\infty}_{z,Ed}}{\sqrt{6}K_z} \\ &= -\frac{z}{2L_{S_c}} \cdot \left[\sqrt{6} \cdot K_z + dL \cdot I_{M,d}\right] \end{aligned} \tag{2.55}$$

$$\begin{aligned} I^{\infty}_{S,q} &= \frac{T^{\infty}_{\theta_m,D}}{pzK_z\sqrt{6}} \\ &= -z \cdot \frac{dL}{2L_{S_c}} \cdot I_{M,q} \end{aligned} \tag{2.56}$$

It allows to express the reluctant force in function of the motor current, but also to explain the origin of the suspension currents. Indeed these equations show that an axial displacement of the rotor has two different effects.

First, as already presented for the SMPM machines in [29], the flux increases in the winding whose rotor is approaching, and conversely for the other. It increases the EMFs and unbalance the distribution of current provided by the source in favour of the nearest winding. This imbalance of current is represented by the first term of 2.55, which express an increase in absolute value of suspension current on the d-axis, the flux being aligned with the d-axis and zero on the q-axis.

Secondly, the axial dependence of the inductance coefficients means that the inductance, and then the impedance of the windings whose rotor is approaching increases and inversely for the other one. The voltage being imposed by the source, it decreases the current in the winding closest to the rotor in contrast to the variation of flux. This is expressed by the other terms of 2.55 and the terme of 2.56

Both phenomena are fully decoupled, the first one being relative to the fluxes provided by the PMs, and the latter to the variation of the magnetic circuit defining the inductances.

2.4.2.b Total force and torque at high speed

All the components of the force and of the torque applied on the rotor developed in previous sections can be expressed only depending on the motor currents.
The total axial force applied on the rotor is composed of three terms: an electrodynamic, a reluctant and a detent force[11]:

$$\begin{aligned} F_{z,tot}^{\infty} =& F_{z,Ed}^{\infty} + F_{z,rel}^{\infty} + F_{z,d} \\ =& -\sqrt{\frac{3}{2}} \cdot \frac{K_z}{L_{S_c}} \cdot z \cdot \left[\sqrt{6} \cdot K_z + dL \cdot I_{M,d}\right] \\ & + (I_{M,d} \cdot I_{S,d}^{\infty} + I_{M,q} \cdot I_{S,q}^{\infty}) \cdot dL \\ & - k_{z,d} \cdot z \end{aligned} \tag{2.57}$$

Equations 2.55 and 2.56 allow to obtain an expression of the total axial force only depending on the axial position and on the motor currents:

$$F_{z,tot}^{\infty} = -z \cdot \left[\frac{\left[dL \cdot I_{M,d} + \sqrt{6} \cdot K_z\right]^2}{2L_{S_c}} + \frac{dL^2}{2L_{S_c}} \cdot I_{M,q}^2 + k_{z,d} \right] \tag{2.58}$$

Then it is possible to compute the asymptotic total axial stiffness of the machine:

$$k_t^{\infty} = \frac{-F_{z,tot}^{\infty}}{z} = \underbrace{\frac{3K_z^2}{L_{S_c}} + \sqrt{6}K_z \cdot \frac{dL}{L_{S_c}} \cdot I_{M,d}}_{\substack{\text{Electrodynamic} \\ \text{stiffness}}} + \underbrace{\frac{1}{2}dL \cdot \frac{dL}{L_{S_c}} \cdot \left(I_{M,d}^2 + I_{M,q}^2\right)}_{\substack{\text{Reluctant} \\ \text{stiffness}}} + \underbrace{k_{z,d}}_{\substack{\text{Detent} \\ \text{stiffness}}} \tag{2.59}$$

As it can be observed in Equation 2.59, this stiffness can be split in three components: the electrodynamic, the reluctant and the detent component. The former contains two terms, the first of which was already presented in [29] for a SMPM machine. The second part of the electrodynamic stiffness can be modulated through the direct component of the motor current, which adds a new possibility in the control of the rotor stiffness. It is important to specify that this is not a position control as such, the position cannot be controlled as an active self-bearing machine, but the stiffness can be partially modulated through the direct current, conversely to [29] where this current was set to zero. It could even be considered to inject a negative current to reduce the total stiffness, depending on the situation. The higher $\frac{dL}{L_{S_c}}$, the relative variation of the inductance coefficients with respect to the axial position, will be, the greater the influence of the direct current on the stiffness.

Axial variation of the inductance coefficients also adds a reluctant component which, by definition, does not depend on the PMs. Then the model shows that a passive suspension could be reached without any PM. This stiffness, and then the resulting force created by an axial shift are due to the imbalance of current created by the variation of inductances of upper and lower windings, as explained in 2.4.2.a.

[11] Developments available in Appendix G.1

In turn, the total torque applied on the rotor at high speed can be expressed as:

$$\begin{aligned} \mathrm{T}^{\infty}_{\theta_\mathrm{m},\mathrm{tot}} =& \mathrm{T}_{\theta_\mathrm{m},\mathrm{M}} + \mathrm{T}^{\infty}_{\theta_\mathrm{m},\mathrm{D}} \\ =& \sqrt{\frac{3}{2}} \cdot \mathrm{p} \cdot \left[\mathrm{K}_{\theta_\mathrm{m}} - \mathrm{z}^2 \cdot \frac{\mathrm{K_z} \cdot \mathrm{dL}}{\mathrm{L_{S_c}}} \right] \cdot \mathrm{I_{M,q}} \end{aligned} \tag{2.60}$$

Contrary to a SMPM machine, the total torque at high speed presents a negative component opposed to the driving torque which is also proportional to the quadrature motor current. As for the stiffness, the higher the relative axial variation $\frac{\mathrm{dL}}{\mathrm{L_{s,c}}}$ of the inductance coefficient, the greater the drag torque in a decentred position of the rotor.

2.4.3 Quasi-Static analysis of a rotor with magnetic saliency

The second evolution consists in taking into account the magnetic saliency of the rotor. The axial variation of inductance coefficients is conserved, then all the observations made in Section 2.4.2 are still valid but will not be repeated. This situation is considered during the rest of this master's thesis. The coefficients $\mathrm{L_2}, \mathrm{M_2}$ and $\mathrm{dL_2}$ are then no longer nil, which provides the following expression for the axial electrodynamic force:

$$\mathrm{F_{z,Ed}} = \sqrt{\frac{3}{2}} \cdot \mathrm{K_z} \cdot \mathrm{z} \left[\frac{\mathrm{dL_q}}{\mathrm{R}} \cdot \left(1 - \frac{\omega^2}{\left[\frac{\mathrm{R}^2}{\mathrm{p}^2 \mathrm{L_{S,d}} \mathrm{L_{S,q}}} + \omega^2 \right]} \right) \cdot \mathrm{p}\omega \cdot \mathrm{I_{M,q}} - \frac{\omega^2}{\left[\frac{\mathrm{R}^2}{\mathrm{p}^2 \mathrm{L_{S,d}} \mathrm{L_{S,q}}} + \omega^2 \right]} \cdot \left[\frac{\mathrm{dL_d}}{\mathrm{L_{S,d}}} \cdot \mathrm{I_{M,d}} + \sqrt{6} \cdot \frac{\mathrm{K_z}}{\mathrm{L_{S,d}}} \right] \right] \tag{2.61}$$

which reaches, when the speed exceeds significantly the electrical pole $\omega_\mathrm{e} = \frac{\mathrm{R}}{\mathrm{p} \cdot \sqrt{\mathrm{L_{S,d}}, \mathrm{L_{S,q}}}}$, the asymptotic value is defined as:

$$\mathrm{F^{\infty}_{z,Ed}} = \lim_{\omega \to \infty} \mathrm{F_{z,Ed}} = -\sqrt{\frac{3}{2}} \cdot \frac{\mathrm{K_z}}{\mathrm{L_{S,d}}} \cdot \mathrm{z} \cdot \left[\sqrt{6} \cdot \mathrm{K_z} + \mathrm{dL_d} \cdot \mathrm{I_{M,d}} \right] \tag{2.62}$$

Concerning the electrodynamic drag torque in quasi-static conditions, its expression can be computed as:

$$\mathrm{T}_{\theta_\mathrm{m},\mathrm{D}} = -\mathrm{z}^2 \cdot \sqrt{\frac{3}{2}} \cdot \frac{\mathrm{K_z} \cdot \mathrm{R}}{\mathrm{L_{S,d}} \mathrm{L_{S,q}}} \cdot \frac{\omega}{\left[\frac{\mathrm{R}^2}{\mathrm{p}^2 \mathrm{L_{S,d}} \mathrm{L_{S,q}}} + \omega^2 \right]} \cdot \left[\frac{\mathrm{L_{S,d}} \cdot \mathrm{dL_q}}{\mathrm{R}} \cdot \mathrm{p}\omega \cdot \mathrm{I_{M,q}} + \mathrm{dL_d} \cdot \mathrm{I_{M,d}} + \sqrt{6} \cdot \mathrm{K_z} \right] \tag{2.63}$$

And this expression, at high rotation speed, tends to:

$$\mathrm{T^{\infty}_{\theta_m,D}} = -\mathrm{z}^2 \cdot \sqrt{\frac{3}{2}} \cdot \mathrm{p} \cdot \frac{\mathrm{K_z} \cdot \mathrm{dL_q}}{\mathrm{L_{S,q}}} \cdot \mathrm{I_{M,q}} \tag{2.64}$$

The asymptotic expressions defined here are very similar to 2.52 and 2.54 respectively, and comparisons made in Section 2.4.2 are still valid. However, the consideration of the saliency changes the coefficient $\mathrm{L_{S,c}}$ either in $\mathrm{L_{S,d}}$ or $\mathrm{L_{S,q}}$, and these modifications are discussed in Section 2.4.3.b where all the forces and torques are gathered and expressed according to the motor currents.

2.4.3.a Expression of suspension currents

Similarly to what has been done in Section 2.4.2.a, suspension currents need to be expressed according to the motor currents. Equations 2.36, 2.37, 2.62 and 2.64 allow to obtain these expressions at speed significantly higher than the electrical pole:

$$I_{S,d}^{\infty} = -\frac{z}{2L_{S,d}} \cdot \left[dL_d \cdot I_{M,d} + \sqrt{6} \cdot K_z \right] \qquad (2.65) \qquad I_{S,q}^{\infty} = -z \cdot \frac{dL_q}{2L_{S,q}} \cdot I_{M,q} \qquad (2.66)$$

2.4.3.b Total Force and torque at high speed

All the components of the force and the torque applied on the rotor have been developed and can be expressed only depending on the motor currents.
Similarly to the developments made in 2.4.2.b, the total axial force applied on the rotor is composed of three terms: an electrodynamic, a reluctant and a detente force [12]:

$$\begin{aligned} F_{z,tot}^{\infty} =& F_{z,Ed}^{\infty} + F_{z,rel}^{\infty} + F_{z,d} \\ =& -\sqrt{\frac{3}{2}} \cdot \frac{K_z}{L_{S,d}} \cdot z \cdot \left[dL_d \cdot I_{M,d} + \sqrt{6} \cdot K_z \right] \\ & + I_{M,d} \cdot I_{S,d}^{\infty} \cdot dL_d + I_{M,q} \cdot I_{S,q}^{\infty} \cdot dL_q \\ & - k_{z,d} \cdot z \end{aligned} \qquad (2.67)$$

Equations 2.65 and 2.66 allow to obtain an expression of the total axial force only depending on the axial position and on the motor currents:

$$F_{z,tot}^{\infty} = -z \cdot \left[\frac{\left[dL_d \cdot I_{M,d} + \sqrt{6} \cdot K_z \right]^2}{2L_{S,d}} + \frac{dL_q^2}{2L_{S,q}} \cdot I_{M,q}^2 + k_{z,d} \right] \qquad (2.68)$$

And this expression leads to the asymptotic total axial stiffness of the machine:

$$k_t^{\infty} = \frac{-F_{z,tot}}{z} = \underbrace{\frac{3K_z^2}{L_{S,d}} + \sqrt{6} \cdot K_z \cdot \frac{dL_d}{L_{S,d}} \cdot I_{M,d}}_{\text{Electrodynamic stiffness}} \underbrace{+ \frac{dL_d^2}{2L_{S,d}} \cdot I_{M,d}^2 + \frac{dL_q^2}{2L_{S,q}} \cdot I_{M,q}^2}_{\text{Induced reluctant stiffness}} + \underbrace{k_{z,d}}_{\text{Detent stiffness}} \qquad (2.69)$$

All the analysis made in Section 2.4.2.b still applies here, but the reluctant term is now split into two parts, each one depending respectively on the relative variation of the direct or quadrature inductance.

[12] Developments available in Appendix G.1

The total torque applied on the rotor can also be expressed, by adding the reluctant torque induced by the magnetic saliencies expressed in 2.39:

$$\begin{aligned} T^{\infty}_{\theta_m,tot} =& T_{\theta_m,M} + T^{\infty}_{\theta_m,D} + T^{\infty}_{\theta_m,rel} \\ =& \sqrt{\frac{3}{2}} \cdot p \cdot \left[K_{\theta_m} - z^2 \cdot \frac{K_z \cdot dL_q}{L_{S,q}} \right] \cdot I_{M,q} \\ &+ 3p \cdot \left[(L_2 + M_2) \cdot \left[\frac{I_{M,d} I_{M,q}}{2} \right] + (L_2 - M_2) \cdot \left[2 I^{\infty}_{S,d} I^{\infty}_{S,q} \right] + z \cdot dL_2 \cdot \left[I_{M,d} I^{\infty}_{S,q} + I^{\infty}_{S,d} I_{M,q} \right] \right] \end{aligned} \tag{2.70}$$

Equations 2.65 and 2.66 allow to suppress the suspension currents of the expression:

$$\begin{aligned} T^{\infty}_{\theta_m,tot} =& \underbrace{3p \cdot I_{M,q} \left[\frac{K_{\theta_m}}{\sqrt{6}} - z^2 \cdot \frac{K_z}{\sqrt{6}} \cdot \left(\frac{dL_d}{L_{S,d}} \right) \right]}_{\text{Electrodynamic torque}} \\ &+ \underbrace{3p \cdot \frac{I_{M,d} \cdot I_{M,q}}{2} \cdot \left[(L_2 + M_2) + z^2 \cdot \left[(L_2 - M_2) \cdot \left(\frac{dL_d \cdot dL_q}{L_{S,d} \cdot L_{S,q}} \right) - dL_2 \cdot \left(\frac{dL_d}{L_{S,d}} + \frac{dL_q}{L_{S,q}} \right) \right] \right]}_{\text{Reluctant torque}} \end{aligned} \tag{2.71}$$

This total torque can be divided into two parts, the first one being the electrodynamic torque, similar to the Equation 2.60.

The second term is a reluctant torque, which is, in centred position, directly proportional to $L_2 + M_2$, the total inductance variation seen by the power supply.

In the following reasoning, the coefficients L_2 and M_2 are assumed to have the same sign[13]. The sign of $L_2 + M_2$ influences the sign of the direct motor current $I_{M,d}$. Indeed in case of a negative value of $L_2 + M_2$, the direct current must be negative to obtain a reluctant torque which participates to the driving torque. However it could decrease the total stiffness since the second term of equation 2.69 could becomes negative in turn if the ratio $\frac{dL_d}{L_{S,d}}$ is positive. Then to take advantage of all stiffness and torque components, the sign of $L_2 + M_2$ must be positive and it is interesting to note that it can be anticipated: The sign of L_2, and then of $L_2 + M_2$, is fixed by the reluctance seen by the winding when its aligned with the d and q-axis, and then by the topology of the rotor and the pitch of the coils. In the case of a TLST rotor for example, Figure 2.2 (a) and (b) shows a pitch which makes the magnetic field created by the coils pass through less ferromagnetic materials on the d-axis than the q-axis, which means a bigger inductance on the q-axis, and then a negative coefficient L_2 due to definitions 2.25 and 2.26.

[13] This assumption will be confirmed in section 3.3.1.

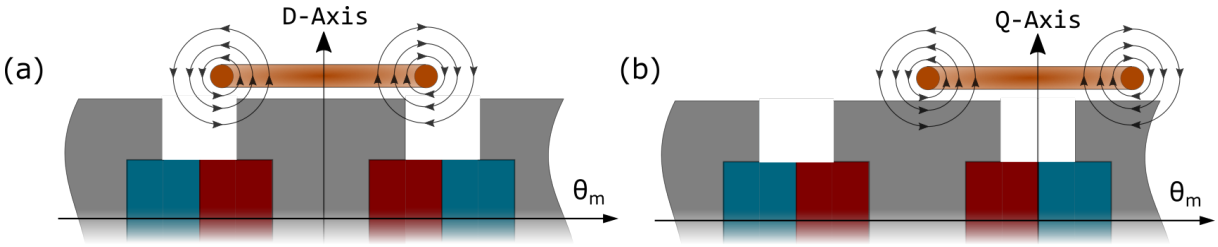

Figure 2.2: Pitch leading to a negative coefficient L_2 for a TLST topology. Windings are aligned with: (a) the d-axis of the rotor (b) the q-axis of the rotor.

On the other hand, Figure 2.3 (a) and (b) shows a winding pitch leading to a positive L_2 coefficient.

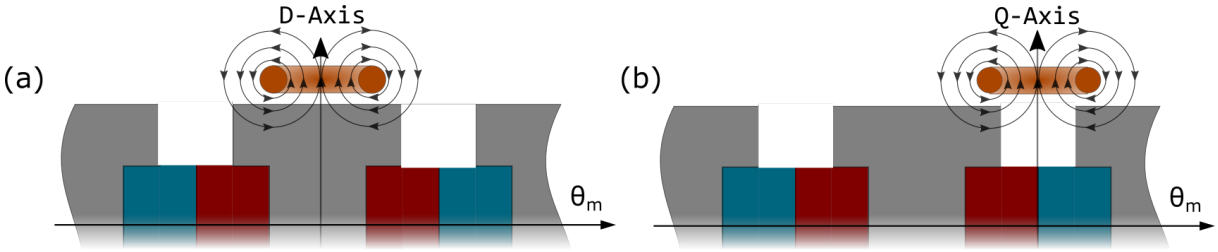

Figure 2.3: Pitch leading to a positive coefficient L_2 for a TLST topology. Windings are aligned with: (a) the d-axis of the rotor (b) the q-axis of the rotor

However, a positive value of the coefficient L_2 does not mean that the machine will provide better performances, but only that all the components of stiffness and torque will be beneficial. Indeed the pitch will also fix the values of the inductance coefficients, whose average values (without saliency) could lead to better performances despite the negative values of some torque/force components.

2.5 Conclusions

This chapter presented an electromechanical model describing the axial and spin dynamic of a fully passively levitated self-bearing machine with a BPM rotor. Similarly to [29], the set of state equations depends on parameters which can be determined through static FEM. The quasi-static behaviour of the machine has been realised in two steps, by first adding the axial variation of inductance coefficients, and then the magnetic saliency. The former highlights three elements not present in the electromechanical model of a machine with a SMPM rotor: First, an additional electrodynamic term is added to the stiffness and shows that some modulation can be applied on the stiffness through direct motor current, while this current is usually set to 0 for classical synchronous machine with SMPM rotor. Secondly the axial variation of these coefficients adds a reluctant force which shows that a passive suspension can be reached at high speed without any PM.
Finally the drag torque does not tend to 0 at high speed contrary to the SMPM machine but becomes proportional to the quadrature motor current. All these supplementary terms are directly proportional to the relative variation of the inductance according to axial position. The axial variation of the inductance coefficients has positive effect on the stiffness but negative effect on the motor performances when the rotor is decentred.
In addition to these results, the magnetic saliencies generate a reluctant torque that depends on $(L_2 + M_2)$, the total variation of inductance seen by the power supply.

CHAPTER 3

FEM MODELLING

This chapter presents the finite element models and the numerical method applied to determine parameters presented in Chapter 2 and to validate through simulations, the assumptions 5,6 and 7 made in Section 2.1.
Section 3.1, describes the different finite element models used. Then, the approach to determine the parameters is presented in Section 3.2. Finally, the three assumptions are verified in Section 3.3.

3.1 Description of the models

The models built to compute the required parameters and to validate the assumptions are 3D FEM models based on the software COMSOL Multiphysics. Three dimensions are needed to be able to determine the magnetic flux in the machines while taking into account the rotor and winding topologies. These models use magnetostatic laws, described in Section 3.2. There are five main models, divided in two categories. On one hand, there is a model which derives the flux constants linked to the flux coming from the PM and intercepted by the windings. On the other hand, there are the models used to calculate the inductance coefficients. All of these models are single-turn, this means that the winding is modelled as one coil comprising one turn. As these models are also used to optimise several criteria detailed in the next chapter, they are all built with a parametric geometry represented in Figure 3.1. To reduce the computation time during the optimisation, symmetries are exploited through boundary conditions when it is possible. Two types of conditions are used: the perfect magnetic conductor and the magnetic insulation. The purpose of the first is to only keep the normal component of the magnetic field and the tangential component of the current density across the boundary while the second keeps only the tangential component of the magnetic flux density and the normal component of the current density across the boundary.

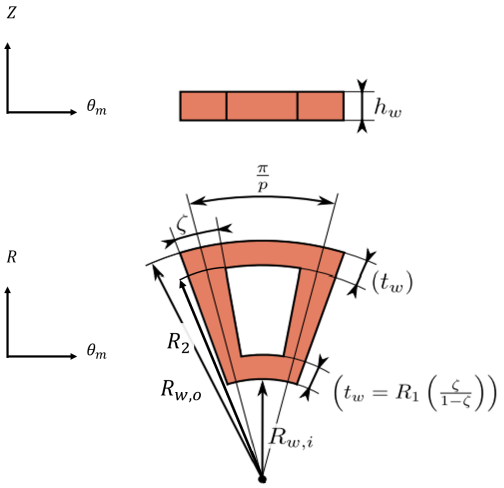

(a) Overlapping coils geometry [53].

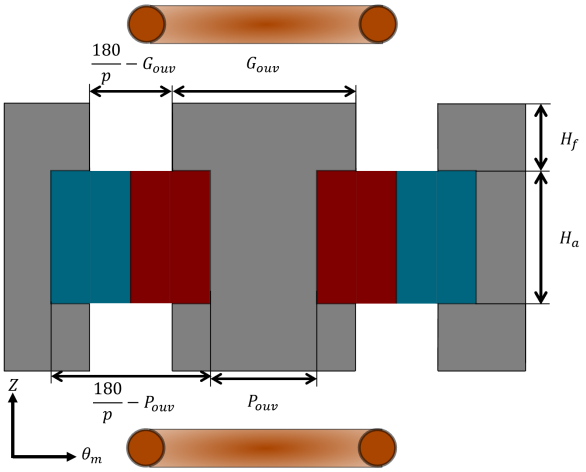

(b) Main design parameters of the rotor.

Figure 3.1: Winding and rotor configuration.

Then the rotor is created following the geometry represented in Figure 3.1b. Five parameters characterise its dimensions:

- H_a, the height of the permanent magnet;
- H_f, the height of the superior ferromagnetic part;
- G_{ouv}, the angular span of a ferromagnetic part;
- P_{ouv}, the angular span between two PMs;
- p, the number of pole pairs;

In these models the coils are made of copper, the ferromagnetic pieces are made of soft iron with μ_r=1000 and the PMs are modelled with air as their magnetic properties are assumed to be similar. The internal and external radius of the rotor correspond to the same radius than the winding.

3.1.1 Flux constants models

Two models compose this first category. The first one, depicted in Figure 3.2a is used to validate the assumption 5. There is only a symmetry with respect to the horizontal plane. This choice has been made to be able to evaluate the evolution of the flux constants over one electrical period by rotating the rotor. If it is verified, then the second model represented in Figure 3.2b can be used to compute the flux constants during the optimisation. In addition to the symmetry with respect to the horizontal plane, this model has also a symmetry with respect to the angular position. In fact, during the optimisation, the flux must be computed in a single angular position as it will be explained in Section 3.2.2. Consequently, the model is limited to one pole, reducing the computation time.

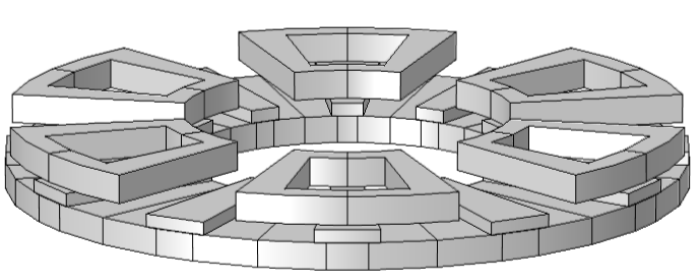

(a) Flux constants model used to validate the assumptions.

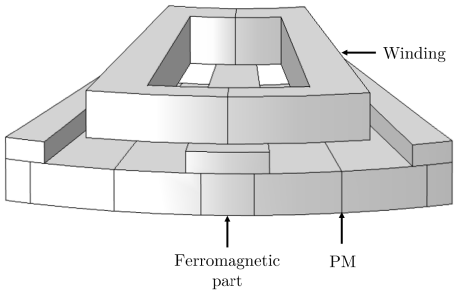

(b) Flux constants model used to determine the value of the parameters.

Figure 3.2: Models used to determine the flux constants.

The mesh applied to the model is a compromise between fast computation time and accuracy of the solution. This leads to a very fine mesh on the coil because this is where measurements are done and a more coarse on the other parts. The computation time of the model in Figure 3.2b is about 10s and differences with a global extra fine mesh are less than 1%.

3.1.2 Inductance coefficients models

The second category of model can also be split into two other branches, with on one side two single-phase models and on the other side one two-phase model. Two phases are necessary to calculate the mutual inductance coefficients between two different phases for both upper and lower windings. The single-phase models are presented in Figures 3.3a and 3.3b. They use both an axial and angular symmetry as in Figure 3.2b but do not have any PM since only the flux created by current is needed. They both evaluate the inductance coefficient of the windings in centred axial position but in two different angular positions of the rotor, one time aligned on the d-axis and the second time aligned on the q-axis.

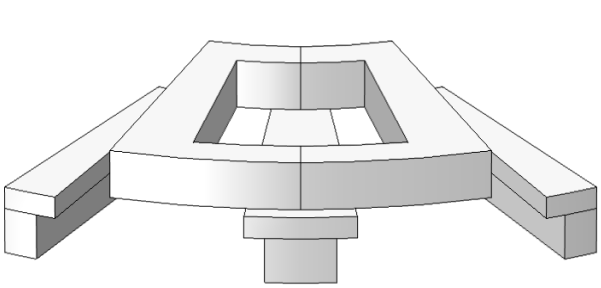

(a) Winding aligned with the d-axis.

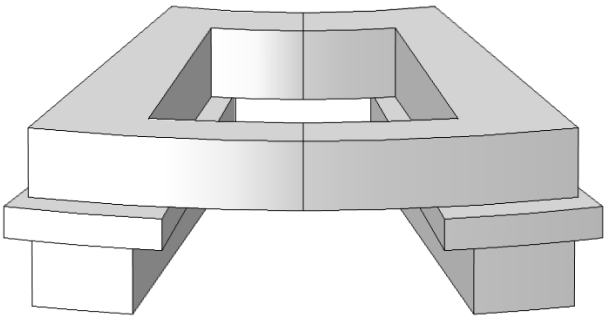

(b) Winding aligned with the q-axis.

Figure 3.3: Single-phase models used to determine inductance coefficients.

Once again, due to the angular symmetry these models cannot be used to verify the assumptions made in Section 2.1. Thus another model, which is a two-phase complete model of the machine allows to verify the three assumptions for all the required inductance coefficients. It is depicted in Figure 3.4.

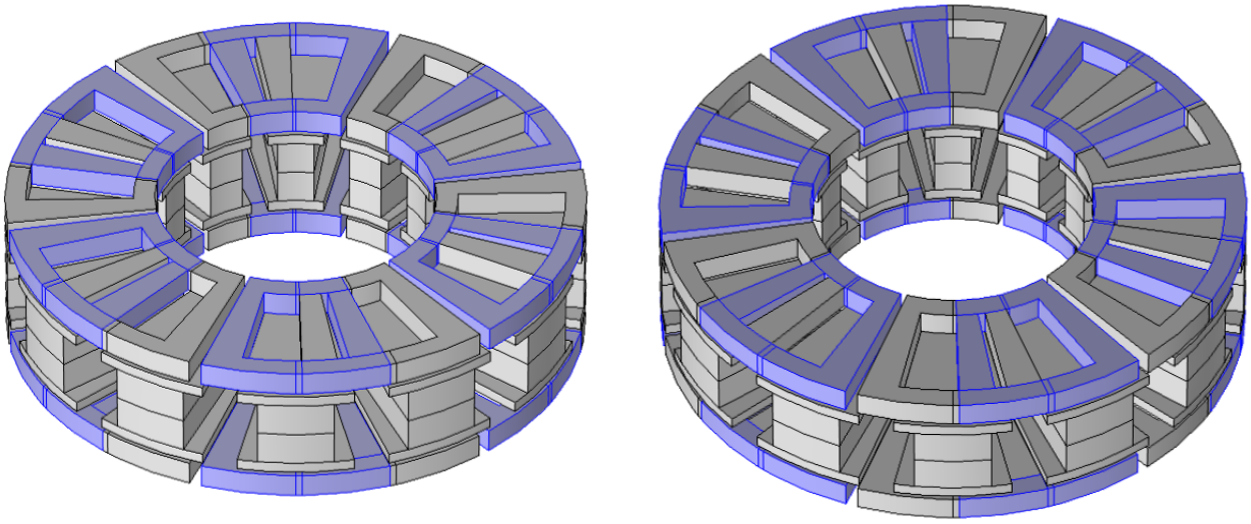

(a) Winding of phase a.

(b) Winding of phase b.

Figure 3.4: Full model to validate the assumptions on the inductance coefficients.

Since the model is a complete representation of the machine the computation time is bigger than for the symmetrised models. For similar mesh it takes 10s for one simulation on a symmetrised model while it takes 1min15s on the full model. Furthermore, the crossing areas between two phases are very small and as a consequence lead to a very fine mesh. The advantage of this model is that it is a whole in one. One evaluation gives all the needed inductance coefficients.

3.2 Determination of the parameters

The parameters listed here below are determined using the two types of finite element models described in Section 3.1. All the parameters presented in Section 2 are not separately determined. In order to highlight both the rotor axial and angular positions dependencies of the inductance coefficients, the parameters that represent these variations are put together such as L_2 and M_2 for the rotor angular position. To take the number of turns N into account, all the flux values have to be multiplied by N and all the inductance coefficients by a factor N^2.

- K_{θ_m}, the flux amplitude in axial centred position;
- K_z, the flux gradient linked to the axial position of the rotor;
- $L_2 + M_2$, the summation of the sinusoidal components of the self and mutual inductance coefficients;

- $L_{S,d}$ and $L_{S,q}$, respectively the direct and quadratic inductance of suspension;
- dL_d and dL_q, respectively the axial variation of direct and quadratic self inductance;

3.2.1 Methodology

The methodology to compute either the magnetic flux or the inductance coefficients is the same. In fact in both type of models, a flux computation on the windings is needed. It is generally done by integrating the magnetic flux density $\mathbf{B}$ on a surface $\mathbf{S}$ and is written as:

$$\boldsymbol{\phi} = \iint_{\mathbf{S}} \mathbf{B} \cdot \mathrm{d}\mathbf{S} \tag{3.1}$$

However it is not trivial to choose on which surface of the winding to integrate. To solve this issue, based on Maxwell-Thomson's equation:

$$\nabla \cdot \mathbf{B} = 0$$

Since magnetic flux density is divergence free, it can be expressed as:

$$\nabla \times \mathbf{A} = \mathbf{B}$$

where $\mathbf{A}$ is the magnetic potential vector. Using Stoke's theorem, the flux can be expressed as:

$$\boldsymbol{\phi} = \iint_{\mathbf{S}} \boldsymbol{\nabla} \times \mathbf{A} \cdot \mathrm{d}\mathbf{S} = \oint_{\boldsymbol{\Gamma}} \mathbf{A} \cdot \mathrm{d}\boldsymbol{\Gamma} \tag{3.2}$$

where $\boldsymbol{\Gamma}$ is the contour of integration. Computing the integral on the contour $\boldsymbol{\Gamma}$ is still not a easy thing to do, especially if the number of turn comprising the winding is not known. For ease of calculation, an equivalent computation is done on the volume of the winding. It is written as:

$$\boldsymbol{\phi} = \iiint_{\mathbf{V}} \mathbf{A} \cdot \frac{\mathbf{J}}{\mathbf{I}} \cdot \mathrm{d}\mathbf{V} \tag{3.3}$$

where $\mathbf{J}$ is the current density vector and $\mathbf{I}$ is the current vector. It respects the dimension of a magnetic flux. The ratio $\frac{\mathbf{J}}{\mathbf{I}}$ corresponds to the ratio of the current density over the current both injected in the windings, which correponds to a vector that indicates the direction of the conductors. In practice, to determine magnetic flux only coming from PM to obtain the flux constants, there must be no current into the windings. Therefore to be able to perform this integral, virtual currents are injected into the windings. To determine the total flux, the expression above has to be multiplied by the number of pole pairs p. However, to compute inductance coefficient, current is needed in the windings, unless the ratio $\frac{\mathbf{J}}{\mathbf{I}}$ is known. The relation between the inductance coefficient and the flux is:

$$\mathrm{L} = \frac{\phi}{\mathrm{I}}$$

where I is the current circulating in the windings.

3.2.2 Flux constants

Firstly, the total flux arising from the PM and intercepted by the windings has been characterised. Its expression developed in Section 2.2.2 is based on two parameters: K_{θ_m} and K_z. These two parameters are obtained by computing the flux of the PM intercepted by the windings for different axial positions of the rotor. By applying Equation 3.3, one evaluation over the volume of interest is sufficient to determine the total flux coming from the PM.
Furthermore, the angular position of the rotor is fixed such that the flux reaches its maximum value. This gives the following expression:

$$\begin{cases} \Phi_{U,k}(\theta_m = 0, z) = (K_{\theta_m} + zK_z) \\ \Phi_{L,k}(\theta_m = 0, z) = (K_{\theta_m} - zK_z) \end{cases}$$

with $k = 1, 2, 3$

Thus by evaluating the flux in the centred position, K_{θ_m} is obtained:

$$K_{\theta_m} = \Phi_k(\theta_m = 0, z = 0)$$

Then by changing the axial position of the rotor,$z = z_1$ with $z_1 \neq 0$, a second value of flux is computed, which permits to derive the value of K_z:

$$K_z = \frac{\Phi_{U,k}(\theta_m = 0, z = z_1) - \Phi_{U,k}(\theta_m = 0, z = 0)}{z_1} = \frac{\Phi_{U,k}(\theta_m = 0, z = z_1) - K_{\theta_m}}{z_1}$$

3.2.3 Inductance coefficients

Secondly, the inductance coefficients detailed in the list above have to be determined. Models 3.3a and 3.3b together give $L_2 + M_2$ and $L_0 + M_{ii}$ and the one depicted in Figure 3.4 is used to find out the coefficients L_{sd}, L_{sq}, dL_d and dL_q. Contrarily to the flux model, no PM is needed but in this case current circulates into the coils.

In order to determine the coefficients $L_2 + M_2$ and $L_0 + M_{ii}$ using the single-phase models, current is directly injected in upper windings. Through boundaries conditions this current is virtually injected in the lower windings in the opposite direction, respecting the formalism presented in Figure 1.11.

$$\begin{cases} L_x = \frac{\Phi_k}{I_k}(\theta_m = 0) = L_0 + L_2 + M_{ii} + M_2 & (d - axis) \\ L_y = \frac{\Phi_k}{I_k}(\theta_m = \frac{\pi}{2p}) = \underbrace{L_0 - L_2}_{i_{a,U}=1} + \underbrace{M_{ii} - M_2}_{i_{a,L}=1} & (q - axis) \end{cases}$$

The first model, aligned on the d-axis, gives the inductance coefficient L_x while the second, aligned on the q-axis, returns L_y. Then by recombining theses two results the needed coefficients are obtained:

$$\begin{cases} L_2 + M_2 = \frac{L_x - L_y}{2} \\ L_0 + M_{ii} = \frac{L_x + L_y}{2} \end{cases}$$

Contrarily to the two previous models, the third one is a two-phase model. In order to determine the needed coefficients and due to the geometry of the rotor, symmetry is not possible. This leads to a full model of the machine and so a longer computation time. The current is injected in both upper windings and lower windings of both phases with the same magnitude. The currents in the upper windings of phase a and in the lower windings of phase b, $i_{a,U}$ and $i_{b,L}$, are positive regarding the convention of the mating terminals described in Section 1.2.1. On the other hand the upper windings of phase b and the lower windings of phase a, $i_{b,U}$ and $i_{a,L}$ are negative regarding the convention. It permits in centred axial position to deduce the value of $L_{S,d}$ and $L_{S,q}$. $L_{S,d}$ is obtained when the rotor is aligned with the d-axis and $L_{S,q}$ is computed when the rotor is aligned with the q-axis. Although the stator geometry has changed the integration volume has not. The numerical integration is still done on one upper or lower winding of one phase. This can be summarised as:

$$\begin{cases} L_{S,d} = \frac{\Phi_k}{I_k}(\theta_m = 0) = L_0 + L_2 - (M_0 + L_2\cos(\frac{2\pi}{3})) - (M_{ii} + M_2) + (M_{ij} + M_2\cos(\frac{2\pi}{3})) \\ L_{S,q} = \frac{\Phi_k}{I_k}(\theta_m = \frac{\pi}{2p}) = \underbrace{L_0 - L_2}_{i_{a,U}=1} \underbrace{-(M_0 - L_2\cos(\frac{2\pi}{3}))}_{i_{b,U}=-1} \underbrace{-(M_{ii} - M_2)}_{i_{a,L}=-1} + \underbrace{(M_{ij} - M_2\cos(\frac{2\pi}{3}))}_{i_{b,L}=1} \end{cases}$$

Once these simulations are done, the axial position of the rotor is changed ($z \neq 0$) in order to evaluate the coefficients dL_d and dL_q. Consequently, by calculating the flux along the d-axis and the q-axis for two axial positions, these coefficients can be determined using a linear approximation.

$$dL_d = \frac{L_{sd}(z \neq 0) - L_{sd}(z = 0)}{\Delta z} \qquad dL_q = \frac{L_{sq}(z \neq 0) - L_{sq}(z = 0)}{\Delta z}$$

3.3 Assumption validation

Simulations have been realised to validate the assumptions on which the analytical model relies. Among the assumptions this Section focuses on the dominance of the fundamental component of magnetic flux and the inductance coefficients. After that, the linearity of the magnetic flux and the inductance coefficients with the axial position of the rotor is verified. And from that, the independence of the mutual inductance coefficient with the axial rotor position is shown. The validation is based on a six pole pairs machine. Its geometrical dimensions are arbitrary chosen but of the same order of magnitude as the ones used for the last prototype described in [1]. They are summarised in the following table:

Table 3.1: **Rotor**.

H_a[mm]	H_f[mm]	G_{ouv}[°]	P_{ouv}[°]	**p**
8.3	2	11	7	6

Table 3.2: **Stator**.

h_w[mm]	R_1[mm]	R_2[mm]	$R_{w,i}$[mm]	$R_{w,o}$[mm]	t_w[mm]
44	28.9	48	25.1	51.8	3.8

Main dimensions of the rotor and the stator

3.3.1 Dominance of the fundamental harmonic

Magnetic flux

Based on the model described in Figure 3.2a, a parametric sweep is done on the mechanical angular position of the rotor over one electrical period, $\frac{2\pi}{p}$. At each angular step, the flux intercepted by the windings is computed. As it is represented in Figure 3.5a, the flux has a sinusoidal shape. Indeed, by inspecting the harmonic content depicted in Figure 3.5b, the fundamental is dominant over the others. For example the second and third harmonics represent respectively 3.2 % and 3.5% of the fundamental which is negligible. Therefore, it is reasonable to neglect all the others harmonics as it is said in assumption 5.

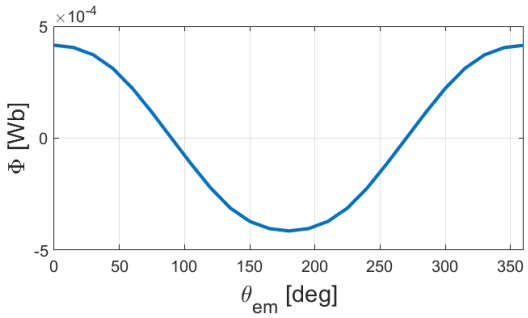

(a) Amplitude variation according to the electrical angular position.

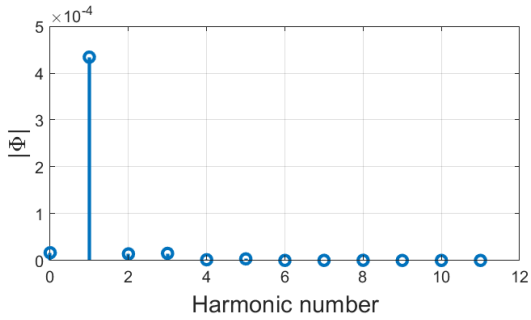

(b) Harmonic content of an electrical period (60 mechanical degrees).

Figure 3.5: Axial component of the magnetic flux for a six pole TLST Machine.

Inductance coefficients

Then, the harmonic content of the inductance coefficients listed here below is analysed. The model used to derive these coefficients is shown in Figure 3.4. Conversely to subsection 3.2.3, the current is here only injected in upper windings of phase a, positively in relation to the convention. As for the flux constants, a parametric sweep on the angular position of the rotor is done over one electrical period.

- $L_{U_a} = L_0 + L_2 \cdot \cos(2\theta_{em})$, the self-inductance of the upper windings of phase a;
- $M_{U_aU_b} = M_0 + L_2 \cdot \cos(120 + 2\theta_{em})$, the mutual inductance coefficient between the upper windings of phase a and the upper windings of phase b;
- $M_{U_aL_a} = M_{ii} + M_2 \cdot \cos(2\theta_{em})$, the mutual inductance coefficient between the upper and lower windings of phase a;

- $M_{U_aL_b} = M_{ij} + M_2 \cdot \cos(120 + 2\theta_{em})$, the mutual inductance coefficient between the upper windings of phase a and lower windings of phase b;

As shown in Figure 3.6a, L_{U_a} is obtained by measuring the flux intercepted by the upper windings of phase a. Then the mutual inductance coefficient between phase a and b of upper windings, $M_{U_aU_b}$, is measured on upper windings of phase b as depicted in Figure 3.6b.

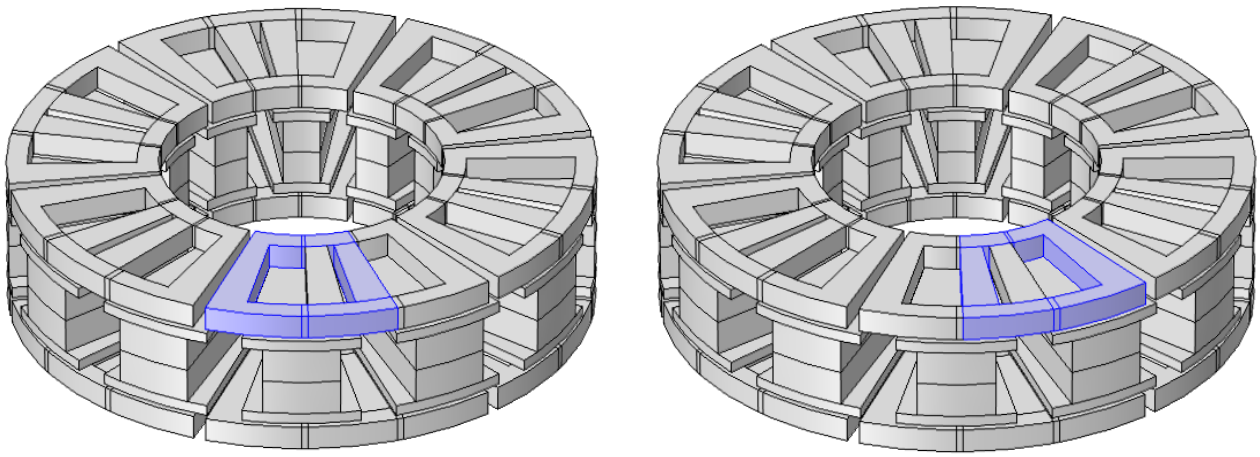

(a) L_{U_a} integration volume.

(b) $M_{U_aU_b}$ integration volume.

Figure 3.6: Representation on the model of the inductance coefficients L_{U_a} and $M_{U_aU_b}$.

The third coefficient, $M_{U_aL_a}$ is calculated on lower windings of phase a, as highlighted in Figure 3.7a. After that, the mutual inductance coefficient between the upper windings of phase a and the lower windings of phase b, $M_{U_aL_b}$is computed on lower windings of phase b as presented in Figure 3.7b.

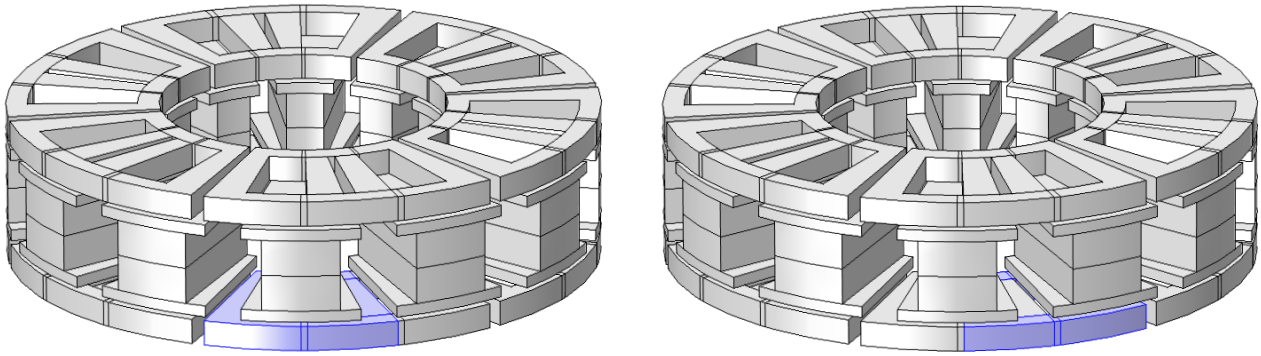

(a) $M_{U_aL_a}$ integration volume.

(b) $M_{U_aL_b}$ integration volume.

Figure 3.7: Representation on the model of the inductance coefficients $M_{U_aL_a}$ and $M_{U_aL_b}$.

Contrarily to the magnetic flux and as expected by assumption 8 and equation 2.1, the period of the coefficient is two times smaller, thus the fundamental harmonic is harmonic number two on the following graphs. In Figures 3.8b and 3.9b, the DC components are removed in order to properly observe the impact of the different harmonics. L_{U_a} has a less sinusoidal shape than the magnetic flux as it is shown in Figure 3.8a. Indeed, one can see in Figure 3.8b that harmonic number six has an negative impact. It represents 5.7% of the fundamental. Furthermore, harmonics number 1, 3, 4, respectively represent 4.1%, 3%, and 2.6% of the fundamental.

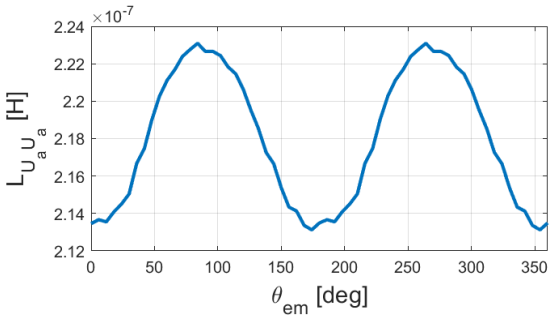

(a) Amplitude variation according to the electrical angular position.

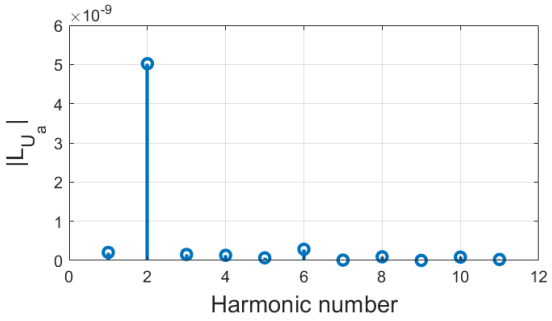

(b) Harmonic content of an electrical period (30 mechanical degrees), the continuous component has been suppressed for clarity reason.

Figure 3.8: L_{U_A}, the self inductance of one phase for a six pole TLST Machine.

Then for $M_{U_aU_b}$ this negative impact is even bigger, as depicted in Figures 3.9a and 3.9b, it looks like a combination of multiple sinusoidal waves at different frequencies. Harmonic number four represents 87.3% of the fundamental and other harmonics have also an impact. The origin of the non-sinusoidal form of this mutual inductance will be discussed in the following pages. Finally the two last coefficients $M_{U_aL_a}$ and $M_{U_aL_b}$ have a more sinusoidal shape. Harmonics number four and one represent respectively 16.2% and 5% for $M_{U_aL_a}$ and 6.8% and 2.8% for $M_{U_aL_b}$. Although these values are bigger than for L_{U_a}, the impact of the other harmonics is smaller than for L_{U_a}. Therefore assumption 6 is verified for $M_{U_aL_a}$, $M_{U_aL_b}$. This assumption is weaker for L_{U_a} and is not verified for $M_{U_aU_b}$. However the variation of amplitude of this inductance coefficient is one order of magnitude smaller than L_{U_a}, thus although this assumption is not verified, the modelling done previously will not be significantly impacted.

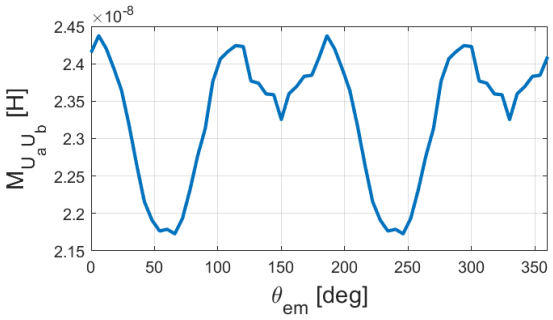

(a) Amplitude variation according to the electrical angular position.

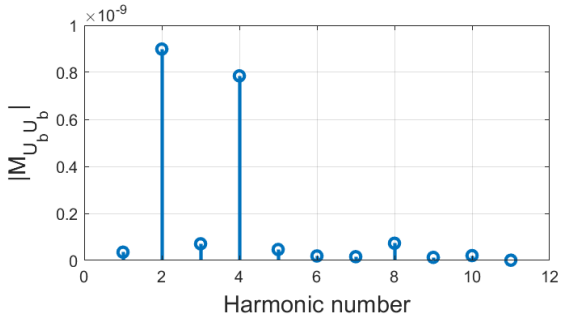

(b) Harmonic content of an electrical period (30 mechanical degrees), the continuous component has been suppressed for clarity reason.

Figure 3.9: $M_{U_aU_b}$, the mutual inductance between two phases of the upper winding for a six pole TLST Machine.

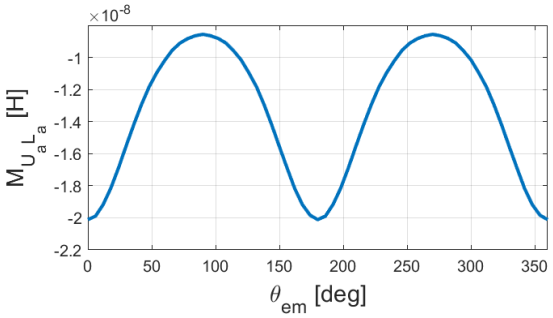

(a) Amplitude variation according to the electrical angular position.

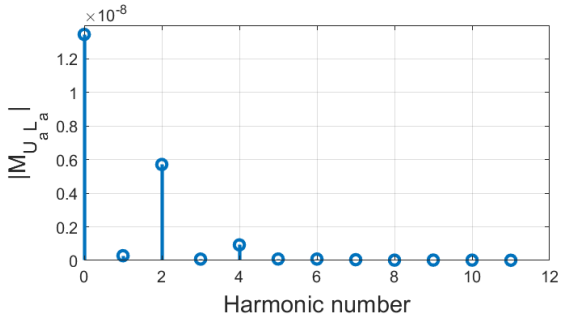

(b) Harmonic content of an electrical period (30 mechanical degrees).

Figure 3.10: $M_{U_aL_a}$, the Mutual inductance between upper and lower winding of one phase for a six pole TLST Machine.

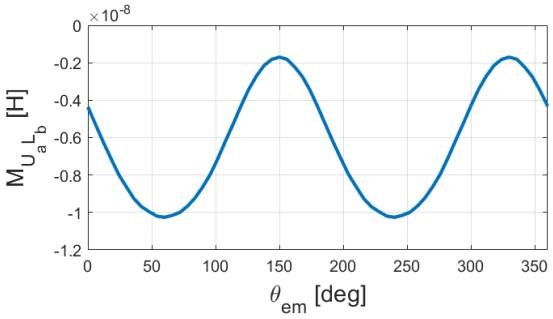

(a) Amplitude variation according to the electrical angular position.

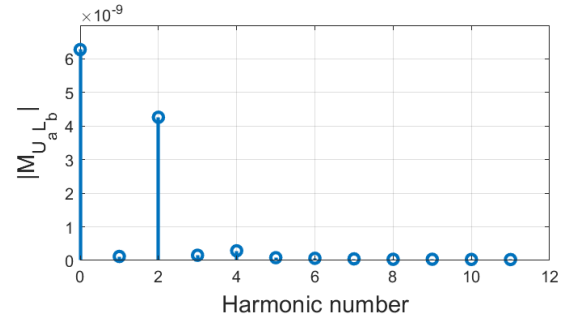

(b) Harmonic content of an electrical period (30 mechanical degrees).

Figure 3.11: $M_{U_aL_b}$,the mutual inductance between a phase of an upper winding and another for a lower winding for a six pole TLST Machine.

Origin of the non-sinusoidal form of the mutual inductance between two phases of the upper winding

As shown in Figure 3.9, the mutual inductance between two phases of the upper windings is mainly composed of two sinusoidal functions, the second and fourth harmonic. It results in a mutual inductance coefficient which has a minimum value when the rotor is shifted by 60 electrical degrees with respect to the magnetic axis of phase "a" and two maxima in $\theta_{em} = 114°$ and 186°. A local minimum is also present for the angular position $\theta_{em} = 150°$. These four situations are represented in Figure 3.12.

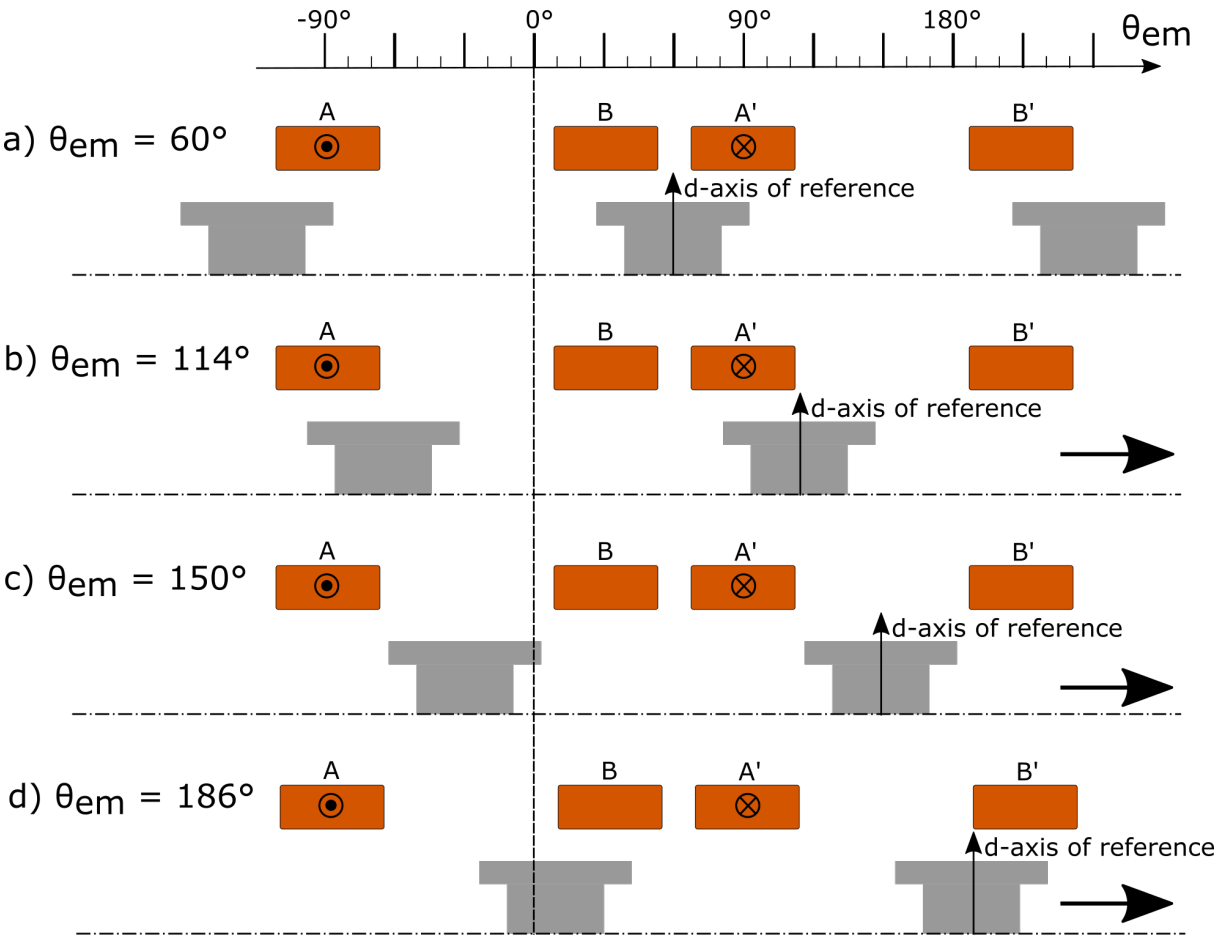

Figure 3.12: Unrolled view of the TLST rotor and overlapped windings, with proportions corresponding to the Tables 3.1 and 3.2. The d-axis of the rotor is shifted of a) 60, b) 114, c) 150 and d) 186 electrical degrees with respect to the magnetic axis of the phase "a".

The minimum value of the inductance appears when only one ferromagnetic part is involved in the magnetic circuit which links phase "a" and "b", as shown on Figure 3.12.a. Indeed the two other ferromagnetic parts are on the outside of the angular span covered by the two phases, then the reluctance has a maximum value for this configuration. For the three other cases, two ferromagnetic parts are fully inside this angular span, which reduce the reluctance of the magnetic circuit and explain the higher value of the inductance for these positions.

The local minimum appears when the ferromagnetic parts are centred between the windings of two different phases where the current, if it was injected in both phases, would flow in the same direction (as shown on Figure 3.12.c). It may lead to believe that no local minimum appears for non-overlapped windings since this situation no longer exists with this type of winding, which means that the assumption could be verified for concentrated winding.

The situations (presented on Figure 3.12.b and 3.12.d) form magnetic circuits which are symmetric, which result to identical values of inductance. The maximum value of the inductance is reached when the center of the ferromagnetic part and the end of the winding are aligned[1].

3.3.2 Linearization with respect to the axial position of the rotor

The models used in the subsection 3.3.1 are evaluated for seven different axial rotor positions.

Linearization of the flux coming from PM

By doing these simulations to obtain the values of the flux, one can observe in Figure 3.13 that the magnetic flux is increasing when the rotor is approaching the upper windings and inversely. The coefficient of determination R^2 expressed on Figure 3.13 allows to evaluate the quality of the linear approximation. The closer to 1, the better the linear approximation. Based on these results, assumption 7 is verified for the magnetic flux.

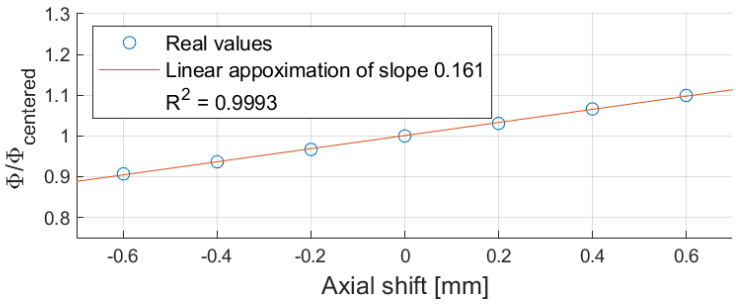

Figure 3.13: Relative variation of the flux intercepted by upper windings according to the axial shift of the rotor.

Linearization of the inductance coefficients

In addition to the seven simulations, in order to isolate the different inductance coefficients, the models are also evaluated on two different angular positions: one time on the d-axis and the other one on the q-axis. As shown in Figures 3.14a, 3.14c, and 3.14b the

[1] In reality, the dimensions of the model are such that both elements are aligned for a angular position $\theta_{em} = 112.5°$ and $\theta_{em} = 187.5°$, but these positions have not been evaluated by the simulation since the inductance have been measured for every mechanical degree, which corresponds to 6 electrical degrees.

inductance coefficients are increasing with the axial shift of the rotor. Once again, the coefficient of determination R^2 allows to validate assumption 7 for the coefficients L_2, L_0 and M_0.

Then the mutual inductance coefficients between upper and lower windings represented in Figures 3.15a, 3.15c can be assumed as constant with respect to the rotor axial position, as assumed in 2.2.3. Indeed the slope of the linear approximation is nearly zero. The small variance of the measurements expressed in Figures 3.15a, 3.15c allows to consider these coefficients as constant[2]. In Figure 3.15b, a slope of -3.1% per [mm] is observed despite the constant value assumption made in 2.2.3. However, as shown in Figure 3.11a, this inductance coefficient varies little and is one order of magnitude smaller than the two others, so its dependency can be assumed as negligible. Thus as assumed in Section 2.2.1.b, the mutual inductance coefficients between upper and lower winding can be considered as constant with respect to the axial position of the rotor.

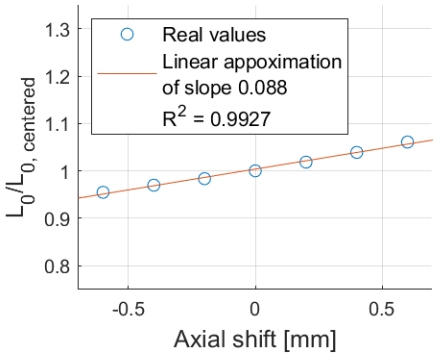

(a) L_0, the mean value of the self inductance of the upper winding of one phase.

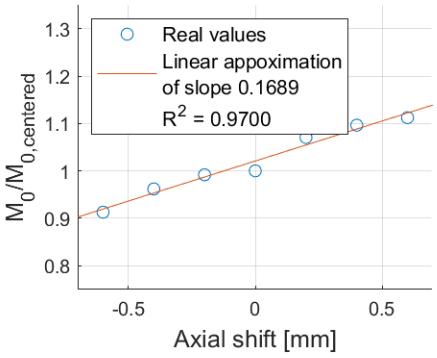

(b) M_0, the mean value of the mutual inductance of upper winding between two phases.

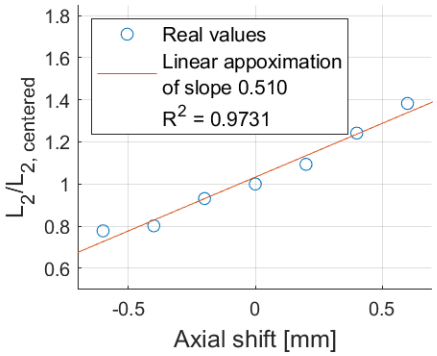

(c) L_2, the amplitude of angular variation of coefficients L_0 and M_0.

Figure 3.14: Relative variation of the terms of equation 2.1 according to the axial position of the rotor.

[2]This time, the coefficient R^2 is not relevant due to the almost constant value of the measurements. Indeed R^2 measures the correlation between two variables, if one of these variables is constant, their is no correlation and then the coefficient R^2 is nearly equal to zero

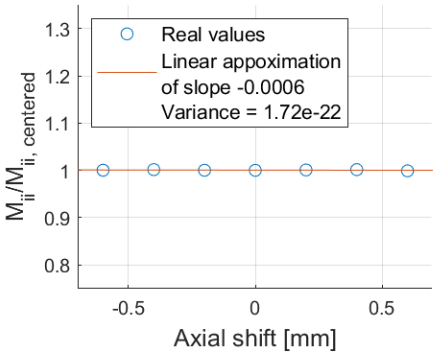

(a) M_{ii}, the mean value of the mutual inductance between the upper and the lower winding of the same phase.

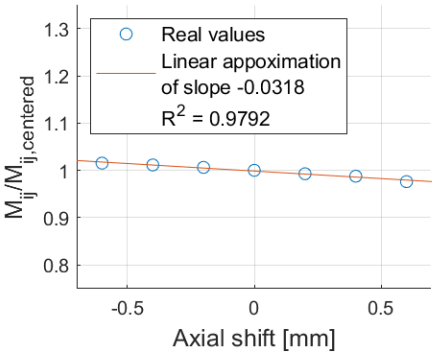

(b) M_{ij}, the mean value of the mutual inductance between the upper and the lower winding of two different phases.

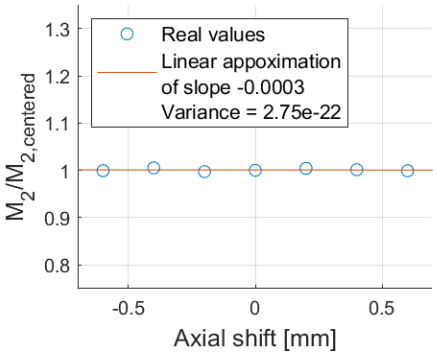

(c) M_2, the amplitude of angular variation of coefficients M_{ii} and M_{ij}.

Figure 3.15: Relative variation of the terms of equation 2.5 according to the axial position of the rotor.

3.4 Conclusions

This chapter presented the two families of finite element models, one for the flux constants related to the flux coming from the PM and the other for all the inductance coefficients. They aim to first determine parameters such as the flux constants and the required inductance coefficients and secondly to validate assumptions 5, 7, 8 through simulations. Limitations encountered during modelling led to several big models although the objective was to have fast computation while being accurate. The methodology applied is based on the volume integral of the product between the magnetic potential vector and the quotient between the current density and the current. Concerning the dominance of the fundamental harmonic, it appears to be reasonable for the coefficients L_a, $M_{U_aL_a}$ and $M_{U_aL_b}$. However this is a big assumption for the coefficient $M_{U_aU_b}$. Then regarding the linearity with respect to the axial rotor position is acceptable for the flux, L_0, M_0 and L_2. Finally the independence with respect to this axial position is also acceptable for the coefficients M_{ii}, M_{ij} and M_2. Even though M_{ij} changes with the axial position, its variation is very limited and the value of this coefficient is one order of magnitude below the two other coefficients.

CHAPTER 4

OPTIMISATION AND COMPARISON

This chapter presents and develops the optimisation processes used in order to optimally sized the machine. Section 4.1 details the objectives of the optimisation and the two optimisation processes applied on the design chosen in Chapter 1, using the FEM models presented in Chapter 3. On the one hand the d-axis motor current $I_{M,d}$ is fixed to zero and on the other hand it is considered as different from zero into the process. Finally, a comparison between the two optimised machines is done in Section 4.2 in order to choose a study case to characterise in next chapter.

4.1 Optimal sizing process

This section presents the optimal approach used to size the rotor of the machine. Besides the optimal sizing, two objectives are followed during the process. They consist of minimising the losses while maximising the total axial stiffness of the machine. The algorithm used to realise this study is an NSGA-II genetic algorithm. It applies variable dimensions to a set of initial candidates, each candidate representing a machine. Then based on the performances computed the algorithm keeps the best candidates and do mutation and crossing with them. After that, the algorithm proceeds to another evaluation with the new candidates. This algorithm has been chosen because it is already used in [1] for another optimisation process. Some performances and dimensions are already fixed and are based on the results obtained in [1]: The machine has to produce a torque of 7.5 [mNm] at a rotating speed of 14000 [rpm] while using a fixed Volume of Permanent Magnet (VPM) corresponding to the dimensions of the rotor described in [20]. This volume is $4.1 \cdot 10^{-5}$ [m^3]. The dimensions of a stator winding are the same as the one presented in Table 3.2 except for h_w which is a parameter of the optimisation. Two optimisations processes are realised in parallel. Their difference lies in the problem formulation. Indeed, firstly no $I_{M,d}$ current is considered. Then in the second process, this current is taken into account in the torque and Joule losses computation, and the results of the optimisations are compared.

4.1.1 Optimisation parameters

Five parameters are used to do the optimisations of the TLST machine. There are listed here below:

- C_{h_w}, a coefficient that fixed the height of a winding;
- g_{ouv}, a coefficient that fixed the angular span of a ferromagnetic part;
- p_{ouv}, a coefficient that fixed the angular span between two PM;
- h_f, a coefficient that fixed the height of superior ferromagnetic part;
- p, the number of pole pairs;

Among them, g_{ouv}, p_{ouv}, h_f and p dictate the dimensions of the PM while C_{h_w} and p fix the dimensions of the winding. The number of pole pairs, p, belongs to the interval [5; 10], which has been arbitrary chosen. The coefficients g_{ouv}, p_{ouv}, h_f, $C_{h_w} \in [0;1]$. Based on their values, they respectively fixed the dimensions G_{ouv}, P_{ouv}, H_f and h_w reminded in Figures 4.1a and 4.1b. The height H_a is deduced from the other dimensions to conserve the VPM fixed before.

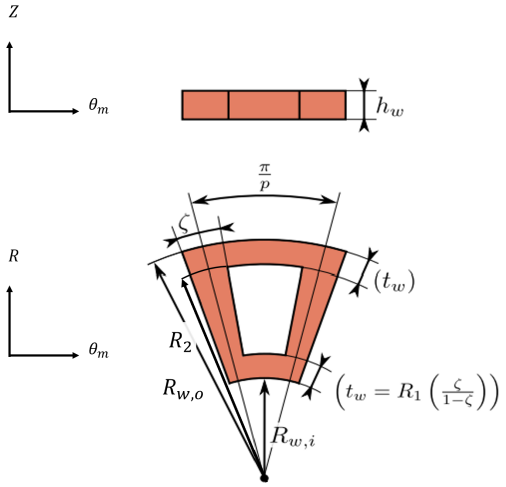

(a) Overlapping coils geometry [53].

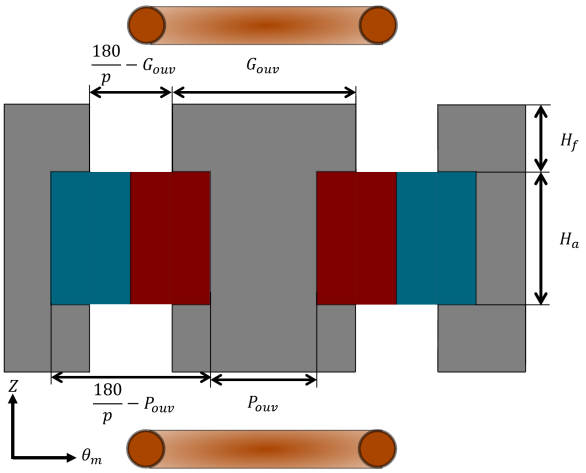

(b) Design parameters of the rotor.

Figure 4.1: Winding and rotor configuration.

Furthermore, to avoid mesh problems minimum and maximum values are imposed for G_{ouv}, P_{ouv}, H_f. The coefficients g_{ouv} and p_{ouv} must respect the following arbitrary condition to conserve a TLST rotor shape: $g_{ouv} - p_{ouv} > 0.2$. To keep reasonable winding dimensions, h_w is also fixed between two values. These dimensions are summarised in Table 4.1:

Table 4.1: **Minimum and maximum dimensions**.

G_{ouv}[°]	P_{ouv} [°]	H_f [mm]	h_w [mm]
$[\frac{180}{6p}; \frac{180 \cdot 5}{6p}]$	$[\frac{180}{6p}; \frac{180 \cdot 5}{6p}]$	[2; 12.5]	[4; 8]

4.1.2 Problem formulation

This section consists of deriving the problem formulation related to the two optimisation processes. First, the case without the current $I_{M,d}$ is considered and then the second part of the section is dedicated to the case with $I_{M,d} \neq 0$.

Optimisation with $I_{M,d} = 0$

Although the rotor contains ferromagnetic parts, iron losses are arbitrary assumed as negligible as well as the windage losses. It is also assumed that no external force $F_{z,e}$ is applied on the rotor. Therefore the machine stabilises itself in a centered position, $z = 0$. Among all the losses, it remains the Joule losses coming from the circulation of the motor current $I_{M,q}$. Since $I_{M,d} = 0$ and the rotor is in an axial centered position, the torque is purely electrodynamic. As explained in Chapter 2, this current is linked to the driving torque $T_{\theta_m,M}$ through Equation 2.37. Thus the current can be express as:

$$I_{M,q} = \frac{T_{\theta_m,M}}{\sqrt{\frac{3}{2}} p K_{\theta_m}} \tag{4.1}$$

The power losses, the first objective function, can be written as:

$$P_M = \frac{R}{2} \cdot I_{M,q}^2 \tag{4.2}$$

with R the total resistance of the windings which depends on the parameter h_w and evaluate thanks to the Pouillet's law.

Secondly, by taking the expressions of the electrodynamic axial force given by equation 2.61 and the detent axial force given by equation 2.38, the expression of the second objective function, the stiffness in axial centred position can be obtained:

$$\begin{aligned} k_{z,tot}|_{z=0} =& -\frac{F_{z,Ed} + F_{z,d}}{z} \\ =& \sqrt{\frac{3}{2}} \cdot K_z \left[\frac{dL_q}{R} \cdot \left(\frac{\omega^2}{\left[\frac{R^2}{p^2 L_{S,d} L_{S,q}} + \omega^2 \right]} - 1 \right) \cdot p\omega \cdot I_{M,q} + \frac{\omega^2}{\left[\frac{R^2}{p^2 L_{S,d} L_{S,q}} + \omega^2 \right]} \cdot \left[\sqrt{6} \cdot \frac{K_z}{L_{S,d}} \right] \right] \\ &+ k_{z,d} \end{aligned}$$

The coefficient $k_{z,d}$ is fixed to 0 during the optimisation process.

Optimisation with $I_{M,d} \neq 0$

If we now consider the motor current $I_{M,d} \neq 0$, the expression of the power losses changes and a reluctant torque component appears. By combining the electrodynamic and the reluctant component of the torque, one can derive the total torque in axial centered position:

$$T_{\theta_m,tot}|_{z=0} = \sqrt{\frac{3}{2}} \cdot p K_{\theta_m} \cdot I_{M,q} + 3p \cdot (L_2 + M_2) \cdot \left[\frac{I_{M,d} I_{M,q}}{2} \right] \tag{4.3}$$

As both current are now implied in the total torque, they must be fixed. Then the pair of current is chosen to minimise the Joule losses while providing the total torque of 7.5 [mNm].

Due to the new current implied in the joule losses, the first objective function becomes:

$$\mathrm{P_M} = \frac{\mathrm{R}}{2} \cdot (\mathrm{I_{M,q}^2} + \mathrm{I_{M,d}^2}) \tag{4.4}$$

And the total axial stiffness[1] in $\mathrm{z} = 0$ is still the second objective. Its expression, which takes into account the direct current, can be expressed as:

$$\begin{aligned} \mathrm{k_{z,tot}}|_{\mathrm{z}=0} = & \left(\sqrt{\frac{3}{2}} \cdot \mathrm{K_z} + \frac{\mathrm{I_{M,d}} \cdot \mathrm{dL_d}}{2} \right) \cdot \left[\frac{\mathrm{dL_q}}{\mathrm{R}} \cdot \left(\frac{\omega^2}{\left[\frac{\mathrm{R}^2}{\mathrm{p}^2 \mathrm{L_{S,d}} \mathrm{L_{S,q}}} + \omega^2 \right]} - 1 \right) \cdot \mathrm{p}\omega \cdot \mathrm{I_{M,q}} \right. \\ & \left. + \frac{\omega^2}{\left[\frac{\mathrm{R}^2}{\mathrm{p}^2 \mathrm{L_{S,d}} \mathrm{L_{S,q}}} + \omega^2 \right]} \cdot \left[\frac{\mathrm{dL_d}}{\mathrm{L_{S,d}}} \cdot \mathrm{I_{M,d}} + \sqrt{6} \cdot \frac{\mathrm{K_z}}{\mathrm{L_{S,d}}} \right] \right] \\ & + \mathrm{I_{M,q}} \cdot \frac{1}{2\mathrm{p}} \cdot \frac{\mathrm{R}}{\mathrm{L_{S,d}} \mathrm{L_{S,q}}} \cdot \frac{\omega}{\left[\frac{\mathrm{R}^2}{\mathrm{p}^2 \mathrm{L_{S,d}} \mathrm{L_{S,q}}} + \omega^2 \right]} \cdot \left[\frac{\mathrm{L_{S,d}} \cdot \mathrm{dL_q}}{\mathrm{R}} \cdot \mathrm{p}\omega \cdot \mathrm{I_{M,q}} + \mathrm{dL_d} \cdot \mathrm{I_{M,d}} + \sqrt{6} \cdot \mathrm{K_z} \right] \cdot \mathrm{dL_q} \end{aligned} \tag{4.5}$$

Both optimisation process can be formulated as follow:

$$\begin{aligned} & \text{minimise } \mathrm{P_M} \text{ and maximise } \mathrm{k_{z,tot}}, \\ & \{\mathrm{C_{h_w}}, \mathrm{g_{ouv}}, \mathrm{p_{ouv}}, \mathrm{h_f}, \mathrm{p}\} \\ & \text{subject to VPM} = 4.1 \cdot 10^{-5} \ [\mathrm{m^3}], \\ & \mathrm{T_{\theta_m,tot}} = 7.5 \ [\mathrm{mNm}], \\ & \omega = \frac{1400\pi}{3} \ [\mathrm{rad/s}], \\ & \mathrm{g_{ouv}}, \mathrm{p_{ouv}}, \mathrm{h_f}, \mathrm{C_{h_w}} \in [0; 1], \\ & \mathrm{p} \in [5, 10], \\ & \mathrm{g_{ouv}} - \mathrm{p_{ouv}} > 0.2, \\ & \mathrm{h_w} \in [4; 8] \ [\mathrm{mm}], \\ & \mathrm{G_{ouv}}, \mathrm{P_{ouv}} \in \left[\frac{180}{6\mathrm{p}}; \frac{180 \cdot 5}{6\mathrm{p}} \right] \ [^\circ], \\ & \mathrm{H_f} \in [2; 12.5] \ [\mathrm{mm}] \end{aligned}$$

[1] Developments available in Appendix G.2

4.1.3 Results

In this section the results of the optimisation process are presented. First, the results without $I_{M,d}$ are detailed and then the second results take it into account. As it is noticeable in the following figures, the Pareto[2] front is not yet achieved. This is due to the facts that some models, as described in section 3.1, are not symmetrised and thus take a lot of time to run. Then the optimisation processes have been stopped because of the lack of time. The most important results will be discussed here, and Figures representing the evolution of the main geometrical dimensions with respect to the objective functions are available in Appendix H.

Optimisation with $I_{M,d} = 0$

The results show that the process tends to high values of pole pairs. However, when $p > 9$, the performances decrease, as represented in Figure 4.2. Among the three points of the Pareto front shown in Figure 4.2, the higher the number of pole pair the higher the stiffness but also the higher the Joule losses. However the stiffness start to decrease when the number of pole pair is equal to 10. Between the case with $p = 7$ and the one with $p = 9$ the stiffness increases by 52.3% while the Joule losses increase by 6.7%. As a consequence $p = 9$ is chosen. Then between the two machines with $p = 9$, the stiffness increases by 14.7% while the Joule losses increase by 4.5%. Therefore the machine with higher stiffness and losses is selected. It develops a stiffness of 112 [N/mm] and losses of 3 [mW]. The parameters of this machine are summarised in Tables 4.2 and 4.3.

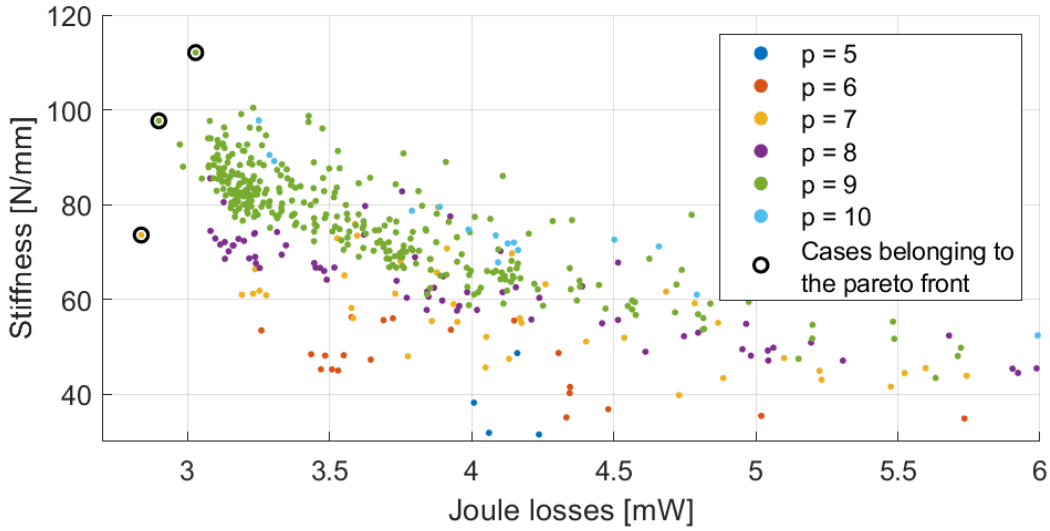

Figure 4.2: Stiffness and Joule losses obtained for each candidate tested during the first optimisation. Each candidate is coloured according to its number of pole pair p.

[2]During the rest of the chapter, the term Pareto front will be used to describe the best candidates although this is not yet a Pareto front.

Table 4.2: **Rotor**.

H_a[mm]	h_f	H_f[mm]	g_{ouv}	G_{ouv}[°]	p_{ouv}	P_{ouv}[°]	p
11.5	0	2	0.812	14.2	0.415	8.9	9

Table 4.3: **Stator**.

h_w[mm]	R_1[mm]	R_2[mm]	$R_{w,i}$[mm]	$R_{w,o}$[mm]	t_w[mm]
49	27.5	49.4	25.1	51.8	2.4

Main optimised dimensions of the rotor and the stator.

As it can be seen in Table 4.2, the coefficient h_f is equal to zero. Thus the height H_f is equal to its minimum value, 2 [mm]. This means that the process tends to reduces this height of ferromagnetic material as much as possible. Lower this coefficient, better the performances as depicted in Figure 4.3. This observation highlight some design amelioration which will be discussed in Chapter 5.

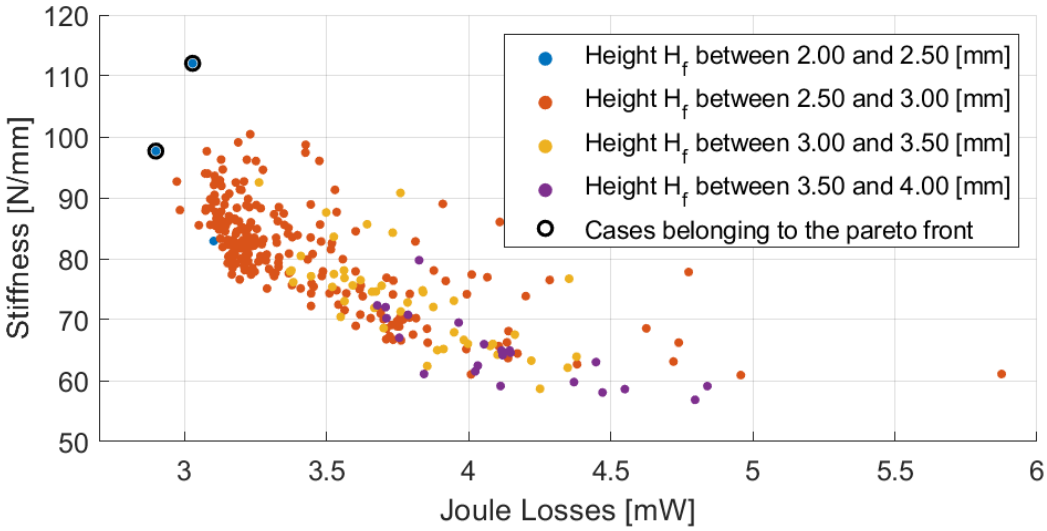

Figure 4.3: Stiffness and Joule losses obtained for all candidates where p = 9 during the first optimisation. Each candidate is coloured according to its height H_f.

Optimisation with $I_{M,d} \neq 0$

When $I_{M,d} \neq 0$, as highlighted in Figure 4.4, p = 9 and p = 10 belong to the Pareto front. Between the two available points, there is a stiffness increase of 4.8% and Joule losses increase by 17.5%. Therefore the machine with p = 9 is chosen because of smaller Joule losses. It is characterised by a stiffness of 100 [N/mm] and Joule losses of 2.9 [mW] for the given torque. Its optimised dimensions are listed in Tables 4.4 an 4.5.

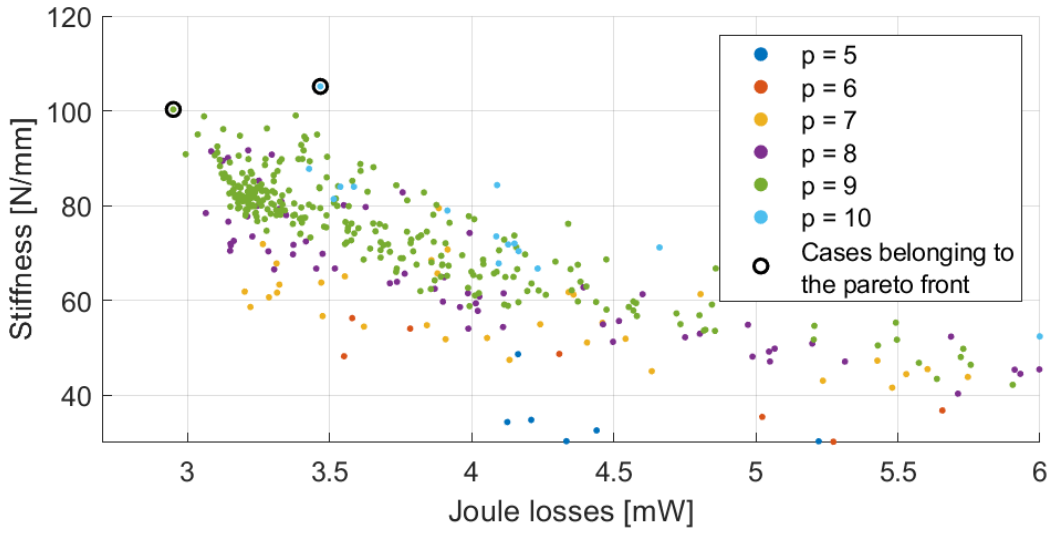

Figure 4.4: Stiffness and Joule losses obtained for each candidate tested during the second optimisation. Each candidate is coloured according to its number of pole pair p.

Table 4.4: **Rotor**.

H_a[mm]	h_f	H_f[mm]	g_{ouv}	G_{ouv}[°]	p_{ouv}	P_{ouv}[°]	**p**
11.5	0.06	2.6	0.665	12.2	0.419	8.9	9

Table 4.5: **Stator**.

h_w[mm]	R_1[mm]	R_2[mm]	$R_{w,i}$[mm]	$R_{w,o}$[mm]	t_w[mm]
51	27.5	49.4	25.1	51.8	2.4

Main optimised dimensions of the rotor and the stator.

Once again, the coefficient h_f is nearly equal to zero and thus H_f is close to its minimum. In fact, as shown in Figure 15, this process tends also to reduce this height.

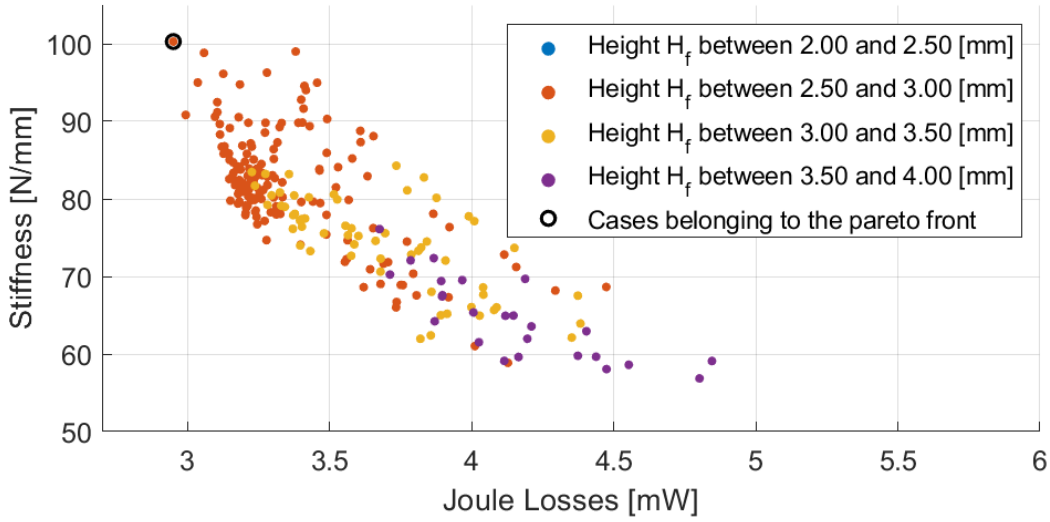

Figure 4.5: Stiffness and Joule losses obtain for all candidates where p = 9 during the second optimisation. Each candidate is coloured according to its height H_f.

4.2 Comparison of the performances of the optimised machines

As it is noticeable in the previous tables, the two machines tend toward similar dimensions. However, there are differences in the resulting performances. Indeed the stiffness increases by 12% and losses increase by 3.4% when no current $I_{M,d}$ is considered. Thus by considering motor current on the d-axis, the optimisation process leads to a lower the axial stiffness but also to lower Joule losses. By taking the optimal machine obtained with $I_{M,d} \neq 0$ and by equalling this current to zero, no difference is observed in terms of stiffness and losses. In fact, $I_{M,d}$ represents 1.8% of $I_{M,q}$ and thus the impact of $I_{M,d}$ is negligible. It results that the optimisation process that does not use $I_{M,d}$ appears to be more interesting in terms of performance. Nevertheless as the processes were stopped before reaching the Pareto front, these differences may variate, that is why the influence of the d-axis motor current is investigated in Chapter 5.

4.3 Conclusions

In this chapter two optimisation processes on the TLST machine are covered. The aim of the optimisation is to size the rotor of the machine and the height of the winding. The two processes used an NSGA-II algorithm and pursue the two same objectives: minimising the Joule losses while maximising the axial stiffness in centred position. The difference between the optimisations lies in the value of the direct axis motor current $I_{M,d}$. The first machine is sized considering $I_{M,d} = 0$ [A] whereas the second used $I_{M,d} \neq 0$ [A]. As explained in Section 4.1.3, the optimisation process has been stopped without achieving the Pareto front because of the lack of time. This implies that better performances can be achieved by the TLST machine. The results obtained give machines that have similar dimensions. Moreover, it appears that the height H_f tends to its minimal value, which means that the purpose of these ferromagnetic parts may be questioned and will be discussed in Chapter 5. Results showed that the machine which has no $I_{M,d}$ has more stiffness and also losses but in a lesser extent. Because of the negligible influence of $I_{M,d}$ on the performances, the model without $I_{M,d}$ is chosen and will be analysed in Chapter 5. This machine reaches 112 [N/mm] of stiffness and limits the Joule losses to 3 [mW] in axial centred position.

CHAPTER 5

CASE STUDY

This chapter aims to study the performances reached by an Electrodynamic Thrust Self Bearing Machine ETSBM equipped with a TLST rotor and highlights improvements caused by the use of BPMs. To do so, the paper [29] about the dynamical modelling of the ETSBM with SMPM rotor will be used as reference during the followings sections. It allows to directly compare both machines. However, the results must be viewed with caution since both machines have different air-gap and volume of PM. Indeed both dimensions of the case study are smaller than for the machine presented in [29]: 0.75 [mm] of airgap instead of 2.2 [mm] and 41 [cm^3] instead of 47 [cm^3].

This chapter is organised as follows: first the dimensions and parameters of the case study are summarised. Then, a quasi-static and a dynamic study compare the performances achieved by the TLST rotor to the SMPM rotor. Next, the study is focused on the influence of the motor currents on the stiffness and a discussion about the design choice concludes the chapter.

5.1 Dimensions of the case study

Let us consider the ETSBM with a TLST rotor. The optimisation performed in Chapter 4 gives the dimensions of the machine which are used in this case study. These dimensions are represented in Figure 4.1 and resumed in Tables 4.2 and 4.3. Based on these dimensions, FEM simulations presented in Chapter 3 provide the value of the different coefficients used in the analytical model of Chapter 2. These values are gathered in Table 5.1. The armature resistance has been identified through Pouillet's law while the rotor mass m and polar moment of inertia J_p have been estimated by considering the dimensions of the PM and the iron parts provided by the optimisation. An aluminium shaft with similar dimensions to Figure 9 has also been considered for both mass and moment of inertia. Finally, axial and angular damping coefficients, respectively noted C_z and C_{θ_m}, have been set arbitrarily to 10 [kg/m] and 10^{-6} [$kg \cdot m^2/s$][1] to ensure the stability of the system.

[1]This value fixes the viscous torque to approximately 100 [μNm].

Table 5.1: **Model parameters for the TLST rotor**

R $[\Omega]$	$L_{M,d}$ $[\mu H]$	$L_{M,q}$ $[\mu H]$	$L_{S,d}$ $[\mu H]$	$L_{S,q}$ $[\mu H]$
0.22	21.82	23.86	24.67	23.86

L_2 $[\mu H]$	M_2 $[\mu H]$	dL_d $[\mu H/mm]$	dL_q $[\mu H/mm]$	dL_2 $[\mu H/mm]$
-0.325	-1.66	-2.31	-2.72	0.138

K_θ [mWb]	K_z [Wb/m]	$k_{z,d}$ [N/m]	m [kg]	J_p $[gm^2]$
4.12	1.17	0	0.49	0.81

5.2 Quasi-static analysis

Figures 5.1a and 5.1b provide the evolution of the axial stiffness k_z and the drag torque for the ETSBM with respectively the SMPM and the TLST rotor. For the latter, both curves are defined by Equations 4.5 and 2.63 while the first figure is provided by [29]. The first thing to observe is the biggest value of both terms for the TLST rotor. Indeed, the stiffness reaches its asymptotic value k_z^∞ equal to 164 [N/mm] for speed higher than 80000 [rpm] while the SMPM rotor provides a maximal stiffness of 122 [N/mm]. The same remark can be made for the maximal value of the drag torque, which goes from 155 [mNm] for SMPM rotor to 321 [mNm] for the TLST topology. This maximal value is reached more quickly by the TLST rotor due to the higher value of the inductances, resulting in a lower value of its electrical pole: $\omega_e = \frac{R}{p\sqrt{L_{S,d}L_{S,q}}} = 9622$ [rpm] instead of 15575 [rpm] for the SMPM rotor. This lower electrical pole also allows to reach faster a higher stiffness for classical speed range, since it is equal to 47.5 [N/mm] for a speed of 6000 [rpm] while the SMPM provides 15.8 [N/mm].

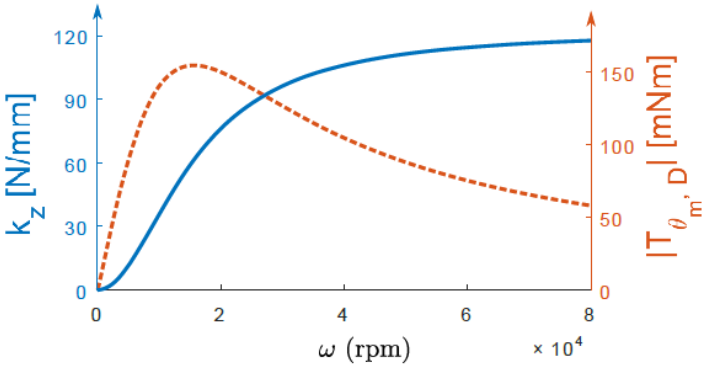

(a) For the SMPM rotor (from [29]).

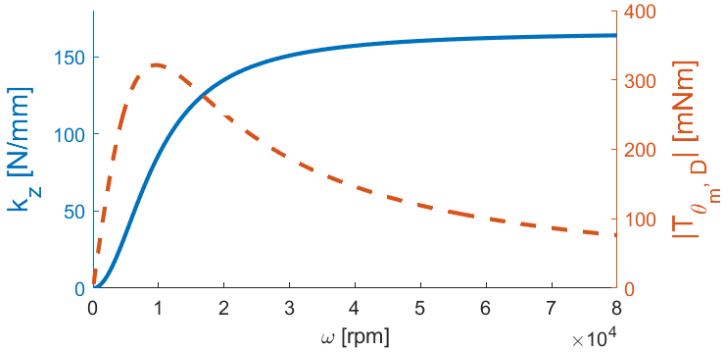

(b) For the case study with the TLST rotor.

Figure 5.1: Evolution of the axial stiffness k_z (solid line) and the drag torque $T_{\theta_{m,D}}$ (dashed line) with the rotation speed ω for a fixed axial displacement of 0.65 [mm].

This increase of the drag torque may seem problematic, but it is important to note that it has a quadratic dependence to the axial position as expressed by Equation 2.63. The gain of stiffness has then indirectly a significant influence on the drag torque and reduce its negative impact.

It must be noted that this quasi-static study considers the direct and the quadrature motor currents respectively set to 0 and 0.169 [A], the second value allowing to produce a motor torque of 7.5 [mNm]. It corresponds to the torque fixed during the optimisation. The influence of these currents is studied later in Section 5.7, but it is already possible to highlight the difference of stiffness and drag torque created by the motor current of 0.169 [A]. To do so, the stiffness and drag torque according to the rotation speed have also been computed for a zero quadrature motor current and subtracted to the curve of Figure 5.1b. The result is shown in Figure 5.2. The figure shows than both values of quadrature current provide performances which are extremely similar. Indeed, the maximum difference is smaller than 0.2% for drag torque and $4.1 \cdot 10^{-6}$% for the stiffness. The nonzero asymptotic drag torque expressed in Section 2.4.3 is in fact fully negligible compare to the total drag torque for this axial shift since it is equal to 0.104 [mNm].

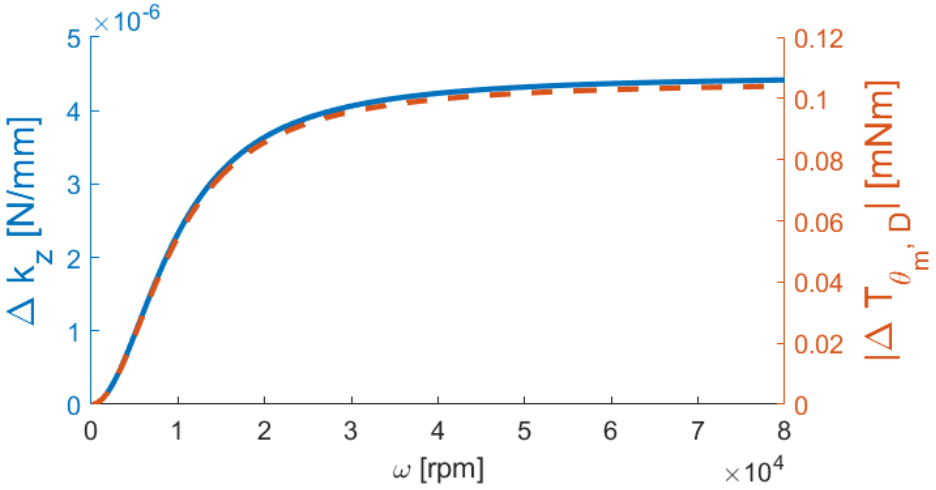

Figure 5.2: Increase of axial stiffness and drag torque for the case study with TLST rotor when the quadrature currents switches from 0 to 0.169 [A].

5.3 Dynamic analysis

Figure 5.4 presents the block diagram of a classical two-levels controller with back-EMF compensation. The control is directly applied on the direct and quadrature voltages u_d and u_q. Decoupling of direct and quadrature voltage equations is also applied but does not take into account the potential axial shift which adds coupling between equations in decentred position of the rotor, as shown by equation 2.43 and 2.43. The high-level controller uses a Proportional-Integral (PI) controller with a settling time of 10 [sec] while both low-level controllers, which control the voltages, use PI with settling time of 0.5 [sec]. The direct motor current is set to zero as for classical synchronous machines but can be independently modulated to highlight its influence on the motor and suspension performances. The

ETSBM start-up is available in Figure 5.4.

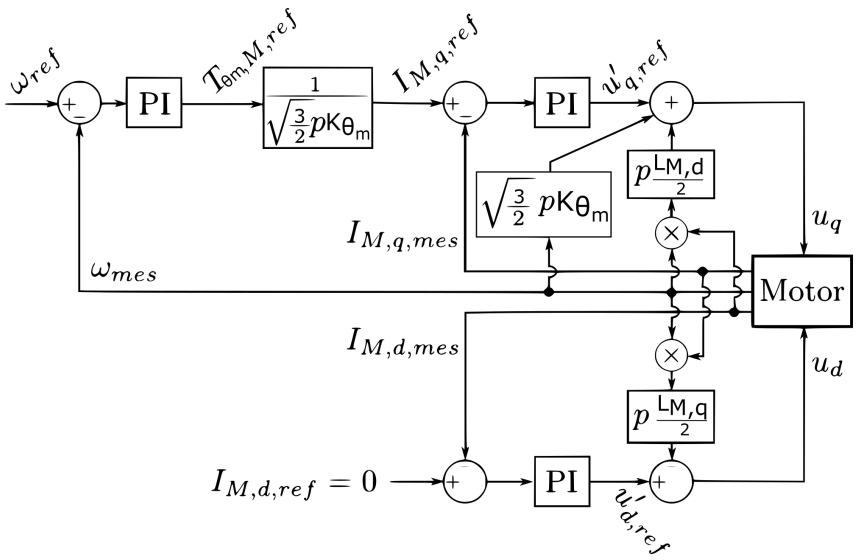

Figure 5.3: Motor control block diagram (modification of Figure from [29]).

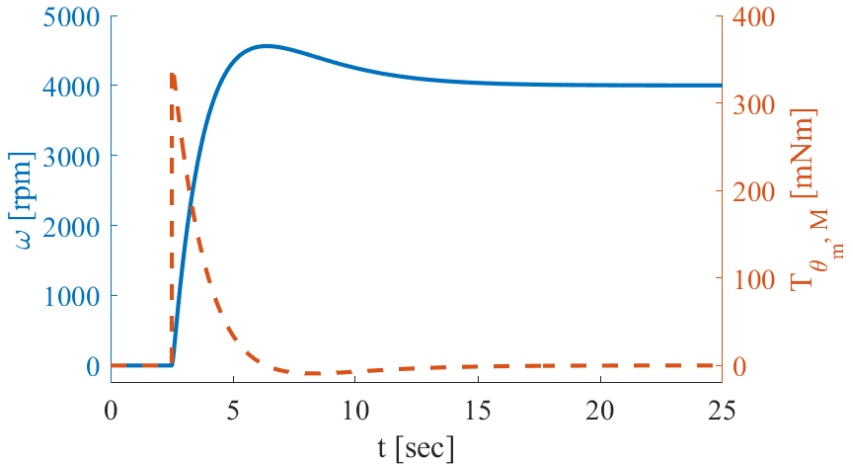

Figure 5.4: Evolution of the rotor spin speed (solid line) and the motor torque $T_{\theta_m,M}$ (dashed line) during the start-up.

In the paper [29] about the dynamic modelling of the ETSBM with SMPMs, two situations are analysed to study the coupling between the suspensions and motor functions. To continue the comparison between both types of rotor, these two tests will also be performed on the case study.

The first one consists of a step of external axial force $F_{z,e}$ applied on the rotor when the speed setpoint is fixed to 4000 [rpm]. This step is applied after 10 [sec] and maintained during 20 [sec]. For both machines, the axial external force shifts the rotor from its centred axial position, and this shift creates an opposite electrodynamic force noted F_z in Figure 5.5. The rotor stabilises in a position where the electrodynamic force compensates

exactly the external one. In the same time, the axial shift creates a drag torque, which is compensated by the controller by injecting quadrature current to create a driving torque and to maintain the motor at its rotation speed setpoint. When the external force is removed, the induced electrodynamic force brings back the rotor in a balanced position and the drag torque is removed in turn. Figures 5.5 (a) and (c) provide the results available in [29] while 5.5 (b) and (d) show the performances reached with the TLST topology:

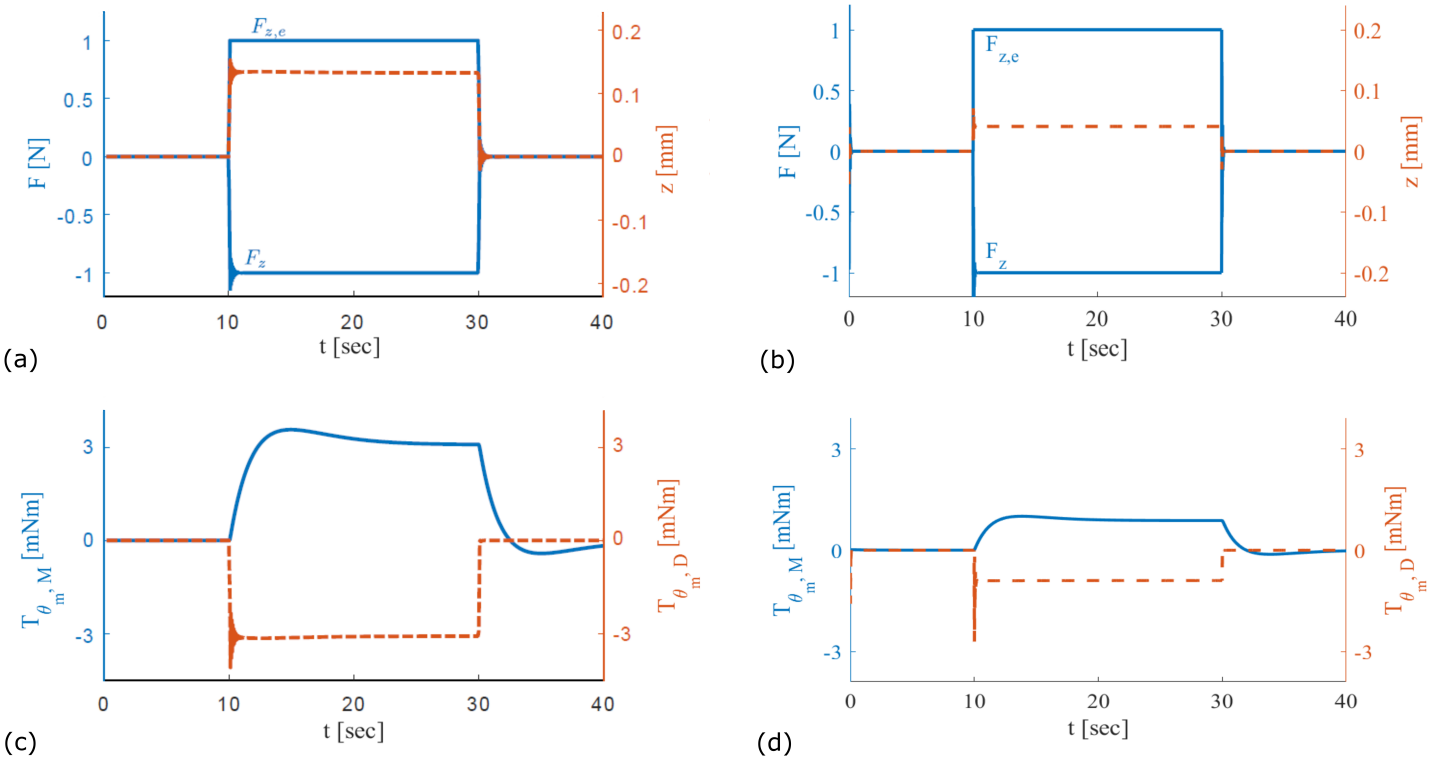

Figure 5.5: Dynamic behaviour following a step of external force $F_{z,e}$ when the rotor spin speed setpoint is fixed to 4000 [rpm]. Evolution of the electrodynamic force F_z (solid line) and the axial displacement z (dashed line) in Figure (a) for a SMPM rotor (from [29]) and in Figure (b) for a TLST rotor. Evolution of the driving torque $T_{\theta_m,M}$ (solid line) and the drag torque $T_{\theta_m,D}$ (dashed line) in Figure (c) for a SMPM rotor (from [29]) and in Figure (d) for a TLST rotor.

Figures 5.5 (a) and (b) show the reaction of both machines to the step force: as it can be seen, both provide the same opposite electrodynamic axial force, but the axial shift of the rotor goes from 0.13 [mm] for the SMPM rotor to 0.04 [mm] for the TLST topology. This difference is related to the gain of stiffness due to BPMs already highlighted in the quasi-static study. Indeed as shown on Figure 5.1, the stiffness at low speed increases by a factor 3 between the SMPM rotor and the TLST one, and it results in an axial shift 3 times smaller.

This increase of stiffness also influences the drag torque as it is proportional to the square of the rotor axial position z: Figures 5.5 (c) and (d) show the decrease of the drag torque from 3 [mNm] to 0.9 [mNm]. Thanks to the higher stiffness, a smaller driving torque is needed to counter the drag torque created by a given axial force, then the needed

quadratic motor current is reduced and the same goes for Joules losses caused by this axial force.

The second case studied consists of a linear variation of the speed setpoint from 4000 [rpm] to 6000 [rpm] in 20 [sec] with an external axial force fixed to 1 [N]. No external torque is applied. Figures 5.6 (a) and (b) show the evolution of rotation speed and axial shift of both machine while Figures 5.6 (c) and (d) describe the evolution of the driving torque and the drag torque, noted $T_{\theta_{m,M}}$ and $T_{\theta_{m,D}}$.

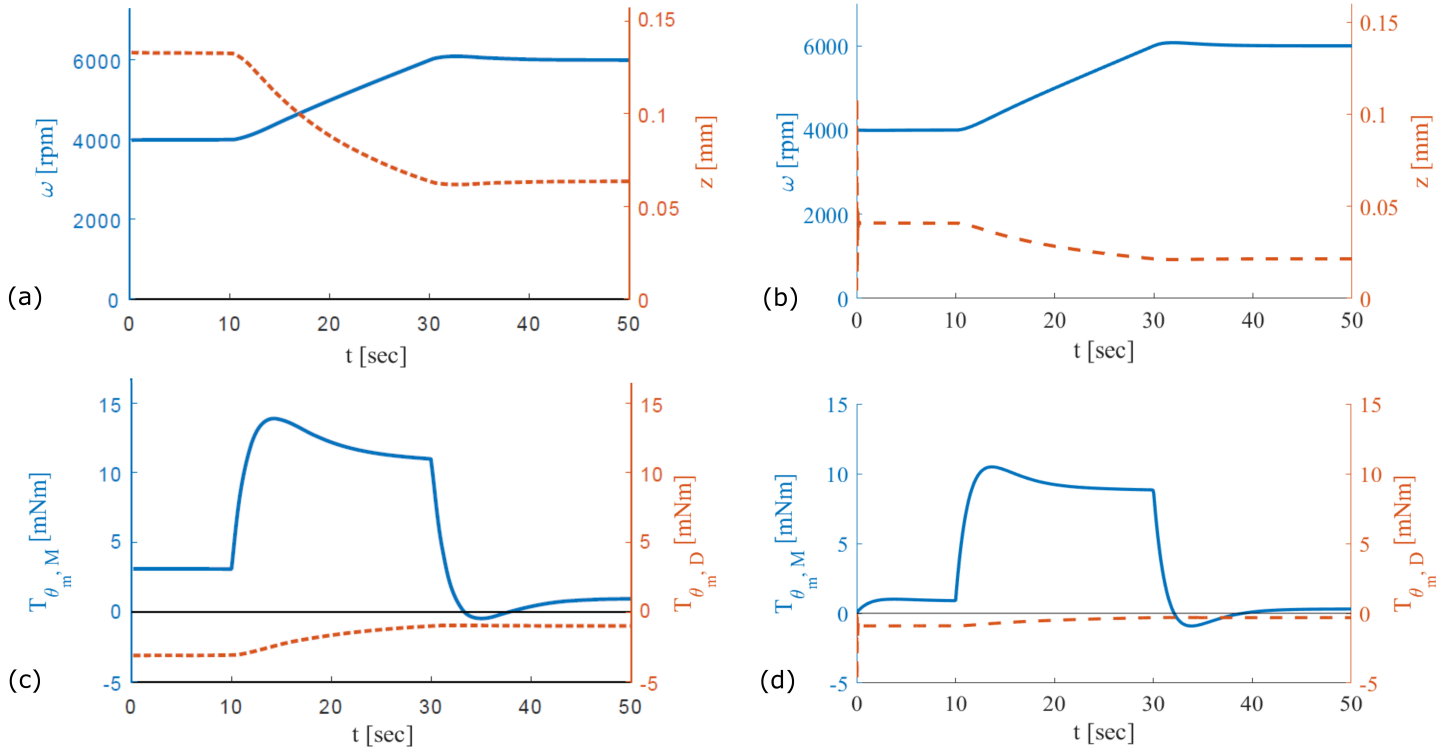

Figure 5.6: Dynamic behaviour for a fixed external force $F_{z,e}$ equal to 1 [N] when the rotor spin speed varies linearly from 4000 [rpm] to 6000 [rpm]. Evolution of the spin speed (solid line) and the axial displacement z (dashed line) in Figure (a) for a SMPM rotor (from [29]) and in Figure (b) for a TLST rotor. Evolution of the motor torque $T_{\theta_{m,M}}$ (solid line) and the drag torque $T_{\theta_{m}D}$ (dashed line) in Figure (c) for a SMPM rotor (from [29]) and in Figure (d) for a TLST rotor.

The constant external force leads to an axial shift and the latter results in turn in a drag torque present at the start of the experiment as shown in Figure 5.6 (c) and (d). This drag torque is compensated for both machines by the driving torque. During the linear variation of speed, the driving torque increases to accelerate the rotor, and the stiffness increases in turn which results in a simultaneous decrease of the axial shift and the drag torque. When the speed reaches the 6000 [rpm] plateau, the driving torque decreases since it only compensates the drag torque. Figure 5.6 (c) and (d) show that the diminution of axial shift leads to a smaller drag torque. Once again, the higher stiffness of the TLST, the smaller the axial shift and the drag torque.

5.4 Influence of the motor currents on the suspension

The quasi-static study has already shown the negligible influence of the quadrature current on the stiffness, but no variation of the current has been applied. The purpose of this section is to study the evolution of the stiffness for a larger range of direct and quadrature current. To do so, each one is linearly injected for two constant rotation speed setpoints, a high speed of 14000 [rpm] and a low speed, chosen as 5% of the last one, thus equal to 700 [rpm]. However, injecting quadrature current increases the driving torque which increases the speed, and it is not the purpose in this case. To solve this problem, a negative torque is linearly applied on the motor, which makes the controller increases the quadrature current to maintain the rotation speed. Secondly, the external torque is maintained to a constant value while the direct motor current is linearly injected. Figure 5.7 provides the dynamic behaviour of the rotor.

First in (1), no external torque is applied as shown in Figure (a), which results in zero currents and Joule losses as represented in Figure (b), and a constant rotation speed and stiffness depicted in Figures (c) and (d).

Then in (2), the external torque starts to increase and in reaction to that a quadrature current is injected by the controller to create a driving torque which maintains the rotor at constant speed. However the delay in the controller leads to a speed decrease, and therefore also to a stiffness decrease as shown in Figures 5.7 (c) and (d) in area (2).

The driving torque compensates exactly the external torque in the area (3). However this external torque continues to increase, so the quadrature current and the Joule losses too. Despite the increasing value of this current, no variation of stiffness is visible in Figures 5.7 (c) and (d) in this area.

The external torque stops to increase in area (4), which fixes the driving torque and then the quadrature current. The speed comes back to its setpoint as well as the stiffness comes back to its initial value. This last one has not been significantly increased by the quadrature current despite its high value.

Then the direct current is injected linearly in the area (5). This current is chosen as negative to take advantage of all the components of stiffness and torque as expressed in Equations 2.69 and 2.71, since the coefficients dL_d and $(L_2 + M_2)$ are negatives in this case study. As it can be seen in Figure 5.7 (c) in the area (5), no significant stiffness variation can be observed at low speed. However at high speed, a linear increase of the stiffness appears, as shown in the same area of 5.7 (d). This difference between low and high speed can be explained with the model. Indeed by reminding the equation 2.61 of the electrodynamic axial force created by the motor:

$$F_{z,Ed} = \sqrt{\frac{3}{2}} \cdot K_z \cdot z \left[\frac{dL_q}{R} \cdot \left(1 - \frac{\omega^2}{\left[\frac{R^2}{p^2 L_{S,d} L_{S,q}} + \omega^2 \right]} \right) \cdot p\omega \cdot I_{M,q} - \underbrace{\frac{\omega^2}{\left[\frac{R^2}{p^2 L_{S,d} L_{S,q}} + \omega^2 \right]} \cdot \left[\frac{dL_d}{L_{S,d}} \cdot I_{M,d} \right.}_{\text{Term A}} + \sqrt{6} \cdot \frac{K_z}{L_{S,d}} \right]$$

The term A in the equation above is proportional to the direct current but almost zero at low speed, which explains that no variation is observed in Figure 5.7 (c). On the opposite, when the speed has exceeded the electrical pole, this term is no more zero and a linear increase of the stiffness is observed. However, the increase of the stiffness for a direct current of -1 [A] is approximately equal to 0.2% of the total stiffness, which is still very low and not significant. To improve the relative influence of the direct current on the stiffness compare the the axial flux variation K_z, the ratio $\frac{dL_d \cdot I_{M,d}}{K_z}$ must be significantly increased.

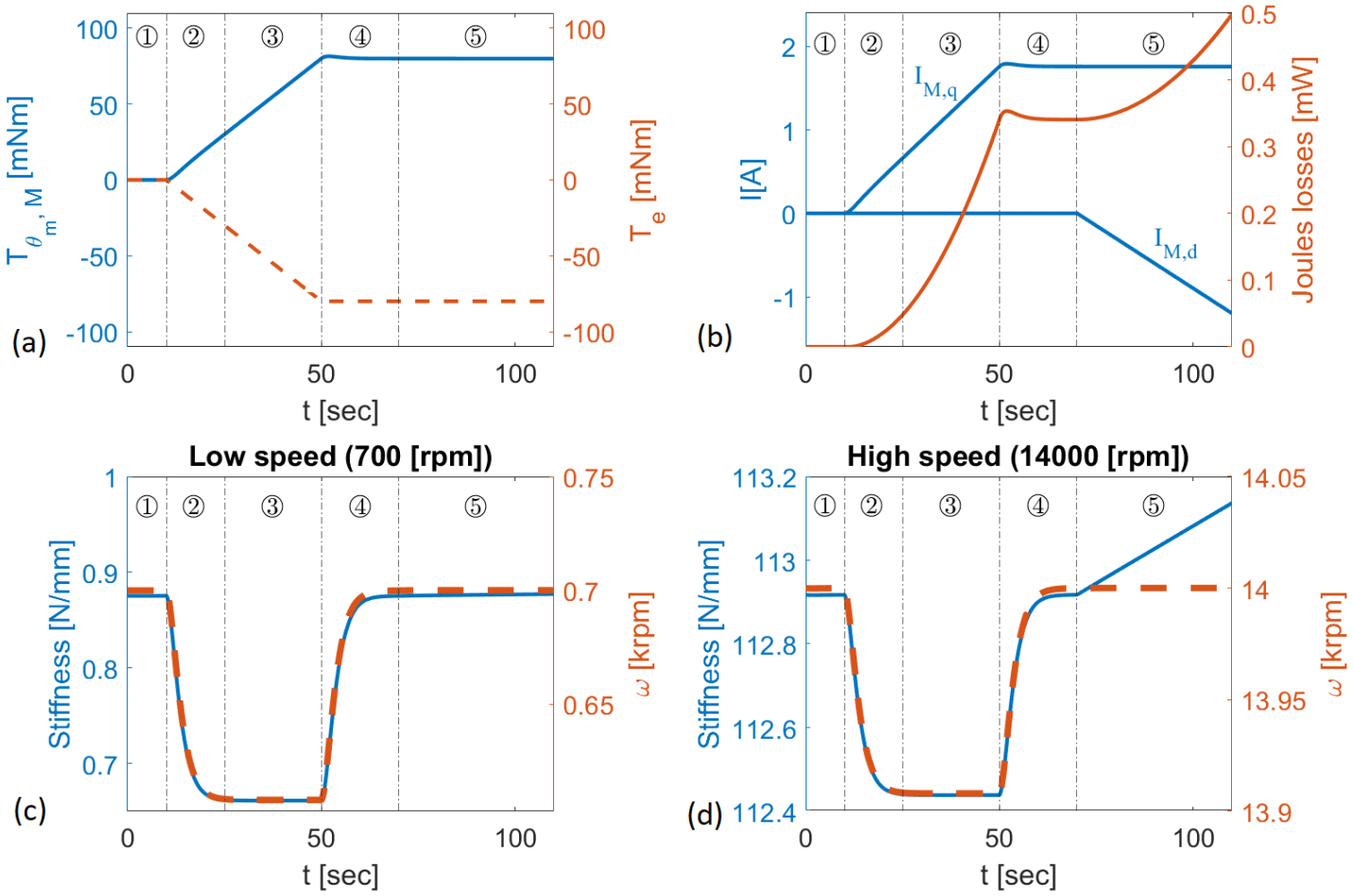

Figure 5.7: Dynamic behaviour of the ETSBM with a TLST rotor: linear increase of the external torque during 40 [sec] as it can be seen in Figure (a) at constant speed in centred position. The external torque is applied after 10 [sec] and results in an increase of the quadrature current as depicted in Figure (b). Next, a negative direct current is linearly injected after 70 [sec]. The evolution of the stiffness and speed is shown for low and high speed, respectively 700 [rpm] in Figure (c) and 14000 [rpm] in Figure (d). Figures (a) and (b) are valid for both situations since torques and currents are independent of the speed.

Another analyse can be made in this figure and is about the non-significant influence of the reluctant terms in the stiffness and the torque. Indeed, no quadratic increase of the stiffness according to the currents is observed for both cases despite the form of reluctant terms in Equations 2.69, which shows that they are negligible for the stiffness. Moreover, the

presence of a significant reluctant torque should result in a diminution of the quadrature current. Indeed, this additional torque leads to an acceleration of the rotor. Consequently, the controller should reduce the electrodynamic torque to maintain the constant speed by reducing this current. But no significant diminution of the quadrature current is visible on area (5) of Figure 5.7 (b) despite the high values of $I_{M,d}$ and $I_{M,q}$. These observations allow to conclude that the reluctant term of the total torque in Equation 2.71 is negligible for the case study. Indeed, for $I_{M,d} = -1$ [A] and $I_{M,q} = 1$ [A], Equations 2.71 and 2.69 give at high speed a reluctant torque of 26.7 [μNm] and a reluctant stiffness of 0.26 [N/m] for the case study, which are completely negligible.

5.5 Discussion

The high stiffness of this case study brings positive results for the use of BPMs but some criticisms can be made. First, in order to realise the prototype initially planned for this Master's thesis, it has been decided in the middle of the project to modify the TLST topology to use segment-shaped PMs. These PMs are easier to manufacture and to obtain than the initial PMs of this topology represented in Figure 5.8a. However, using segment-shaped PMs with the ferromagnetic parts of the TLST topology, it keeps the PMs away from the windings. Moreover it also creates a path for the magnetic field which can circulate between two consecutive ferromagnetic parts without going through the windings, as shown in Figure 5.8b. In fact, without the PMs on the height H_f defined in Figure 3.1b, the ferromagnetic parts on this height are disadvantageous from a flux point of view. It explains why the optimisation performed in Chapter 4 tends to a value of H_f near to 2 [mm]. This height was indeed the minimal value allowed by the code : the bigger this height, the lower the fluxes and so the performances.

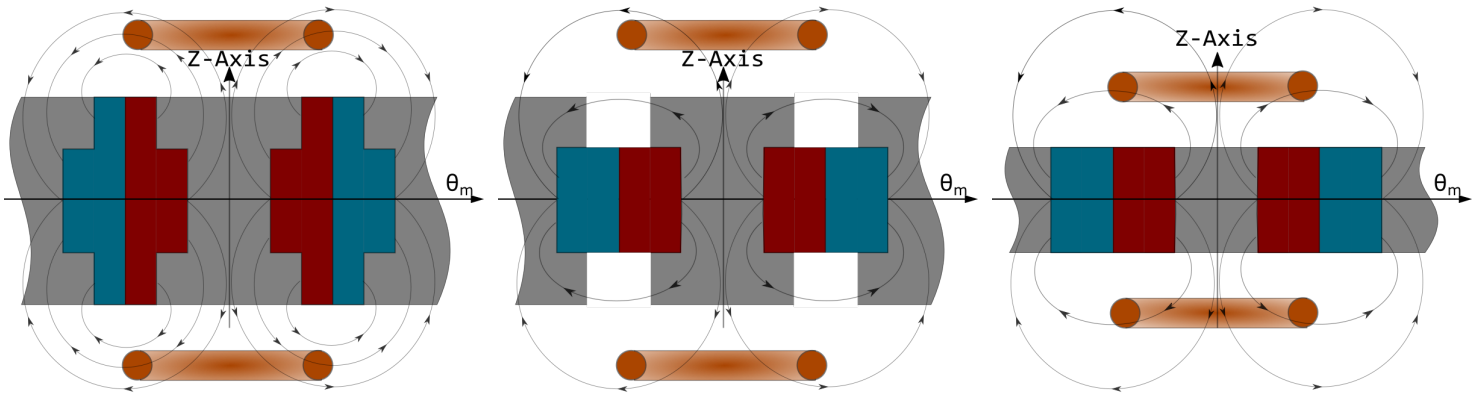

(a) Topology TLST chosen at the start of the master thesis.

(b) Adaptation of the topology to segment-shaped magnet.

(c) ST topology increasing the flux in winding for the same VPM.

Figure 5.8

To support this proposition, simulations have been performed on a rotor where all the dimensions have been conserved excepted the height of ferromagnetic material which has been removed. The windings have been brought closer to the PM to conserve the same airgap than before. This rotor, represented in Figure 5.8c, corresponds to a Spoke Type ST topology. A quasi-static study, presented in Figure 5.9, allows to highlight the gain of stiffness obtained by removing this ferromagnetic thickness. This modification allows to reach stiffness higher than 300 [N/mm] despite the fact that no optimisation has been performed on the topology. These observations show that the choice made in this Master's thesis leads to a non-optimal topology.

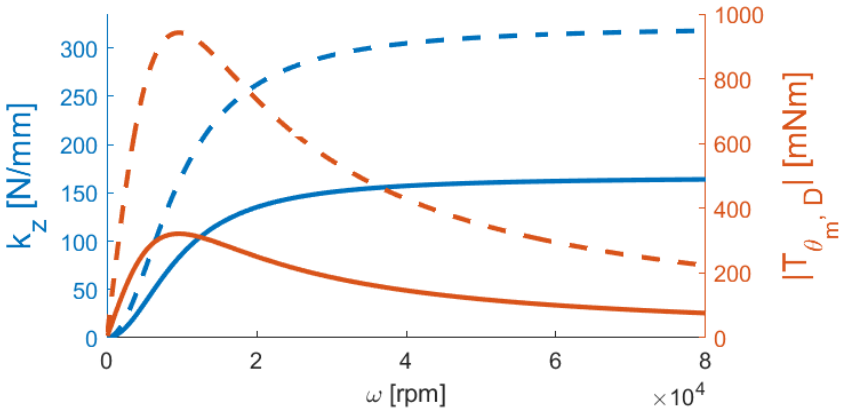

Figure 5.9: Comparison of the quasi-static stiffness and the drag torque for the case study with the TLST rotor (solid line) and the same rotor without the thickness of ferromagnetic material on the height H_f (dashed line), corresponding to a ST topology.

5.6 Conclusions

This case study performed a quasi-static and dynamic analysis of an Electrodynamic Thrust Self-Bearing Machine (ETSBM) using the TLST rotor, the latter having been sized by the optimisation of Chapter 4. The suspension performances have been compared to the ETSBM using a rotor with surface mounted PMs, studied in [29]. The comparisons have shown an important gain of stiffness which allows to reduce the parasitic drag torque caused by axial shift of the rotor. Moreover the bigger inductances values of the TLST topology allow to reduce the electrical pole of the machine which increases consequently the stiffness for low speed compared to the initial machine.

Next the influence of the motor currents on the stiffness has been studied. It has been determined that these currents do not allow to modulate the stiffness as expected in Chapter 2, due to the too small value of the axial inductance variation compared to the axial flux variation. The reluctant torque and stiffness are also non-significant for the machine performances. Therefore, the direct current must be set to zero as for classical synchronous machines, the torque and stiffness being almost completely caused by electrodynamic effects. However, no optimisation to improve the influence of the direct current has been performed, which means that a higher influence of this current could be obtained with more specific researches.

Finally, a discussion on the chosen design has been proposed to highlight the bad association of TLST topology with segment-shaped PMs leading to a decrease of stiffness. This last section showed that, despite the improvements of stiffness reached by the use of BPM, better performance can still be achieved by improving the design of the rotor.

CONCLUSION

The work done in [1] by J. Van Verdeghem on the axial-flux ETSBM machines using SMPMs is the starting point of this Master's thesis. In order to contextualise it a review of the different topologies of AFPM bearingless machine is done and the principle of operation of the ETSBM described in [37] is detailed. As shown by the review, all the presented machines use classical SMPM rotor despite the fact that BPM should increase the suspension performances. Then this master thesis aims to study the modification of performance provided by the use of a BPM rotor on the ETSBM.

This work is thus divided in five mains objectives: First, realising the state of the art of axial-flux machines having a rotor with BPMs and choosing one of them to design and characterise. Next, deriving the electromechanical model of ETSBM with a BPM rotor and validate it through static FEM simulations. Then, optimising the dimensions of the chosen machine. Finally, based on the optimal dimensions computed and on the state-space model derived, analysing in both quasi-static and dynamic conditions the behaviour of the motor.

Chapter 1 first reviewed the different rotor topologies with BPMs. Among them, it appears that the TLST topology, thanks to the improvement of the THD while keeping a good reachable range of speed and manufacturablity, was a good candidate. Then, a design proposal using 3D-printed parts to position correctly all the different elements composing the rotor was described.

Chapter 2 derived the electromechanical model of the considered motor. Thanks to it the axial and spin dynamic behaviours were described. One of the big difference with respect to the machine developed in [29] was the dependencies of the inductance coefficients with the axial and the angular position of the rotor due to its ferromagnetic parts. This axial dependence adds some terms proportional to the motor currents in the expression of the axial stiffness, which open the way of a potential modulation of the suspension through these currents in addition to the passive suspension reached by ETSBM. However this dependence also modified the expression of the drag torque which does not tend to zero anymore at high speed, contrarily to the machine presented in [37]. Indeed at high speed the drag torque becomes proportional to the quadrature motor current. Finally in

addition to the electrodynamic effects already present in the initial motor using SMPM rotor, reluctant effects appear.

Chapter 3 determined the global parameters of the analytical model and validated the assumptions made in Chapter 2 with static FEM. First two categories of FEM models were detailed. The first category computed the flux constants while the second computed the inductance coefficients. Both models used the same methodology which is based on an adapted version of the integral of the magnetic flux density over a surface. All the assumptions were validated except for one parameter. It appeared that the mutual inductance coefficient between two phases of the upper winding did not evolve in a purely sinusoidal way with respect to the rotor angular position. However, the impact of this non-sinusoidal form has been shown as negligible, which allows to validate the electromechanical model of Chapter 2.

Chapter 4 presented the optimisation processes applied on the chosen machine in order to determine its dimensions. The two processes followed the same objectives: minimising the losses while maximising the total axial stiffness. The constraints applied were the speed of rotation, the torque and the VPM, and they were based on the performances and the dimensions given in [20]. The first process did not take the current $I_{M,d}$ into account while the second did. The results showed that it was more interesting to not take this current into account during the optimisation because of its limited impact on the performances. As the model used were time-consuming, the front Pareto obtained was not yet finished and so better performances could be obtained. The best candidate was nevertheless selected to perform a case study in the last chapter of this work.

Chapter 5 analysed the performance of the machine which has been sized in the previous chapter. The purpose was to use the state space model developed in Chapter 2, to first validate the passive axial suspension of the rotor and secondly, to compare the performances reached by the new topology to the ETSBM using SMPM rotor described in [29]. The improvement in stiffness for the new topology highlights the main interest of the use of BPM rotor for bearingless machines. Moreover, the higher value of inductance coefficients shows that high stiffness are quickly reached at low speed due to the decrease of the electrical pole of the machine. The chapter has then investigated the influence of the motor currents on the suspension. Despite the high current values tested, no significant influence of those have been observed on the suspension, which showed that the suspension of the machine is still mainly achieved by electrodynamic effect. Finally, some design improvement have been put forward to highlight the fact than better stiffness may still be reached.

This work paves the way for the use of BPM for axial flux bearingless machine by highlighting the improvement of the suspension function. Moreover, other topologies of BPM rotor should be investigated to potentially improve the influence of the motor currents on this suspension and take more advantage of the reluctant component brought by BPM.

BIBLIOGRAPHY

[1] J. Van Verdeghem, "Design, modelling and experimental validation of a novel bearingless machine with fully passive magnetic suspension," Ph.D. dissertation, UCL-Université Catholique de Louvain, 2020.

[2] E. L. Severson, "Bearingless motor technology for industrial and transportation applications," in *2018 IEEE Transportation Electrification Conference and Expo (ITEC)*. IEEE, 2018, pp. 266–273.

[3] A. Martowicz, J. Roemer, S. Kantor, P. Zdziebko, G. Żywica, and P. Bagiński, "Gas foil bearing technology enhanced with smart materials," *Applied Sciences*, vol. 11, no. 6, 2021. [Online]. Available: https://www.mdpi.com/2076-3417/11/6/2757

[4] W. Zhang and H. Zhu, "Radial magnetic bearings: An overview," *Results in Physics*, vol. 7, pp. 3756–3766, 2017. [Online]. Available: https://www.sciencedirect.com/science/article/pii/S221137971730863X

[5] T. S. Slininger, W. Chan, E. L. Severson, and B. Jawdat, "An overview on passive magnetic bearings," in *2021 IEEE International Electric Machines Drives Conference (IEMDC)*, 2021, pp. 1–8.

[6] J. Chen, J. Zhu, and E. L. Severson, "Review of bearingless motor technology for significant power applications," *IEEE Transactions on Industry Applications*, vol. 56, no. 2, pp. 1377–1388, 2020.

[7] T. Pei, D. Li, J. Liu, J. Li, and W. Kong, "Review of bearingless synchronous motors: Principle and topology," *IEEE Transactions on Transportation Electrification*, 2022.

[8] A. Chiba, T. Fukao, O. Ichikawa, M. Oshima, M. Takemoto, and D. G. Dorrell, *Magnetic bearings and bearingless drives*. Elsevier, 2005.

[9] X. Sun, L. Chen, and Z. Yang, "Overview of bearingless induction motors," *Mathematical Problems in Engineering*, vol. 2014, 2014.

[10] L. Ramdane, J. Da Silva, E. Helene, F. Ponson, and U. Schroeder, "Electric centrifugal compressor for vehicles," Dec. 26 2013, uS Patent App. 13/925,390.

[11] M. Neff, N. Barletta, and R. Schob, "Bearingless centrifugal pump for highly pure chemicals," in *Proc. 8th Int. Symp. Magnetic Bearings*, 2002, pp. 283–287.

[12] Y. Zhang, L. Hu, R. Su, and X. Ruan, "Design method of bearingless permanent magnet slice motor for maglev centrifugal pump based on performance metric cluster," in *Actuators*, vol. 10, no. 7. Multidisciplinary Digital Publishing Institute, 2021, p. 153.

[13] W. Bauer and W. Amrhein, "Electrical design considerations for a bearingless axial-force/torque motor," *IEEE Transactions on Industry Applications*, vol. 50, no. 4, pp. 2512–2522, 2014.

[14] H. Sugimoto, I. Shimura, and A. Chiba, "A novel stator structure for active axial force improvement in a one-axis actively positioned single-drive bearingless motor," *IEEE Transactions on Industry Applications*, vol. 53, no. 5, pp. 4414–4421, 2017.

[15] W. Gruber, W. Bauer, D. Wetsch, B. Klammer, and N. Kurita, "Implementation of a bearingless axial-force/torque motor fan with flex-pcb windings," in *2019 IEEE International Electric Machines Drives Conference (IEMDC)*, 2019, pp. 179–184.

[16] W. Li, K. T. Chau, T. W. Ching, Y. Wang, and M. Chen, "Design of a high-speed superconducting bearingless machine for flywheel energy storage systems," *IEEE Transactions on Applied Superconductivity*, vol. 25, no. 3, pp. 1–4, 2015.

[17] M. Ooshima, S. Kobayashi, and H. Tanaka, "Magnetic suspension performance of a bearingless motor/generator for flywheel energy storage systems," in *IEEE PES General Meeting*, 2010, pp. 1–4.

[18] Y. Yuan, Y. Sun, and Y. Huang, "Design and analysis of bearingless flywheel motor specially for flywheel energy storage," *Electronics Letters*, vol. 52, no. 1, pp. 66–68, 2016.

[19] J. Zhou and K. Tseng, "A disk-type bearingless motor for use as satellite momentum-reaction wheel," in *2002 IEEE 33rd Annual IEEE Power Electronics Specialists Conference. Proceedings (Cat. No.02CH37289)*, vol. 4, 2002, pp. 1971–1975 vol.4.

[20] J. Van Verdeghem and B. Dehez, "Fully passively levitated self-bearing machine implemented within a reaction wheel," *IEEE Transactions on Industry Applications*, pp. 1–1, 2021.

[21] T. Reichert, T. Nussbaumer, W. Gruber, and J. W. Kolar, "Bearingless permanent-magnet motor with 4/12 slot-pole ratio for bioreactor stirring applications," *IEEE/ASME Transactions on Mechatronics*, vol. 16, no. 3, pp. 431–439, 2011.

[22] T. Reichert, T. Nussbaumer, and J. W. Kolar, "Investigation of exterior rotor bearingless motor topologies for high-quality mixing applications," *IEEE Transactions on Industry Applications*, vol. 48, no. 6, pp. 2206–2216, 2012.

[23] ——, "Bearingless 300-w pmsm for bioreactor mixing," *IEEE Transactions on industrial electronics*, vol. 59, no. 3, pp. 1376–1388, 2011.

[24] B. Warberger, R. Kaelin, T. Nussbaumer, and J. W. Kolar, "50-N · m/2500-w bearingless motor for high-purity pharmaceutical mixing," *IEEE Transactions on Industrial Electronics*, vol. 59, no. 5, pp. 2236–2247, 2012.

[25] R. John, J. W. Long, H. T. Massey, B. P. Griffith, B. C. Sun, A. J. Tector, O. H. Frazier, and L. D. Joyce, "Outcomes of a multicenter trial of the levitronix centrimag ventricular assist system for short-term circulatory support," *The Journal of thoracic and cardiovascular surgery*, vol. 141, no. 4, pp. 932–939, 2011.

[26] N. Barletta and R. Schob, "Design of a bearingless blood pump," in *NASA CONFERENCE PUBLICATION*. NASA, 1996, pp. 265–274.

[27] Y. Okada, N. Yamashiro, K. Ohmori, T. Masuzawa, T. Yamane, Y. Konishi, and S. Ueno, "Mixed flow artificial heart pump with axial self-bearing motor," *IEEE/ASME Transactions on Mechatronics*, vol. 10, no. 6, pp. 658–665, 2005.

[28] H. Hoshi, T. Shinshi, and S. Takatani, "Third-generation blood pumps with mechanical noncontact magnetic bearings," *Artificial organs*, vol. 30, no. 5, pp. 324–338, 2006.

[29] J. Van Verdeghem, M. Lefebvre, V. Kluyskens, and B. Dehez, "Dynamical modeling of passively levitated electrodynamic thrust self-bearing machines," *IEEE Transactions on Industry Applications*, vol. 55, no. 2, pp. 1447–1460, 2018.

[30] S. Ueno and Y. Okada, "Characteristics of axial force and rotating torque and their control of permanent magnet type axial gap self-bearing motor," *Electrical Engineering in Japan*, vol. 132, no. 1, pp. 81–91, 2000.

[31] ——, "Characteristics and control of a bidirectional axial gap combined motor-bearing," *IEEE/ASME transactions on mechatronics*, vol. 5, no. 3, pp. 310–318, 2000.

[32] H. Asper, "Passive dynamically stabilizing magnetic bearing and drive unit," Dec. 14 2006, uS Patent App. 10/514,612.

[33] J. Asama, Y. Hamasaki, T. Oiwa, and A. Chiba, "Proposal and analysis of a novel single-drive bearingless motor," *IEEE Transactions on Industrial Electronics*, vol. 60, no. 1, pp. 129–138, 2012.

[34] J. Asama, D. Watanabe, T. Oiwa, and A. Chiba, "Development of a one-axis actively regulated bearingless motor with a repulsive type passive magnetic bearing," in *2014 International Power Electronics Conference (IPEC-Hiroshima 2014-ECCE ASIA)*. IEEE, 2014, pp. 988–993.

[35] J. Asama, T. K. Tai, and A. Chiba, "Development of axial-flux single-drive bearingless motor with one-axis active positioning," *IEEE Transactions on Industry Applications*, 2021.

[36] H. Sugimoto, I. Shimura, and A. Chiba, "A novel stator structure for active axial force improvement in a one-axis actively positioned single-drive bearingless motor," *IEEE Transactions on Industry Applications*, vol. 53, no. 5, pp. 4414–4421, 2017.

[37] J. Van Verdeghem and B. Dehez, "Fully passively levitated self-bearing machines with combined windings," in *2020 IEEE Energy Conversion Congress and Exposition (ECCE)*. IEEE, 2020, pp. 254–261.

[38] S. Ueno, M. Tomoda, and C. Jiang, "Development of an axial-flux self-bearing motor using two permanent magnet attractive type passive magnetic bearings," *International Journal of Applied Electromagnetics and Mechanics*, no. Preprint, pp. 1–7, 2020.

[39] G. Cavalcanterubio, Y. Fujii, and A. Chiba, "A bearingless motor with passive electrodynamic suspension in axial direction," *IEEE Transactions on Industry Applications*, 2021.

[40] G. C. Rubio and A. Chiba, "Design and analysis of a bearingless motor with passive axial suspension through null-flux coils," in *2019 IEEE International Electric Machines & Drives Conference (IEMDC)*. IEEE, 2019, pp. 779–786.

[41] F. G. Capponi, G. De Donato, and F. Caricchi, "Recent advances in axial-flux permanent-magnet machine technology," *IEEE Transactions on Industry Applications*, vol. 48, no. 6, pp. 2190–2205, 2012.

[42] B. Tekgun, T. Husain, S. Das, Y. Sozer, and M. Hamdan, "Design of a novel interior permanent magnet axial flux machine," in *2017 IEEE Energy Conversion Congress and Exposition (ECCE)*, 2017, pp. 314–320.

[43] J. Gieras, R.-J. Wang, and M. Kamper, *Axial Flux Permanent Magnet Brushless Machines*, 01 2008.

[44] P. Van Tichelen and E. Peeters, "Design of a new axial flux permanent magnet generator for hybrid electric vehicles," in *2003 IEEE 58th Vehicular Technology Conference. VTC 2003-Fall (IEEE Cat. No.03CH37484)*, vol. 5, 2003, pp. 3192–3196 Vol.5.

[45] E. Peeters, J. Bael, and P. Van Tichelen, "Different 600kw designs of an axial flux permanent magnet machine for wind turbines," 01 2007.

[46] S. Neethu, S. Pal, A. K. Wankhede, and B. G. Fernandes, "High performance axial flux permanent magnet synchronous motor for high speed applications," in *IECON 2017 - 43rd Annual Conference of the IEEE Industrial Electronics Society*, 2017, pp. 5093–5098.

[47] A. Binder, T. Schneider, and M. Klohr, "Fixation of buried and surface mounted magnets in high-speed permanent magnet synchronous motors," in *Fourtieth IAS Annual Meeting. Conference Record of the 2005 Industry Applications Conference, 2005.*, vol. 4, 2005, pp. 2843–2848 Vol. 4.

[48] F. Chai, Y. Bi, and Y. Pei, "Magnet shape optimization of two-layer spoke-type axial flux interior permanent magnet machines," *Energies*, vol. 11, no. 1, 2018. [Online]. Available: https://www.mdpi.com/1996-1073/11/1/15

[49] Y. Bi, Y. Pei, and F. Chai, "A novel axial flux interior permanent magnet motor with high torque density," in *2019 22nd International Conference on Electrical Machines and Systems (ICEMS)*, 2019, pp. 1–5.

[50] M. Aydin and M. Gulec, "A new coreless axial flux interior permanent magnet synchronous motor with sinusoidal rotor segments," *IEEE Transactions on Magnetics*, vol. 52, no. 7, pp. 1–4, 2016.

[51] S.-o. Kwon, S.-i. Kim, P. Zhang, and J.-p. Hong, "Performance comparison of ipmsm with distributed and concentrated windings," in *Conference Record of the 2006 IEEE Industry Applications Conference Forty-First IAS Annual Meeting*, vol. 4, 2006, pp. 1984–1988.

[52] MarkForged, "Onyx material," *https://markforged.com/materials/plastics/onyx?___geom=%E2%9C%AA*.

[53] J. Van Verdeghem and B. Dehez, "Performance comparison of wire-wound and pcb windings for passively levitated self-bearing machines," 10 2021, pp. 116–120.

Appendices

A Electrical equations with motor and suspension variables

Starting from:

$$\begin{cases} \mathbf{U} = \mathrm{R} \cdot \mathbf{I_U} + \dfrac{\mathrm{d}(\mathbf{L_U} \cdot \mathbf{I_U})}{\mathrm{dt}} + \dfrac{\mathrm{d}(\mathbf{M_{UL}} \cdot \mathbf{I_L})}{\mathrm{dt}} + \dfrac{\mathrm{d}\boldsymbol{\Phi}_\mathbf{U}}{\mathrm{dt}} \\ \mathbf{U} = \mathrm{R} \cdot \mathbf{I_L} + \dfrac{\mathrm{d}(\mathbf{L_L} \cdot \mathbf{I_L})}{\mathrm{dt}} + \dfrac{\mathrm{d}(\mathbf{M_{UL}} \cdot \mathbf{I_U})}{\mathrm{dt}} + \dfrac{\mathrm{d}\boldsymbol{\Phi}_\mathbf{L}}{\mathrm{dt}} \end{cases} \tag{A.1}$$

The following system can be obtained:

$$\begin{cases} \mathbf{U} = \mathrm{R} \cdot \dfrac{\mathbf{I_U} + \mathbf{I_L}}{2} + \dfrac{\mathrm{d}}{\mathrm{dt}} \left(\dfrac{\mathbf{L_U} + \mathbf{M_{UL}}}{2} \cdot \mathbf{I_U} + \dfrac{\mathbf{L_L} + \mathbf{M_{UL}}}{2} \cdot \mathbf{I_L} \right) + \dfrac{\mathrm{d}}{\mathrm{dt}} \left(\dfrac{\boldsymbol{\Phi}_\mathbf{U} + \boldsymbol{\Phi}_\mathbf{L}}{2} \right) & \text{By averaging the two equations of A.1} \\ 0 = \mathrm{R} \cdot (\mathbf{I_U} - \mathbf{I_L}) + \dfrac{\mathrm{d}}{\mathrm{dt}} \left((\mathbf{L_U} - \mathbf{M_{UL}}) \cdot \mathbf{I_U} + (\mathbf{M_{UL}} - \mathbf{L_L}) \cdot \mathbf{I_L} \right) + \dfrac{\mathrm{d}}{\mathrm{dt}} (\boldsymbol{\Phi}_\mathbf{U} - \boldsymbol{\Phi}_\mathbf{L}) & \text{By subtracting equations of A.1} \end{cases}$$

By injecting the motor and suspension currents and fluxes:

$$\begin{cases} \mathbf{I_U} = \frac{\mathbf{I_M}}{2} + \mathbf{I_S} \\ \mathbf{I_L} = \frac{\mathbf{I_M}}{2} - \mathbf{I_S} \end{cases} \iff \begin{cases} \mathbf{I_M} = \mathbf{I_L} + \mathbf{I_U} \\ \mathbf{I_S} = \frac{\mathbf{I_U} - \mathbf{I_L}}{2} \end{cases} \quad \text{and} \quad \begin{cases} \boldsymbol{\Phi}_\mathbf{M} = \dfrac{\boldsymbol{\Phi}_\mathrm{L} + \boldsymbol{\Phi}_\mathrm{U}}{2} \\ \boldsymbol{\Phi}_\mathbf{S} = \boldsymbol{\Phi}_\mathrm{U} - \boldsymbol{\Phi}_\mathrm{L} \end{cases}$$

It gives:

$$\begin{cases} \mathbf{U} = \dfrac{\mathrm{R}}{2} \cdot \mathbf{I_M} + \dfrac{\mathrm{d}}{\mathrm{dt}} \left(\dfrac{\mathbf{L_U} + \mathbf{M_{UL}}}{2} \cdot \left(\dfrac{\mathbf{I_M}}{2} + \mathbf{I_S} \right) + \dfrac{\mathbf{L_L} + \mathbf{M_{UL}}}{2} \cdot \left(\dfrac{\mathbf{I_M}}{2} - \mathbf{I_S} \right) \right) + \dfrac{\mathrm{d}\boldsymbol{\Phi}_\mathbf{M}}{\mathrm{dt}} \\ 0 = 2\mathrm{R} \cdot \mathbf{I_S} + \dfrac{\mathrm{d}}{\mathrm{dt}} \left((\mathbf{L_U} - \mathbf{M_{UL}}) \cdot \left(\dfrac{\mathbf{I_M}}{2} + \mathbf{I_S} \right) + (\mathbf{M_{UL}} - \mathbf{L_L}) \cdot \left(\dfrac{\mathbf{I_M}}{2} - \mathbf{I_S} \right) \right) + \dfrac{\mathrm{d}\boldsymbol{\Phi}_\mathbf{S}}{\mathrm{dt}} \end{cases}$$

Which is equivalent to:

$$\begin{cases} \mathbf{U} = \dfrac{\mathrm{R}}{2} \cdot \mathbf{I_M} + \dfrac{\mathrm{d}}{\mathrm{dt}} \left(\left(\dfrac{\mathbf{L_U + L_L}}{2} + \mathbf{M_{UL}} \right) \cdot \dfrac{\mathbf{I_M}}{2} + \left(\dfrac{\mathbf{L_U - L_L}}{2} \right) \cdot \mathbf{I_S} \right) + \dfrac{\mathrm{d}\boldsymbol{\Phi}_\mathbf{M}}{\mathrm{dt}} \\ 0 = 2\mathrm{R} \cdot \mathbf{I_S} + \dfrac{\mathrm{d}}{\mathrm{dt}} \left(\left(\dfrac{\mathbf{L_U - L_L}}{2} \right) \cdot \mathbf{I_M} + (\mathbf{L_U + L_L - 2M_{UL}}) \cdot \mathbf{I_S} \right) + \dfrac{\mathrm{d}\boldsymbol{\Phi}_\mathbf{S}}{\mathrm{dt}} \end{cases}$$

Finally, after having introduced the "average" inductance matrix $\mathbf{L_{AV}}$ and the "variation inductance" $\mathbf{L_V}$ defined in 2.13 and 2.14, the new version of the electrical equations[2] is obtained:

$$\begin{cases} \mathbf{U} = \dfrac{\mathrm{R}}{2} \cdot \mathbf{I_M} + \dfrac{\mathrm{d}}{\mathrm{dt}} \left(\left(\dfrac{\mathbf{L_{AV} + M_{UL}}}{2} \right) \cdot \mathbf{I_M} + \mathbf{L_V} \cdot \mathbf{I_S} \right) + \dfrac{\mathrm{d}\boldsymbol{\Phi}_\mathbf{M}}{\mathrm{dt}} \\ 0 = 2\mathrm{R} \cdot \mathbf{I_S} + \dfrac{\mathrm{d}}{\mathrm{dt}} \left(\mathbf{L_V} \cdot \mathbf{I_M} + 2 \left(\mathbf{L_{AV} - M_{UL}} \right) \cdot \mathbf{I_S} \right) + \dfrac{\mathrm{d}\boldsymbol{\Phi}_\mathbf{S}}{\mathrm{dt}} \end{cases} \tag{A.2}$$

[2]Come back to the section concerning this appendix: Section 2.2.3.a

B Concordia transformation

B.1 Electrical equations

The Concordia transformation must be applied on:

- The first equation of A.2

$$\mathbf{U} = \frac{\mathrm{R}}{2} \cdot \mathbf{I_M} + \frac{\mathrm{d}}{\mathrm{dt}} \left(\left(\frac{\mathbf{L_{AV}} + \mathbf{M_{UL}}}{2} \right) \cdot \mathbf{I_M} + \mathbf{L_V} \cdot \mathbf{I_S} \right) + \frac{\mathrm{d}\boldsymbol{\Phi}_\mathbf{M}}{\mathrm{dt}}$$

By applying the Concordia transformation

$$\mathbf{T} \cdot \mathbf{U^S} = \frac{\mathrm{R}}{2} \cdot \mathbf{T} \cdot \mathbf{I_M^S} + \frac{\mathrm{d}}{\mathrm{dt}} \left(\left(\frac{\mathbf{L_{AV}} + \mathbf{M_{UL}}}{2} \right) \cdot \mathbf{T} \cdot \mathbf{I_M^S} + \mathbf{L_V} \cdot \mathbf{T} \cdot \mathbf{I_S^S} \right) + \frac{\mathrm{d}\mathbf{T} \cdot \boldsymbol{\Phi}_\mathbf{M}^\mathbf{S}}{\mathrm{dt}}$$

$$\mathbf{U^S} = \frac{\mathrm{R}}{2} \cdot \mathbf{T^{-1}T} \cdot \mathbf{I_M^S} + \mathbf{T^{-1}} \frac{\mathrm{d}}{\mathrm{dt}} \left(\left(\frac{\mathbf{L_{AV}} + \mathbf{M_{UL}}}{2} \right) \cdot \mathbf{T} \cdot \mathbf{I_M^S} + \mathbf{L_V} \cdot \mathbf{T} \cdot \mathbf{I_S^S} \right) + \mathbf{T^{-1}} \frac{\mathrm{d}\mathbf{T} \cdot \boldsymbol{\Phi}_\mathbf{M}^\mathbf{S}}{\mathrm{dt}}$$

$\mathbf{T}^{-1}$ being time-invariant, it can go into the derivative,

and as $\mathbf{T}$ is orthogonal, $\mathbf{T^{-1} \cdot T} = \mathbf{I_3}$ the identity matrix

$$= \frac{\mathrm{R}}{2} \cdot \mathbf{I_M^S} + \frac{\mathrm{d}}{\mathrm{dt}} \left(\left(\frac{\mathbf{L_{AV}^S} + \mathbf{M_{UL}^S}}{2} \right) \cdot \mathbf{I_M^S} + \mathbf{L_V^S} \cdot \mathbf{I_S^S} \right) + \frac{\mathrm{d}\boldsymbol{\Phi}_\mathbf{M}^\mathbf{S}}{\mathrm{dt}}$$

Where $\mathbf{L_{AV}^S} = \mathbf{T^{-1}} \cdot \mathbf{L_{AV}} \cdot \mathbf{T}$, $\mathbf{M_{UL}^S} = \mathbf{T^{-1}} \cdot \mathbf{M_{UL}} \cdot \mathbf{T}$ and $\mathbf{L_V^S} = \mathbf{T^{-1}} \cdot \mathbf{L_V} \cdot \mathbf{T}$

- The second equation of A.2

$$0 = 2\mathrm{R} \cdot \mathbf{I_S} + \frac{\mathrm{d}}{\mathrm{dt}} \left(\mathbf{L_V} \cdot \mathbf{I_M} + 2 \left(\mathbf{L_{AV}} - \mathbf{M_{UL}} \right) \cdot \mathbf{I_S} \right) + \frac{\mathrm{d}\boldsymbol{\Phi}_\mathbf{S}}{\mathrm{dt}}$$

$$= 2\mathrm{R} \cdot \mathbf{T} \cdot \mathbf{I_S^S} + \frac{\mathrm{d}}{\mathrm{dt}} \left(\mathbf{L_V} \cdot \mathbf{T} \cdot \mathbf{I_M^S} + 2 \left(\mathbf{L_{AV}} - \mathbf{M_{UL}} \right) \cdot \mathbf{T} \cdot \mathbf{I_S^S} \right) + \frac{\mathrm{d}\mathbf{T} \cdot \boldsymbol{\Phi}_\mathbf{S}^\mathbf{S}}{\mathrm{dt}}$$

By pre-multiplying by $\mathbf{T^{-1}}$

$$= 2\mathrm{R} \cdot \mathbf{T^{-1}} \cdot \mathbf{T} \cdot \mathbf{I_S^S} + \mathbf{T^{-1}} \cdot \frac{\mathrm{d}}{\mathrm{dt}} \left(\mathbf{L_V} \cdot \mathbf{T} \cdot \mathbf{I_M^S} + 2 \left(\mathbf{L_{AV}} - \mathbf{M_{UL}} \right) \cdot \mathbf{T} \cdot \mathbf{I_S^S} \right) + \mathbf{T^{-1}} \cdot \frac{\mathrm{d}\mathbf{T} \cdot \boldsymbol{\Phi}_\mathbf{S}^\mathbf{S}}{\mathrm{dt}}$$

$$= 2\mathrm{R} \cdot \mathbf{I_S^S} + \frac{\mathrm{d}}{\mathrm{dt}} \left(\mathbf{L_V^S} \cdot \mathbf{I_M^S} + 2 \left(\mathbf{L_{AV}^S} - \mathbf{M_{UL}^S} \right) \cdot \mathbf{I_S^S} \right) + \frac{\mathrm{d}\boldsymbol{\Phi}_\mathbf{S}^\mathbf{S}}{\mathrm{dt}}$$

This transformation provides the system[3]:

$$\begin{cases} \mathbf{U^S} = \dfrac{\mathrm{R}}{2} \cdot \mathbf{I_M^S} + \dfrac{\mathrm{d}}{\mathrm{dt}} \left(\left(\dfrac{\mathbf{L_{AV}^S} + \mathbf{M_{UL}^S}}{2} \right) \cdot \mathbf{I_M^S} + \mathbf{L_V^S} \cdot \mathbf{I_S^S} \right) + \dfrac{\mathrm{d}\boldsymbol{\Phi}_\mathbf{M}^\mathbf{S}}{\mathrm{dt}} \\ 0 = 2\mathrm{R} \cdot \mathbf{I_S^S} + \dfrac{\mathrm{d}}{\mathrm{dt}} \left(\mathbf{L_V^S} \cdot \mathbf{I_M^S} + 2 \left(\mathbf{L_{AV}^S} - \mathbf{M_{UL}^S} \right) \cdot \mathbf{I_S}^\mathrm{S} \right) + \dfrac{\mathrm{d}\boldsymbol{\Phi}_\mathbf{S}^\mathbf{S}}{\mathrm{dt}} \end{cases}$$

[3]Come back to the section concerning this appendix: Section 2.2.3.b

B.2 Transformation of the different inductance matrices:

Three new matrices are defined when the Concordia transformation is applied on the electrical equation 2.16. These three matrices, 2.17, 2.18 and 2.19, having the same form, the development will be only done for the first one.
Equation 2.17 is obtained in this way:

$$\begin{aligned}
\mathbf{L^S_{AV}} =& \mathbf{T^{-1}L_{AV}T} \\
=& \mathbf{T^{-1}L_0T} + \mathrm{L_2}\cdot\mathbf{T^{-1}}\cdot[\boldsymbol{2\theta_{em}}]\cdot\mathbf{T} \qquad \text{by using equation 2.13} \\
=& \begin{pmatrix} \mathrm{L_0}+2\mathrm{M_0} & 0 & 0 \\ 0 & \mathrm{L_0}-\mathrm{M_0} & 0 \\ 0 & 0 & \mathrm{L_0}-\mathrm{M_0} \end{pmatrix} + \frac{3}{2}\mathrm{L_2}\cdot\begin{pmatrix} 0 & 0 & 0 \\ 0 & \cos(2\theta_{\mathrm{em}}) & \sin(2\theta_{\mathrm{em}}) \\ 0 & \sin(2\theta_{\mathrm{em}}) & -\cos(2\theta_{\mathrm{em}}) \end{pmatrix}
\end{aligned}$$

As the homopolar component of the current and voltage does not participate to the electrodynamic behaviour of the machine, it will not be represented in the next developments. Then the inductance matrices becomes 2×2- matrices.[4]

B.3 Transformation of fluxes derivatives

First the Concordia transformation can be applied on the fluxes:

$$\begin{aligned}
\boldsymbol{\Phi^S_M} &= \mathbf{T^{-1}}\cdot\left[\mathrm{K}_{\theta_{\mathrm{m}}}\begin{pmatrix}\cos(\theta_{\mathrm{em}})\\ \cos(\theta_{\mathrm{em}}-\frac{2\pi}{3})\\ \cos(\theta_{\mathrm{em}}-\frac{4\pi}{3})\end{pmatrix}\right] \\
&= \sqrt{\frac{3}{2}}\mathrm{K}_{\theta_{\mathrm{m}}}\cdot\begin{pmatrix}0\\ \cos(\theta_{\mathrm{em}})\\ \sin(\theta_{\mathrm{em}})\end{pmatrix}
\end{aligned}
\qquad
\begin{aligned}
\boldsymbol{\Phi^S_S} &= \mathbf{T^{-1}}\cdot\left[2\mathrm{zK_z}\begin{pmatrix}\cos(\theta_{\mathrm{em}})\\ \cos(\theta_{\mathrm{em}}-\frac{2\pi}{3})\\ \cos(\theta_{\mathrm{em}}-\frac{4\pi}{3})\end{pmatrix}\right] \\
&= \sqrt{6}\mathrm{zK_z}\cdot\begin{pmatrix}0\\ \cos(\theta_{\mathrm{em}})\\ \sin(\theta_{\mathrm{em}})\end{pmatrix}
\end{aligned}$$

And their time derivatives [5] are expressed as:

$$\begin{aligned}
\frac{\mathrm{d}\boldsymbol{\Phi^S_M}}{\mathrm{dt}} &= \frac{\mathbf{d}\boldsymbol{\Phi^S_M}}{\mathrm{d}\theta_{\mathrm{em}}}\cdot\frac{\mathrm{d}\theta_{\mathrm{em}}}{\mathrm{d}\theta_{\mathrm{m}}}\cdot\frac{\mathrm{d}\theta_{\mathrm{m}}}{\mathrm{dt}} \\
&= \sqrt{\frac{3}{2}}\mathrm{K}_{\theta_{\mathrm{m}}}\cdot\begin{pmatrix}0\\ -\sin(\theta_{\mathrm{em}})\\ \cos(\theta_{\mathrm{em}})\end{pmatrix}\cdot\mathrm{p}\dot{\theta}_{\mathrm{m}}
\end{aligned}
\qquad
\begin{aligned}
\frac{\mathrm{d}\boldsymbol{\Phi^S_S}}{\mathrm{dt}} &= \frac{\mathbf{d}\boldsymbol{\Phi^S_S}}{\mathrm{d}\theta_{\mathrm{em}}}\cdot\frac{\mathrm{d}\theta_{\mathrm{em}}}{\mathrm{d}\theta_{\mathrm{m}}}\cdot\frac{\mathrm{d}\theta_{\mathrm{m}}}{\mathrm{dt}} + \frac{\mathbf{d}\boldsymbol{\Phi^S_S}}{\mathrm{dz}}\cdot\frac{\mathrm{dz}}{\mathrm{dt}} \\
&= \sqrt{6}\mathrm{zK_z}\cdot\left[\mathrm{z}\cdot\begin{pmatrix}0\\ -\sin(\theta_{\mathrm{em}})\\ \cos(\theta_{\mathrm{em}})\end{pmatrix}\cdot\mathrm{p}\dot{\theta}_{\mathrm{m}} + \dot{\mathrm{z}}\begin{pmatrix}0\\ \cos(\theta_{\mathrm{em}})\\ \sin(\theta_{\mathrm{em}})\end{pmatrix}\right]
\end{aligned}$$

[4] Come back to the section concerning this appendix: Section 2.2.3.b
[5] Come back to the section concerning this appendix: Section 2.2.3.b

C Park transformation

C.1 Park transformation of the first equation of 2.16

The Park transformation an be applied on the motor electrical equation which is the first equation of 2.16. It gives:

$$\mathbf{U^S} = \frac{\mathrm{R}}{2} \cdot \mathbf{I_M^S} + \frac{\mathrm{d}}{\mathrm{dt}} \left(\left(\frac{\mathbf{L_{AV}^S} + \mathbf{M_{UL}^S}}{2} \right) \cdot \mathbf{I_M^S} + \mathbf{L_V^S} \cdot \mathbf{I_S^S} \right) + \frac{\mathrm{d}\boldsymbol{\Phi}_\mathbf{M}^\mathbf{S}}{\mathrm{dt}}$$

By applying the Park transformation on the currents it gives

$$\mathbf{P} \cdot \mathbf{U^P} = \frac{\mathrm{R}}{2} \cdot \mathbf{P} \cdot \mathbf{I_M^P} + \frac{\mathrm{d}}{\mathrm{dt}} \left(\left(\frac{\mathbf{L_{AV}^S} + \mathbf{M_{UL}^S}}{2} \right) \cdot \mathbf{P} \cdot \mathbf{I_M^P} + \mathbf{L_V^S} \cdot \mathbf{P} \cdot \mathbf{I_S^P} \right) + \frac{\mathrm{d}\boldsymbol{\Phi}_\mathbf{M}^\mathbf{S}}{\mathrm{dt}}$$

The Park transformation being time-dependent, $\mathbf{P^{-1}}$ cannot go into the derivative and the different terms will be developed in the following subsections

$$\mathbf{U^P} = \frac{\mathrm{R}}{2} \cdot \mathbf{I_M^P} + \underbrace{\mathbf{P^{-1}} \frac{\mathrm{d}}{\mathrm{dt}} \left(\left(\frac{\mathbf{L_{AV}^S} + \mathbf{M_{UL}^S}}{2} \right) \cdot \mathbf{P} \cdot \mathbf{I_M^P} \right)}_{\text{Term "a" developed in C.1.a}} + \underbrace{\mathbf{P^{-1}} \frac{\mathrm{d}}{\mathrm{dt}} \left(\mathbf{L_V^S} \cdot \mathbf{P} \cdot \mathbf{I_S^P} \right)}_{\text{Term "b" developed in C.1.b}} + \underbrace{\mathbf{P^{-1}} \frac{\mathrm{d}\boldsymbol{\Phi}_\mathbf{M}^\mathbf{S}}{\mathrm{dt}}}_{\text{Term "c" developed in C.1.c}} \tag{C.1}$$

C.1.a Term "a" of equation C.1

$$\begin{aligned} \mathbf{P^{-1}} \frac{\mathrm{d}}{\mathrm{dt}} \left(\left(\frac{\mathbf{L_{AV}^S} + \mathbf{M_{UL}^S}}{2} \right) \cdot \mathbf{P} \cdot \mathbf{I_M^P} \right) &= \mathbf{P^{-1}} \frac{\mathrm{d}}{\mathrm{dt}} \left(\left(\frac{\mathbf{L_{AV}^S} + \mathbf{M_{UL}^S}}{2} \right) \right) \cdot \mathbf{P} \cdot \mathbf{I_M^P} \\ &+ \mathbf{P^{-1}} \left(\frac{\mathbf{L_{AV}^S} + \mathbf{M_{UL}^S}}{2} \right) \cdot \frac{\mathrm{d}\mathbf{P}}{\mathrm{dt}} \cdot \mathbf{I_M^P} \\ &+ \mathbf{P^{-1}} \left(\frac{\mathbf{L_{AV}^S} + \mathbf{M_{UL}^S}}{2} \right) \cdot \mathbf{P} \cdot \frac{\mathrm{d}\mathbf{I_M^P}}{\mathrm{dt}} \end{aligned}$$

Each sub-term multiplying the currents or their derivatives can be developed by using expressions 2.17 and 2.18:

- The first one:

$$\begin{aligned} \mathbf{P^{-1}} \frac{\mathrm{d}}{\mathrm{dt}} \left(\left(\frac{\mathbf{L_{AV}^S} + \mathbf{M_{UL}^S}}{2} \right) \right) \cdot \mathbf{P} &= \frac{3}{2} \mathrm{p} \dot{\theta}_\mathrm{m} \cdot (\mathrm{L_2} + \mathrm{M_2}) \cdot \left(\mathbf{P^{-1}} \cdot \begin{pmatrix} -\sin(2\theta_\mathrm{em}) & \cos(2\theta_\mathrm{em}) \\ \cos(2\theta_\mathrm{em}) & \sin(2\theta_\mathrm{em}) \end{pmatrix} \cdot \mathbf{P} \right) \\ &= \frac{3}{2} \mathrm{p} \dot{\theta}_\mathrm{m} \cdot (\mathrm{L_2} + \mathrm{M_2}) \cdot \begin{pmatrix} 0 & 1 \\ 1 & 0 \end{pmatrix} \\ &= \frac{\mathrm{p} \dot{\theta}_\mathrm{m}}{2} \cdot \begin{pmatrix} 0 & 3(\mathrm{L_2} + \mathrm{M_2}) \\ 3(\mathrm{L_2} + \mathrm{M_2}) & 0 \end{pmatrix} \end{aligned}$$

- The second one:

$$\mathbf{P^{-1}} \cdot \left(\frac{\mathbf{L^S_{AV}} + \mathbf{M^S_{UL}}}{2}\right) \cdot \frac{\mathrm{d}\mathbf{P}}{\mathrm{dt}} = \mathbf{P^{-1}} \cdot \begin{pmatrix} \frac{\mathrm{L_0}-\mathrm{M_0}+\mathrm{M_{ii}}-\mathrm{M_{ij}}}{2} & 0 \\ 0 & \frac{\mathrm{L_0}-\mathrm{M_0}+\mathrm{M_{ii}}-\mathrm{M_{ij}}}{2} \end{pmatrix} \cdot \frac{\mathrm{d}\mathbf{P}}{\mathrm{dt}} + \frac{1}{2} \cdot \left(\frac{3}{2}\mathrm{L_2} + \frac{3}{2}\mathrm{M_2}\right) \cdot \mathbf{P^{-1}} \cdot \begin{pmatrix} \cos(2\theta_{\mathrm{em}}) & \sin(2\theta_{\mathrm{em}}) \\ \sin(2\theta_{\mathrm{em}}) & -\cos(2\theta_{\mathrm{em}}) \end{pmatrix} \cdot \frac{\mathrm{d}\mathbf{P}}{\mathrm{dt}}$$

$$\text{with } \frac{\mathrm{d}\mathbf{P}}{\mathrm{dt}} = \frac{\mathrm{d}\theta_{\mathrm{em}}}{\mathrm{d}\theta_{\mathrm{m}}}\frac{\mathrm{d}\theta_{\mathrm{m}}}{\mathrm{dt}} \cdot \begin{pmatrix} -\sin(\theta_{\mathrm{em}}) & -\cos(\theta_{\mathrm{em}}) \\ \cos(\theta_{\mathrm{em}}) & -\sin(\theta_{\mathrm{em}}) \end{pmatrix} = \mathrm{p}\dot{\theta}_{\mathrm{m}} \cdot \begin{pmatrix} -\sin(\theta_{\mathrm{em}}) & -\cos(\theta_{\mathrm{em}}) \\ \cos(\theta_{\mathrm{em}}) & -\sin(\theta_{\mathrm{em}}) \end{pmatrix}$$

$$= \frac{\mathrm{p}\dot{\theta}_{\mathrm{m}}}{2} \cdot \left[(\mathrm{L_0} - \mathrm{M_0} + \mathrm{M_{ii}} - \mathrm{M_{ij}}) \cdot \begin{pmatrix} 0 & -1 \\ 1 & 0 \end{pmatrix} + \left(\frac{3(\mathrm{L_2} + \mathrm{M_2})}{2}\right) \cdot \begin{pmatrix} 0 & -1 \\ -1 & 0 \end{pmatrix}\right] \quad \text{(C.2)}$$

Definitions 2.25, 2.26,2.27 and 2.28 allow to simplify the expression

$$= \frac{\mathrm{p}\dot{\theta}_{\mathrm{m}}}{2} \cdot \begin{pmatrix} 0 & -(\mathrm{L_d} + \mathrm{M_d}) \\ \mathrm{L_q} + \mathrm{M_q} & 0 \end{pmatrix}$$

- The third one:

$$\mathbf{P^{-1}} \left(\frac{\mathbf{L^S_{AV}} + \mathbf{M^S_{UL}}}{2}\right) \cdot \mathbf{P} = \mathbf{P^{-1}} \cdot \begin{pmatrix} \frac{\mathrm{L_0}-\mathrm{M_0}+\mathrm{M_{ii}}-\mathrm{M_{ij}}}{2} & 0 \\ 0 & \frac{\mathrm{L_0}-\mathrm{M_0}+\mathrm{M_{ii}}-\mathrm{M_{ij}}}{2} \end{pmatrix} \cdot \mathbf{P} + \left(\frac{3(\mathrm{L_2} + \mathrm{M_2})}{4}\right) \cdot \mathbf{P^{-1}} \cdot \begin{pmatrix} \cos(2\theta_{\mathrm{em}}) & \sin(2\theta_{\mathrm{em}}) \\ \sin(2\theta_{\mathrm{em}}) & -\cos(2\theta_{\mathrm{em}}) \end{pmatrix} \cdot \mathbf{P}$$

$$= \begin{pmatrix} \frac{\mathrm{L_0}-\mathrm{M_0}+\mathrm{M_{ii}}-\mathrm{M_{ij}}}{2} & 0 \\ 0 & \frac{\mathrm{L_0}-\mathrm{M_0}+\mathrm{M_{ii}}-\mathrm{M_{ij}}}{2} \end{pmatrix} + \begin{pmatrix} \frac{3(\mathrm{L_2}+\mathrm{M_2})}{4} & 0 \\ 0 & -\frac{3(\mathrm{L_2}+\mathrm{M_2})}{4} \end{pmatrix}$$

Definitions 2.25, 2.26,2.27 and 2.28 allow to simplify the expression

$$= \frac{1}{2} \cdot \begin{pmatrix} \mathrm{L_d} + \mathrm{M_d} & 0 \\ 0 & \mathrm{L_q} + \mathrm{M_q} \end{pmatrix} \quad \text{(C.3)}$$

The final expression of term "a" is:

$$\mathbf{P^{-1}} \frac{\mathrm{d}}{\mathrm{dt}} \left(\left(\frac{\mathbf{L^S_{AV}} + \mathbf{M^S_{UL}}}{2}\right) \cdot \mathbf{P} \cdot \mathbf{I^P_M}\right) = \frac{\mathrm{p}\dot{\theta}_{\mathrm{m}}}{2} \cdot \begin{pmatrix} 0 & -(\mathrm{L_d} + \mathrm{M_d}) + 3(\mathrm{L_2} + \mathrm{M_2}) \\ \mathrm{L_q} + \mathrm{M_q} + 3(\mathrm{L_2} + \mathrm{M_2}) & 0 \end{pmatrix} \cdot \mathbf{I^P_M} + \frac{1}{2} \cdot \begin{pmatrix} \mathrm{L_d} + \mathrm{M_d} & 0 \\ 0 & \mathrm{L_q} + \mathrm{M_q} \end{pmatrix} \cdot \frac{\mathrm{d}\mathbf{I^P_M}}{\mathrm{dt}}$$

Using 2.25, 2.26,2.27 and 2.28 give:

$$= \frac{\mathrm{p}\dot{\theta}_{\mathrm{m}}}{2} \cdot \begin{pmatrix} 0 & -(\mathrm{L_q} + \mathrm{M_q}) \\ \mathrm{L_d} + \mathrm{M_d} & 0 \end{pmatrix} \cdot \mathbf{I^P_M} + \frac{1}{2} \cdot \begin{pmatrix} \mathrm{L_d} + \mathrm{M_d} & 0 \\ 0 & \mathrm{L_q} + \mathrm{M_q} \end{pmatrix} \cdot \frac{\mathrm{d}\mathbf{I^P_M}}{\mathrm{dt}}$$

C.1.b Term "b" of equation C.1

$$\mathbf{P^{-1}}\frac{\mathrm{d}}{\mathrm{dt}}\left(\mathbf{L_V^S}\cdot\mathbf{P}\cdot\mathbf{I_S^P}\right)=\mathbf{P^{-1}}\frac{\mathrm{d}\mathbf{L_V^S}}{\mathrm{dt}}\cdot\mathbf{P}\cdot\mathbf{I_S^P}+\mathbf{P^{-1}}\mathbf{L_V^S}\frac{\mathrm{d}\mathbf{P}}{\mathrm{dt}}\cdot\mathbf{I_S^P}+\mathbf{P^{-1}}\mathbf{L_V^S}\mathbf{P}\cdot\frac{\mathrm{d}\mathbf{I_S^P}}{\mathrm{dt}}$$

Each sub-term multiplying the currents or their derivatives can be developed by using expression 2.19:

- The first one:

$$\begin{aligned}\mathbf{P^{-1}}\frac{\mathrm{d}\mathbf{L_V^S}}{\mathrm{dt}}\cdot\mathbf{P}=&\mathbf{P^{-1}}\cdot\left(\frac{\mathrm{d}\mathbf{L_V^S}}{\mathrm{dz}}\cdot\dot{\mathrm{z}}+\frac{\mathrm{d}\mathbf{L_V^S}}{\mathrm{d}\theta_{\mathrm{em}}}\cdot\frac{\mathrm{d}\theta_{\mathrm{em}}}{\mathrm{d}\theta_{\mathrm{m}}}\frac{\mathrm{d}\theta_{\mathrm{m}}}{\mathrm{dt}}\right)\cdot\mathbf{P}\\ =&\mathbf{P^{-1}}\left[\dot{\mathrm{z}}\cdot\begin{pmatrix}\mathrm{dL_0}-\mathrm{dM_0}&0\\0&\mathrm{dL_0}-\mathrm{dM_0}\end{pmatrix}+\dot{\mathrm{z}}\frac{3}{2}\mathrm{dL_2}\cdot\begin{pmatrix}\cos(2\theta_{\mathrm{em}})&\sin(2\theta_{\mathrm{em}})\\\sin(2\theta_{\mathrm{em}})&-\cos(2\theta_{\mathrm{em}})\end{pmatrix}\right.\\ &\left.+3\mathrm{zp}\dot{\theta}_{\mathrm{m}}\mathrm{dL_2}\cdot\begin{pmatrix}-\sin(2\theta_{\mathrm{em}})&\cos(2\theta_{\mathrm{em}})\\\cos(2\theta_{\mathrm{em}})&\sin(2\theta_{\mathrm{em}})\end{pmatrix}\right]\cdot\mathbf{P}\\ =&\dot{\mathrm{z}}\cdot\begin{pmatrix}\mathrm{dL_0}-\mathrm{dM_0}&0\\0&\mathrm{dL_0}-\mathrm{dM_0}\end{pmatrix}+\dot{\mathrm{z}}\frac{3}{2}\mathrm{dL_2}\cdot\begin{pmatrix}1&0\\0&-1\end{pmatrix}\\ &+3\mathrm{zp}\dot{\theta}_{\mathrm{m}}\mathrm{dL_2}\cdot\begin{pmatrix}0&1\\1&0\end{pmatrix}\end{aligned}\tag{C.4}$$

  Definitions 2.33 and 2.34 allow to simplify the expression

$$=\begin{pmatrix}\dot{\mathrm{z}}\mathrm{dL_d}&3\mathrm{zp}\dot{\theta}_{\mathrm{m}}\mathrm{dL_2}\\3\mathrm{zp}\dot{\theta}_{\mathrm{m}}\mathrm{dL_2}&\dot{\mathrm{z}}\mathrm{dL_q}\end{pmatrix}$$

- The second one:

$$\begin{aligned}\mathbf{P^{-1}}\mathbf{L_V^S}\frac{\mathrm{d}\mathbf{P}}{\mathrm{dt}}=&\mathbf{P^{-1}}\cdot\mathrm{z}\cdot\begin{pmatrix}\mathrm{dL_0}-\mathrm{dM_0}&0\\0&\mathrm{dL_0}-\mathrm{dM_0}\end{pmatrix}\cdot\frac{\mathrm{d}\mathbf{P}}{\mathrm{dt}}\\ &+\frac{3}{2}\mathrm{zdL_2}\cdot\mathbf{P^{-1}}\cdot\begin{pmatrix}\cos(2\theta_{\mathrm{em}})&\sin(2\theta_{\mathrm{em}})\\\sin(2\theta_{\mathrm{em}})&-\cos(2\theta_{\mathrm{em}})\end{pmatrix}\cdot\frac{\mathrm{d}\mathbf{P}}{\mathrm{dt}}\end{aligned}$$

  Since the matrix product has the same form as the one performed for equation C.2, then only the final result is given

  Definitions 2.33 and 2.34 allow to simplify the expression

$$\begin{aligned}=&\mathrm{zp}\dot{\theta}_{\mathrm{m}}\cdot\begin{pmatrix}0&-(\mathrm{L_0}-\mathrm{dM_0})-\frac{3}{2}\mathrm{dL_2}\\\mathrm{dL_0}-\mathrm{dM_0}-\frac{3}{2}\mathrm{dL_2}&0\end{pmatrix}\\ =&\mathrm{zp}\dot{\theta}_{\mathrm{m}}\cdot\begin{pmatrix}0&-\mathrm{dL_d}\\\mathrm{dL_q}&0\end{pmatrix}\end{aligned}$$

- The last one: the development is very similar to the one made for equation C.3, then

it will not be as detailed:

$$\begin{aligned}\mathbf{P^{-1}L_V^S P} &= \mathrm{z}\cdot\begin{pmatrix}\mathrm{dL_0}-\mathrm{dM_0}+\frac{3}{2}\mathrm{dL_2} & 0\\ 0 & \mathrm{dL_0}-\mathrm{dM_0}-\frac{3}{2}\mathrm{dL_2}\end{pmatrix}\\ &= \begin{pmatrix}\mathrm{z}\cdot\mathrm{dL_d} & 0\\ 0 & \mathrm{z}\cdot\mathrm{dL_q}\end{pmatrix}\end{aligned}$$

The final expression of term "b" is:

$$\begin{aligned}\mathbf{P^{-1}}\frac{\mathrm{d}}{\mathrm{dt}}\left(\mathbf{L_V^S}\cdot\mathbf{P}\cdot\mathbf{I_S^P}\right) &= \begin{pmatrix}\dot{\mathrm{z}}\mathrm{dL_d} & 3\mathrm{zp}\dot{\theta}_\mathrm{m}\mathrm{dL_2}\\ 3\mathrm{zp}\dot{\theta}_\mathrm{m}\mathrm{dL_2} & \dot{\mathrm{z}}\mathrm{dL_q}\end{pmatrix}\cdot\mathbf{I_S^P}+\mathrm{zp}\dot{\theta}_\mathrm{m}\cdot\begin{pmatrix}0 & -\mathrm{dL_d}\\ \mathrm{dL_q} & 0\end{pmatrix}\cdot\mathbf{I_S^P}\\ &\quad+\begin{pmatrix}\mathrm{z}\cdot\mathrm{dL_d} & 0\\ 0 & \mathrm{z}\cdot\mathrm{dL_q}\end{pmatrix}\cdot\frac{\mathrm{d}\mathbf{I_S^P}}{\mathrm{dt}}\\ &= \begin{pmatrix}\dot{\mathrm{z}}\mathrm{dL_d} & -\mathrm{zp}\dot{\theta}_\mathrm{m}\mathrm{dL_q}\\ \mathrm{zp}\dot{\theta}_\mathrm{m}\mathrm{dL_d} & \dot{\mathrm{z}}\mathrm{dL_q}\end{pmatrix}\cdot\mathbf{I_S^P}+\begin{pmatrix}\mathrm{z}\cdot\mathrm{dL_d} & 0\\ 0 & \mathrm{z}\cdot\mathrm{dL_q}\end{pmatrix}\cdot\frac{\mathrm{d}\mathbf{I_S^P}}{\mathrm{dt}}\end{aligned}$$

C.1.c Term "c" of equation C.1

The Park transformation of the time derivative of the motor flux vector is needed. To do so, starting from the expression computed in equation 2.20:

$$\begin{aligned}\mathbf{P^{-1}}\frac{\mathrm{d}\boldsymbol{\Phi}_\mathbf{M}^\mathbf{S}}{\mathrm{dt}} &= \mathbf{P^{-1}}\cdot\sqrt{\frac{3}{2}}\mathrm{K}_{\theta_\mathrm{m}}\cdot\begin{pmatrix}-\sin(\theta_\mathrm{em})\\ \cos(\theta_\mathrm{em})\end{pmatrix}\cdot\mathrm{p}\cdot\dot{\theta}_\mathrm{m}\\ &= \sqrt{\frac{3}{2}}\mathrm{K}_{\theta_\mathrm{m}}\mathrm{p}\dot{\theta}_\mathrm{m}\begin{pmatrix}0\\1\end{pmatrix}\end{aligned}\tag{C.5}$$

C.1.d Final expression of the motor electrical equation

It is now possible to put together all the result to obtain the final form of the motor electrical equation:

$$\begin{aligned}\mathbf{U^P} = &\frac{\mathrm{R}}{2}\cdot\mathbf{I_M^P} + \frac{\mathrm{p}\dot{\theta}_\mathrm{m}}{2}\cdot\begin{pmatrix}0 & -(\mathrm{L_q}+\mathrm{M_q})\\ \mathrm{L_d}+\mathrm{M_d} & 0\end{pmatrix}\cdot\mathbf{I_M^P} + \frac{1}{2}\cdot\begin{pmatrix}\mathrm{L_d}+\mathrm{M_d} & 0\\ 0 & \mathrm{L_q}+\mathrm{M_q}\end{pmatrix}\cdot\frac{\mathrm{d}\mathbf{I_M^P}}{\mathrm{dt}}\\ &+\begin{pmatrix}\dot{\mathrm{z}}\mathrm{dL_d} & -\mathrm{zp}\dot{\theta}_\mathrm{m}\mathrm{dL_q}\\ \mathrm{zp}\dot{\theta}_\mathrm{m}\mathrm{dL_d} & \dot{\mathrm{z}}\mathrm{dL_q}\end{pmatrix}\cdot\mathbf{I_S^P} + \begin{pmatrix}\mathrm{z}\cdot\mathrm{dL_d} & 0\\ 0 & \mathrm{z}\cdot\mathrm{dL_q}\end{pmatrix}\cdot\frac{\mathrm{d}\mathbf{I_S^P}}{\mathrm{dt}}\\ &+\sqrt{\frac{3}{2}}\mathrm{K}_{\theta_\mathrm{m}}\mathrm{p}\dot{\theta}_\mathrm{m}\cdot\begin{pmatrix}0\\1\end{pmatrix}\end{aligned}$$

By using definition 2.29 and 2.30

$$\begin{aligned}\mathbf{U^P} = &\frac{\mathrm{R}}{2}\cdot\mathbf{I_M^P} + \frac{\mathrm{p}\dot{\theta}_\mathrm{m}}{2}\cdot\begin{pmatrix}0 & -\mathrm{L_{M,q}}\\ \mathrm{L_{M,d}} & 0\end{pmatrix}\cdot\mathbf{I_M^P} + \frac{1}{2}\cdot\begin{pmatrix}\mathrm{L_{M,d}} & 0\\ 0 & \mathrm{L_{M,q}}\end{pmatrix}\cdot\frac{\mathrm{d}\mathbf{I_M^P}}{\mathrm{dt}}\\ &+\begin{pmatrix}\dot{\mathrm{z}}\mathrm{dL_d} & -\mathrm{zp}\dot{\theta}_\mathrm{m}\mathrm{dL_q}\\ \mathrm{zp}\dot{\theta}_\mathrm{m}\mathrm{dL_d} & \dot{\mathrm{z}}\mathrm{dL_q}\end{pmatrix}\cdot\mathbf{I_S^P} + \begin{pmatrix}\mathrm{z}\cdot\mathrm{dL_d} & 0\\ 0 & \mathrm{z}\cdot\mathrm{dL_q}\end{pmatrix}\cdot\frac{\mathrm{d}\mathbf{I_S^P}}{\mathrm{dt}}\\ &+\sqrt{\frac{3}{2}}\mathrm{K}_{\theta_\mathrm{m}}\mathrm{p}\dot{\theta}_\mathrm{m}\cdot\begin{pmatrix}0\\1\end{pmatrix}\end{aligned}$$

It finally provides the following system of equation[6]:

$$\begin{cases}\mathrm{U_d} = \dfrac{\mathrm{R}}{2}\cdot\mathrm{I_{M,d}} - \mathrm{p}\dot{\theta}_\mathrm{m}\cdot\dfrac{\mathrm{L_{M,q}}}{2}\cdot\mathrm{I_{M,q}} + \dfrac{\mathrm{L_{M,d}}}{2}\dot{\mathrm{I}}_\mathrm{M,d} + \mathrm{dL_d}\cdot\dfrac{\mathrm{d}}{\mathrm{dt}}(\mathrm{z}\cdot\mathrm{I_{S,d}}) - \mathrm{pz}\dot{\theta}_\mathrm{m}\mathrm{dL_q}\mathrm{I_{S,q}}\\ \mathrm{U_q} = \dfrac{\mathrm{R}}{2}\cdot\mathrm{I_{M,q}} + \mathrm{p}\dot{\theta}_\mathrm{m}\cdot\dfrac{\mathrm{L_{M,d}}}{2}\cdot\mathrm{I_{M,d}} + \dfrac{\mathrm{L_{M,q}}}{2}\dot{\mathrm{I}}_\mathrm{M,q} + \mathrm{dL_q}\cdot\dfrac{\mathrm{d}}{\mathrm{dt}}(\mathrm{z}\cdot\mathrm{I_{S,q}}) + \mathrm{pz}\dot{\theta}_\mathrm{m}\mathrm{dL_d}\mathrm{I_{S,d}} + \sqrt{\dfrac{3}{2}}\mathrm{K}_{\theta_\mathrm{m}}\mathrm{p}\dot{\theta}_\mathrm{m}\end{cases}$$

[6] Come back to the section concerning this appendix: Section 2.2.3.c

C.2 Park transformation of the second equation of 2.16

The reasoning and the matrix forms being very similar to those that have been computed in appendix C.1, the developments will not be as detailed.
Starting from the second equation of 2.16

$$0 = 2\mathrm{R} \cdot \mathbf{I_S^S} + \frac{\mathrm{d}}{\mathrm{dt}} \left(\mathbf{L_V^S} \cdot \mathbf{I_M^S} + 2 \left(\mathbf{L_{AV}^S} - \mathbf{M_{UL}^S} \right) \cdot \mathbf{I_S^S} \right) + \frac{\mathrm{d}\boldsymbol{\Phi}_\mathbf{S}^\mathbf{S}}{\mathrm{dt}}$$

By applying the Park transformation on the currents we get

$$0 = 2\mathrm{R} \cdot \mathbf{P} \cdot \mathbf{I_S^P} + \frac{\mathrm{d}}{\mathrm{dt}} \left(\mathbf{L_V^S} \cdot \mathbf{P} \cdot \mathbf{I_M^P} + 2 \left(\mathbf{L_{AV}^S} - \mathbf{M_{UL}^S} \right) \cdot \mathbf{P} \cdot \mathbf{I_S^P} \right) + \frac{\mathrm{d}\boldsymbol{\Phi}_\mathbf{S}^\mathbf{S}}{\mathrm{dt}}$$

By pre-multiplying by $\mathbf{P^{-1}}$ we obtain

$$0 = 2\mathrm{R} \cdot \mathbf{I_S^P} + \underbrace{\mathbf{P^{-1}} \frac{\mathrm{d}}{\mathrm{dt}} \left(\mathbf{L_V^S} \cdot \mathbf{P} \cdot \mathbf{I_M^P} \right)}_{\text{Very similar to the term developed in C.1.b}} + \underbrace{\mathbf{P^{-1}} \frac{\mathrm{d}}{\mathrm{dt}} \left(2 \left(\mathbf{L_{AV}^S} - \mathbf{M_{UL}^S} \right) \cdot \mathbf{P} \cdot \mathbf{I_S^P} \right)}_{\text{Very similar to the term developed in C.1.a}} + \underbrace{\mathbf{P^{-1}} \frac{\mathrm{d}\boldsymbol{\Phi}_\mathbf{S}^\mathbf{S}}{\mathrm{dt}}}_{\text{Developed below}}$$

Each term can be developed to obtain the final system of electrical suspension equations:

- The term similar to the one developed in appendix C.1.b is expressed as:

$$\mathbf{P^{-1}} \frac{\mathrm{d}}{\mathrm{dt}} \left(\mathbf{L_V^S} \cdot \mathbf{P} \cdot \mathbf{I_M^P} \right) = \begin{pmatrix} \dot{\mathrm{z}}\mathrm{dL_d} & -\mathrm{zp}\dot{\theta}_\mathrm{m}\mathrm{dL_q} \\ \mathrm{zp}\dot{\theta}_\mathrm{m}\mathrm{dL_d} & \dot{\mathrm{z}}\mathrm{dL_q} \end{pmatrix} \cdot \mathbf{I_M^P} + \begin{pmatrix} \mathrm{z} \cdot \mathrm{dL_d} & 0 \\ 0 & \mathrm{z} \cdot \mathrm{dL_q} \end{pmatrix} \cdot \frac{\mathrm{d}\mathbf{I_M^P}}{\mathrm{dt}}$$

- The one similar to the term of appendix C.1.a is expressed as:

$$\mathbf{P^{-1}} \frac{\mathrm{d}}{\mathrm{dt}} \left(2 \left(\mathbf{L_{AV}^S} - \mathbf{M_{UL}^S} \right) \cdot \mathbf{P} \cdot \mathbf{I_S^P} \right) = 2\mathrm{p}\dot{\theta}_\mathrm{m} \cdot \begin{pmatrix} 0 & -(\mathrm{L_q} - \mathrm{M_q}) \\ \mathrm{L_d} - \mathrm{M_d} & 0 \end{pmatrix} \cdot \mathbf{I_S^P} + 2 \cdot \begin{pmatrix} \mathrm{L_d} - \mathrm{M_d} & 0 \\ 0 & \mathrm{L_q} - \mathrm{M_q} \end{pmatrix} \cdot \frac{\mathrm{d}\mathbf{I_S^P}}{\mathrm{dt}}$$

This expression can be simplified by using definition 2.31 and 2.32

$$= 2\mathrm{p}\dot{\theta}_\mathrm{m} \cdot \begin{pmatrix} 0 & -\mathrm{L_{S,q}} \\ \mathrm{L_{S,d}} & 0 \end{pmatrix} \cdot \mathbf{I_S^P} + 2 \cdot \begin{pmatrix} \mathrm{L_{S,d}} & 0 \\ 0 & \mathrm{L_{S,q}} \end{pmatrix} \cdot \frac{\mathrm{d}\mathbf{I_S^P}}{\mathrm{dt}}$$

- The last term concerning the flux derivatives, starting from equation 2.21, is expressed as:

$$\begin{aligned} \mathbf{P^{-1}} \frac{\mathrm{d}\boldsymbol{\Phi}_\mathbf{S}^\mathbf{S}}{\mathrm{dt}} &= \mathbf{P^{-1}} \cdot \sqrt{6}\mathrm{K_z} \cdot \left[\mathrm{z} \cdot \begin{pmatrix} -\sin(\theta_\mathrm{em}) \\ \cos(\theta_\mathrm{em}) \end{pmatrix} \cdot \mathrm{p}\dot{\theta}_\mathrm{m} + \dot{\mathrm{z}} \begin{pmatrix} \cos(\theta_\mathrm{em}) \\ \sin(\theta_\mathrm{em}) \end{pmatrix} \right] \\ &= \sqrt{6}\mathrm{K_z} \cdot \left[\mathrm{z} \cdot \begin{pmatrix} 0 \\ 1 \end{pmatrix} \cdot \mathrm{p}\dot{\theta}_\mathrm{m} + \dot{\mathrm{z}} \begin{pmatrix} 1 \\ 0 \end{pmatrix} \right] \end{aligned} \tag{C.6}$$

C.2.a Final expression of the electrical suspension equations

By gathering all the terms, the final expression of the suspension electrical equation is:

$$\begin{aligned} 0 = {} & 2\mathrm{R}\cdot\mathbf{I_S^P} + 2\mathrm{p}\dot{\theta}_\mathrm{m}\cdot\begin{pmatrix}0 & -\mathrm{L_{S,q}}\\ \mathrm{L_{S,d}} & 0\end{pmatrix}\cdot\mathbf{I_S^P} + 2\cdot\begin{pmatrix}\mathrm{L_{S,d}} & 0\\ 0 & \mathrm{L_{S,q}}\end{pmatrix}\cdot\frac{\mathrm{d}\mathbf{I_S^P}}{\mathrm{dt}} \\ & + \begin{pmatrix}\dot{\mathrm{z}}\mathrm{dL_d} & -\mathrm{zp}\dot{\theta}_\mathrm{m}\mathrm{dL_q}\\ \mathrm{zp}\dot{\theta}_\mathrm{m}\mathrm{dL_d} & \dot{\mathrm{z}}\mathrm{dL_q}\end{pmatrix}\cdot\mathbf{I_M^P} + \begin{pmatrix}\mathrm{z}\cdot\mathrm{dL_d} & 0\\ 0 & \mathrm{z}\cdot\mathrm{dL_q}\end{pmatrix}\cdot\frac{\mathrm{d}\mathbf{I_M^P}}{\mathrm{dt}} + \sqrt{6}\mathrm{K_z}\cdot\begin{pmatrix}\dot{\mathrm{z}}\\ \mathrm{p}\dot{\theta}_\mathrm{m}\mathrm{z}\end{pmatrix} \end{aligned}$$

Which provides the following system[7]:

$$\begin{cases} 0 = 2\mathrm{R}\cdot\mathrm{I_{S,d}} - 2\mathrm{p}\dot{\theta}_\mathrm{m}\mathrm{L_{S,q}}\cdot\mathrm{I_{S,q}} + 2\mathrm{L_{S,d}}\dot{\mathrm{I}}_\mathrm{S,d} + \mathrm{dL_d}\cdot\dfrac{\mathrm{d}}{\mathrm{dt}}(\mathrm{z}\cdot\mathrm{I_{M,d}}) - \mathrm{pz}\dot{\theta}_\mathrm{m}\mathrm{dL_q}\cdot\mathrm{I_{M,q}} + \sqrt{6}\mathrm{K_z}\cdot\dot{\mathrm{z}} \\ 0 = 2\mathrm{R}\cdot\mathrm{I_{S,q}} + 2\mathrm{p}\dot{\theta}_\mathrm{m}\mathrm{L_{S,d}}\cdot\mathrm{I_{S,d}} + 2\mathrm{L_{S,q}}\dot{\mathrm{I}}_\mathrm{S,q} + \mathrm{dL_q}\cdot\dfrac{\mathrm{d}}{\mathrm{dt}}(\mathrm{z}\cdot\mathrm{I_{M,q}}) + \mathrm{pz}\dot{\theta}_\mathrm{m}\mathrm{dL_d}\cdot\mathrm{I_{M,d}} + \sqrt{6}\mathrm{K_z}\mathrm{p}\dot{\theta}_\mathrm{m}\cdot\mathrm{z} \end{cases}$$

[7] Come back to the section concerning this appendix: Section 2.2.3.c

D Electrodynamics forces and torques

D.1 Axial electrodynamic force

Starting from its definition it gives [8]:

$$\begin{aligned}
\mathrm{F_{z,Ed}} &= [\mathbf{I_U}]^{\mathrm{T}} \cdot \frac{\partial \boldsymbol{\Phi}_\mathbf{U}}{\partial \mathrm{z}} + [\mathbf{I_L}]^{\mathrm{T}} \cdot \frac{\partial \boldsymbol{\Phi}_\mathbf{L}}{\partial \mathrm{z}} \\
&= \left[\frac{\mathbf{I_M}}{2} + \mathbf{I_S}\right]^{\mathrm{T}} \cdot \frac{\partial \boldsymbol{\Phi}_\mathbf{U}}{\partial \mathrm{z}} + \left[\frac{\mathbf{I_M}}{2} - \mathbf{I_S}\right]^{\mathrm{T}} \cdot \frac{\partial \boldsymbol{\Phi}_\mathbf{L}}{\partial \mathrm{z}} \\
&= [\mathbf{I_M}]^{\mathrm{T}} \cdot \frac{\partial \left(\frac{\boldsymbol{\Phi}_\mathbf{U} + \boldsymbol{\Phi}_\mathbf{L}}{2}\right)}{\partial \mathrm{z}} + [\mathbf{I_S}]^{\mathrm{T}} \cdot \frac{\partial \left(\boldsymbol{\Phi}_\mathbf{U} - \boldsymbol{\Phi}_\mathbf{L}\right)}{\partial \mathrm{z}} \\
&= [\mathbf{I_M}]^{\mathrm{T}} \cdot \frac{\partial \boldsymbol{\Phi}_\mathbf{M}}{\partial \mathrm{z}} + [\mathbf{I_S}]^{\mathrm{T}} \cdot \frac{\partial \boldsymbol{\Phi}_\mathbf{S}}{\partial \mathrm{z}}
\end{aligned}$$

The first term having no z-dependency, is reduced to:

$$= 0 + [\mathbf{I_S}]^{\mathrm{T}} \cdot \frac{\partial \boldsymbol{\Phi}_\mathbf{S}}{\partial \mathrm{z}}$$

The Park and Concordia transformation can be applied on the currents to obtain:

$$\begin{aligned}
&= \left[\mathbf{T} \cdot \mathbf{P} \cdot \mathbf{I_S^P}\right]^{\mathrm{T}} \cdot \frac{\partial \boldsymbol{\Phi}_\mathbf{S}}{\partial \mathrm{z}} \\
&= \left[\mathbf{I_S^P}\right]^{\mathrm{T}} \cdot \mathbf{P^T} \cdot \mathbf{T^T} \frac{\partial \boldsymbol{\Phi}_\mathbf{S}}{\partial \mathrm{z}}
\end{aligned}$$

Both transformations being orthogonal, the expression becomes

$$\begin{aligned}
&= \left[\mathbf{I_S^P}\right]^{\mathrm{T}} \cdot \mathbf{P^{-1}} \cdot \mathbf{T^{-1}} \frac{\partial \boldsymbol{\Phi}_\mathbf{S}}{\partial \mathrm{z}} \\
&= \left[\mathbf{I_S^P}\right]^{\mathrm{T}} \cdot \mathbf{P^{-1}} \cdot \mathbf{T^{-1}} \cdot 2\mathrm{K_z} \begin{pmatrix} \cos(\theta_{\mathrm{em}}) \\ \cos(\theta_{\mathrm{em}} - \frac{2\pi}{3}) \\ \cos(\theta_{\mathrm{em}} - \frac{4\pi}{3}) \end{pmatrix} \\
&= \left[\mathbf{I_S^P}\right]^{\mathrm{T}} \cdot \mathbf{P^{-1}} \cdot \sqrt{6}\mathrm{K_z} \cdot \begin{pmatrix} 0 \\ \cos(\theta_{\mathrm{em}}) \\ \sin(\theta_{\mathrm{em}}) \end{pmatrix} \\
&= \left[\begin{pmatrix} \mathrm{I_{S,d}} \\ \mathrm{I_{S,q}} \end{pmatrix}\right]^{\mathrm{T}} \cdot \sqrt{6}\mathrm{K_z} \cdot \begin{pmatrix} 1 \\ 0 \end{pmatrix}
\end{aligned}$$

$$\mathrm{F_{z,Ed}} = \sqrt{6}\mathrm{K_z} \cdot \mathrm{I_{S,d}}$$

[8] Come back to the section concerning this appendix: Section 2.2.4

D.2 Electrodynamic torque

Starting from the definition of the electrodynamic torque, the expression can be developed as[9]:

$$\mathrm{T}_{\theta_\mathrm{m},\mathrm{Ed}} = [\mathbf{I_U}]^\mathrm{T} \cdot \frac{\partial \boldsymbol{\Phi}_\mathbf{U}}{\partial \theta_\mathrm{m}} + [\mathbf{I_L}]^\mathrm{T} \cdot \frac{\partial \boldsymbol{\Phi}_\mathbf{L}}{\partial \theta_\mathrm{m}}$$

Using the motor and suspension currents defined in 2.9 allow to express the equation as:

$$\begin{aligned}
&= \left[\frac{\mathbf{I_M}}{2} + \mathbf{I_S}\right]^\mathrm{T} \cdot \frac{\partial \boldsymbol{\Phi}_\mathbf{U}}{\theta_\mathrm{m}} + \left[\frac{\mathbf{I_M}}{2} - \mathbf{I_S}\right]^\mathrm{T} \cdot \frac{\partial \boldsymbol{\Phi}_\mathbf{L}}{\theta_\mathrm{m}} \\
&= [\mathbf{I_M}]^\mathrm{T} \cdot \frac{\partial \left(\frac{\boldsymbol{\Phi}_\mathbf{U} + \boldsymbol{\Phi}_\mathbf{L}}{2}\right)}{\theta_\mathrm{m}} + [\mathbf{I_S}]^\mathrm{T} \cdot \frac{\partial \left(\boldsymbol{\Phi}_\mathbf{U} - \boldsymbol{\Phi}_\mathbf{L}\right)}{\theta_\mathrm{m}} \\
&= [\mathbf{I_M}]^\mathrm{T} \cdot \frac{\partial \boldsymbol{\Phi}_\mathbf{M}}{\theta_\mathrm{m}} + [\mathbf{I_S}]^\mathrm{T} \cdot \frac{\partial \boldsymbol{\Phi}_\mathbf{S}}{\theta_\mathrm{m}} \\
&= \left[\mathbf{T} \cdot \mathbf{P} \cdot \mathbf{I_M^P}\right]^\mathrm{T} \cdot \frac{\partial \boldsymbol{\Phi}_\mathbf{M}}{\theta_\mathrm{m}} + \left[\mathbf{T} \cdot \mathbf{P} \cdot \mathbf{I_S^P}\right]^\mathrm{T} \cdot \frac{\partial \boldsymbol{\Phi}_\mathbf{S}}{\theta_\mathrm{m}} \\
&= \left[\mathbf{I_M^P}\right]^\mathrm{T} \cdot \mathbf{P^{-1}} \cdot \mathbf{T^{-1}} \cdot \frac{\partial \boldsymbol{\Phi}_\mathbf{M}}{\theta_\mathrm{m}} + \left[\mathbf{I_S^P}\right]^\mathrm{T} \cdot \mathbf{P^{-1}} \cdot \mathbf{T^{-1}} \cdot \frac{\partial \boldsymbol{\Phi}_\mathbf{S}}{\theta_\mathrm{m}}
\end{aligned}$$

These transformations and partial derivatives have already been computed in C.6 and C.5

$$\begin{aligned}
&= \left[\begin{pmatrix} \mathrm{I_{M,d}} \\ \mathrm{I_{M,q}} \end{pmatrix}\right]^\mathrm{T} \cdot \sqrt{\frac{3}{2}} \mathrm{K}_{\theta_\mathrm{m}} \mathrm{p} \dot{\theta}_\mathrm{m} \begin{pmatrix} 0 \\ 1 \end{pmatrix} + \left[\begin{pmatrix} \mathrm{I_{S,d}} \\ \mathrm{I_{S,q}} \end{pmatrix}\right]^\mathrm{T} \cdot \sqrt{6} \mathrm{zK_z} \cdot \mathrm{p} \dot{\theta}_\mathrm{m} \begin{pmatrix} 0 \\ 1 \end{pmatrix} \\
\mathrm{T}_{\theta_\mathrm{m},\mathrm{Ed}} &= \underbrace{\mathrm{pK}_{\theta_\mathrm{m}} \sqrt{\frac{3}{2}} \cdot \mathrm{I_{M,q}}}_{\mathrm{T}_{\theta_\mathrm{m},\mathrm{M}}} + \underbrace{\mathrm{pzK_z}\sqrt{6} \cdot \mathrm{I_{S,q}}}_{\mathrm{T}_{\theta_\mathrm{m},\mathrm{D}}}
\end{aligned}$$

[9] Come back to the section concerning this appendix: Section 2.2.4

E Reluctant force and torque

E.1 Axial reluctant force

Starting from the axial electrodynamic force and developing its expression[10], it gives:

$$\begin{aligned}
\mathrm{F_{z,rel}} =& \frac{1}{2} \cdot \begin{pmatrix} \mathbf{I_U} \\ \mathbf{I_L} \end{pmatrix}^{\mathrm{T}} \cdot \frac{\partial}{\partial \mathrm{z}} \cdot \begin{pmatrix} \mathbf{L_U} & \mathbf{M_{UL}} \\ \mathbf{M_{UL}}^{\mathrm{T}} & \mathbf{L_L} \end{pmatrix} \cdot \begin{pmatrix} \mathbf{I_U} \\ \mathbf{I_L} \end{pmatrix} \\
=& \frac{1}{2} \cdot [\mathbf{I_U}]^{\mathrm{T}} \cdot \frac{\partial \mathbf{L_U}}{\partial \mathrm{z}} \cdot \mathbf{I_U} + \frac{1}{2} \cdot [\mathbf{I_L}]^{\mathrm{T}} \cdot \frac{\partial \mathbf{L_L}}{\partial \mathrm{z}} \cdot \mathbf{I_L} + [\mathbf{I_U}]^{\mathrm{T}} \cdot \underbrace{\frac{\partial \mathbf{M_{UL}}}{\partial \mathrm{z}}}_{=0 \text{ because no z-dependency}} \cdot \mathbf{I_L}
\end{aligned}$$

Using the motor and suspension currents defined in 2.9 allow to express the equation as:

$$\begin{aligned}
=& \frac{1}{2} \cdot \left[\frac{\mathbf{I_M}}{2} + \mathbf{I_S}\right]^{\mathrm{T}} \cdot \frac{\partial \mathbf{L_U}}{\partial \mathrm{z}} \cdot \left[\frac{\mathbf{I_M}}{2} + \mathbf{I_S}\right] + \frac{1}{2} \cdot \left[\frac{\mathbf{I_M}}{2} - \mathbf{I_S}\right]^{\mathrm{T}} \cdot \frac{\partial \mathbf{L_L}}{\partial \mathrm{z}} \cdot \left[\frac{\mathbf{I_M}}{2} - \mathbf{I_S}\right] \\
=& \left[\frac{\mathbf{I_M}}{2}\right]^{\mathrm{T}} \cdot \frac{\partial \left(\frac{\mathbf{L_U}+\mathbf{L_L}}{2}\right)}{\partial \mathrm{z}} \cdot \frac{\mathbf{I_M}}{2} + [\mathbf{I_S}]^{\mathrm{T}} \cdot \frac{\partial \left(\frac{\mathbf{L_U}+\mathbf{L_L}}{2}\right)}{\partial \mathrm{z}} \cdot \mathbf{I_S} \\
&+ \left[\frac{\mathbf{I_M}}{2}\right]^{\mathrm{T}} \cdot \frac{\partial \left(\frac{\mathbf{L_U}-\mathbf{L_L}}{2}\right)}{\partial \mathrm{z}} \cdot \mathbf{I_S} + [\mathbf{I_S}]^{\mathrm{T}} \cdot \frac{\partial \left(\frac{\mathbf{L_U}-\mathbf{L_L}}{2}\right)}{\partial \mathrm{z}} \cdot \frac{\mathbf{I_M}}{2}
\end{aligned}$$

And then by using definitions 2.13 and 2.14

$$\begin{aligned}
=& \left[\frac{\mathbf{I_M}}{2}\right]^{\mathrm{T}} \cdot \frac{\partial (\mathbf{L_{AV}})}{\partial \mathrm{z}} \cdot \frac{\mathbf{I_M}}{2} + [\mathbf{I_S}]^{\mathrm{T}} \cdot \frac{\partial (\mathbf{L_{AV}})}{\partial \mathrm{z}} \cdot \mathbf{I_S} \\
&+ \left[\frac{\mathbf{I_M}}{2}\right]^{\mathrm{T}} \cdot \frac{\partial (\mathbf{L_V})}{\partial \mathrm{z}} \cdot \mathbf{I_S} + [\mathbf{I_S}]^{\mathrm{T}} \cdot \frac{\partial (\mathbf{L_V})}{\partial \mathrm{z}} \cdot \frac{\mathbf{I_M}}{2}
\end{aligned}$$

As $\frac{\partial \mathbf{L_{AV}}}{\partial \mathrm{z}} = 0$ and $\frac{\partial \mathbf{L_V}}{\partial \mathrm{z}} = \mathbf{dL_0} + \mathrm{dL_2} \cdot [\boldsymbol{2\theta_{em}}]$ it becomes:

$$= \left[\frac{\mathbf{I_M}}{2}\right]^{\mathrm{T}} \cdot [\mathbf{dL_0} + \mathrm{dL_2} \cdot [\boldsymbol{2\theta_{em}}]] \cdot \mathbf{I_S} + [\mathbf{I_S}]^{\mathrm{T}} \cdot [\mathbf{dL_0} + \mathrm{dL_2} \cdot [\boldsymbol{2\theta_{em}}]] \cdot \frac{\mathbf{I_M}}{2}$$

The Park and Concordia transformations can be applied on the currents to obtain:

$$\begin{aligned}
=& \left[\mathbf{P} \cdot \mathbf{T} \cdot \frac{\mathbf{I_M^P}}{2}\right]^{\mathrm{T}} \cdot [\mathbf{dL_0} + \mathrm{dL_2} \cdot [\boldsymbol{2\theta_{em}}]] \cdot \mathbf{P} \cdot \mathbf{T} \cdot \mathbf{I_S^P} \\
&+ \left[\mathbf{P} \cdot \mathbf{T} \cdot \mathbf{I_S^P}\right]^{\mathrm{T}} \cdot [\mathbf{dL_0} + \mathrm{dL_2} \cdot [\boldsymbol{2\theta_{em}}]] \cdot \mathbf{P} \cdot \mathbf{T} \cdot \frac{\mathbf{I_M^P}}{2}
\end{aligned}$$

[10] Come back to the section concerning this appendix: Section 2.2.5

Both transformations being orthogonal

$$= \left[\frac{\mathbf{I_M^P}}{2}\right]^{\mathrm{T}} \cdot \mathbf{P^{-1}} \cdot \mathbf{T^{-1}} \left[\mathbf{dL_0} + \mathrm{dL_2} \cdot [\boldsymbol{2\theta_{em}}]\right] \cdot \mathbf{P} \cdot \mathbf{T} \cdot \mathbf{I_S^P}$$
$$+ \left[\mathbf{I_S^P}\right]^{\mathrm{T}} \mathbf{P^{-1}} \cdot \mathbf{T^{-1}} \cdot \left[\mathbf{dL_0} + \mathrm{dL_2} \cdot [\boldsymbol{2\theta_{em}}]\right] \cdot \mathbf{P} \cdot \mathbf{T} \cdot \frac{\mathbf{I_M^P}}{2}$$

Transformations of the matrices similar to those made in C.4

$$= \left[\frac{\mathbf{I_M^P}}{2}\right]^{\mathrm{T}} \cdot \begin{pmatrix} \mathrm{dL_d} & 0 \\ 0 & \mathrm{dL_q} \end{pmatrix} \cdot \mathbf{I_S^P} + \left[\mathbf{I_S^P}\right]^{\mathrm{T}} \begin{pmatrix} \mathrm{dL_d} & 0 \\ 0 & \mathrm{dL_q} \end{pmatrix} \cdot \frac{\mathbf{I_M^P}}{2}$$

$$\mathrm{F_{z,rel}} = \mathrm{I_{M,d}} \cdot \mathrm{I_{S,d}} \cdot \mathrm{dL_d} + \mathrm{I_{M,q}} \cdot \mathrm{I_{S,q}} \cdot \mathrm{dL_q}$$

E.2 Reluctant torque

$$\mathrm{T}_{\theta_\mathrm{m},\mathrm{rel}} = \frac{1}{2} \cdot [\mathbf{I_U}]^{\mathrm{T}} \cdot \frac{\partial \mathbf{L_U}}{\partial \theta_\mathrm{m}} \cdot \mathbf{I_U} + \frac{1}{2} \cdot [\mathbf{I_L}]^{\mathrm{T}} \cdot \frac{\partial \mathbf{L_L}}{\partial \theta_\mathrm{m}} \cdot \mathbf{I_L} + [\mathbf{I_U}]^{\mathrm{T}} \cdot \frac{\partial \mathbf{M_{UL}}}{\partial \theta_\mathrm{m}} \cdot \mathbf{I_L}$$

By using the motor and suspension currents defined in 2.9
allow to express the equation as:

$$= \frac{1}{2} \cdot \left[\frac{\mathbf{I_M}}{2} + \mathbf{I_S}\right]^{\mathrm{T}} \cdot \frac{\partial \mathbf{L_U}}{\partial \theta_\mathrm{m}} \cdot \left[\frac{\mathbf{I_M}}{2} + \mathbf{I_S}\right]$$
$$+ \frac{1}{2} \cdot \left[\frac{\mathbf{I_M}}{2} - \mathbf{I_S}\right]^{\mathrm{T}} \cdot \frac{\partial \mathbf{L_L}}{\partial \theta_\mathrm{m}} \cdot \left[\frac{\mathbf{I_M}}{2} - \mathbf{I_S}\right]$$
$$+ \left[\frac{\mathbf{I_M}}{2} + \mathbf{I_S}\right]^{\mathrm{T}} \cdot \frac{\partial \mathbf{M_{UL}}}{\partial \theta_\mathrm{m}} \cdot \left[\frac{\mathbf{I_M}}{2} - \mathbf{I_S}\right]$$

And applying the Concordia and Park transformation provides:

$$= \frac{1}{2} \cdot \left[\frac{\mathbf{I_M^P}}{2} + \mathbf{I_S^P}\right]^{\mathrm{T}} \cdot \mathbf{P}^{-1} \cdot \mathbf{T}^{-1} \cdot \frac{\partial \mathbf{L_U}}{\partial \theta_\mathrm{m}} \cdot \mathbf{T} \cdot \mathbf{P} \cdot \left[\frac{\mathbf{I_M^P}}{2} + \mathbf{I_S^P}\right]$$
$$+ \frac{1}{2} \cdot \left[\frac{\mathbf{I_M^P}}{2} - \mathbf{I_S^P}\right]^{\mathrm{T}} \cdot \mathbf{P}^{-1} \cdot \mathbf{T}^{-1} \cdot \frac{\partial \mathbf{L_L}}{\partial \theta_\mathrm{m}} \cdot \mathbf{T} \cdot \mathbf{P} \cdot \left[\frac{\mathbf{I_M^P}}{2} - \mathbf{I_S^P}\right]$$
$$+ \left[\frac{\mathbf{I_M^P}}{2} + \mathbf{I_S^P}\right]^{\mathrm{T}} \cdot \mathbf{P}^{-1} \cdot \mathbf{T}^{-1} \cdot \frac{\partial \mathbf{M_{UL}}}{\partial \theta_\mathrm{m}} \cdot \mathbf{T} \cdot \mathbf{P} \cdot \left[\frac{\mathbf{I_M^P}}{2} - \mathbf{I_S^P}\right]$$

Knowing that

- $\frac{\partial \mathbf{L_U}}{\partial \theta_\mathrm{m}} = (\mathrm{L_2} + \mathrm{z} \cdot \mathrm{dL_2}) \cdot \frac{\partial \theta_\mathrm{em}}{\theta_\mathrm{m}} \cdot \frac{\partial [\boldsymbol{2\theta_{em}}]}{\theta_\mathrm{em}} = \mathrm{p} \cdot (\mathrm{L_2} + \mathrm{z} \cdot \mathrm{dL_2}) \cdot \frac{\partial [\boldsymbol{2\theta_{em}}]}{\theta_\mathrm{em}}$ with $[\boldsymbol{2\theta_{em}}]$ defined in 2.4
- $\frac{\partial \mathbf{L_L}}{\partial \theta_\mathrm{m}} = \mathrm{p} \cdot (\mathrm{L_2} - \mathrm{z} \cdot \mathrm{dL_2}) \cdot \frac{\partial [\boldsymbol{2\theta_{em}}]}{\theta_\mathrm{em}}$
- $\frac{\partial \mathbf{M_{UL}}}{\partial \theta_\mathrm{m}} = \mathrm{p} \cdot \mathrm{M_2} \cdot \frac{\partial [\boldsymbol{2\theta_{em}}]}{\theta_\mathrm{em}}$

It becomes:

$$\begin{aligned}
\mathrm{T}_{\theta_\mathrm{m},\mathrm{rel}} = & \frac{1}{2} \cdot \left[\frac{\mathbf{I_M^P}}{2} + \mathbf{I_S^P} \right]^\mathrm{T} \cdot \mathbf{P}^{-1} \cdot \mathbf{T}^{-1} \cdot \mathrm{p} \cdot (\mathrm{L}_2 + \mathrm{z} \cdot \mathrm{dL}_2) \cdot \frac{\partial[\boldsymbol{2\theta_{em}}]}{\theta_\mathrm{em}} \cdot \mathbf{T} \cdot \mathbf{P} \cdot \left[\frac{\mathbf{I_M^P}}{2} + \mathbf{I_S^P} \right] \\
& + \frac{1}{2} \cdot \left[\frac{\mathbf{I_M^P}}{2} - \mathbf{I_S^P} \right]^\mathrm{T} \cdot \mathbf{P}^{-1} \cdot \mathbf{T}^{-1} \cdot \mathrm{p} \cdot (\mathrm{L}_2 - \mathrm{z} \cdot \mathrm{dL}_2) \cdot \frac{\partial[\boldsymbol{2\theta_{em}}]}{\theta_\mathrm{em}} \cdot \mathbf{T} \cdot \mathbf{P} \cdot \left[\frac{\mathbf{I_M^P}}{2} - \mathbf{I_S^P} \right] \\
& + \left[\frac{\mathbf{I_M^P}}{2} + \mathbf{I_S^P} \right]^\mathrm{T} \cdot \mathbf{P}^{-1} \cdot \mathbf{T}^{-1} \cdot \mathrm{p} \cdot \mathrm{M}_2 \cdot \frac{\partial[\boldsymbol{2\theta_{em}}]}{\theta_\mathrm{em}} \cdot \mathbf{T} \cdot \mathbf{P} \cdot \left[\frac{\mathbf{I_M^P}}{2} - \mathbf{I_S^P} \right]
\end{aligned}$$

Then the following expression can be developed:

$$\begin{aligned}
\mathbf{P}^{-1} \cdot \mathbf{T}^{-1} \cdot \frac{\partial[\boldsymbol{2\theta_{em}}]}{\theta_\mathrm{em}} \cdot \mathbf{T} \cdot \mathbf{P} &= -2 \cdot \mathbf{P}^{-1} \cdot \mathbf{T}^{-1} \cdot \begin{pmatrix} \sin(2\theta_\mathrm{em}) & \sin(2\theta_\mathrm{em} - 2\pi/3) & \sin(2\theta_\mathrm{em} - 4\pi/3) \\ \sin(2\theta_\mathrm{em} - 2\pi/3) & \sin(2\theta_\mathrm{em} - 4\pi/3) & \sin(2\theta_\mathrm{em}) \\ \sin(2\theta_\mathrm{em} - 4\pi/3) & \sin(2\theta_\mathrm{em}) & \sin(2\theta_\mathrm{em} - 2\pi/3) \end{pmatrix} \cdot \mathbf{T} \cdot \mathbf{P} \\
&= 3 \cdot \mathbf{P}^{-1} \cdot \begin{pmatrix} 0 & 0 & 0 \\ 0 & -\sin(2\theta_\mathrm{em}) & \cos(2\theta_\mathrm{em}) \\ 0 & \cos(2\theta_\mathrm{em}) & \sin(2\theta_\mathrm{em}) \end{pmatrix} \cdot \mathbf{P} \\
&= \begin{pmatrix} 0 & 0 & 0 \\ 0 & 0 & 3 \\ 0 & 3 & 0 \end{pmatrix}
\end{aligned}$$

which will be noted without the homopolar component:

$$= \begin{pmatrix} 0 & 3 \\ 3 & 0 \end{pmatrix}$$

Then the next expression can be developed[a]:

$$
\begin{aligned}
\mathrm{T}_{\theta_\mathrm{m},\mathrm{rel}} = \quad & \frac{1}{2}\cdot\left[\frac{\mathbf{I_M^P}}{2}+\mathbf{I_S^P}\right]^{\mathrm{T}}\cdot \mathrm{p}\cdot(\mathrm{L}_2+\mathrm{z}\cdot\mathrm{dL}_2)\cdot\begin{pmatrix}0&3\\3&0\end{pmatrix}\cdot\left[\frac{\mathbf{I_M^P}}{2}+\mathbf{I_S^P}\right]\\
& +\frac{1}{2}\cdot\left[\frac{\mathbf{I_M^P}}{2}-\mathbf{I_S^P}\right]^{\mathrm{T}}\cdot \mathrm{p}\cdot(\mathrm{L}_2-\mathrm{z}\cdot\mathrm{dL}_2)\cdot\begin{pmatrix}0&3\\3&0\end{pmatrix}\cdot\left[\frac{\mathbf{I_M^P}}{2}-\mathbf{I_S^P}\right]\\
& +\left[\frac{\mathbf{I_M^P}}{2}+\mathbf{I_S^P}\right]^{\mathrm{T}}\cdot \mathrm{p}\cdot\mathrm{M}_2\cdot\begin{pmatrix}0&3\\3&0\end{pmatrix}\cdot\left[\frac{\mathbf{I_M^P}}{2}-\mathbf{I_S^P}\right]\\
\\
= \quad & \frac{3}{2}\mathrm{p}\cdot(\mathrm{L}_2+\mathrm{z}\cdot\mathrm{dL}_2)\cdot\left[\begin{pmatrix}\frac{\mathrm{I_{M,d}}}{2}+\mathrm{I_{S,d}}\\ \frac{\mathrm{I_{M,q}}}{2}+\mathrm{I_{S,q}}\end{pmatrix}\right]^{\mathrm{T}}\cdot\begin{pmatrix}0&1\\1&0\end{pmatrix}\cdot\begin{pmatrix}\frac{\mathrm{I_{M,d}}}{2}+\mathrm{I_{S,d}}\\ \frac{\mathrm{I_{M,q}}}{2}+\mathrm{I_{S,q}}\end{pmatrix}\\
& +\frac{3}{2}\mathrm{p}\cdot(\mathrm{L}_2-\mathrm{z}\cdot\mathrm{dL}_2)\cdot\left[\begin{pmatrix}\frac{\mathrm{I_{M,d}}}{2}-\mathrm{I_{S,d}}\\ \frac{\mathrm{I_{M,q}}}{2}-\mathrm{I_{S,q}}\end{pmatrix}\right]^{\mathrm{T}}\cdot\begin{pmatrix}0&1\\1&0\end{pmatrix}\cdot\begin{pmatrix}\frac{\mathrm{I_{M,d}}}{2}-\mathrm{I_{S,d}}\\ \frac{\mathrm{I_{M,q}}}{2}-\mathrm{I_{S,q}}\end{pmatrix}\\
& +3\mathrm{p}\cdot\mathrm{M}_2\cdot\left[\begin{pmatrix}\frac{\mathrm{I_{M,d}}}{2}+\mathrm{I_{S,d}}\\ \frac{\mathrm{I_{M,q}}}{2}+\mathrm{I_{S,q}}\end{pmatrix}\right]^{\mathrm{T}}\cdot\begin{pmatrix}0&1\\1&0\end{pmatrix}\cdot\begin{pmatrix}\frac{\mathrm{I_{M,d}}}{2}-\mathrm{I_{S,d}}\\ \frac{\mathrm{I_{M,q}}}{2}-\mathrm{I_{S,q}}\end{pmatrix}\\
\\
= \quad & \frac{3}{2}\mathrm{p}\cdot(\mathrm{L}_2+\mathrm{z}\cdot\mathrm{dL}_2)\cdot\left[\begin{pmatrix}\frac{\mathrm{I_{M,q}}}{2}+\mathrm{I_{S,q}}\\ \frac{\mathrm{I_{M,d}}}{2}+\mathrm{I_{S,d}}\end{pmatrix}\right]^{\mathrm{T}}\cdot\begin{pmatrix}\frac{\mathrm{I_{M,d}}}{2}+\mathrm{I_{S,d}}\\ \frac{\mathrm{I_{M,q}}}{2}+\mathrm{I_{S,q}}\end{pmatrix}\\
& +\frac{3}{2}\mathrm{p}\cdot(\mathrm{L}_2-\mathrm{z}\cdot\mathrm{dL}_2)\cdot\left[\begin{pmatrix}\frac{\mathrm{I_{M,q}}}{2}-\mathrm{I_{S,q}}\\ \frac{\mathrm{I_{M,d}}}{2}-\mathrm{I_{S,d}}\end{pmatrix}\right]^{\mathrm{T}}\cdot\begin{pmatrix}\frac{\mathrm{I_{M,d}}}{2}-\mathrm{I_{S,d}}\\ \frac{\mathrm{I_{M,q}}}{2}-\mathrm{I_{S,q}}\end{pmatrix}\\
& +3\mathrm{p}\cdot\mathrm{M}_2\cdot\left[\begin{pmatrix}\frac{\mathrm{I_{M,q}}}{2}+\mathrm{I_{S,q}}\\ \frac{\mathrm{I_{M,d}}}{2}+\mathrm{I_{S,d}}\end{pmatrix}\right]^{\mathrm{T}}\cdot\begin{pmatrix}\frac{\mathrm{I_{M,d}}}{2}-\mathrm{I_{S,d}}\\ \frac{\mathrm{I_{M,q}}}{2}-\mathrm{I_{S,q}}\end{pmatrix}\\
\\
= \quad & \frac{3}{2}\mathrm{p}\cdot(\mathrm{L}_2+\mathrm{z}\cdot\mathrm{dL}_2)\cdot\left[\frac{\mathrm{I_{M,d}I_{M,q}}}{2}+2\mathrm{I_{S,d}I_{S,q}}+\mathrm{I_{M,d}I_{S,q}}+\mathrm{I_{S,d}I_{M,q}}\right]\\
& +\frac{3}{2}\mathrm{p}\cdot(\mathrm{L}_2-\mathrm{z}\cdot\mathrm{dL}_2)\cdot\left[\frac{\mathrm{I_{M,d}I_{M,q}}}{2}+2\mathrm{I_{S,d}I_{S,q}}-\mathrm{I_{M,d}I_{S,q}}-\mathrm{I_{S,d}I_{M,q}}\right]\\
& +3\mathrm{p}\cdot\mathrm{M}_2\left[\frac{\mathrm{I_{M,d}I_{M,q}}}{2}-2\mathrm{I_{S,d}I_{S,q}}\right]\\
\\
= \quad & 3\mathrm{p}\cdot\mathrm{L}_2\cdot\left[\frac{\mathrm{I_{M,d}I_{M,q}}}{2}+2\mathrm{I_{S,d}I_{S,q}}\right]+3\mathrm{p}\cdot\mathrm{M}_2\left[\frac{\mathrm{I_{M,d}I_{M,q}}}{2}-2\mathrm{I_{S,d}I_{S,q}}\right]\\
& +3\mathrm{p}\cdot\mathrm{z}\cdot\mathrm{dL}_2\cdot[\mathrm{I_{M,d}I_{S,q}}+\mathrm{I_{S,d}I_{M,q}}]
\end{aligned}
$$

To finally reach the expression:

$$
\begin{aligned}
\mathrm{T}_{\theta_\mathrm{m},\mathrm{rel}} = \quad & 3\mathrm{p}\cdot(\mathrm{L}_2+\mathrm{M}_2)\cdot\left[\frac{\mathrm{I_{M,d}I_{M,q}}}{2}\right]+3\mathrm{p}\cdot(\mathrm{L}_2-\mathrm{M}_2)\cdot[2\mathrm{I_{S,d}I_{S,q}}]\\
& +3\mathrm{p}\cdot\mathrm{z}\cdot\mathrm{dL}_2\cdot[\mathrm{I_{M,d}I_{S,q}}+\mathrm{I_{S,d}I_{M,q}}]
\end{aligned}
$$

[a] Come back to the section concerning this appendix: Section 2.2.5

F State-space model

The purpose of this appendix is to express the different equations of 2.35 and 2.41 with the chosen state-space variables.

F.1 Modification of the electrical equations:

Concerning the electrical equations, the relations F.1 and F.2 based on 2.36 and 2.37 defined below, allow to make the following modifications:

$$F_{z,Ed} = \sqrt{6}K_z \cdot I_{S,d} \quad \Longleftrightarrow \quad I_{S,d} = \frac{1}{\sqrt{6}K_z} \cdot F_{z,Ed} \tag{F.1}$$

$$T_{\theta_m,D} = pK_z z\sqrt{6} \cdot I_{S,q} \quad \Longleftrightarrow \quad I_{S,q} = \frac{1}{\sqrt{6}pK_z}\left(\frac{T_{\theta_m,D}}{z}\right) \tag{F.2}$$

1. **State equations of the direct motor current and the axial force**

   Starting from the first electrical equation of 2.35:

$$\begin{aligned} U_d = &\frac{R}{2} \cdot I_{M,d} \quad + \quad \frac{L_{M,d}}{2}\dot{I}_{M,d} \quad - \quad p\dot{\theta}_m \cdot \frac{L_{M,q}}{2} \cdot I_{M,q} \\ &+ \quad dL_d \cdot \frac{d}{dt}(z \cdot I_{S,d}) \quad - \quad dL_q \cdot z \cdot p\dot{\theta}_m \cdot I_{S,q} \end{aligned}$$

   One can use expression F.1 and F.2 to modify the equation as

$$\begin{aligned} U_d = &\frac{R}{2} \cdot I_{M,d} \quad + \quad \frac{L_{M,d}}{2}\dot{I}_{M,d} \quad - \quad p\dot{\theta}_m \cdot \frac{L_{M,q}}{2} \cdot I_{M,q} \\ &+ \quad \frac{dL_d}{\sqrt{6}K_z} \cdot \frac{d}{dt}(z \cdot F_{z,Ed}) \quad - \quad z\dot{\theta}_m \frac{dL_q}{\sqrt{6}K_z}\left(\frac{T_{\theta_m,D}}{z}\right) \end{aligned}$$

   The $I_{M,d}$-derivative can be isolated to obtain:

$$\begin{aligned} \dot{I}_{M,d} = &\frac{2 \cdot U_d}{L_{M,d}} \quad - \quad \frac{R}{L_{M,d}} \cdot I_{M,d} \quad + \quad p\dot{\theta}_m \cdot \frac{L_{M,q}}{L_{M,d}} \cdot I_{M,q} \\ &- \quad \sqrt{\frac{2}{3}}\frac{dL_d}{K_z \cdot L_{M,d}} \cdot \left(\dot{z} \cdot F_{z,Ed} + z \cdot \dot{F}_{z,Ed}\right) \quad + \quad z\dot{\theta}_m\sqrt{\frac{2}{3}}\frac{dL_q}{K_z \cdot L_{M,d}}\left(\frac{T_{\theta_m,D}}{z}\right) \end{aligned} \tag{F.3}$$

   This equation is not yet a state equation since it depends on the derivative of the axial force. This derivative has to be replaced.

To do so, starting from the electrical equation of the direct suspension current $I_{S,d}$:

$$\begin{aligned} 0 = 2R \cdot I_{S,d} \quad &+ \quad 2L_{S,d}\dot{I}_{S,d} \quad - \quad 2p\dot{\theta}_m L_{S,q} \cdot I_{S,q} \\ + \quad dL_d \cdot \frac{d}{dt}(z \cdot I_{M,d}) \quad &- \quad dL_q \cdot z \cdot p\dot{\theta}_m \cdot I_{M,q} \quad + \quad \sqrt{6}K_z \cdot \dot{z} \end{aligned}$$

One can use expressions F.1 and F.2 to modify the equation as

$$\begin{aligned} 0 = \quad \sqrt{\frac{2}{3}}\frac{R}{K_z} \cdot F_{z,Ed} \quad &+ \quad \sqrt{\frac{2}{3}}\frac{L_{S,d}}{K_z} \cdot \dot{F}_{z,Ed} \quad - \quad \sqrt{\frac{2}{3}}\frac{L_{S,q}}{K_z}\dot{\theta}_m \cdot \left(\frac{T_{\theta_m,D}}{z}\right) \\ + \quad dL_d \cdot \frac{d}{dt}(z \cdot I_{M,d}) \quad &- \quad dL_q \cdot z \cdot p\dot{\theta}_m \cdot I_{M,q} \quad + \quad \sqrt{6}K_z \cdot \dot{z} \end{aligned}$$

The $F_{z,Ed}$-derivative can be isolated to obtain:

$$\begin{aligned} \dot{F}_{z,Ed} = \quad - \quad \frac{R}{L_{S,d}} \cdot F_{z,Ed} \quad &+ \quad \frac{L_{S,q}}{L_{S,d}}\dot{\theta}_m \cdot \left(\frac{T_{\theta_m,D}}{z}\right) \quad - \quad \sqrt{\frac{3}{2}}\frac{dL_d}{L_{S,d}} \cdot K_z \cdot (\dot{z} \cdot I_{M,d} + z \cdot \dot{I}_{M,d}) \\ + \quad \sqrt{\frac{3}{2}}\frac{dL_q}{L_{S,d}} \cdot K_z \cdot z \cdot p\dot{\theta}_m \cdot I_{M,q} \quad &- \quad 3\frac{K_z^2}{L_{S,d}} \cdot \dot{z} \end{aligned} \tag{F.4}$$

This expression will also be used in the derivation of the quasi-static model in appendix G and can be injected in F.3 to obtain the first state space equation.

$$\begin{aligned} \dot{I}_{M,d} = \quad & \frac{2 \cdot U_d}{L_{M,d}} \quad - \quad \frac{R}{L_{M,d}} \cdot I_{M,d} \quad + \quad p\dot{\theta}_m \cdot \frac{L_{M,q}}{L_{M,d}} \cdot I_{M,q} \\ - \quad & \sqrt{\frac{2}{3}}\frac{dL_d}{K_z \cdot L_{M,d}} \cdot (\dot{z} \cdot F_{z,Ed}) \quad + \quad z\dot{\theta}_m\sqrt{\frac{2}{3}}\frac{dL_q}{K_z \cdot L_{M,d}}\left(\frac{T_{\theta_m,D}}{z}\right) \\ - & \sqrt{\frac{2}{3}}\frac{dL_d}{K_z \cdot L_{M,d}} \cdot z \cdot \Bigg(\quad - \quad \frac{R}{L_{S,d}} \cdot F_{z,Ed} \quad + \quad \frac{L_{S,q}}{L_{S,d}}\dot{\theta}_m \cdot \left(\frac{T_{\theta_m,D}}{z}\right) \\ - \quad & \sqrt{\frac{3}{2}}\frac{dL_d}{L_{S,d}} \cdot K_z \cdot (\dot{z} \cdot I_{M,d} + z \cdot \dot{I}_{M,d}) \quad + \quad \sqrt{\frac{3}{2}}\frac{dL_q}{L_{S,d}} \cdot K_z \cdot z \cdot p\dot{\theta}_m \cdot I_{M,q} \quad - \quad 3\frac{K_z^2}{L_{S,d}} \cdot \dot{z}\Bigg) \end{aligned}$$

By pre-multiplying by $L_{M,d} \cdot L_{S,d}$, gathering terms for each state variable and isolating $\dot{I}_{M,d}$it gives

$$\begin{aligned} \dot{I}_{M,d} = & \frac{1}{L_{M,d} \cdot L_{S,d} - dL_d^2 \cdot z^2}\Big[\quad 2 \cdot U_d \cdot L_{S,d} \quad + \quad \left(dL_d^2 \cdot z \cdot \dot{z} - R \cdot L_{S,d}\right) \cdot I_{M,d} \\ + \quad & p\dot{\theta}_m \cdot \left(L_{M,q} \cdot L_{S,d} - z^2 \cdot dL_d \cdot dL_q\right) \cdot I_{M,q} \quad + \quad \sqrt{\frac{2}{3}}\frac{dL_d}{K_z} \cdot (z \cdot R - \dot{z} \cdot L_{S,d}) \cdot F_{z,Ed} \\ + \quad & z\dot{\theta}_m\sqrt{\frac{2}{3}}\frac{1}{K_z} \cdot (dL_q \cdot L_{S,d} - dL_d \cdot L_{S,q})\left(\frac{T_{\theta_m,D}}{z}\right) \quad + \quad \sqrt{6}K_z \cdot dL_d \cdot z \cdot \dot{z}\Big] \end{aligned}$$

This expression is the state equation of the direct motor current $I_{M,d}$ and by injecting it into F.4, allows to obtain the state equation of $F_{z,Ed}$:

$$\begin{aligned}
L_{S,d}\cdot\dot{F}_{z,Ed} = \quad & - \quad R\cdot F_{z,Ed} \quad + \quad L_{S,q}\dot{\theta}_m\cdot\left(\frac{T_{\theta_m,D}}{z}\right) \quad - \quad \sqrt{\frac{3}{2}}dL_d\cdot K_z\cdot\dot{z}\cdot I_{M,d} \\
& + \quad \sqrt{\frac{3}{2}}dL_q\cdot K_z\cdot z\cdot p\dot{\theta}_m\cdot I_{M,q} \quad - \quad 3K_z^2\cdot\dot{z} \\
& - \quad \frac{\sqrt{\frac{3}{2}}\cdot K_z\cdot z\cdot dL_d}{L_{M,d}\cdot L_{S,d}-dL_d^2\cdot z^2}\Big[\quad 2\cdot U_d\cdot L_{S,d} \quad + \quad \left(dL_d^2\cdot z\cdot\dot{z}-R\cdot L_{S,d}\right)\cdot I_{M,d} \\
& + \quad p\dot{\theta}_m\cdot\left(L_{M,q}\cdot L_{S,d}-z^2\cdot dL_d\cdot dL_q\right)\cdot I_{M,q} \quad + \quad \sqrt{\frac{2}{3}}\frac{dL_d}{K_z}\cdot(z\cdot R-\dot{z}\cdot L_{S,d})\cdot F_{z,Ed} \\
& + \quad z\dot{\theta}_m\sqrt{\frac{2}{3}}\frac{1}{K_z}\cdot(dL_q\cdot L_{S,d}-dL_d\cdot L_{S,q})\left(\frac{T_{\theta_m,D}}{z}\right) \quad + \quad \sqrt{6}K_z\cdot dL_d\cdot z\cdot\dot{z}\Big]
\end{aligned}$$

Gathering the terms for each state variable allows to obtain the second state equation:

$$\begin{aligned}
\dot{F}_{z,Ed} = \quad & \frac{1}{L_{M,d}\cdot L_{S,d}-z^2dL_d^2}\cdot\Big[\left(z\cdot\dot{z}\cdot dL_d^2-R\cdot L_{M,d}\right)\cdot F_{z,Ed} \quad + \quad \left(L_{S,q}\cdot L_{M,d}-z^2dL_d\cdot dL_q\right)\dot{\theta}_m\cdot\left(\frac{T_{\theta_m,D}}{z}\right) \\
& + \quad \sqrt{\frac{3}{2}}dL_d\cdot K_z\cdot(R\cdot z-L_{M,d}\cdot\dot{z})\cdot I_{M,d} \quad + \quad \sqrt{\frac{3}{2}}\cdot K_z\cdot z\cdot p\dot{\theta}_m\cdot I_{M,q}\cdot(dL_q\cdot L_{M,d}-dL_d\cdot L_{M,q}) \\
& - \quad 3K_z^2\cdot L_{M,d}\cdot\dot{z} \quad - \quad \sqrt{6}\cdot K_z\cdot U_d\cdot z\cdot dL_d\Big]
\end{aligned}$$

2. **State equations of the quadratic motor current and the drag torque:**

   Starting from the second electrical equation of 2.35:

$$\begin{aligned}
U_q = & \frac{R}{2}\cdot I_{M,q} \quad + \quad \frac{L_{M,q}}{2}\dot{I}_{M,q} \quad + \quad p\dot{\theta}_m\cdot\frac{L_{M,d}}{2}\cdot I_{M,d} \\
& + \quad dL_q\cdot\frac{d}{dt}(z\cdot I_{S,q}) \quad + \quad dL_d\cdot z\cdot p\dot{\theta}_m\cdot I_{S,d} \quad + \quad \sqrt{\frac{3}{2}}K_{\theta_m}p\dot{\theta}_m
\end{aligned}$$

   One can use expressions F.1 and F.2 to modify the equation as

$$\begin{aligned}
U_q = \quad & \frac{R}{2}\cdot I_{M,q} \quad + \quad \frac{L_{M,q}}{2}\dot{I}_{M,q} \quad + \quad p\dot{\theta}_m\cdot\frac{L_{M,d}}{2}\cdot I_{M,d} \\
& + \quad \frac{dL_q}{\sqrt{6}pK_z}\cdot\frac{d}{dt}\left(z\cdot\left(\frac{T_{\theta_m,D}}{z}\right)\right) \quad + \quad \frac{dL_d}{\sqrt{6}K_z}\cdot z\cdot p\dot{\theta}_m\cdot F_{z,Ed} \quad + \quad \sqrt{\frac{3}{2}}K_{\theta_m}p\dot{\theta}_m
\end{aligned}$$

The $I_{M,q}$-derivative can be isolated to obtain:

$$\begin{aligned}\dot{I}_{M,q} = \quad & \frac{2 \cdot U_q}{L_{M,q}} \quad - \quad \frac{R}{L_{M,q}} \cdot I_{M,q} \quad - \quad p\dot{\theta}_m \cdot \frac{L_{M,d}}{L_{M,q}} \cdot I_{M,d} \\ & - \quad \sqrt{\frac{2}{3}} \frac{dL_q}{pK_z L_{M,q}} \cdot \left(\dot{z} \cdot \left(\frac{T_{\theta_m,D}}{z} \right) + z \cdot \left(\frac{\dot{T}_{\theta_m,D}}{z} \right) \right) \quad - \quad \sqrt{\frac{2}{3}} \frac{dL_d}{K_z \cdot L_{M,q}} \cdot z \cdot p\dot{\theta}_m \cdot F_{z,Ed} \\ & - \quad \frac{\sqrt{6} K_{\theta_m} p}{L_{M,q}} \dot{\theta}_m \end{aligned} \tag{F.5}$$

It remains to replace the term $\left(\frac{\dot{T}_{\theta_m,D}}{z}\right)$ starting from the last electrical equation of 2.35:

$$\begin{aligned} 0 = \quad & 2R \cdot I_{S,q} \quad + \quad 2L_{S,q}\dot{I}_{S,q} \quad + \quad 2p\dot{\theta}_m L_{S,d} \cdot I_{S,d} \\ & + \quad dL_q \cdot \frac{d}{dt}(z \cdot I_{M,q}) \quad + \quad dL_d \cdot z \cdot p\dot{\theta}_m \cdot I_{M,d} \quad + \quad \sqrt{6} K_z p\dot{\theta}_m \cdot z \end{aligned}$$

Using expression F.1 and F.2 modify the equation as

$$\begin{aligned} 0 = \quad & \sqrt{\frac{2}{3}} R \cdot \frac{1}{pK_z} \left(\frac{T_{\theta_m,D}}{z} \right) \quad + \quad \sqrt{\frac{2}{3}} \frac{L_{S,q}}{pK_z} \left(\frac{\dot{T}_{\theta_m,D}}{z} \right) \quad + \quad \sqrt{\frac{2}{3}} \cdot \frac{L_{S,d}}{K_z} \cdot p\dot{\theta}_m \cdot F_{z,Ed} \\ & + \quad dL_q \cdot \frac{d}{dt}(z \cdot I_{M,q}) \quad + \quad dL_d \cdot z \cdot p\dot{\theta}_m \cdot I_{M,d} \quad + \quad \sqrt{6} K_z p\dot{\theta}_m \cdot z \end{aligned}$$

The $\left(\frac{\dot{T}_{\theta_m,D}}{z}\right)$-derivative can be isolated to obtain:

$$\begin{aligned} \left(\frac{\dot{T}_{\theta_m,D}}{z} \right) = \quad & - \quad \frac{R}{L_{S,q}} \left(\frac{T_{\theta_m,D}}{z} \right) \quad - \quad \frac{L_{S,d}}{L_{S,q}} \cdot p^2 \dot{\theta}_m \cdot F_{z,Ed} \quad - \quad \sqrt{\frac{3}{2}} pK_z \frac{dL_q}{L_{S,q}} \cdot \frac{d}{dt}(z \cdot I_{M,q}) \\ & - \quad \sqrt{\frac{3}{2}} pK_z \frac{dL_d}{L_{S,q}} \cdot z \cdot p\dot{\theta}_m \cdot I_{M,d} \quad - \quad \frac{3K_z^2 p^2}{L_{S,q}} \dot{\theta}_m \cdot z \end{aligned} \tag{F.6}$$

The last equation will be used in the quasi-static study and can be injected in F.5 to obtain the third state equation:

$$\begin{aligned}\dot{I}_{M,q} = \quad & \frac{2\cdot U_q}{L_{M,q}} \quad - \quad \frac{R}{L_{M,q}}\cdot I_{M,q} \quad - \quad p\dot{\theta}_m\cdot\frac{L_{M,d}}{L_{M,q}}\cdot I_{M,d} \quad - \quad \sqrt{\frac{2}{3}}\frac{dL_q}{pK_zL_{M,q}}\cdot(\dot{z})\cdot\left(\frac{T_{\theta_m,D}}{z}\right)\\ - \quad & \sqrt{\frac{2}{3}}\frac{dL_q}{pK_zL_{M,q}}\cdot z\cdot\left(\quad - \quad \frac{R}{L_{S,q}}\left(\frac{T_{\theta_m,D}}{z}\right) \quad - \quad \frac{L_{S,d}}{L_{S,q}}\cdot p^2\dot{\theta}_m\cdot F_{z,Ed}\right.\\ - \quad & \left.\sqrt{\frac{3}{2}}pK_z\frac{dL_q}{L_{S,q}}\cdot(\dot{z}\cdot I_{M,q}+z\cdot\dot{I}_{M,q}) \quad - \quad \sqrt{\frac{3}{2}}pK_z\frac{dL_d}{L_{S,q}}\cdot z\cdot p\dot{\theta}_m\cdot I_{M,d} \quad - \quad \frac{3K_z^2p^2}{L_{S,q}}\dot{\theta}_m\cdot z\right)\\ - \quad & \sqrt{\frac{2}{3}}\frac{dL_d}{K_z\cdot L_{M,q}}\cdot z\cdot p\dot{\theta}_m\cdot F_{z,Ed} \quad - \quad \frac{\sqrt{6}K_{\theta_m}p}{L_{M,q}}\dot{\theta}_m\end{aligned}$$

By pre-multiplying by $L_{M,q}\cdot L_{S,q}$, gathering terms for each state variable and isolating $\dot{I}_{M,q}$ it gives:

$$\begin{aligned}\dot{I}_{M,q} = & \frac{1}{\left(L_{M,q}\cdot L_{S,q}-z^2\cdot dL_q^2\right)}\cdot\left[\quad 2\cdot U_q\cdot L_{S,q} \quad + \quad \left(dL_q^2\cdot z\cdot\dot{z}-R\cdot L_{S,q}\right)\cdot I_{M,q}\right.\\ + \quad & p\dot{\theta}_m\cdot\left[z^2\cdot dL_d\cdot dL_q-L_{M,d}\cdot L_{S,q}\right]\cdot I_{M,d} \quad + \quad \sqrt{\frac{2}{3}}\frac{dL_q}{pK_z}\cdot(z\cdot R-\dot{z}\cdot L_{S,q})\cdot\left(\frac{T_{\theta_m,D}}{z}\right)\\ - \quad & \left.\sqrt{\frac{2}{3}}\frac{L_{S,q}\cdot dL_d-L_{S,d}\cdot dL_q}{K_z}\cdot z\cdot p\dot{\theta}_m\cdot F_{z,Ed} \quad + \quad \sqrt{6}\cdot p\dot{\theta}_m\cdot\left(z^2\cdot K_z\cdot dL_q-K_{\theta_m}\cdot L_{S,q}\right)\right]\end{aligned}$$

The state equation expressed before can be injected in F.6 to obtain the state equation of the drag torque:

$$\begin{aligned}L_{S,q}\cdot\left(\frac{\dot{T_{\theta_m,D}}}{z}\right) = \quad & - \quad R\left(\frac{T_{\theta_m,D}}{z}\right) \quad - \quad L_{S,d}\cdot p^2\dot{\theta}_m\cdot F_{z,Ed} \quad - \quad \sqrt{\frac{3}{2}}K_z\cdot dL_d\cdot z\cdot p^2\dot{\theta}_m\cdot I_{M,d}\\ - \quad & 3K_z^2p^2\dot{\theta}_m\cdot z \quad - \quad \sqrt{\frac{3}{2}}pK_z\cdot dL_q\cdot(\dot{z}\cdot I_{M,q})\\ - \quad & \sqrt{\frac{3}{2}}\cdot\frac{pK_zdL_q\cdot z}{\left(L_{M,q}\cdot L_{S,q}-z^2\cdot dL_q^2\right)}\cdot\left[\quad 2\cdot U_q\cdot L_{S,q} \quad + \quad \left(dL_q^2\cdot z\cdot\dot{z}-R\cdot L_{S,q}\right)\cdot I_{M,q}\right.\\ + \quad & p\dot{\theta}_m\cdot\left[z^2\cdot dL_d\cdot dL_q-L_{M,d}\cdot L_{S,q}\right]\cdot I_{M,d} \quad + \quad \sqrt{\frac{2}{3}}\frac{dL_q}{pK_z}\cdot(z\cdot R-\dot{z}\cdot L_{S,q})\cdot\left(\frac{T_{\theta_m,D}}{z}\right)\\ - \quad & \left.\sqrt{\frac{2}{3}}\frac{L_{S,q}\cdot dL_d-L_{S,d}\cdot dL_q}{K_z}\cdot z\cdot p\dot{\theta}_m\cdot F_{z,Ed} \quad + \quad \sqrt{6}\cdot p\dot{\theta}_m\cdot\left(z^2\cdot K_z\cdot dL_q-K_{\theta_m}\cdot L_{S,q}\right)\right]\end{aligned}$$

By gathering terms for each state variable, it becomes:

$$\begin{aligned}\left(\frac{\dot{T_{\theta_m,D}}}{z}\right) = \quad & \frac{1}{L_{M,q}\cdot L_{S,q}-z^2\cdot dL_q^2}\left[\left(z\dot{z}\cdot dL_q^2-R\cdot L_{M,q}\right)\left(\frac{T_{\theta_m,D}}{z}\right) \quad - p^2\dot{\theta}_m\cdot\left(L_{M,q}\cdot L_{S,d}-z^2dL_d\cdot dL_q\right)\cdot F_{z,Ed}\right.\\ + \quad & \sqrt{\frac{3}{2}}pK_z\cdot dL_q\cdot(z\cdot R-\dot{z}\cdot L_{M,q})\cdot I_{M,q} \quad + \quad \sqrt{\frac{3}{2}}K_z\cdot z\cdot p^2\dot{\theta}_m\left(L_{M,d}\cdot dL_q-L_{M,q}\cdot dL_d\right)\cdot I_{M,d}\\ - \quad & \left.\sqrt{6}\cdot pK_zdL_q\cdot z\cdot U_q \quad + \quad 3p^2\dot{\theta}_m\cdot zK_z\cdot(K_{\theta_m}\cdot dL_q-K_z\cdot L_{M,q})\right.\end{aligned}$$

F.2 Mechanical state equations:

The last equation can be modified by using the relations 2.36, 2.37, 2.38, 2.39 and 2.40 reminded and modified (with F.1 and F.2) below:

- The axial detent force:

$$F_{z,d} = -k_{z,d} \cdot z$$

- The electrodynamic driving torque

$$T_{\theta_m,M} = pK_{\theta_m}\sqrt{\frac{3}{2}} \cdot I_{M,q}$$

- The axial reluctant force

$$\begin{aligned} F_{z,rel} &= I_{M,d} \cdot I_{S,d} \cdot dL_d + I_{M,q} \cdot I_{S,q} \cdot dL_q \\ &= \frac{1}{\sqrt{6}K_z}\left[dL_d \cdot I_{M,d} \cdot F_{z,Ed} + \frac{dL_q}{p} \cdot I_{M,q} \cdot \left(\frac{T_{\theta_m,D}}{z}\right)\right] \end{aligned}$$

- The reluctant torque

$$\begin{aligned} T_{\theta_m,rel} = &\ 3p \cdot (L_2 + M_2) \cdot \left[\frac{I_{M,d}I_{M,q}}{2}\right] \\ &+ 3p \cdot (L_2 - M_2) \cdot [2I_{S,d}I_{S,q}] \\ &+ 3p \cdot z \cdot dL_2 \cdot [I_{M,d}I_{S,q} + I_{S,d}I_{M,q}] \\ = &\ 3p \cdot (L_2 + M_2) \cdot \left[\frac{I_{M,d}I_{M,q}}{2}\right] \\ &+ \frac{1}{K_z^2} \cdot (L_2 - M_2) \cdot \left[F_{z,Ed} \cdot \left(\frac{T_{\theta_m,D}}{z}\right)\right] \\ &+ \sqrt{\frac{3}{2}}\frac{z \cdot dL_2}{K_z} \cdot \left[I_{M,d} \cdot \left(\frac{T_{\theta_m,D}}{z}\right) + p \cdot F_{z,Ed} \cdot I_{M,q}\right] \end{aligned}$$

These expressions can be injected in the mechanical system reminded below:

$$\begin{aligned} m\ddot{z} + C_z\dot{z} &= F_{z,Ed} + F_{z,d} + F_{z,rel} + F_{z,e} \\ J_p\ddot{\theta}_m + C_{\theta_m}\dot{\theta}_m &= T_{\theta_m,D} + T_{\theta_m,M} + T_{\theta_m,rel} + T_{\theta_m,e} \end{aligned}$$

to obtain, after some manipulations:

$$\ddot{z} = \frac{F_{z,Ed}}{m} - \frac{k_{z,d}}{m} \cdot z + \frac{1}{\sqrt{6}mK_z}\left[dL_d \cdot I_{M,d} \cdot F_{z,Ed} + \frac{dL_q}{p} \cdot I_{M,q} \cdot \left(\frac{T_{\theta_m,D}}{z}\right)\right] - \frac{C_z}{m}\dot{z} + \frac{F_{z,e}}{m}$$

$$\begin{aligned} \ddot{\theta}_m = &\ \left(\frac{T_{\theta_m,D}}{z}\right) \cdot \frac{z}{J_p} + \frac{pK_{\theta_m}}{J_p}\sqrt{\frac{3}{2}} \cdot I_{M,q} - \frac{C_{\theta_m}}{J_p}\dot{\theta}_m + \frac{3p \cdot (L_2 + M_2)}{J_p} \cdot \left[\frac{I_{M,d}I_{M,q}}{2}\right] \\ &+ \frac{(L_2 - M_2)}{J_pK_z^2} \cdot \left[F_{z,Ed} \cdot \left(\frac{T_{\theta_m,D}}{z}\right)\right] + \sqrt{\frac{3}{2}}\frac{z \cdot dL_2}{J_pK_z} \cdot \left[I_{M,d} \cdot \left(\frac{T_{\theta_m,D}}{z}\right) + p \cdot F_{z,Ed} \cdot I_{M,q}\right] + \frac{T_{\theta_m,e}}{J_p} \end{aligned}$$

F.3 Gathering of equations:

The final state-space model[11] is obtained by gathering all the equations:

$$\begin{aligned}\dot{I}_{M,d} =& \frac{1}{L_{M,d}L_{S,d} - z^2 dL_d^2}\Big[\quad 2U_d \cdot L_{S,d} \quad + \quad \left(dL_d^2 \cdot z \cdot \dot{z} - RL_{S,d}\right) \cdot I_{M,d} \\ &+ \quad p\dot{\theta}_m \cdot \left(L_{M,q}L_{S,d} - z^2 \cdot dL_d dL_q\right) \cdot I_{M,q} \quad + \quad \sqrt{\frac{2}{3}}\frac{dL_d}{K_z} \cdot (z \cdot R - \dot{z} \cdot L_{S,d}) \cdot F_{z,Ed} \\ &+ \quad \sqrt{\frac{2}{3}}\frac{L_{S,d}dL_q - L_{S,q}dL_d}{K_z}\dot{\theta}_m \cdot \left(\frac{T_{\theta_m,D}}{z}\right) \quad + \quad \sqrt{6}K_z dL_d \cdot z \cdot \dot{z}\Big]\end{aligned}$$

$$\begin{aligned}\dot{I}_{M,q} =& \frac{1}{\left(L_{M,q}L_{S,q} - z^2 \cdot dL_q^2\right)} \cdot \Big[\quad 2U_q \cdot L_{S,q} \quad + \quad \left(dL_q^2 \cdot z \cdot \dot{z} - RL_{S,q}\right) \cdot I_{M,q} \\ &+ \quad p\dot{\theta}_m \cdot \left[z^2 \cdot dL_d dL_q - L_{M,d}L_{S,q}\right] \cdot I_{M,d} \quad + \quad \sqrt{\frac{2}{3}}\frac{dL_q}{pK_z} \cdot (z \cdot R - \dot{z} \cdot L_{S,q}) \cdot \left(\frac{T_{\theta_m,D}}{z}\right) \\ &- \quad \sqrt{\frac{2}{3}}\frac{L_{S,q}dL_d - L_{S,d}dL_q}{K_z} \cdot z \cdot p\dot{\theta}_m \cdot F_{z,Ed} \quad + \quad \sqrt{6}\left(z^2 \cdot K_z dL_q - K_{\theta_m}L_{S,q}\right) \cdot p\dot{\theta}_m\Big]\end{aligned}$$

$$\begin{aligned}\dot{F}_{z,Ed} =& \quad \frac{1}{L_{M,d}L_{S,d} - z^2 \cdot dL_d^2} \cdot \Big[\left(z \cdot \dot{z} \cdot dL_d^2 - RL_{M,d}\right) \cdot F_{z,Ed} \quad + \quad \left(L_{M,d}L_{S,q} - z^2 \cdot dL_d dL_q\right) \cdot \dot{\theta}_m \cdot \left(\frac{T_{\theta_m,D}}{z}\right) \\ &+ \quad \sqrt{\frac{3}{2}}K_z dL_d \cdot (z \cdot R - \dot{z} \cdot L_{M,d}) \cdot I_{M,d} \quad + \quad \sqrt{\frac{3}{2}}K_z \left(L_{M,d}dL_q - L_{M,q}dL_d\right) \cdot z \cdot p\dot{\theta}_m \cdot I_{M,q} \\ &- \quad \sqrt{6}K_z dL_d \cdot U_d \cdot z \quad - \quad 3K_z^2 L_{M,d} \cdot \dot{z}\Big]\end{aligned}$$

$$\begin{aligned}\dot{\left(\frac{T_{\theta_m,D}}{z}\right)} =& \quad \frac{1}{L_{M,q}L_{S,q} - z^2 \cdot dL_q^2}\left[\left(z \cdot \dot{z} \cdot dL_q^2 - RL_{M,q}\right)\left(\frac{T_{\theta_m,D}}{z}\right) \quad - \quad \left(L_{M,q}L_{S,d} - z^2 \cdot dL_d dL_q\right) \cdot p^2\dot{\theta}_m \cdot F_{z,Ed}\right. \\ &+ \quad \sqrt{\frac{3}{2}}pK_z dL_q \cdot (z \cdot R - \dot{z} \cdot L_{M,q}) \cdot I_{M,q} \quad + \quad \sqrt{\frac{3}{2}}K_z \left(L_{M,d}dL_q - L_{M,q}dL_d\right) \cdot z \cdot p^2\dot{\theta}_m \cdot I_{M,d} \\ &\left. - \quad \sqrt{6}pK_z dL_q \cdot U_q \cdot z \quad + \quad 3p^2 K_z \cdot \left(K_{\theta_m}dL_q - K_z L_{M,q}\right)\dot{\theta}_m \cdot z\right]\end{aligned}$$

$$\ddot{z} = \frac{F_{z,Ed}}{m} - \frac{k_{z,d}}{m} \cdot z + \frac{1}{\sqrt{6}mK_z}\left[dL_d \cdot I_{M,d} \cdot F_{z,Ed} + \frac{dL_q}{p} \cdot I_{M,q} \cdot \left(\frac{T_{\theta_m,D}}{z}\right)\right] - \frac{C_z}{m}\dot{z} + \frac{F_{z,e}}{m}$$

$$\begin{aligned}\ddot{\theta}_m =& \left(\frac{T_{\theta_m,D}}{z}\right) \cdot \frac{z}{J_p} + \frac{pK_{\theta_m}}{J_p}\sqrt{\frac{3}{2}} \cdot I_{M,q} - \frac{C_{\theta_m}}{J_p}\dot{\theta}_m + \frac{3p(L_2 + M_2)}{J_p} \cdot \left[\frac{I_{M,d}I_{M,q}}{2}\right] \\ &+ \frac{1}{J_p K_z^2} \cdot (L_2 - M_2) \cdot \left[F_{z,Ed} \cdot \left(\frac{T_{\theta_m,D}}{z}\right)\right] + \sqrt{\frac{3}{2}}\frac{dL_2}{J_p K_z} \cdot z \cdot \left[I_{M,d} \cdot \left(\frac{T_{\theta_m,D}}{z}\right) + p \cdot F_{z,Ed} \cdot I_{M,q}\right] + \frac{T_{\theta_m,e}}{J_p}\end{aligned}$$

[11] Come back to the section concerning this appendix: Section 2.4.1

G Quasi-static analysis

All the developments are made for a rotor including saliency and axial variation of the inductance coefficients because it is the most general case. All these expressions can be simplified to a rotor which has no saliency.

By applying the quasi-static conditions, $\dot{I}_{M,d} = \dot{I}_{M,q} = \left(\frac{\dot{T}_{\theta_m,D}}{z}\right) = \dot{F}_{z,Ed} = \dot{z} = \ddot{z} = 0$ and a constant spin speed $\dot{\theta}_m = \omega$, equations F.4 and F.6 are reduced to:

- Equation F.4 becomes:

$$F_{z,Ed} = \frac{L_{S,q}}{R} \cdot \omega \cdot \left(\frac{T_{\theta_m,D}}{z}\right) + \sqrt{\frac{3}{2}}\frac{dL_q}{R} \cdot K_z \cdot z \cdot p\omega \cdot I_{M,q} \tag{G.1}$$

- Equation F.6 becomes:

$$\left(\frac{T_{\theta_m,D}}{z}\right) = -\frac{p^2\omega}{R}\left(L_{S,d} \cdot F_{z,Ed} + \sqrt{\frac{3}{2}}K_z \cdot dL_d z \cdot I_{M,d} + 3K_z^2 \cdot z\right) \tag{G.2}$$

Injecting G.2 expression in equation G.1 provides:

$$\begin{aligned}\left(\frac{T_{\theta_m,D}}{z}\right) = &-\frac{p^2\omega}{R}\left(L_{S,d} \cdot \left[\frac{L_{S,q}}{R} \cdot \omega \cdot \left(\frac{T_{\theta_m,D}}{z}\right) + \sqrt{\frac{3}{2}}\frac{dL_q}{R} \cdot K_z \cdot z \cdot p\omega \cdot I_{M,q}\right]\right.\\ &\left. + \sqrt{\frac{3}{2}}K_z \cdot dL_d z \cdot I_{M,d} + 3K_z^2 \cdot z\right)\end{aligned}$$

$$\left(\frac{T_{\theta_m,D}}{z}\right) \cdot -R \cdot \frac{\left[1 + \frac{p^2 L_{S,d} L_{S,q}}{R^2}\omega^2\right]}{p^2 \cdot \omega} = \sqrt{\frac{3}{2}}\frac{L_{S,d} \cdot dL_q}{R} \cdot K_z \cdot z \cdot p\omega \cdot I_{M,q} + \sqrt{\frac{3}{2}}K_z \cdot z \cdot dL_d \cdot I_{M,d} + 3K_z^2 \cdot z$$

Which finally provides the expression:

$$T_{\theta_m,D} = -z^2 \cdot \sqrt{\frac{3}{2}} \cdot \frac{K_z \cdot R}{L_{S,d} L_{S,q}} \cdot \frac{\omega}{\left[\frac{R^2}{p^2 L_{S,d} L_{S,q}} + \omega^2\right]} \cdot \left[\frac{L_{S,d} \cdot dL_q}{R} \cdot p\omega \cdot I_{M,q} + dL_d \cdot I_{M,d} + \sqrt{6} \cdot K_z\right] \tag{G.3}$$

The expression can be injected in G.1 to obtain:

$$\begin{aligned}F_{z,Ed} = &-\sqrt{\frac{3}{2}} \cdot \frac{K_z \cdot L_{S,q}}{R^2} \cdot z \cdot \frac{p^2 \cdot \omega^2}{\left[1 + \frac{p^2 L_{S,d} L_{S,q}}{R^2}\omega^2\right]} \cdot \left[\frac{L_{S,d} \cdot dL_q}{R} \cdot p\omega \cdot I_{M,q} + dL_d \cdot I_{M,d} + \sqrt{6} \cdot K_z\right]\\ &+ \sqrt{\frac{3}{2}}\frac{dL_q}{R} \cdot K_z \cdot z \cdot p\omega \cdot I_{M,q}\\ =&\sqrt{\frac{3}{2}} \cdot K_z \cdot z \left[-\frac{1}{L_{S,d}} \cdot \frac{\omega^2}{\left[\frac{R^2}{p^2 L_{S,d} L_{S,q}} + \omega^2\right]} \cdot \left[\frac{L_{S,d} \cdot dL_q}{R} \cdot p\omega \cdot I_{M,q} + dL_d \cdot I_{M,d} + \sqrt{6} \cdot K_z\right] + \frac{dL_q}{R} \cdot p\omega \cdot I_{M,q}\right]\\ =&\sqrt{\frac{3}{2}} \cdot K_z \cdot z \left[\frac{dL_q}{R} \cdot \left(1 - \frac{\omega^2}{\left[\frac{R^2}{p^2 L_{S,d} L_{S,q}} + \omega^2\right]}\right) \cdot p\omega \cdot I_{M,q} - \frac{\omega^2}{\left[\frac{R^2}{p^2 L_{S,d} L_{S,q}} + \omega^2\right]} \cdot \left[\frac{dL_d}{L_{S,d}} \cdot I_{M,d} + \sqrt{6} \cdot \frac{K_z}{L_{S,d}}\right]\right]\end{aligned} \tag{G.4}$$

The asymptotic value of this axial force can be computed when ω reach important values[12]:

$$F^{\infty}_{z,Ed} = \lim_{\omega \to \infty} F_{z,Ed} = -\sqrt{\frac{3}{2}} \cdot \frac{K_z}{L_{S,d}} \cdot z \cdot \left[dL_d \cdot I_{M,d} + \sqrt{6} \cdot K_z \right] \tag{G.5}$$

The same reasoning can be applied for the drag torque:

$$T^{\infty}_{\theta_m,D} = -z^2 \cdot \sqrt{\frac{3}{2}} \cdot \frac{K_z}{L_{S,q}} \cdot [dL_q \cdot p \cdot I_{M,q}] \tag{G.6}$$

[12] Come back to the section concerning this appendix: Section 2.4.3

G.1 Total stiffness and torque developed by the machine

The purpose of this appendix is to compute the expression of the total axial force and torque produced by the machine only based on the motors direct and quadratic currents.

Starting from 2.67 and injecting equations 2.65 and 2.66, the total axial force can be expressed as:

$$\begin{aligned}
\mathrm{F}_{\mathrm{z,tot}}^{\infty} =& -\sqrt{\frac{3}{2}} \cdot \frac{\mathrm{K_z}}{\mathrm{L_{S,d}}} \cdot \mathrm{z} \cdot \left[\mathrm{dL_d} \cdot \mathrm{I_{M,d}} + \sqrt{6} \cdot \mathrm{K_z}\right] \\
&+ \mathrm{I_{M,d}} \cdot \frac{\mathrm{F}_{\mathrm{z,Ed}}^{\infty}}{\sqrt{6}\mathrm{K_z}} \cdot \mathrm{dL_d} + \mathrm{I_{M,q}} \cdot \frac{\mathrm{T}_{\theta_\mathrm{m},\mathrm{D}}^{\infty}}{\mathrm{pzK_z}\sqrt{6}} \cdot \mathrm{dL_q} \\
&- \mathrm{k_{z,d}} \cdot \mathrm{z} \\
\\
=& -\sqrt{\frac{3}{2}} \cdot \frac{\mathrm{K_z}}{\mathrm{L_{S,d}}} \cdot \mathrm{z} \cdot \left[\mathrm{dL_d} \cdot \mathrm{I_{M,d}} + \sqrt{6} \cdot \mathrm{K_z}\right] \\
&- \mathrm{I_{M,d}} \cdot \frac{\mathrm{dL_d}}{2\mathrm{L_{S,d}}} \cdot \mathrm{z} \cdot \left[\mathrm{dL_d} \cdot \mathrm{I_{M,d}} + \sqrt{6} \cdot \mathrm{K_z}\right] - \mathrm{z} \cdot \frac{\mathrm{dL_q^2}}{2\mathrm{L_{S,q}}} \cdot \mathrm{I_{M,q}^2} \\
&- \mathrm{k_{z,d}} \cdot \mathrm{z} \\
\\
=& -\frac{\mathrm{z}}{\mathrm{L_{S,d}}} \left[\sqrt{\frac{3}{2}} \cdot \mathrm{K_z} + \frac{\mathrm{I_{M,d}} \cdot \mathrm{dL_d}}{2}\right] \cdot \left[\mathrm{dL_d} \cdot \mathrm{I_{M,d}} + \sqrt{6} \cdot \mathrm{K_z}\right] \\
&- \mathrm{z} \cdot \frac{\mathrm{dL_q^2}}{2\mathrm{L_{S,q}}} \cdot \mathrm{I_{M,q}^2} - \mathrm{k_{z,d}} \cdot \mathrm{z} \\
\\
=& -\frac{\mathrm{z}}{2\mathrm{L_{S,d}}} \cdot \left[\mathrm{dL_d} \cdot \mathrm{I_{M,d}} + \sqrt{6} \cdot \mathrm{K_z}\right]^2 \\
&- \mathrm{z} \cdot \frac{\mathrm{dL_q^2}}{2\mathrm{L_{S,q}}} \cdot \mathrm{I_{M,q}^2} - \mathrm{k_{z,d}} \cdot \mathrm{z} \\
\\
=& -\mathrm{z} \cdot \left[\frac{\left[\mathrm{dL_d} \cdot \mathrm{I_{M,d}} + \sqrt{6} \cdot \mathrm{K_z}\right]^2}{2\mathrm{L_{S,d}}} + \frac{\mathrm{dL_q^2}}{2\mathrm{L_{S,q}}} \cdot \mathrm{I_{M,q}^2} + \mathrm{k_{z,d}}\right]
\end{aligned} \tag{G.7}$$

Based on this result, one can deduce the expression of the total stiffness:

$$\mathrm{k}_{\mathrm{z,tot}}^{\infty} = \frac{\left[\mathrm{dL_d} \cdot \mathrm{I_{M,d}} + \sqrt{6} \cdot \mathrm{K_z}\right]^2}{2\mathrm{L_{S,d}}} + \frac{\mathrm{dL_q^2}}{2\mathrm{L_{S,q}}} \cdot \mathrm{I_{M,q}^2} + \mathrm{k_{z,d}} \tag{G.8}$$

The same reasoning can be made with equation 2.70[13]

$$\begin{aligned}
\mathrm{T}^{\infty}_{\theta_\mathrm{m},\mathrm{tot}} =& \mathrm{T}_{\theta_\mathrm{m},\mathrm{M}} + \mathrm{T}^{\infty}_{\theta_\mathrm{m},\mathrm{D}} + \mathrm{T}^{\infty}_{\theta_\mathrm{m},\mathrm{rel}} \\
=& \sqrt{\frac{3}{2}} \cdot \mathrm{p} \cdot \left[\mathrm{K}_{\theta_\mathrm{m}} - \mathrm{z}^2 \cdot \frac{\mathrm{K_z} \cdot \mathrm{dL_q}}{\mathrm{L_{S,q}}} \right] \cdot \mathrm{I_{M,q}} + 3\mathrm{p} \cdot (\mathrm{L_2} + \mathrm{M_2}) \cdot \left[\frac{\mathrm{I_{M,d}} \mathrm{I_{M,q}}}{2} \right] \\
& + 3\mathrm{p} \cdot (\mathrm{L_2} - \mathrm{M_2}) \cdot \left[2\mathrm{I^{\infty}_{S,d}} \mathrm{I^{\infty}_{S,q}} \right] + 3\mathrm{p} \cdot \mathrm{z} \cdot \mathrm{dL_2} \cdot \left[\mathrm{I_{M,d}} \mathrm{I^{\infty}_{S,q}} + \mathrm{I^{\infty}_{S,d}} \mathrm{I_{M,q}} \right]
\end{aligned}$$

Where the expressions of $\mathrm{I_{S,d}}$ and $\mathrm{I_{S,q}}$ can be replaced (equations 2.65 and 2.66)

$$\begin{aligned}
=& \sqrt{\frac{3}{2}} \cdot \mathrm{p} \cdot \left[\mathrm{K}_{\theta_\mathrm{m}} - \mathrm{z}^2 \cdot \frac{\mathrm{K_z} \cdot \mathrm{dL_q}}{\mathrm{L_{S,q}}} \right] \cdot \mathrm{I_{M,q}} + 3\mathrm{p} \cdot (\mathrm{L_2} + \mathrm{M_2}) \cdot \left[\frac{\mathrm{I_{M,d}} \mathrm{I_{M,q}}}{2} \right] \\
& + 3\mathrm{p} \cdot (\mathrm{L_2} - \mathrm{M_2}) \cdot \left[2 \left(-\frac{\mathrm{z}}{2\mathrm{L_{S,d}}} \cdot \left[\mathrm{dL_d} \cdot \mathrm{I_{M,d}} + \sqrt{6} \cdot \mathrm{K_z} \right] \right) \cdot \left(-\mathrm{z} \cdot \frac{\mathrm{dL_q}}{2\mathrm{L_{S,q}}} \cdot \mathrm{I_{M,q}} \right) \right] \\
& + 3\mathrm{p} \cdot \mathrm{z} \cdot \mathrm{dL_2} \cdot \left[\mathrm{I_{M,d}} \cdot \left(-\mathrm{z} \cdot \frac{\mathrm{dL_q}}{2\mathrm{L_{S,q}}} \cdot \mathrm{I_{M,q}} \right) + \left(-\frac{\mathrm{z}}{2\mathrm{L_{S,d}}} \cdot \left[\mathrm{dL_d} \cdot \mathrm{I_{M,d}} + \sqrt{6} \cdot \mathrm{K_z} \right] \right) \cdot \mathrm{I_{M,q}} \right]
\end{aligned}$$

$$\begin{aligned}
=& 3\mathrm{p} \cdot \mathrm{I_{M,q}} \left[\left[\frac{\mathrm{K}_{\theta_\mathrm{m}}}{\sqrt{6}} - \mathrm{z}^2 \cdot \frac{\mathrm{K_z} \cdot \mathrm{dL_q}}{\sqrt{6}\mathrm{L_{S,q}}} \right] \right. \\
& + (\mathrm{L_2} + \mathrm{M_2}) \cdot \frac{\mathrm{I_{M,d}}}{2} + \mathrm{z}^2 \cdot (\mathrm{L_2} - \mathrm{M_2}) \cdot \frac{\mathrm{dL_q}}{\mathrm{L_{S,d}} \cdot \mathrm{L_{S,q}}} \left[\mathrm{dL_d} \cdot \frac{\mathrm{I_{M,d}}}{2} + \sqrt{\frac{3}{2}} \cdot \mathrm{K_z} \right] \\
& \left. -\mathrm{z}^2 \cdot \mathrm{dL_2} \cdot \left[\frac{\mathrm{I_{M,d}}}{2} \cdot \left(\frac{\mathrm{dL_q}}{\mathrm{L_{S,q}}} \right) + \frac{1}{\mathrm{L_{S,d}}} \cdot \left[\mathrm{dL_d} \cdot \frac{\mathrm{I_{M,d}}}{2} + \sqrt{\frac{3}{2}} \cdot \mathrm{K_z} \right] \right] \right]
\end{aligned}$$

$$\begin{aligned}
=& 3\mathrm{p} \cdot \mathrm{I_{M,q}} \left[\frac{\mathrm{K}_{\theta_\mathrm{m}}}{\sqrt{6}} - \mathrm{z}^2 \cdot \frac{\mathrm{K_z}}{\sqrt{6}} \cdot \left(\frac{\mathrm{dL_q}}{\mathrm{L_{S,q}}} \cdot \left(1 - 3 \cdot \frac{\mathrm{L_2} - \mathrm{M_2}}{\mathrm{L_{S,d}}} \right) + \frac{3 \cdot \mathrm{dL_2}}{\mathrm{L_{S,d}}} \right) \right] \\
& + 3\mathrm{p} \cdot \mathrm{I_{M,q}} \cdot \frac{\mathrm{I_{M,d}}}{2} \cdot \left[\mathrm{L_2} + \mathrm{M_2} + \mathrm{z}^2 \cdot \left[(\mathrm{L_2} - \mathrm{M_2}) \cdot \left(\frac{\mathrm{dL_d} \cdot \mathrm{dL_q}}{\mathrm{L_{S,d}} \cdot \mathrm{L_{S,q}}} \right) - \mathrm{dL_2} \cdot \left(\frac{\mathrm{dL_d}}{\mathrm{L_{S,d}}} + \frac{\mathrm{dL_q}}{\mathrm{L_{S,q}}} \right) \right] \right]
\end{aligned}$$

Definitions in section 2.2.3.c allow to reduce the expression as:

$$\begin{aligned}
=& 3\mathrm{p} \cdot \mathrm{I_{M,q}} \left[\frac{\mathrm{K}_{\theta_\mathrm{m}}}{\sqrt{6}} - \mathrm{z}^2 \cdot \frac{\mathrm{K_z}}{\sqrt{6}} \cdot \left(\frac{\mathrm{dL_d}}{\mathrm{L_{S,d}}} \right) \right] \\
& + 3\mathrm{p} \cdot \mathrm{I_{M,q}} \cdot \frac{\mathrm{I_{M,d}}}{2} \cdot \left[(\mathrm{L_2} + \mathrm{M_2}) + \mathrm{z}^2 \cdot \left[(\mathrm{L_2} - \mathrm{M_2}) \cdot \left(\frac{\mathrm{dL_d} \cdot \mathrm{dL_q}}{\mathrm{L_{S,d}} \cdot \mathrm{L_{S,q}}} \right) - \mathrm{dL_2} \cdot \left(\frac{\mathrm{dL_d}}{\mathrm{L_{S,d}}} + \frac{\mathrm{dL_q}}{\mathrm{L_{S,q}}} \right) \right] \right]
\end{aligned}$$

G.2 Behaviour when the speed is not infinite in centred position

The same development as before are done but without considering an infinite speed. However, the axial position is set to zero. It means that the drag torque is equal to zero:

[13] Come back to the section concerning this appendix: Section 2.4.3

$$
\begin{aligned}
\mathrm{T}_{\theta_\mathrm{m},\mathrm{tot}} =& \mathrm{T}_{\theta_\mathrm{m},\mathrm{M}} + \mathrm{T}_{\theta_\mathrm{m},\mathrm{rel}} \\
=& \sqrt{\frac{3}{2}} \cdot \mathrm{pK}_{\theta_\mathrm{m}} \mathrm{I}_{\mathrm{M,q}} + 3\mathrm{p} \cdot (\mathrm{L}_2 + \mathrm{M}_2) \cdot \left[\frac{\mathrm{I}_{\mathrm{M,d}} \mathrm{I}_{\mathrm{M,q}}}{2} \right] \\
& + 3\mathrm{p} \cdot (\mathrm{L}_2 - \mathrm{M}_2) \cdot [2\mathrm{I}_{\mathrm{S,d}} \mathrm{I}_{\mathrm{S,q}}] + 3\mathrm{p} \cdot \mathrm{z} \cdot \mathrm{dL}_2 \cdot [\mathrm{I}_{\mathrm{M,d}} \mathrm{I}_{\mathrm{S,q}} + \mathrm{I}_{\mathrm{S,d}} \mathrm{I}_{\mathrm{M,q}}]
\end{aligned}
$$

For a centred axial position, the suspension currents are equal to 0, which simplify the expression:

$$
\mathrm{T}_{\theta_\mathrm{m},\mathrm{tot}}\big|_{\mathrm{z}=0} = \sqrt{\frac{3}{2}} \cdot \mathrm{pK}_{\theta_\mathrm{m}} \cdot \mathrm{I}_{\mathrm{M,q}} + 3\mathrm{p} \cdot (\mathrm{L}_2 + \mathrm{M}_2) \cdot \left[\frac{\mathrm{I}_{\mathrm{M,d}} \mathrm{I}_{\mathrm{M,q}}}{2} \right]
$$

The development for the stiffness is:

$$
\begin{aligned}
\mathrm{k}_{\mathrm{z,tot}}(\mathrm{z}=0) =& -\frac{\mathrm{F}_{\mathrm{z,Ed}} + \mathrm{F}_{\mathrm{z,rel}} + \mathrm{F}_{\mathrm{z,d}}}{\mathrm{z}} \\
=& \sqrt{\frac{3}{2}} \cdot \mathrm{K}_\mathrm{z} \left[\frac{\mathrm{dL}_\mathrm{q}}{\mathrm{R}} \cdot \left(\frac{\omega^2}{\left[\frac{\mathrm{R}^2}{\mathrm{p}^2 \mathrm{L}_{\mathrm{S,d}} \mathrm{L}_{\mathrm{S,q}}} + \omega^2 \right]} - 1 \right) \cdot \mathrm{p}\omega \cdot \mathrm{I}_{\mathrm{M,q}} + \frac{\omega^2}{\left[\frac{\mathrm{R}^2}{\mathrm{p}^2 \mathrm{L}_{\mathrm{S,d}} \mathrm{L}_{\mathrm{S,q}}} + \omega^2 \right]} \cdot \left[\frac{\mathrm{dL}_\mathrm{d}}{\mathrm{L}_{\mathrm{S,d}}} \cdot \mathrm{I}_{\mathrm{M,d}} + \sqrt{6} \cdot \frac{\mathrm{K}_\mathrm{z}}{\mathrm{L}_{\mathrm{S,d}}} \right] \right] \\
& - \frac{\mathrm{I}_{\mathrm{M,d}} \cdot \mathrm{I}_{\mathrm{S,d}} \cdot \mathrm{dL}_\mathrm{d} - \mathrm{I}_{\mathrm{M,q}} \cdot \mathrm{I}_{\mathrm{S,q}} \cdot \mathrm{dL}_\mathrm{q}}{\mathrm{z}} + \mathrm{k}_{\mathrm{z,d}}
\end{aligned}
$$

Equations 2.36, 2.37, 2.61 and 2.63 allow to replace the suspension currents

$$
\begin{aligned}
=& \sqrt{\frac{3}{2}} \cdot \mathrm{K}_\mathrm{z} \left[\frac{\mathrm{dL}_\mathrm{q}}{\mathrm{R}} \cdot \left(\frac{\omega^2}{\left[\frac{\mathrm{R}^2}{\mathrm{p}^2 \mathrm{L}_{\mathrm{S,d}} \mathrm{L}_{\mathrm{S,q}}} + \omega^2 \right]} - 1 \right) \cdot \mathrm{p}\omega \cdot \mathrm{I}_{\mathrm{M,q}} + \frac{\omega^2}{\left[\frac{\mathrm{R}^2}{\mathrm{p}^2 \mathrm{L}_{\mathrm{S,d}} \mathrm{L}_{\mathrm{S,q}}} + \omega^2 \right]} \cdot \left[\frac{\mathrm{dL}_\mathrm{d}}{\mathrm{L}_{\mathrm{S,d}}} \cdot \mathrm{I}_{\mathrm{M,d}} + \sqrt{6} \cdot \frac{\mathrm{K}_\mathrm{z}}{\mathrm{L}_{\mathrm{S,d}}} \right] \right] \\
& - \mathrm{I}_{\mathrm{M,d}} \cdot \frac{\mathrm{F}_{\mathrm{z,ed}}}{\mathrm{z} \cdot \sqrt{6} \mathrm{K}_\mathrm{z}} \cdot \mathrm{dL}_\mathrm{d} - \mathrm{I}_{\mathrm{M,q}} \cdot \frac{\mathrm{T}_{\theta_\mathrm{m},\mathrm{D}}}{\mathrm{z}^2 \cdot \sqrt{6} \cdot \mathrm{pK}_\mathrm{z}} \cdot \mathrm{dL}_\mathrm{q} + \mathrm{k}_{\mathrm{z,d}}
\end{aligned}
$$

$$
\begin{aligned}
=& \sqrt{\frac{3}{2}} \cdot \mathrm{K}_\mathrm{z} \left[\frac{\mathrm{dL}_\mathrm{q}}{\mathrm{R}} \cdot \left(\frac{\omega^2}{\left[\frac{\mathrm{R}^2}{\mathrm{p}^2 \mathrm{L}_{\mathrm{S,d}} \mathrm{L}_{\mathrm{S,q}}} + \omega^2 \right]} - 1 \right) \cdot \mathrm{p}\omega \cdot \mathrm{I}_{\mathrm{M,q}} + \frac{\omega^2}{\left[\frac{\mathrm{R}^2}{\mathrm{p}^2 \mathrm{L}_{\mathrm{S,d}} \mathrm{L}_{\mathrm{S,q}}} + \omega^2 \right]} \cdot \left[\frac{\mathrm{dL}_\mathrm{d}}{\mathrm{L}_{\mathrm{S,d}}} \cdot \mathrm{I}_{\mathrm{M,d}} + \sqrt{6} \cdot \frac{\mathrm{K}_\mathrm{z}}{\mathrm{L}_{\mathrm{S,d}}} \right] \right] \\
& + \frac{\mathrm{I}_{\mathrm{M,d}} \cdot \mathrm{dL}_\mathrm{d}}{2} \cdot \left[\frac{\mathrm{dL}_\mathrm{q}}{\mathrm{R}} \cdot \left(\frac{\omega^2}{\left[\frac{\mathrm{R}^2}{\mathrm{p}^2 \mathrm{L}_{\mathrm{S,d}} \mathrm{L}_{\mathrm{S,q}}} + \omega^2 \right]} - 1 \right) \cdot \mathrm{p}\omega \cdot \mathrm{I}_{\mathrm{M,q}} + \frac{\omega^2}{\left[\frac{\mathrm{R}^2}{\mathrm{p}^2 \mathrm{L}_{\mathrm{S,d}} \mathrm{L}_{\mathrm{S,q}}} + \omega^2 \right]} \cdot \left[\frac{\mathrm{dL}_\mathrm{d}}{\mathrm{L}_{\mathrm{S,d}}} \cdot \mathrm{I}_{\mathrm{M,d}} + \sqrt{6} \cdot \frac{\mathrm{K}_\mathrm{z}}{\mathrm{L}_{\mathrm{S,d}}} \right] \right] \\
& + \mathrm{I}_{\mathrm{M,q}} \cdot \frac{1}{2\mathrm{p}} \cdot \frac{\mathrm{R}}{\mathrm{L}_{\mathrm{S,d}} \mathrm{L}_{\mathrm{S,q}}} \cdot \frac{\omega}{\left[\frac{\mathrm{R}^2}{\mathrm{p}^2 \mathrm{L}_{\mathrm{S,d}} \mathrm{L}_{\mathrm{S,q}}} + \omega^2 \right]} \cdot \left[\frac{\mathrm{L}_{\mathrm{S,d}} \cdot \mathrm{dL}_\mathrm{q}}{\mathrm{R}} \cdot \mathrm{p}\omega \cdot \mathrm{I}_{\mathrm{M,q}} + \mathrm{dL}_\mathrm{d} \cdot \mathrm{I}_{\mathrm{M,d}} + \sqrt{6} \cdot \mathrm{K}_\mathrm{z} \right] \cdot \mathrm{dL}_\mathrm{q} + \mathrm{k}_{\mathrm{z,d}}
\end{aligned}
$$

$$
\begin{aligned}
\mathrm{k}_{\mathrm{z,tot}}\big|_{\mathrm{z}=0} =& \left(\sqrt{\frac{3}{2}} \cdot \mathrm{K}_\mathrm{z} + \frac{\mathrm{I}_{\mathrm{M,d}} \cdot \mathrm{dL}_\mathrm{d}}{2} \right) \cdot \left[\frac{\mathrm{dL}_\mathrm{q}}{\mathrm{R}} \cdot \left(\frac{\omega^2}{\left[\frac{\mathrm{R}^2}{\mathrm{p}^2 \mathrm{L}_{\mathrm{S,d}} \mathrm{L}_{\mathrm{S,q}}} + \omega^2 \right]} - 1 \right) \cdot \mathrm{p}\omega \cdot \mathrm{I}_{\mathrm{M,q}} \right. \\
& \left. + \frac{\omega^2}{\left[\frac{\mathrm{R}^2}{\mathrm{p}^2 \mathrm{L}_{\mathrm{S,d}} \mathrm{L}_{\mathrm{S,q}}} + \omega^2 \right]} \cdot \left[\frac{\mathrm{dL}_\mathrm{d}}{\mathrm{L}_{\mathrm{S,d}}} \cdot \mathrm{I}_{\mathrm{M,d}} + \sqrt{6} \cdot \frac{\mathrm{K}_\mathrm{z}}{\mathrm{L}_{\mathrm{S,d}}} \right] \right] \\
& + \mathrm{I}_{\mathrm{M,q}} \cdot \frac{1}{2\mathrm{p}} \cdot \frac{\mathrm{R}}{\mathrm{L}_{\mathrm{S,d}} \mathrm{L}_{\mathrm{S,q}}} \cdot \frac{\omega}{\left[\frac{\mathrm{R}^2}{\mathrm{p}^2 \mathrm{L}_{\mathrm{S,d}} \mathrm{L}_{\mathrm{S,q}}} + \omega^2 \right]} \cdot \left[\frac{\mathrm{L}_{\mathrm{S,d}} \cdot \mathrm{dL}_\mathrm{q}}{\mathrm{R}} \cdot \mathrm{p}\omega \cdot \mathrm{I}_{\mathrm{M,q}} + \mathrm{dL}_\mathrm{d} \cdot \mathrm{I}_{\mathrm{M,d}} + \sqrt{6} \cdot \mathrm{K}_\mathrm{z} \right] \cdot \mathrm{dL}_\mathrm{q} + \mathrm{k}_{\mathrm{z,d}}
\end{aligned}
$$

H Optimisation results

This appendix presents the dimensions of the machine toward which the optimisation process tends[14].

H.1 $I_{M,d} = 0$

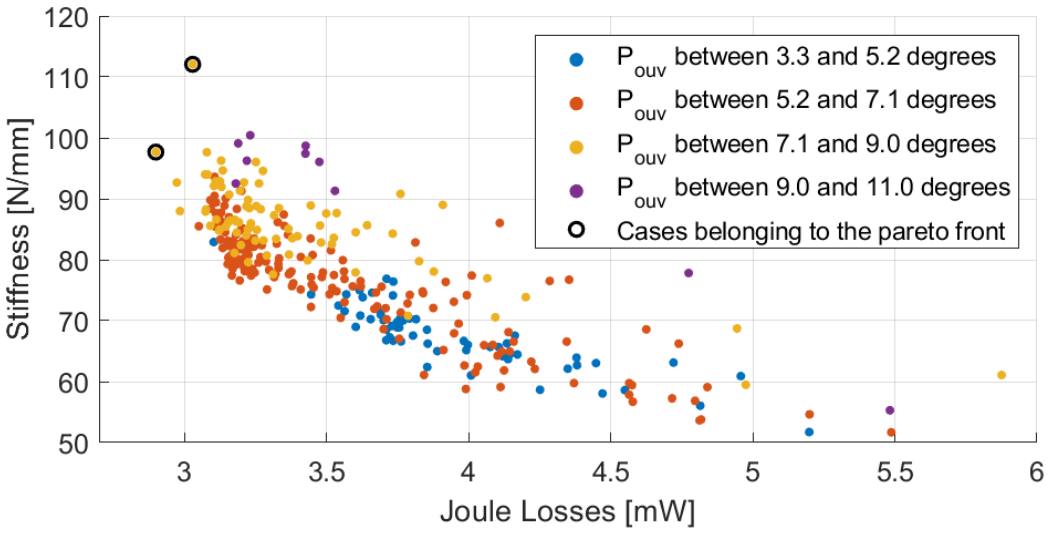

Figure 10: Stiffness and Joule losses obtained for all candidates where p = 9 during the first optimisation. Each candidate is coloured according to its value P_{ouv}.

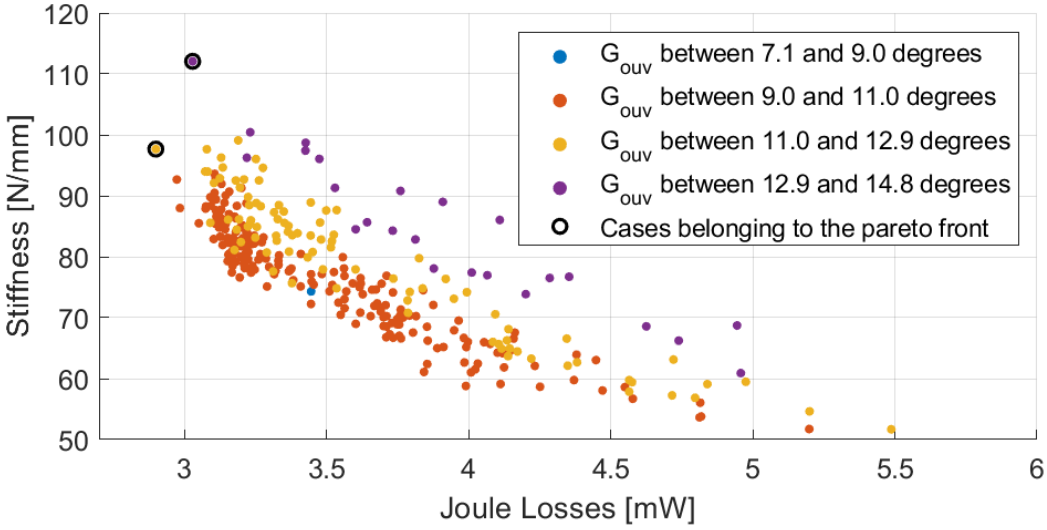

Figure 11: Stiffness and Joule losses obtained for all candidates where p = 9 during the first optimisation. Each candidate is coloured according to its value G_{ouv}.

[14]Come back to the Section concerning this appendix: Section 4.1.3

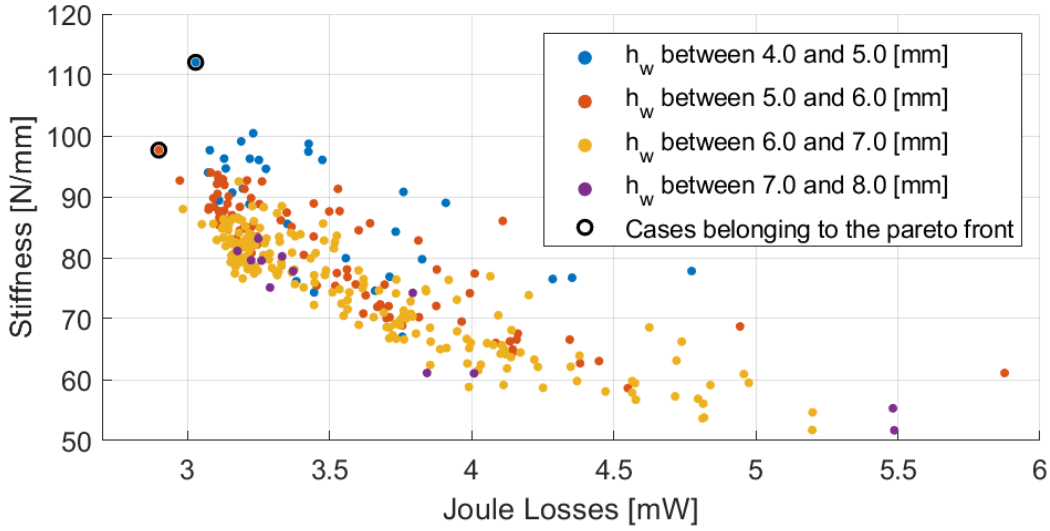

Figure 12: Stiffness and Joule losses obtained for all candidates where p = 9 during the first optimisation. Each candidate is coloured according to its value h_w.

H.2 $I_{M,d} \neq 0$

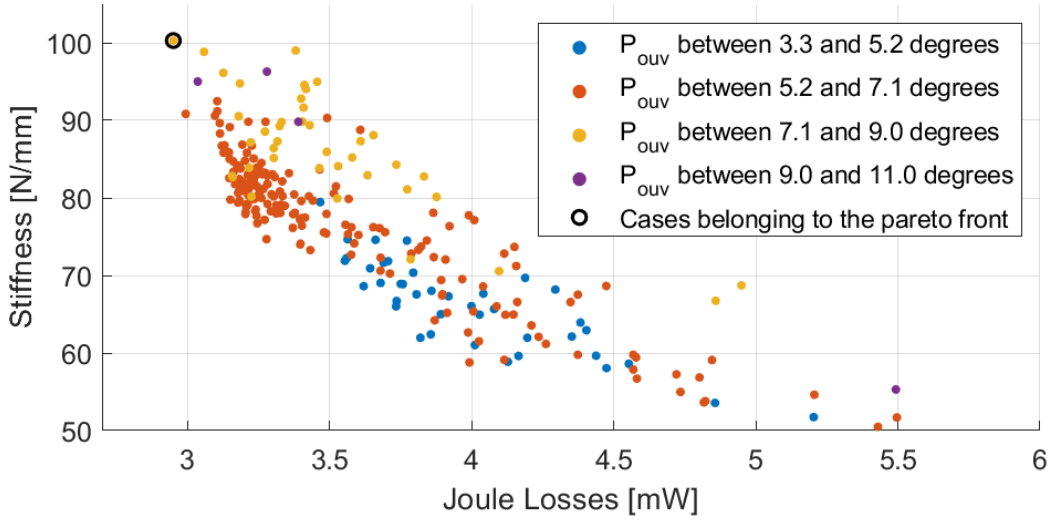

Figure 13: Stiffness and Joule losses obtained for all candidates where p = 9 during the second optimisation. Each candidate is coloured according to its value P_{ouv}.

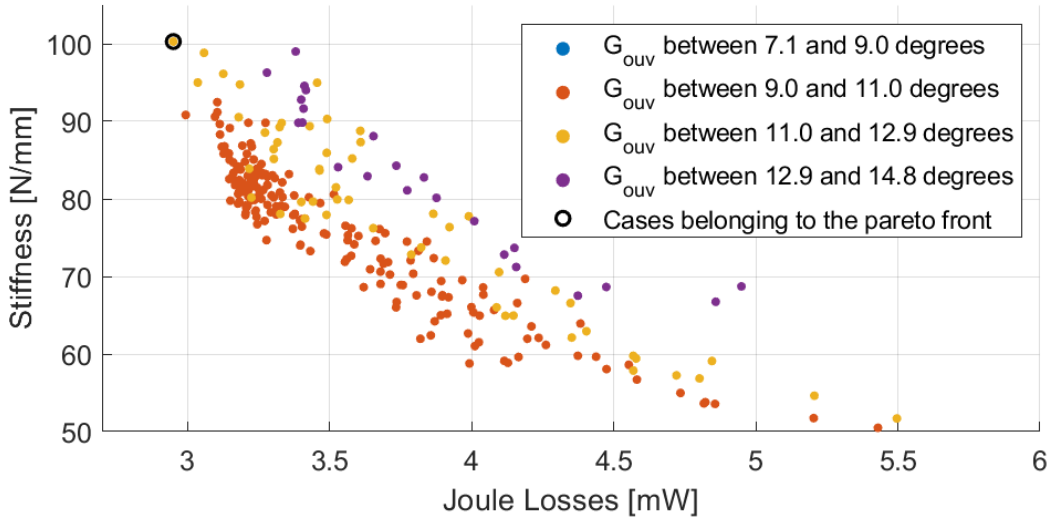

Figure 14: Stiffness and Joule losses obtained for all candidates where p = 9 during the second optimisation. Each candidate is coloured according to its value G_{ouv}.

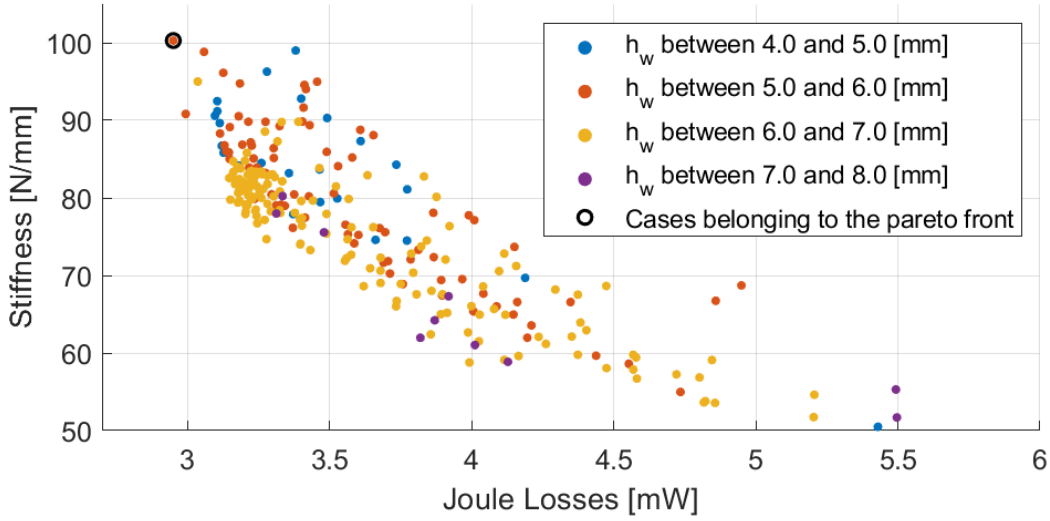

Figure 15: Stiffness and Joule losses obtained for all candidates where p = 9 during the second optimisation. Each candidate is coloured according to its value h_w.

Secret Appendix

Figure 16: Smiles of the authors after this nice year, thank's for reading ! (The crazy girl in background is not one of the authors)

UNIVERSITÉ CATHOLIQUE DE LOUVAIN
École polytechnique de Louvain
Rue Archimède, 1 bte L6.11.01, 1348 Louvain-la-Neuve, Belgique | **www.uclouvain.be/epl**